(2,

CONSTITUTIVE MODELS FOR GEOLOGIC MATERIALS AND THEIR APPLICATION TO EXCAVATION PROBLEMS

Feng ZHANG

School of Civil Engineering

Kyoto University

1994

CONTENTS

Acknowledgments

This paper is completed at the Department of Transportation Engineering, Kyoto University in the period from April 1992 to March 1995.

I am much indebted to Prof. T. ADACHI of Kyoto University, my academic supervisor, for his active support of my research. Since I came to Kyoto University in 1989, he has being provided me with a stimulating environment for my research and writing this paper, for his energetic efforts to impart rudimentary knowledge of geomechanics to me, for his ceaselessly encouragement and advice to my research, for which I am very grateful. Without his overall guidance and keen insight, I could hardly do anything.

Thanks are also given to Prof. F. OKA of Gifu University, for his constant valuable suggestion and encouragement. His ideas often cleared out vague points existed in the paper.

Heartily gratitude should be given to Asso. Prof. M. KIMURA. In nearly five years, he has being responsible for my detail research work, in his unique, powerful and intensive way. It is him who guided me to Japanese society of civil engineering, and also the Japanese culture. As we are in the same age, we need not take much care of the way in our conversation. I cannot remember how many times I was criticized by him on this or that kind of mistakes that when he went out for errand, I would miss his 'noisy' criticism. Moreover, this paper was fully checked by him when he was very busy at the time.

Thanks should be given to Prof. Y. OHNISHI for kind helping in my understanding computer; Asso. Prof. T. TAMURA of Kyoto University, for his comprehensive explanation of finite element analysis; Asso. Prof. A. YASHIMA of Gifu University, Lecturer N. YOSHIDA, Technician T. YANO of Kyoto University, Mr. T. HASHIMOTO, vice director of Osaka Soil Testing Laboratory, Instructor M. TANAKA of Kyoto University, for their valuable suggestion and supports.

Particular thanks should be given to all the students in Adachi and Ohnishi labs. I would like to name some of them. Mr. Y. WAKAYAMA, Mr. K. KOZUKI, Mr. H. SORAOKA and Mr. A. KOIKE, the members of 'constitutive-model group'; Mr. H. KAMEI and Mr. H. KOBAYASHI, the members of 'pile group'. They provided me with a harmonic and pleasant environment. I enjoyed very much the life of the community where we took lesson, did experiments, wrote reports, made discussion and did research together. Part of the result in this paper was the harvest of their industrious effort. In the final stage of the paper, many students helped me in checking the paper.

I and my family would also give thanks to Mr. Y. HACHISUKA and Mr. H. OKAMOTO for their generous support both in daily life and research environment.

I am also grateful to all of my teachers and colleagues at Kyoto University and elsewhere who have contributed significantly and often indirectly to all aspects of my research.

As a cooperative brought up doctoral student send by Chinese government, I came to Japan and started this research on November 1989. At that time, it had been two years since I enrolled in doctor course in Tongji University in September 1987 and former research topic was thoroughly changed. I have to start present research from original point. Here, I would like to give my best regards to Professor Xueyuan HOU, my academic advisor in China, for his enthusiastic encouragement to go on this research, for his guidance and active support in my early research work of finite element analyses in Tongji University. I also would like to extend very special thanks to Professor Zhongxiong HU and Professor Weimin CAI, who were associate academic advisors and responsible for my detail research in Tongji University, for their precious advice and helping.

Finally, truly unbounded thanks are due to Ying MAO and Keying ZHANG, my dear wife and son, who with their love and patience, supported me in writing this paper.

Feng ZHANG
Kyoto University
October, 1994

Chapter 1

Introduction

Soil is a such kind of engineering material that it is not only related to daily life of human being but also to nearly every aspect of engineering problems. Comparing with other engineering materials such as metals, glass and concrete, however, it is more difficult to consider the mechanical behavior of soil. First of all, strictly speaking, soil is not a continuous material. It is composed of solid granules, water and void. Its characteristics of deformation and strength is dependent on the properties of contact surface between soil granules, the displacement and deformation of soil granule on contact surface. Secondly, soil is not homogeneous material. Even in the same place, the property of soil may be different. Thirdly, soil is not isotropic. Because of the fact that soil particles usually arrange in horizontal direction and the difference of soil structure in microscopy, the deformation and strength of soil is different along different directions. Moreover, soil is porous material and is more loosen compared to other materials. In laboratory test, it is nearly impossible to obtain an undisturbed sample or an sample undergone no change of mechanical properties in sampling. Besides, soil is time dependent material. Soils, such as over-consolidated clay, dense sand and soft rock, show time dependent behavior, that is, strain rate dependency, creep and stress relaxation.

In spite of these specialties inherent in soil, continuum theory is still the foundation of soil mechanics. Being different to structure mechanics, hydraulics and other material mechanics, soil mechanics takes the soil as research opponent. Therefore, the constitutive model of soil will be different to those of metals, concrete and other materials. It is very important for soil mechanics to establish a constitutive model which can well describe the mechanical behavior of soils. However, a constitutive model is only a mathematical expression. It is not easy to fully describe real behavior of soils exist in this world. In the early stage of soil mechanics, the material described by certain constitutive model was nonetheless a kind of theoretical or fictional material. Very often it might be the materials such as theoretic gas, theoretic fluid and elastic body.

In order to estimate the deformation and stress of soil subjected to external force, the constitutive model which gives the relation between stress and strain of soil body should be established in advance and then the analysis of mechanical behavior of soil ground, the interaction between soil and structure can be conducted according to the condition of ground stratum and boundary or initial condition. In the early stage of soil mechanics, only elasticity and elasto-perfect-plasticity were introduced to the study of deformation and strength of soil in geotechnical engineering. Main effort was focused on the research of shear strength and influence factors. Little attention was paid to the stress-strain relation because of the difficult to obtain a theoretical solution in mathematics. Since the later 1960s, however, great change has being happened because of the development both in numerical methods and computer technology. It is possible to use complicated constitutive model to describe more precisely the mechanical behavior of geologic material.

Up to present time, the methods in the analysis of deformation and strength of soil are divided mainly into two parts, one is the simplified and empirical method which are still widely used in engineering design, another is the strict method in which general constitutive model is established based on the characteristics of stress, strain and strength. Needless to say, though the strict method has not been applied widely to engineering problems at present time and cannot fully substitute for empirical methods, it stand for the tendency of development of soil mechanics.

The strict analytical method mainly consists of three parts. Firstly, it is necessary to establish a constitutive model which can properly describe the mechanical behaviors of geologic materials. Secondly, a method with which all the parameters involved in the constitutive model can be determined should be given. Thirdly, because of the difficulty to obtain a theoretical result of boundary/initial problems, it is necessary to establish a suitable numerical method based on the constitutive model so that the model can be applied to practical engineering problems.

The main purpose of this paper, is to establish fitting constitutive models for geologic materials such as dense sand, over-consolidated clay and soft rock. Then numerical analyses based on the models proposed in this paper are also conducted with finite element and joint element method in order to establish a numerical designing method for geological engineering problems. In order to make sure that the numerical analyses carried out in this paper be convincing, mathematical verification of the numerical procedures proposed in this paper is carried out. Case studies are also done for some geomechanical problems such as tunneling and progressive failure in cut slop.

In chapter 2, a general review on the development in the research of constitutive models for geologic materials is given. Much attention is paid to the model with strain softening. Among the model describing the mechanical behavior of over-consolidated soils and soft sediment rock, the model with strain-hardening and strain-softening proposed by T. Adachi and F. Oka is discussed thoroughly. Moreover, the improvements of the model, which involves the determination of the parameters in the model, the generalization of parameter for different confining stress and the modification of the yielding function are conducted. The capability of applying the model to different stress paths is also verified in this chapter.

In chapter 3, a constitutive model with strain-hardening and strain-softening is proposed to describe the discontinuous behavior of joint materials. Unlike most of other researchers doing, in the model, continuum theory is still used to describe the discontinuous behavior of joint materials. Application of the theory to the direct shear test of geologic material under constant normal stress and constant stiffness shows good agreement between experimental results and computed results based on the model.

In chapter 4, a series of analyses with FEM(Finite Element Method) and JEM(Joint Element Method) based on the constitutive models with strain softening are presented. For the materials with strain softening, great precaution had to be taken in finite element calculation. It is well known that the strain softening is associated with localization. If no precaution is taken, the region of localization will dependent on the size of the mesh used for spatial discretization. Obviously, this mesh-dependency is unacceptable. In order to make sure that the numerical calculation used in the analyses is convincing, the commonly used techniques in FEM for strain hardening material such as initial stress method is examined and compared with a new numerical procedure developed in this paper. The numerical analyses are conducted both in plane-strain and axisymmetrical condition.

In chapter 5, the mechanical behavior of trap door is first simulated with different numerical methods, among which the idea that softening behavior can be localized to a shear band is adopted and performed by introducing joint element to intact soil body. Then a series of finite element analyses on the mechanical behavior of tunneling with NATM based on fitting constitutive models with strain softening are conducted. In order to properly design and construct a tunnel, it is very important to understand the behavior of ground, lining and the interaction of ground-lining caused by tunnel excavation and to establish an analytical method with suitable constitutive model which can not only synthetically explain the surface subsidence, the displacement of adjacent ground but also the stability of the tunnel excavation. The finite element analyses were carried out in following ways for the shallow tunnels with NATM as; (a) elastic finite element analysis (b) elasto-plastic finite element analysis based on the constitutive model with strain softening (c) elastic finite element analysis with elasto-plastic joint element analysis and (d) elasto-plastic joint element together with elasto-plastic finite element analysis with strain softening. The discontinuous deformation observed in the tunnel excavation is simulated by the analyses with joint elements. Moreover, the behavior characterized by Fenner-Pacher curve in NATM is analyzed based on the constitutive model with strain softening. Because of the difficulties to simulate various kinds of lining used in tunnel excavation such as rock bolt, steel arch and shotcrete in FEM analysis, some simplification has to be used to make it possible for numerical analyses.

In chapter 6, an elasto-viscoplastic model with memory is proposed for geologic materials. The main purpose of proposing the model is to describe not only all the aspects of time dependency as strain rate dependency, creep and stress relaxation but also the strain softening behavior for geologic materials. Because of the fact that this model is proposed based on the constitutive model with strain-hardening and strain-softening proposed by Oka and Adachi, it is desirable that most of the parameters involved in the model should be determined in same way as previous one without losing specialty. The new parameters introduced in this model should also be definitely determined by triaxial test and drained creep test.

In chapter 7, based on the elasto-viscoplastic model developed in chapter 6, a finite element analysis was carried out to investigate the mechanism of progressive failure in cut slope on model ground. Main attention was paid to the factors related to instability of cut slope such as deterioration of ground and progressive failure in relation to boundary value condition. The analytical result is also compared with classical method in soil mechanics. It is found that the cut slope in model ground will not fail by classical method. While for finite element analysis, localized failure occurs in the cut slope of model ground.

In chapter 8, based on the elasto-viscoplastic model developed in chapter 6, a finite element analysis is carried out to investigate the mechanical behavior of tunnel excavation concerning time dependency. Special attention was paid to the time dependent behavior of post tunnel excavation with lining. It is known that when tunnel is excavated in swelling ground, the deformation of tunnel section and the change of earth pressure on lining with time cannot be neglected. Through the analysis conducted in this chapter is a very primitive one, it is interesting to confirm by numerical analysis how much the influence of time dependency will be.

Chapter 2

Constitutive model for continuous geologic materials

2-1 Introduction

Theoretically, an ideal constitutive model for geologic materials should satisfies following conditions:

(a) It should be able to describe the stress-strain-time relation for the material considered.

(b) The rupture criteria can be clearly defined.

(c) The material parameters involved in model could be limited to the number as few as possible and act independently in the model.

(d) It is easy to determined the material parameters involved in model.

(e) The expressions for the model should be as simple and clear as possible.

Needless to say, among the above mentioned conditions, the first one is the most important factor and must be satisfied. However, in order to establish a constitutive model that can well describe the real behavior of the material considered, the constitutive equations may become very complicated and the conditions (c)-(e) cannot be all satisfied. As a result, such models cannot be easily applied to engineering materials. Though the models proposed up to now for the geologic materials cannot satisfy all the conditions mentioned above, the research on this field has being developed very rapidly since the later 1950s.

It is known that the characteristics of deformation and strength of geologic materials are dependent both on the constructive properties of soil such as grain size distribution, the shape of grain, mineralogical composition, the degree of consolidation and state conditions such as gravity, water content, loading rate, confining pressure, loading history and stress. Therefore, it is almost impossible to derive a constitutive model that can describe all these complicated properties. The one of the most important thing in the establishment of a constitutive model is how to simplify these problem without loss of the most fundamental properties of the mechanical behavior of considered materials. Another important thing is how to apply established constitutive models to real engineering problem.

Generally speaking, geologic material is three-phases materials composed of soil particles, water and air. Throughout this paper, it is always assumed that the materials considered here are saturated, namely, the materials considered here is composed of incompressible water and soil skeleton

In this paper, the following assumptions are adopted: (1) infinitesimal deformation is assumed for a general body when subjected to an arbitrary load; (2) The body is in static gravitational field and thermal effect is not considered. (3) only drained condition is considered. Therefore, the total stress will always be equal to effective stress and seepage problems is not considered.

2-2 Review on the development of constitutive models

As the computer technology develops very rapidly recently, the numerical methods, including finite element method, become more and more powerful in dealing with geotechnical engineering problems. It is possible to use the approximate method to solve various kinds of boundary and initial problems in geotechnical engineering. For this reason, it becomes possible to get the solution for those initial/boundary value problems based on the constitutive models that are not restricted to simple models such as elasticity or elasto-perfect plasticity. From this viewpoint, it is badly needed to make further investigation on the constitutive models which can describe the general behavior of the geologic materials even if it may be somehow sophisticated. Many researchers have being worked hard on the establishment of such constitutive model. their researches can be divided into three categories, that is, (1) the constitutive model for cohesive soil based on continuum theory of elasto-plasticity; (2) the constitutive model for cohesionless soil; (3) the constitutive model considering the time dependency, namely, elasto-viscoplasticity.

The first category is so-called the Cambridge category. Roscoe et al.(1963), Roscoe and Schofield(1963), Roscoe and Poorooshasb(1963), Schofield and Wroth(1968) developed the model known as 'Cam-Clay model'. It bases on the assumption that the cohesive soil is an idea elasto-

plastic body. In the model, the main idea is the critical-state-energy theory. Based on Drucker's plasticity theory(1951) and taking into consideration the critical state of the cohesive soil, they firstly introduced the energy dissipating relation for the soil and then derived the model. Cam-Clay model can be regarded as a simple but easy-applied model because it has only four parameters to be determined by conventional triaxial test. The disadvantage of Cam-Clay model is that it has the tendency to underestimate the deviatoric strain and cannot describe time dependency. Burland(1965) improved the model later on. Shibata(1963), Shibata and Karube(1969) did research on dilatancy by experiment and proposed a relation for the dilatancy. Ohta(1971) combined the relation with Drucker plasticity theory to derive a model similar to the Cam-Clay model.

The second category is related the research concerning cohesionless soil, such as sand. Newland and Alley(1957), Rowe(1962), Murayama(1964) etc., based on the rule of friction between granular of sand, tried to predict the mechanical behavior of sand. Among the researches, the relation between stress and dilatancy proposed by Rowe affected greatly the later researches performed by Horn(1962), Murayama(1975) and Oda(1977). Some researchers developed the so-called Granta-Gravel constitutive model, treating sand as an elasto-plastic continuous body. Among them, Lade and Duncan(1975) used non-associated flow theory in their elasto-plasticity, Tatsuoka et al.(1976), combining the granular theory and continuous theory, proposed the model based on the Rowe's equation for stress-dilatancy and yielding function.

The third category is related to the research on cohesive clay or soft rock which show time-dependency. Murayama and Shibata(1958) first proposed the rheologic model, then Singh and Mitchill(1968), Shibata and Karube(1969) published their research on this field. Yong and Japp(1969) proposed the stress-strain relation which is dependent on the rate of strain. Murayama proposed the empirical equation for stress-relaxation. The later research make it clear that it is necessary to combine the former researches to give more precise description of the mechanical behavior for cohesive soils which exhibit both dilatancy and time dependency. Adachi and Okano(1974), based on the research of the time dependent behavior of cohesive clay by Akai et al.(1974), using Perzyna's elasto-plasticity theory(1963), extended the Cam-Clay model to describe time dependent behavior and established an elasto-viscoplastic constitutive model which can describe both the dilatancy and time dependency. Adachi and Oka(1982) proposed the so-called over-stress-model based on the Perzyna's elasto-viscoplastic theory and Cam-Clay model for normal consolidated clay. The over-stress model can not only describe the time-dependency behavior of the soft clay but also more precisely describe the relation of deviatoric stress-strain and the relation of pore water pressure-deviatoric strain than Cam-Clay model. Sekiguchi(1977), Sekiguchi(1984) introduced the so-called non-stationary-flow-surface theory and proposed a constitutive model.

The research on over-consolidated clay, dense sand and soft rock which exhibit both strain hardening and strain softening has drawn more and more attention of researchers. The strain softening behavior is considered to be a very important factor related to progressive failure in geologic engineering problems. Therefore, it is very important to establish a constitutive model that can describe strain softening. However, there are two different viewpoints in dealing with softening behavior.

In the first viewpoint, the softening behavior of geologic materials is considered to be a inherited characteristics in stress-strain relation, that is, strain softening or material soften. The researchers who share with this viewpoint try to establish a constitutive model that can describe strain softening. The researches on this field can be found in the works by Höeg, K.(1972), Nayak and Zienkiewicz(1972), Lo and Lee(1973), Prevost and Höeg(1979), Banerjee and Stipho(1979), Kawahara et al.(1981) and Matumoto and Ko(1982).

However, as some researchers pointed out that when a strain softening model is applied to finite element analysis, the stiff matrix will become negative in softening region and the boundary value problem cannot be defined and solved uniquely. Such kind of problem had being considered by some researchers, for example, Aifantis(1984), Bazant and Pijaudier-Cabot(1988)

In the second viewpoint, the softening behavior is regarded as a consequence of non-uniform deformation occurred in a material undergone loading, in other words, the result of localization in deformation. The researchers who share with this viewpoint insist that softening is related to localization where a decrease of apparent stress occurs not by strain softening but by a reduction of effective area due to the coalescence of void and micro cracks, and that strain-hardening is the inherited characteristics

of geologic materials. Because the localization of deformation is the main reasons that result in softening behavior, the softening behavior can be illustrated by solving the boundary value problems based on strain hardening models.

It is, however, difficult to say that softening behavior can be fully described by the analyses based on strain hardening models. The decline of strength caused by structural deterioration in geologic materials can never be neglected. It seems reasonable to say that the soften behavior is caused both by localization in deformation and structural deterioration in geologic materials. For an engineering approach, the choice of a procedure for providing a drop in nominal stress with strain can be based on convenience because a rigorous development of the methods based on two different viewpoints should provide the same results on macroscopic basis.

Oka(1985), Oka and Adachi(1985) proposed an elasto-plastic model for soft rock considering the strain-hardening-softening. Adachi et al.(1990) proposed an elasto-viscoplastic model which can both describe the strain rate effect and strain softening for frozen sand. Those models have an advantage of being capable to obtain a unique solution for the initial value problem on Valanis's sense(1985).

In the following sections, Adachi-Oka's model is introduced at first and then the improvement of the model is discussed systematically.

2-3 Constitutive models with strain hardening and softening in one-dimension

Generally speaking, for over-consolidated clay and soft rock, the mechanical behavior usually shows strain hardening-strain softening and time dependency.

Valanis(1971) proposed the so-called endochronic method in which the internal variable is introduced. Oka and Adachi(1985), based on the concept of general simple body proposed by Wang(1969), proposed a one dimensional constitutive model that can describe the behavior of strain softening by introducing the internal variable and stress history. The stress history is defined as

$$\sigma^* = \frac{1}{\tau}\int_0^z \exp(-\frac{z-z'}{\tau})\sigma(z')dz' \quad (2\text{-}1)$$

here, τ is stress history parameter, z is time or strain measure and z' is within the interval [0, z]. Eq.2-1 is only for one dimension problem, the general form will be discussed later. Here, the strain measure is assumed to be

$$dz = d\varepsilon \quad (2\text{-}2)$$

and the increment of strain can be expressed as

$$d\varepsilon = d\varepsilon^e + d\varepsilon^p = \frac{d\sigma}{E} + d\varepsilon^p \quad (2\text{-}3)$$

where, ε : strain, σ : stress, E : Young's modules.

As for the plastic component, the following associated flow rule is adopted

$$d\varepsilon^p = \Lambda\, df_y \quad (2\text{-}4)$$

where f_y is yield function. The yielding function is given as

$$f_y = \frac{\sigma^*}{\sigma_0} - \kappa_s = 0 \quad (2\text{-}5)$$

where σ_o =1 kgf/cm². κ_s is a strain-hardening and strain-softening parameter and is introduced as an evolutional equation expressed as

$$\dot{\kappa}_s = \frac{G'(M_f^* - \kappa_s)^2}{M_f^{*2}}\dot{\varepsilon}^p \quad (2\text{-}6)$$

In the case of proportional loading, it can be integrated as

$$\kappa_s = \frac{M_f^* G'\varepsilon^p}{M_f^* + G'\varepsilon^p} \quad (2\text{-}7)$$

where M_f* is the value of stress history σ^*/σ_0 at the residual stress state and G' is the initial tangential modules of the hyperbolic relation.

Prager's compatibility relation for plastic loading is given by

$$df_y = d(\sigma^*/\sigma_0 - \kappa_s) = 0$$

$$\Rightarrow \quad d(\sigma^*/\sigma_0) - \frac{\partial\kappa_s}{\partial\varepsilon^p}d\varepsilon^p = 0 \quad (2\text{-}8)$$

Substituting Eq.2-3 into the above relation, the following relation can be obtained:

$$d(\sigma^* / \sigma_0) - \frac{\partial\kappa_s}{\partial\varepsilon^p}\Lambda\, df_y = 0 \quad (2\text{-}9)$$

and

$$\Lambda = \frac{d(\sigma^*/\sigma_0)}{\frac{\partial\kappa_s}{\partial\varepsilon^p}df_y} \quad (2\text{-}10)$$

Substituting this relation into Eq.2-3 will results in

$$d\varepsilon^p = \frac{d(\sigma^*/\sigma_0)}{\partial\kappa_s / \partial\varepsilon^p} \quad (2\text{-}11)$$

in which

$$\frac{\partial\kappa_s}{\partial\varepsilon^p} = \frac{\partial}{\partial\varepsilon^p}(\frac{M_f^* G'\varepsilon^p}{M_f^* + G'\varepsilon^p}) = \frac{M_f^{*2}G'}{(M_f^* + G'\varepsilon^p)^2} \quad (2\text{-}12)$$

From Eq.2-5 and Eq.2-7, the following relation can be obtained:

$$\frac{\sigma^*}{\sigma_0} = \kappa_s = \frac{M_f^* G'\varepsilon^p}{M_f^* + G'\varepsilon^p} \tag{2-13}$$

Eq.2-13 can be rewritten as

$$G'\varepsilon^p = \frac{M_f^*(\sigma^*/\sigma_0)}{M_f^* - (\sigma^*/\sigma_0)} \tag{2-14}$$

Substituting Eq.2-14 into Eq.2-12, the following relation can be obtained:

$$\frac{\partial \kappa_s}{\partial \varepsilon^p} = \frac{G[M_f^* - (\sigma^*/\sigma_0)]^2}{M_f^{*2}} \tag{2-15}$$

Therefore, Eq.2-11 becomes

$$d\varepsilon^p = \frac{M_f^{*2}}{G'[M_f^* - (\sigma^*/\sigma_0)]^2}\frac{d\sigma^*}{\sigma_0} \tag{2-16}$$

It is easy to prove that the following relation is valid from the definition of the stress history:

$$d\sigma^* = \frac{1}{\tau}(\sigma - \sigma^*)dz \tag{2-17}$$

The plastic incremental strain can be expressed as

$$d\varepsilon^p = \frac{M_f^{*2}}{G'[M_f^* - (\sigma^* / \sigma_0)]^2}\frac{1}{\tau\sigma_0}(\sigma - \sigma^*)dz \quad . \tag{2-18}$$

Finally, from Eq.2-3 and Eq.2-18 the detailed expression for the constitutive equation can be given as

$$d\varepsilon = \frac{d\sigma}{E} + \frac{M_f^{*2}}{G'[M_f^* - (\sigma^*/\sigma_0)]^2}\frac{1}{\tau\sigma_0}(\sigma - \sigma^*)dz \tag{2-19}$$

or

$$d\sigma = E\,(d\varepsilon - \frac{M_f^{*2}}{G'[M_f^* - (\sigma^*/\sigma_0)]^2}\frac{1}{\tau\sigma_0}(\sigma - \sigma^*)dz\,) = E\,(d\varepsilon - d\varepsilon^p) \tag{2-20}$$

or

$$d\sigma = Ed\varepsilon\,\{1 - \frac{M_f^{*2}}{G'(M_f^* - [\sigma^*/\sigma_0])^2}\frac{1}{\tau\sigma_0}(\sigma - \sigma^*)\} \tag{2-21}$$

Eq.2-21 can also be expressed in following way according to the definition of stress history

$$\frac{d\sigma(\varepsilon)}{d\varepsilon} = E\,\{1 - \frac{M_f^{*2}}{G'[M_f^* - (\frac{1}{\tau}e^{-\varepsilon}I(\varepsilon)/\sigma_0)]^2}\frac{1}{\tau\sigma_0}[\sigma(\varepsilon) - \frac{1}{\tau}e^{-\varepsilon}I(\varepsilon)]\} \tag{2-22}$$

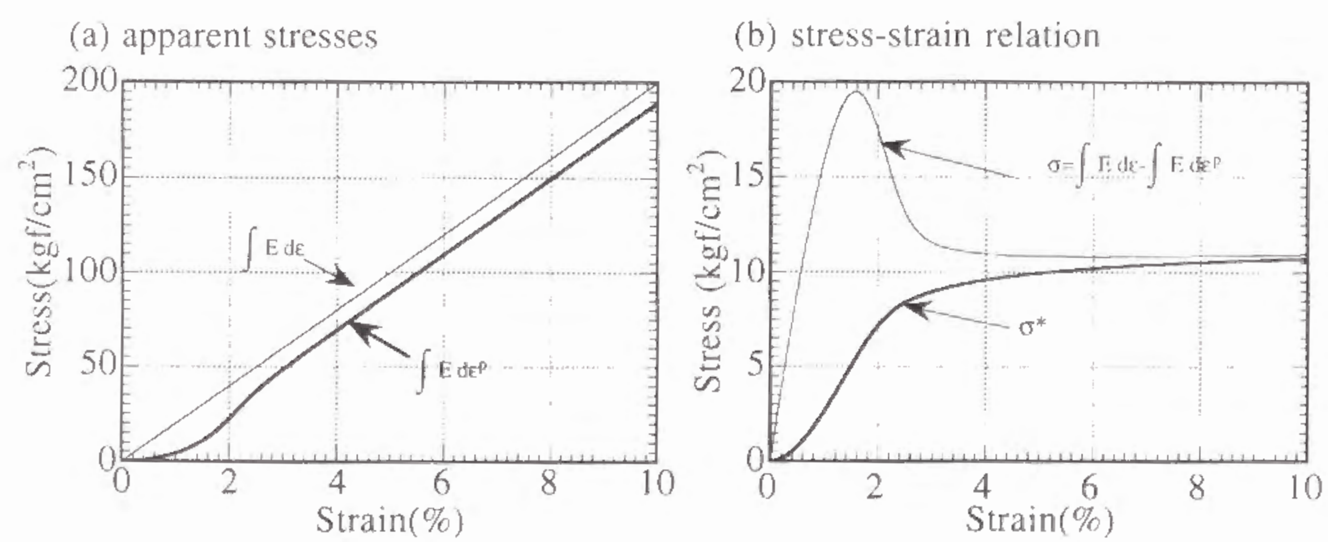

Fig.2-1　Explanation of strain softening behavior in one-dimension

$$I(\varepsilon) = \int_0^{\varepsilon} e^{z'/\tau} \sigma(z')dz' \Rightarrow \quad \frac{dI(\varepsilon)}{d\varepsilon} = e^{\varepsilon/\tau}\sigma(\varepsilon) \qquad (2\text{-}23)$$

Eq.2-22 and Eq.2-23 is a typical associated differential equations of one order and can be easily solved with numerical procedure such as Runge-Kutta method.

Four parameters are involved in the model. That is, Young' modules E, the strain hardening-softening parameter M_f^* and G', the stress historical parameter τ. Fig.2-1 shows the calculated stress-strain curve based on Eq.2-22 and Eq.2-23 and illustrates the physical meanings of first and second terms in right side of Eq.2-19. In Fig.2-1a, two integrations are monotonously increasing functions and their difference results in stress. As the second integration increases faster than the first one at certain strain level, the difference of the two integration or stress converts to decreasing with strain developing. As a result, the strain softening behavior occurred at the strain level as shown in Fig.2-1b.

Fig.2-2 explains schematically the strain softening behavior according to the composition of shear strength. The shear strength can be divided into two parts, that is the strength due to cementation or bonding and the strength due to friction. The strength due to cementation will gradually diminish with the increase of shear strain, resulting in strain softening.

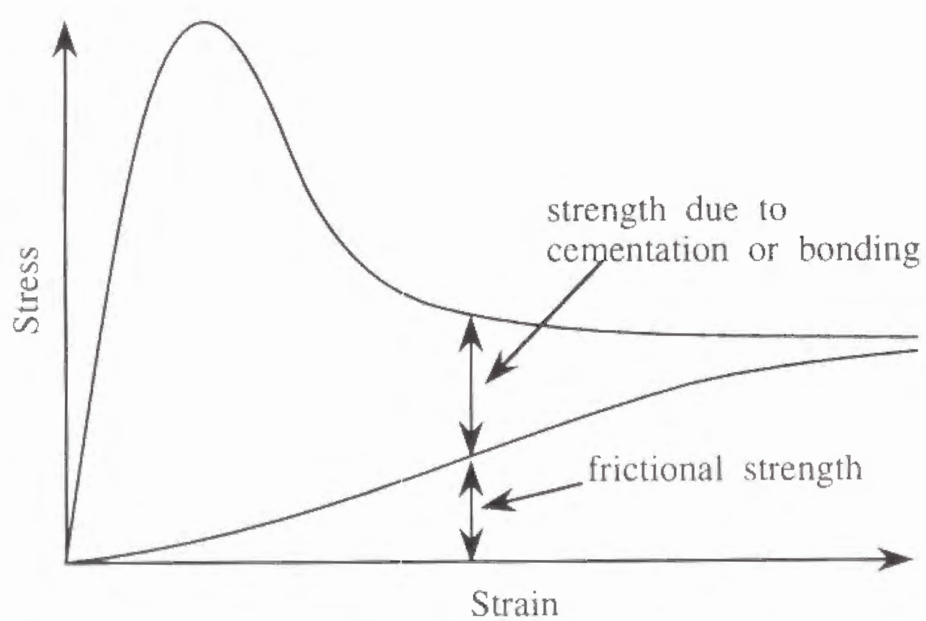

Fig.2-2 Strain softening and composition of shear strength

2-4 Constitutive models with strain hardening and softening in three-dimension

The constitutive model mentioned in the previous section is only an one-dimensional model. A generalized 3-dimensional model is much more needed. Using the generalized strain measure, Oka and Adachi(1985) proposed an elasto-plastic model for soft rocks considering the strain-softening effect. The strain measure used in this model is similar to the concept proposed by Valanis(1971). In Valanis theory, strain measure z takes the form

$$dz = P_{ijkl}\, d\varepsilon_{ij}\, d\varepsilon_{kl} \qquad (2\text{-}24)$$

where P_{ijkl} is a fourth-order tensor and ε_{ij} is a deviatoric strain tensor. In Adachi-Oka's model, z takes the following form as

$$dz = \sqrt{de_{ij}\, de_{ij}} \qquad (2\text{-}25)$$

The stress history tensor is expressed as

$$\sigma_{ij}^* = \frac{1}{\tau}\int_0^z \exp(-\frac{z-z'}{\tau})\sigma_{ij}(z')dz' \qquad (2\text{-}26)$$

where τ is the stress history parameter and physically stands for the retardation of stress with respect to strain. Non-associated flow rule is adopted

$$d\varepsilon_{ij}^p = \Lambda \frac{\partial f_p}{\partial \sigma_{ij}} df \qquad (2\text{-}27)$$

The plastic yield function can be written as

$$f = \eta^* - \kappa_s = 0 \qquad (2\text{-}28)$$

here η^* is defined as

$$\eta^* = \left(\frac{s_{ij}^*}{\sigma_{me}}\frac{s_{ij}^*}{\sigma_{me}}\right)^{1/2} / \left(\frac{\sigma_m^*}{\sigma_{me}}\right)^{\beta_R} \tag{2-29}$$

in which $\sigma_{me}=1\ kgf/cm^2$, s_{ij}^* is the deviatoric part of stress history and σ_m^* is the mean stress history. η^* is a stress history ratio invariant which is different from the original definition proposed by Oka and Adachi(1985) where η^* took the form as $\eta^*=(s_{ij}^*s_{ij}^*)^{1/2}/\sigma_m^*$. As a matter of fact, the residual strength of soft sediment rock is found to be(Adachi et al., 1981)

$$\frac{(s_{ij}^*\ s_{ij}^*)^{1/2}}{\sigma_{me}} = M_f^*\left(\frac{\sigma_m}{\sigma_{me}}\right)^{\beta_R} \tag{2-30}$$

here, M_f^*, β_R are material constants which are independent of stress state and can be determined by conventional drained triaxial test. As β_R usually is not equal to 1, the ratio of $(s_{ij}^*s_{ij}^*)^{1/2}/\sigma_m^*$ will not be a constant at residual state. From Eq.2-29 and 2-30, it is easy to see that the parameter M_f^* is directly related to the value of η^* at residual state. Based on the relation $\lim_{t\to\infty}\sigma^*=\sigma$, It can also be concluded that M_f^* can be uniquely determined with the stress ratio of $\sqrt{s_{ij}s_{ij}}/\sigma_m^{\beta_R}$ at residual state

κ_s is the strain hardening-softening index and can be expressed by following evolutional equation

$$\dot{\kappa}_s = \frac{G'(M_f^* - \kappa_s)^2}{M_f^{*2}}\dot{\gamma}^p \tag{2-31}$$

where $\dot{\gamma}^p=(\dot{e}_{ij}^p\dot{e}_{ij}^p)^{1/2}$ and G' is a strain hardening parameter. In the case of proportional loading, Eq.2-31 can be integrated as(See Appendix II) $\kappa_s=(M_f^*G'\gamma^p)/(M_f^*+G'\gamma^p)$, here $\gamma^p=(e_{ij}^p\,e_{ij}^p)^{1/2}$ is the second invariant of the deviatoric plastic strain.

The loading criteria is given as follow

$$\begin{aligned} f&=\eta^*-\kappa_s=0 \quad \text{and} \quad df>0 \quad \textit{Loading}\\ f&=\eta^*-\kappa_s=0 \quad \text{and} \quad df=0 \quad \textit{Neutral}\\ f&=\eta^*-\kappa_s=0 \quad \text{and} \quad df<0 \quad \textit{Unloading}\end{aligned} \tag{2-32}$$

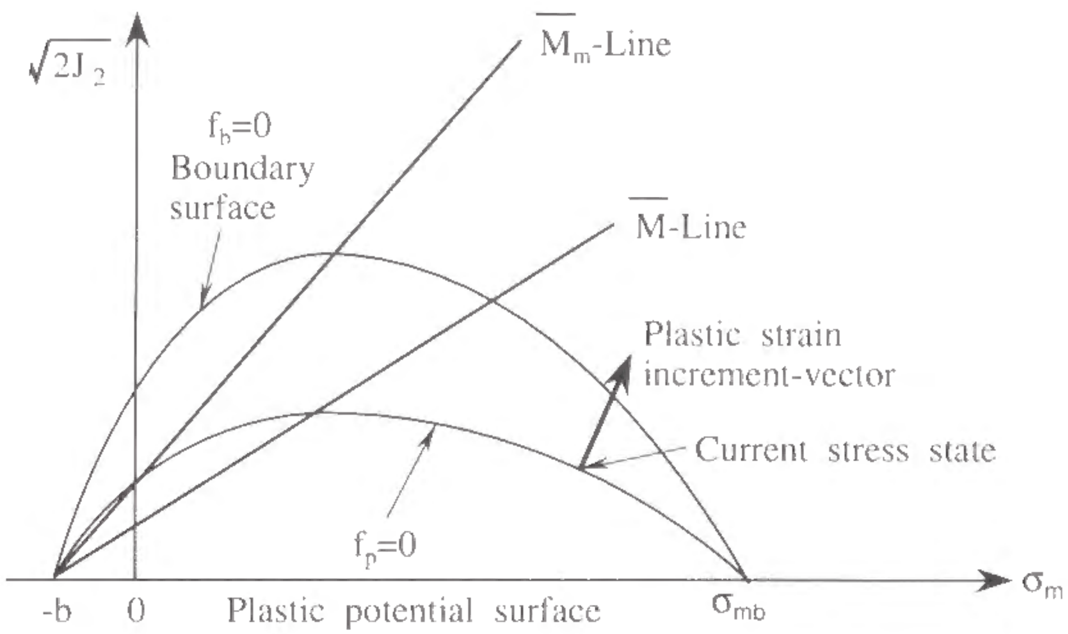

Fig.2-3 Illustration of plastic potential function and boundary surface

The boundary surface which defines the boundary between normally consolidated region($f_b\geq0$) and over-consolidated region($f_b<0$) is shown in Fig.2-3 and its expression is given as follow

$$f_b = \eta + \overline{M}_m \ln\left(\frac{\sigma_m+b}{\sigma_{mb}+b}\right) = 0 \tag{2-33}$$

where, $\overline{M}_m$ is a parameter determining the boundary of over-consolidated region and σ_{mb}, b are plastic potential parameters which will be discussed later.

The plastic potential takes the form as

$$f_p = \eta + \overline{M} \ln\left(\frac{\sigma_m+b}{\sigma_{mb}+b}\right) = 0 \tag{2-34}$$

where $\eta=(s_{ij}s_{ij})^{1/2}/(\sigma_m+b)$ and $\overline{M}$ is determined based on following equation

$$\bar{M} = -\frac{\eta}{\ln\left(\dfrac{\sigma_m+b}{\sigma_{mb}+b}\right)} \qquad f_b<0$$

$$\bar{M} = \bar{M}_m \qquad f_b \geq 0 \tag{2-35}$$

Combining the Prager condition, it is easy to obtain the expression for A (See Appendix II) as

$$A = \frac{\dfrac{\partial \eta^*}{\partial \sigma_{ij}^*} d\sigma_{ij}^*}{\dfrac{G'(M_f^* - \eta^*)^2}{M_f^{*2}} \left\{\dfrac{\partial f_p}{\partial s_{ij}} \dfrac{\partial f_p}{\partial s_{ij}}\right\}^{1/2} df} \tag{2-36}$$

Eq.2-27 can also expressed in another form as

$$d\varepsilon_{ij}^p = A \frac{\partial f_p}{\partial \sigma_{ij}} \frac{\partial \eta^*}{\partial \sigma_{mn}^*} d\sigma_{mn}^*$$

$$A = \frac{M_f^{*2}}{G'(M_f^*-\eta^*)^2} (\sigma_{mb}+b) \tag{2-37}$$

By some calculation, it is easy to prove that, $\lim_{\tau \to 0} \sigma_{ij}^*(z)=\sigma_{ij}(z)$, which means that the stress history tensor satisfied the principle of fading memory. It should be pointed out that Eq.2-17 is also valid for stress tensor, that is

$$d\sigma_{ij}^* = \frac{1}{\tau} (\sigma_{ij} - \sigma_{ij}^*)\, dz \tag{2-38}$$

The detailed expression of the plastic incremental strain tensor in present constitutive equations can be, after some algebraic, expressed as follow

$$d\varepsilon_{ij}^p = \sigma_{me}^{\beta_R-1} \frac{A}{\sigma_m^{*\beta_R}} \left(\frac{S_{kl}^*}{\sqrt{2J_2^*}} - \beta_R \frac{\sqrt{2J_2^*}}{\sigma_m^*} \frac{\delta_{kl}}{3}\right) d\sigma_{kl}^* \left(\frac{S_{ij}}{\sqrt{2J_2}} - \frac{\sqrt{2J_2}}{\sigma_m+b} \frac{\delta_{ij}}{3} + \bar{M}\frac{\delta_{ij}}{3}\right) \frac{1}{\sigma_m+b} \tag{2-39}$$

The total strain increment tensor can be divided by combining the elastic and plastic component as

$$d\varepsilon_{ij} = d\varepsilon_{ij}^e + d\varepsilon_{ij}^p \tag{2-40}$$

$$d\sigma_{ij} = D\, d\varepsilon_{ij}^e = D\, d\varepsilon_{ij} - D\, d\varepsilon_{ij}^p \tag{2-41}$$

where

$$D = G \begin{bmatrix} \begin{matrix} \alpha\ \beta\ \beta \\ \beta\ \alpha\ \beta \\ \beta\ \beta\ \alpha \end{matrix} & 0 \\ 0 & I_{3\times3} \end{bmatrix}$$

$$\alpha = \frac{K}{G} + \frac{4}{3},\ \beta = \frac{K}{G} - \frac{2}{3} \tag{2-42}$$

In axisymmetric condition, it is easy to obtain the more detailed expression for Eq.2-39 as

$$d\varepsilon_{11}^p = \sigma_{me}^{\beta_R-1} \frac{A}{\sigma_m^{*\beta_R}} \sqrt{\frac{2}{3}} \left((q-q^*) \frac{dz}{\tau} - \beta_R \frac{q^*}{\sigma_m^*} (\sigma_m-\sigma_m^*) \frac{dz}{\tau}\right) \left(\sqrt{\frac{2}{3}} - \frac{1}{3}\left(\frac{q}{\sigma_m+b} \sqrt{\frac{2}{3}} - \bar{M}\right)\right) \frac{1}{\sigma_m+b}$$

$$d\varepsilon_{22}^p = \sigma_{me}^{\beta_R-1} \frac{A}{\sigma_m^{*\beta_R}} \sqrt{\frac{2}{3}} \left((q-q^*) \frac{dz}{\tau} - \beta_R \frac{q^*}{\sigma_m^*} (\sigma_m - \sigma_m^*) \frac{dz}{\tau}\right) \left(-\sqrt{\frac{1}{6}} - \frac{1}{3}\left(\frac{q}{\sigma_m+b} \sqrt{\frac{2}{3}} - \bar{M}\right) \frac{1}{\sigma_m+b}\right.$$

$$dv^p = \sigma_{me}^{\beta_R-1} \frac{A}{\sigma_m^{*\beta_R}} \sqrt{\frac{2}{3}} \left((q-q^*)\frac{dz}{\tau} - \beta_R \frac{q^*}{\sigma_m^*}(\sigma_m - \sigma_m^*) \frac{dz}{\tau}\right) \left(-\left(\frac{q}{\sigma_m+b} \sqrt{\frac{2}{3}} - \bar{M}\right)\right) \frac{1}{\sigma_m+b} \tag{2-43}$$

where q, σ_m is defining as

$$q = \sigma_1 - \sigma_2, \quad \sigma_m = \frac{\sigma_{ii}}{3} \tag{2-44}$$

The constitutive model is examined by drained triaxial test of soft sedimentary rock and over-consolidated clay. Two kinds of stress path in axisymmetric condition are evaluated and compared with experimental results. In case I, the confining stress σ_3 is kept constant and only σ_1 increase. The sample is soft sedimentary rock. In case II, the mean stress σ_m is kept constant. The sample is remolded clays pre-consolidated at different confining pressures.

In case I, the stress and strain state can be specified as,

$$\begin{aligned} &\sigma_{33} = \sigma_{22},\ \dot{\sigma}_{33} = \dot{\sigma}_{22} = 0 \\ &\dot{\varepsilon}_{33} = \dot{\varepsilon}_{22},\ \dot{\varepsilon}^p_{33} = \dot{\varepsilon}^p_{22},\ \varepsilon_{33} = \varepsilon_{22},\ e^p_{33} = e^p_{22} \end{aligned} \tag{2-45}$$

The equation for the case I now can be written as follow,

$$\frac{dq}{G} = (\alpha - \beta)\left(\frac{\alpha+2\beta}{\alpha+\beta}\right)(d\varepsilon_{11} - d\varepsilon^p_{11}), \quad d\sigma_m = dq/3 \tag{2-46a}$$

$$dv = \frac{\alpha-\beta}{\alpha+\beta} d\varepsilon_{11} + 2d\varepsilon^p_{22} + \frac{2\beta}{\alpha+\beta} d\varepsilon^p_{11} \tag{2-46b}$$

$$de_{11} = d\varepsilon_{11} - \frac{dv}{3} \tag{2-46c}$$

In case II, σ_m is kept constant, then

$$dq = d\sigma_1 - d\sigma_2 = 3G\,de^e_{11} = 3G(de_{11} - de^p_{11}) \tag{2-46d}$$

$$d\sigma_m = K(dv - dv^p) = 0 \tag{2-46e}$$

Saturated samples of Ohya stone(porous tuff) deposited in Miocene Epoch of Tertiary Period were tested in previous study(Adachi and Ogawa,

1980). The material is fairly a representative of soft rock and can exhibits typical mechanical behavior of soft rock.

Physical properties of the material are listed in Table 2-1. Cylindrical specimens were prepared in 5 cm of diameter and 10 cm of height. The specimens were saturated by applying vacuum to a vessel in which specimen were submerged in water for at least 24 hours. Drained triaxial tests were carried out at some prescribed confining pressure.

The experimental results and the theoretical results of Ohya stone are given in Fig.2-4.

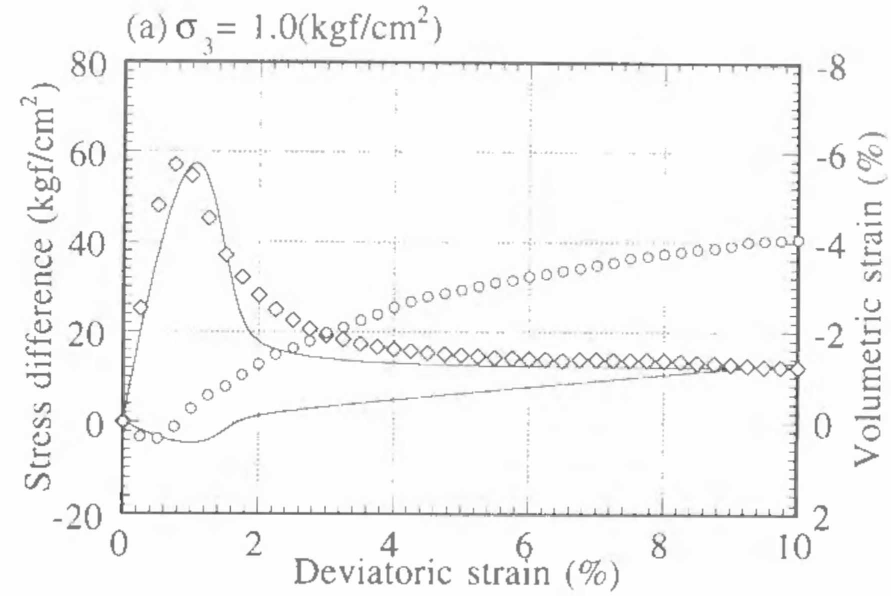

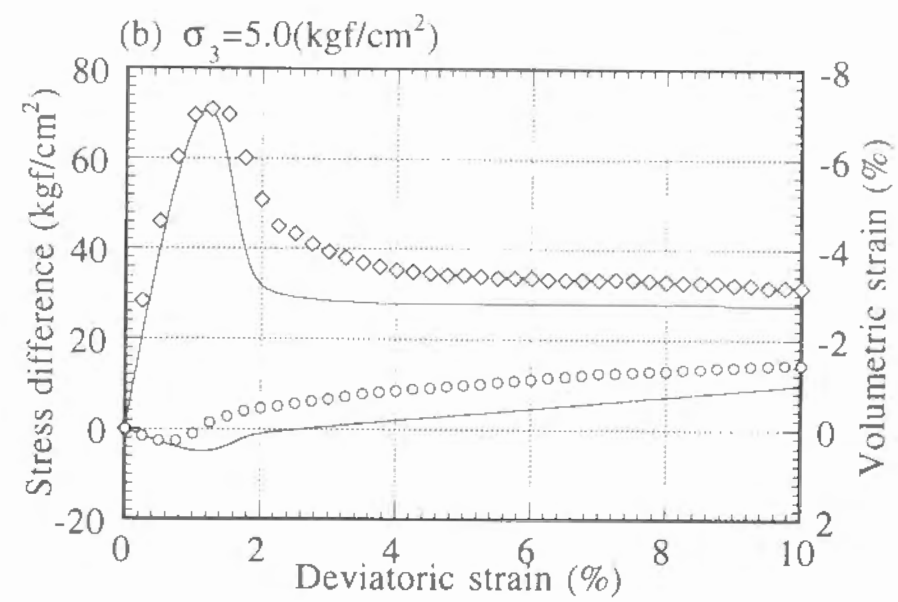

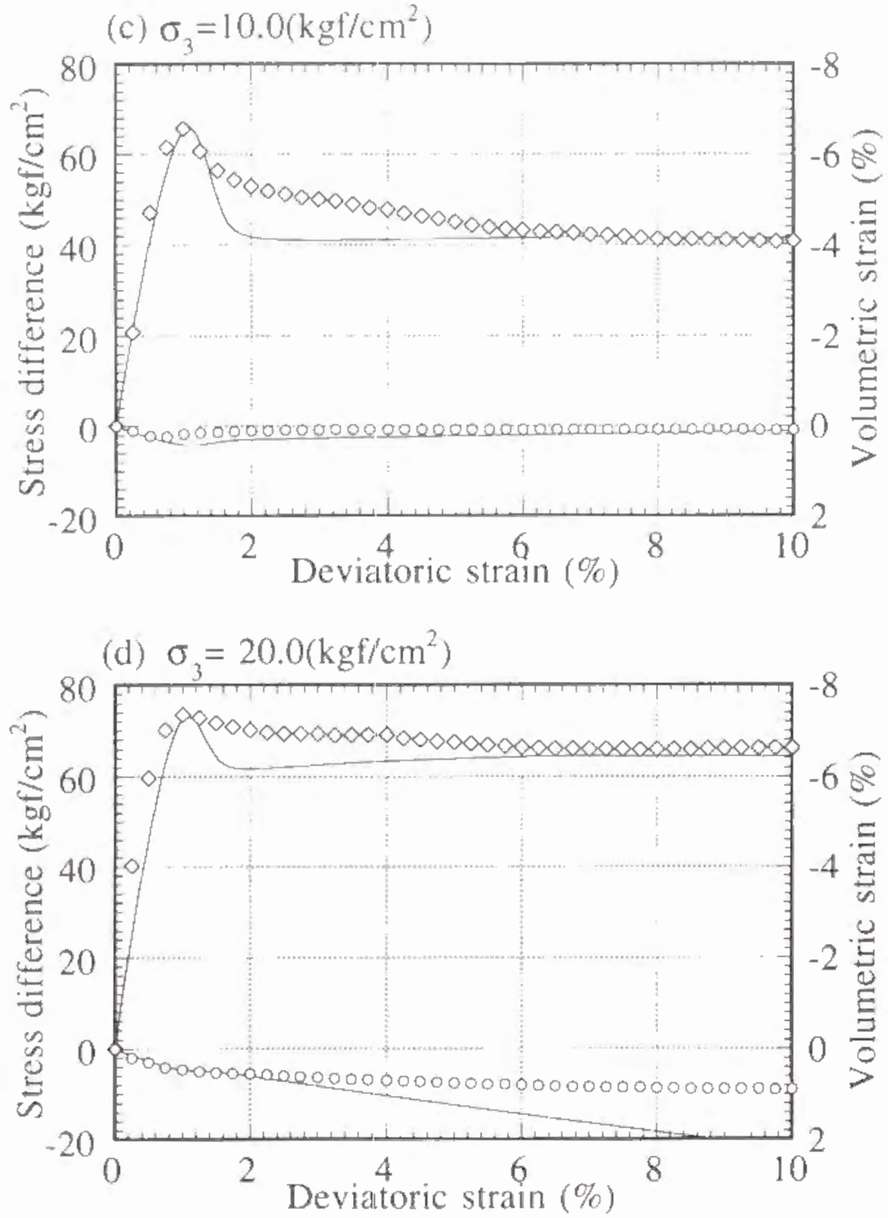

Fig.2-4 Theoretical and experimental results of stress-strain relation and deviatoric strain-volumetric strain relation(Ohya stone)

The material parameters of an over-consolidated clay are listed in Table 2-2. The experimental results and the theoretical results are given in Fig.2-5.

From these figures, it can be concluded that the model can well describe the mechanical behaviors of geologic materials, such as strain-hardening, strain-softening and dilatancy.

Table 2-1 Material parameters of Ohya stone

Test No.	CD-1	CD-5	CD-10	CD-20
σ_3 (kgf/cm^2)	1.0	5.0	10.0	20.0
G (kgf/cm^2)	4301	4346	4569	5253
ν	0.081	0.138	0.163	0.156
α_R (M_f^*)	2.74	2.74	2.74	2.74
β_R	0.80	0.80	0.80	0.80
G'	1501	1501	1501	1501
σ_{mb} (kgf/cm^2)	100	100	100	100
b (kgf/cm^2)	18	18	18	18
$\overline{M}_m$	1.126	1.126	1.126	1.126
τ	0.0619	0.0290	0.0139	0.0078

Table 2-2 Material parameters of an over-consolidated clay

Test No.	OCR-2	OCR-4	OCR-8	OCR-12
σ_m(kgf/cm^2)	2.0	2.0	2.0	2.0
G(kgf/cm^2)	132.9	196.2	322.9	449.5
ν	0.40	0.40	0.40	0.40
α_R (M_f^*)	1.173	1.173	1.173	1.173
β_R	1.00	1.00	1.00	1.00
G'	132.9	196.2	322.9	449.5
σ_{mb}(kgf/cm^2)	4.0	8.0	16.0	24.0
b(kgf/cm^2)	1.0	1.0	1.0	1.0
$\overline{M}_m$	1.173	1.173	1.173	1.173
τ	0.012	0.009	0.007	0.005

(a) OCR=2

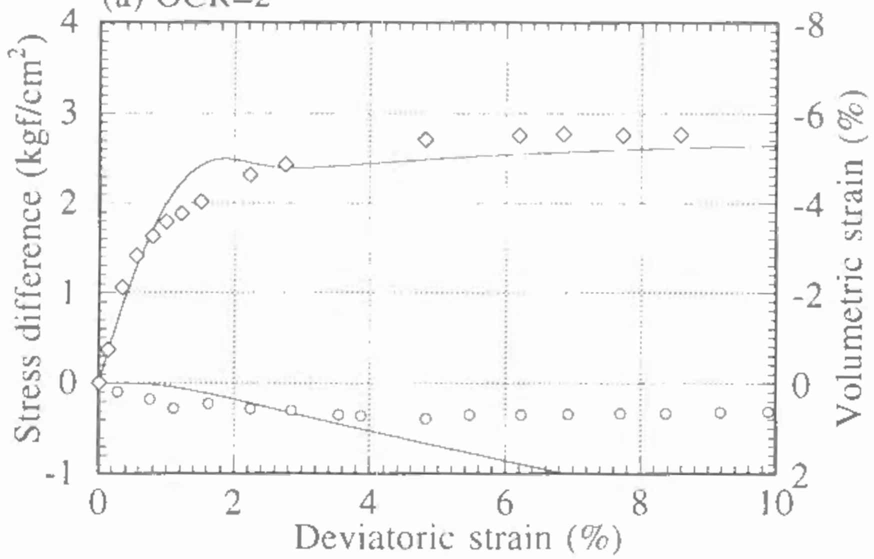

(b) OCR=4

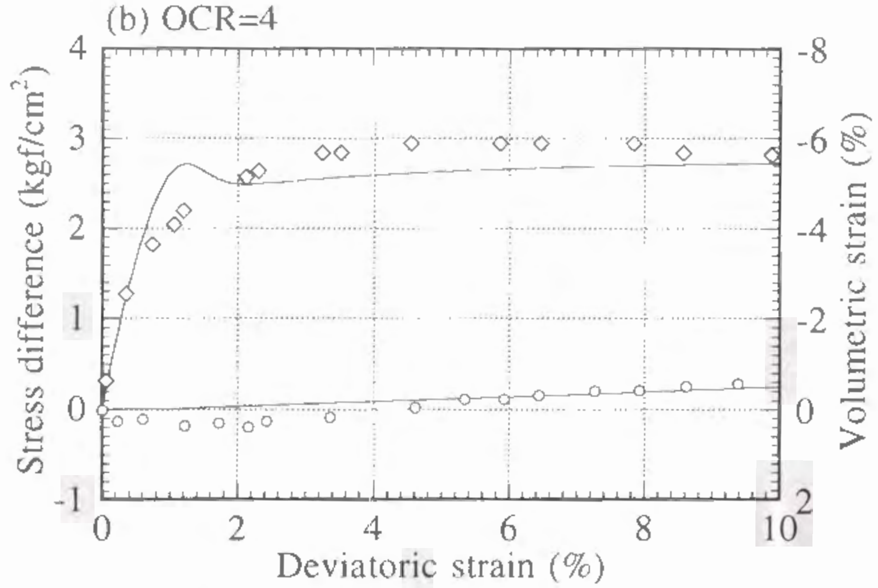

(c) OCR=8

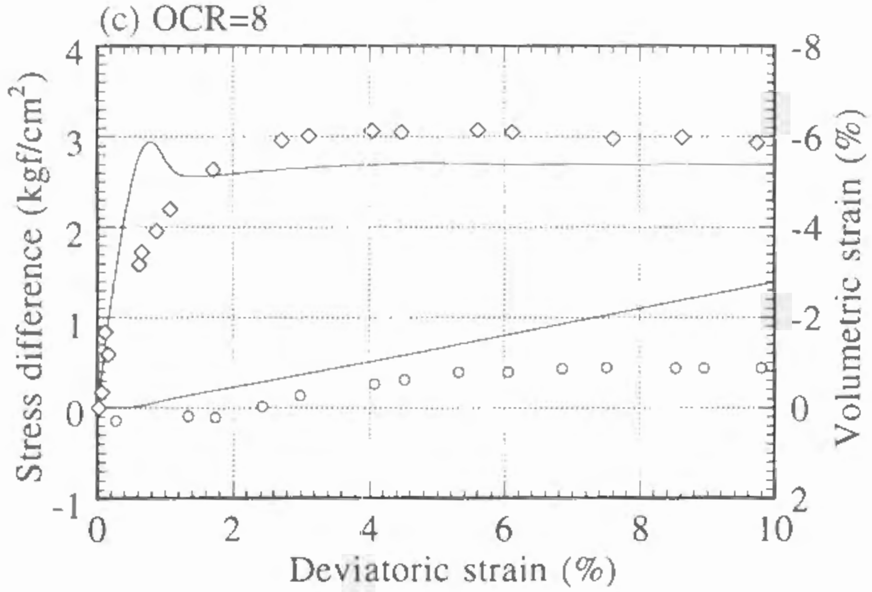

(d) OCR=12

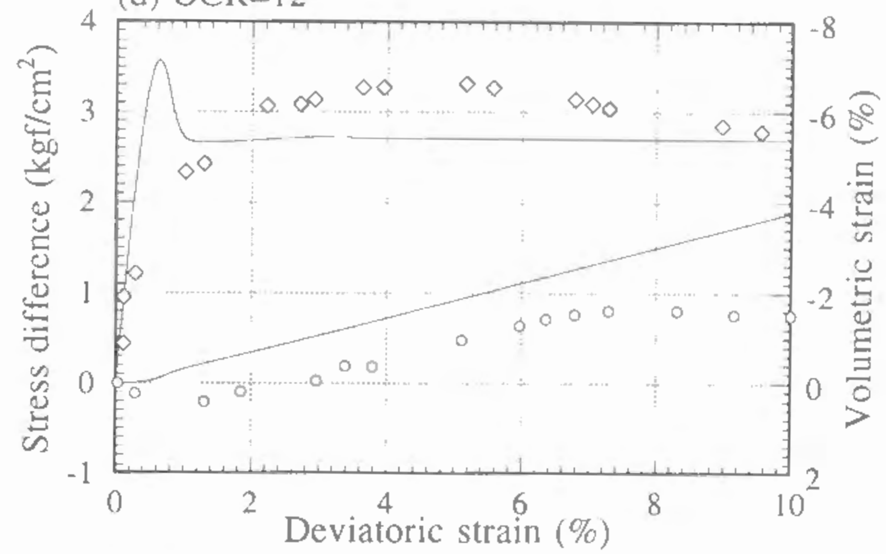

Fig.2-5 Theoretical and experimental results of stress-strain relation and deviatoric strain-volumetric strain relation(clay)

Eight parameters are involved in the constitutive model and their determination are as follow;

(a) G, ν shear modules and Poisson ratio, is determined by conventional triaxial test. The equations to calculate the G and ν are as follow,

$$G = \frac{\Delta q}{3\Delta e_{11}} \Big|_{e_{11}=0}$$

$$\nu = \left\{ \frac{3 - 2\Delta\varepsilon_{ii} / \Delta e_{11}}{6 + 2\Delta\varepsilon_{ii} / \Delta e_{11}} \right\} \Big|_{e_{11}=0} \qquad (2\text{-}47)$$

(b) M_f^*, the strain hardening-softening parameter, is determined by the value of η^* at the state at which residual strength is reached.

(c) G', strain hardening parameter, can be determined as the initial gradient of stress-strain curve in unloading-reloading process at residual state.

(d) σ_{mb}, plastic potential parameter, is determined by isotropic consolidation test and takes the value of pre-consolidated stress.

(e) b, plastic potential parameter. The purpose of introducing this parameter is to explain the dilatancy. It can be determined by the assumption that the stress ratio η is kept constant in over-consolidated region along M_m-line as shown in Fig.2-3.

(f) $\bar{M}_m$, parameter determining the boundary of over-consolidated region, is the value of η^* at the state at which the maximum compression takes place.

(g) τ, the stress historical parameter, is determined by curve fitting method in such a way that the peak stress is best fitted with experiment result. If it takes the value of zero, which means the retardation is zero, the stress history will always be current stress. Fig.2-6 shows schematically the influence of τ on peak strength.

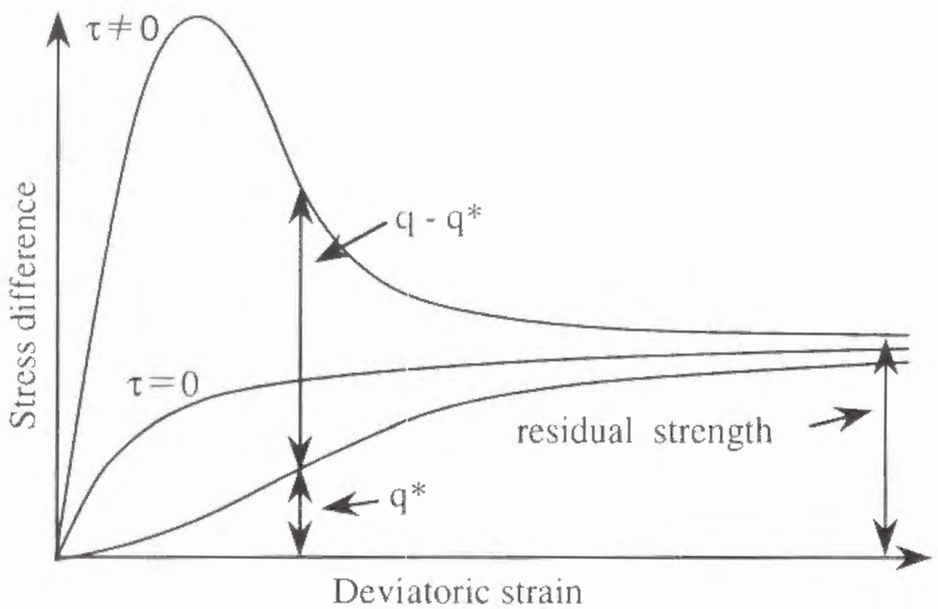

Fig.2-6 Influence of stress history parameter τ on stress-strain relation

The validity of the model is proved by experimental results only in special stress and strain condition. For τ, the parameter that determines the peak stress in stress-strain relation, is founded to be dependent on over-consolidation ratio(OCR), detailed expression for the τ can be given as

$$\tau = \alpha_\tau OCR^{\beta_\tau} = \alpha_\tau \left(\frac{\sigma_{m0}}{\sigma_{mc}}\right)^{\beta_\tau} \tag{2-48}$$

where α_τ and β_τ are material parameters which can be determined by conventional drained triaxial tests combined with a curve fitting method.

σ_{m0} is initial mean stress and σ_{mc} is pre-consolidated mean stress that the undisturbed samples undergone once upon a time. Comparison between the original model and the improved model proposed here shows almost the same results(Wakayama, 1993), which means that the model has been generalized in a general stress state.

2-5 Conclusions

A general review on the development of the constitutive models for geologic materials is given and discussed in this chapter. Some new ideas are presented and added to Adachi-Oka's model with strain hardening and softening. It is found that the stress history parameter τ has great influence on the peak strength and is dependent on stress state, and that the residual strength of soft rock is also dependent on stress state. The expressions for the parameter of τ and yielding function proposed in this chapter have the advantage of taking into consideration the dependency on the state of stress. Therefore the model can be more easily applied in boundary and initial value problems with finite element analysis. The application of the model to over-consolidated clay and soft rock in different stress paths shows that the model can well describe the mechanical behavior of geologic materials such as strain-hardening, strain-softening and dilatancy.

Appendix I

The following relation can easily be proven,

$$s_{ij} = \sigma_{ij} - \sigma_m \delta_{ij}, \quad \sigma_m = \sigma_{ij}\delta_{ij}/3$$

then,

$$\begin{aligned}\frac{\partial f}{\partial \sigma_{ij}} &= \frac{\partial f}{\partial s_{ij}}\frac{\partial s_{ij}}{\partial \sigma_{ij}} + \frac{\partial f}{\partial \sigma_m}\frac{\partial \sigma_m}{\partial \sigma_{ij}} \\ &= \frac{\partial f}{\partial s_{ij}} + \frac{\partial f}{\partial \sigma_m}\frac{\delta_{ij}}{3}\end{aligned} \tag{a-1}$$

In a constitutive model expressed in following equation,

$$d\varepsilon_{ij}^p = d\lambda \frac{\partial f_p}{\partial \sigma_{ij}} \tag{a-2}$$

here, f_p is plastic potential function. If f_p is only dependent on first and second invariant of stress tensor, that is, $f_p=f_p(\sigma_m,J_2)$, then,

$$d\varepsilon_{ij}^p = d\lambda \frac{\partial f_p}{\partial \sigma_{ij}} = d\lambda \frac{\partial f_p}{\partial s_{ij}} + d\lambda \frac{\partial f_p}{\partial \sigma_m} \frac{\delta_{ij}}{3}$$

$$= d\lambda \frac{\partial f_p}{\partial J_2} \frac{s_{ij}}{J_2} + d\lambda \frac{\partial f_p}{\partial \sigma_m} \frac{\delta_{ij}}{3} \tag{a-3}$$

Based on Eq.a-3, it is easy to obtain the following relation, considering the relation of s_{ii}=0.

$$d\varepsilon_m^p = d\varepsilon_v^p/3 = d\lambda \frac{\partial f_p}{\partial \sigma_m} \tag{a-4}$$

From Eq.a-3 and Eq.a-4, we can obtain,

$$de_{ij}^p = d\varepsilon_{ij}^p - d\varepsilon_m^p \delta_{ij} = \frac{\partial f_p}{\partial J_2} \frac{d\lambda}{J_2} s_{ij} = B s_{ij} \tag{a-5}$$

or $$de_{ij}^p = d\lambda \frac{\partial f_p}{\partial s_{ij}} \tag{a-6}$$

From Eq.a-5 and Eq.a-6, it is easy to show that,

$$s_{ij}\, de_{ij}^p = \sqrt{2J_2^2}\; d\sqrt{2I_2^2} \tag{a-7}$$

Appendix II

The Prager condition is expressed as,

$$df = df(\sigma_{ij}^*, e_{ij}^p) = \frac{\partial f}{\partial \sigma_{ij}^*} d\sigma_{ij}^* + \frac{\partial f}{\partial e_{ij}^p} de_{ij}^p = 0 \tag{a-8}$$

$$\Rightarrow \frac{\partial \eta^*}{\partial \sigma_{ij}^*} d\sigma_{ij}^* - \frac{\partial \kappa_s}{\partial e_{ij}^p} de_{ij}^p = 0 \tag{a-9}$$

From Eq.2-87, it is easy to show that

$$\Rightarrow \frac{\partial \kappa_s}{\partial e_{ij}^p} de_{ij}^p = d\kappa_s = \frac{G'(M_f^* - \kappa_s)^2}{M_f^{*2}} (de_{ij}^p\, e_{ij}^p)^{1/2} \tag{a-10}$$

Combining Eq.a-6, a-9 and a-10, we can obtain,

$$\frac{\partial \eta^*}{\partial \sigma_{ij}^*} d\sigma_{ij}^* - \frac{G'(M_f^* - \kappa_s)^2}{M_f^{*2}} \left(\frac{\partial f_p}{\partial s_{ij}} \frac{\partial f_p}{\partial s_{ij}}\right)^{1/2} \wedge df = 0 \tag{a-11}$$

From the definition of f_p, it is easy to prove that

$$\frac{\partial f_p}{\partial s_{ij}} = \frac{s_{ij}}{(\sigma_m + b)\,(s_{ij}\, s_{ij})^{1/2}} \tag{a-12}$$

therefore,

$$\frac{\partial f_p}{\partial s_{ij}} \frac{\partial f_p}{\partial s_{ij}} = \frac{1}{(\sigma_m + b)^2} \tag{a-13}$$

Based on Eq.a-11 and a-13, it is easy to obtain the Eq.2-37.

References

(1) Adachi, T. and Ogawa, T. (1980) : "Mechanical Properties and failure criteria of soft rock," Proc. JSCE, No.295, pp.51-62(In Japanese).

(2) Adachi, T. and Okano, M.(1974) : "A constitutive equation for normally consolidated clay," Soils and Foundations, Vol.14, No.4, pp.55-73.

(3) Adachi, T. and Oka, F. (1982) : "Constitutive equations for normally consolidated clay based on elasto-viscoplasticity," Soils and Foundations, Vol. 22, No.4, pp.57-70.

(4) Adachi, T., Oka, F. and Poorooshasb, H. B. (1990) : "A Constitutive Model for Frozen Sand," Trans. of ASME, Vol.112, pp.208-212.

(5) Aifantis, E. C. (1984) : "On the microstructureal origin of certain inelastic models," Trans. ASME, J. Mat. Eng. Tech., Vol.106, pp.326-330.

(6) Akai, K., Adachi, T. and Fujimoto, K. (1974) : "Constitutive Equations for geomechanical materials based on elasto-viscoplasticity," Proc. of Speciality Session 9, 9th ICSMFE, PP.1-10.

(7) Banerjee, P. K. and Stipho, A. S. (1979) : "An elasto-plastic model for undrained behavior of heavily over-consolidated clays," Short Communication, Int. J. Num. Methods in Geomechanics, Vol.3, pp.97-103.

(8) Bazant, Z. P. and Pijaudier-Cabot, G. (1988) : "Non-local continuum damage, localization, instability and convergence," J. Appl. Mech., ASME, Vol.55, pp.287-293.

(9) Burland, J. B. (1965) : "The Yield and Dilation of Clay," Correspondence, Geotechnique, Vol.15, No.2, pp.211-214.

(10) Drucker, D. C. (1951) : "A more fundamental approach to plastic stress-strain relations," Proc. 1st. U.S. National Congr. Appl. Mech., New York, pp.487-491.

(11) Horn, H. M. and Deere, D. V. (1962) : "Frictional characteristics of minerals," Geotechnique, Vol.12, No.4, pp.319-334.

(12) Höeg, K. (1972) : "Finite element analysis of strain softening clay," J. Soil Mech., ASCE, Vol.98, SM-1, pp.43-58.

(13) Kawahara, M., Kanho, Y., Kaneko, N. and Yada, K. (1981) : "Strain-softening finite element analysis of rock applied to tunnel excavation," Proc. Int. Symp. on Weak Rock, Tokyo, pp.713-719.

(14) Lade, P. V. and Duncan, J. M. (1975) : "Elastoplastic stress-strain theory for cohesionless soil," Proc. ASCE, Vol.101, No.GT10, pp.1037-1053.

(15) Lo, K. Y. and Lee, C. F. (1973) : "Stress analysis and slope stability in strain softening soils," Gotechnique, Vol.23, pp.1-11.

(16) Matumoto, T. and Ko, H. Y. (1982) : "Finite Element Analysis of Strain-Softening soil," Proc. 4th Int. Conf. on Numerical Method In Geomechanics, I, pp213-222.

(17) Murayama, S. and Shibata, T. (1958) : "On the Rheological characters of clay-Part I," Bulletin, Disaster. Prev. Res. Inst., Kyoto Univ. No.26, pp.1-43.

(18) Murayama, S. (1964) : "A theoretical consideration on a behavior of sand," Proc. IUTAM Symp. on Rheology and Soil Mech., pp.146-159

(19) Murayama, S. (1975) : "A constituitve model for sand in plastic condition," Proc. of JSCE, No.236, pp.125-137(In Japanese).

(20) Nayak, G. C. and Zienkiewicz, O. C. (1972) : "Elasto-plastic stress analysis, A generalization for various constitutive relations including strain softening," Int. J. Anal. Methods In Geomechanics, Vol.5, pp. 113-135.

(21) Newland, P. L. and Allely, B. H. (1957) : "Volume change in drained triaxial tests on granular materials," Geotechnique, Vol.7, No.1, pp.17-34

(22) Oda, M. (1977) : "Co-ordination number and its relation to shear strength of granular material," Soils and Foundations, Vol.17, No.2, pp.29-42.

(23) Ohta, H. (1971) : "Analysis of deformations of soils based on the theory of plasticity and its application to settlement of embarkments," Doctoral Theses, Kyoto University.

(24) Oka, F. (1985) : "Elasto/viscoplastic constitutive equation with memory and internal variables," Computer and Geomechanics, Vol.1, pp.59-69.

(25) Oka, F. and Adachi, T. (1985) : "A elasto-plastic constitutive equation of geologic material with memory," Proc. 5th Int. Conf. on Numerical Methods in Geomechanics, Vol.1, pp. 293-300.

(26) Perzyna, P. (1963) : "The constitutive equations for work hardening and rate sensitive plastic materials," Proc. Vibrational Problems, Warsaw, Vol.4, No.3, pp.281-290.

(27) Prevost, J, H. and Höeg, K. (1979) : "Soil mechanics and plasticity analysis of strain softening," Geotechnique, Vol.25, No.2, pp.279-297.

(28) Roscoe, K. H. and Poorooshasb, H. B. (1963) : "A theoretical and experimental study of strains in triaxial compression test on normally consolidated clays," Geotechnique, Vol.13, No.1, pp.12-38.
(29) Roscoe, K. H., Schofield, A. N. and Thurairajah, A. (1963) : "Yielding of clay in state sweeter than critical," Geothchnique, Vol.13, No.3, pp.211-240.
(30) Roscoe, K. H. and Schofield, A. N. (1963) : "Mechanical behavior of an idealized 'wet clay'," Proc. 2nd. European Conf. Soil Mechanics., Vol.1, pp.47-54.
(31) Rowe, P. W. (1962) : "The stress-dilatancy relation for static equilibrium of an assembly of particles in contact," Proc. Royal Soc., Vol.269, pp.500-527.
(32) Schofield, A. N. and Wroth, C. P. (1968) : "Critical state soil mechanics," Mcgraw-Hill, London.
(33) Sekiguchi, H. (1977) : "Rheological characteristics of clays," Proc. 9th ICSMFE, Vol.1, pp.289-292.
(34) Sekiguchi, H. (1984) : "Theory of undrained creep rupture of normally consolidated clay based on elasto-viscoplasticity," Soils and Foundations, JSSMFE, Vol.24, No.1, pp.129-147.
(35) Shibata, T. (1969) : "A study on the dilatancy of clay," Bulletin, Disaster. Prev. Res. Inst., Kyoto Univ., No.6, pp.128-134.
(36) Shibata, T. and Karube, D. (1969) : "Creep rate and creep strength of clays," Proc. 7th ICSMFE, Vol.1, pp.361-367.
(37) Singh, A. and Mitchell, J. K. (1968) : "General stress-strain-time function for soils," Proc. ASCE, Vol. 94, No.SM1, pp. 21-46.
(38) Tatsuoka, F. (1976) : "Stress-dilatancy relations of anisotropic sands in three dimensional stress condition," Soils and Foundations, Vol.16, No.2, pp.1-18.
(39) Valanis, K. C. (1971) : "A theory of viscoplasticity without a yield surface-I," Arch of Mechanics,Vol.23, pp.535-551.
(40) Valanis, K. C. (1985) : "On the uniqueness of solution of the initial value problem in softening materials," J. Appl. Mech. Vol.52, pp.649-653.
(41) Wakayama, Y. (1993) : "A study on a constitutive model with strain softening for sedimentary rock," Master theses, Kyoto University(In Japanese)

(42) Wang, C. C. (1969) : "Generalized simple bodies," Arcs. Rational Mech. Analysis, No.32, pp.1-30.
(43) Yong, R. N. and Japp, R. D. (1969) : "Stress-strain behavior of clays in dynamic compression," Vibrational effects on earthquakes on soil and foundation, ASTM, STP, 450, pp.233-262.

Chapter 3

Constitutive model with strain softening for discontinuous geologic materials

3-1 Introduction

In the explanation of the mechanical behavior of joint in geologic materials, it is usually assumed that the joint is discontinuous and its mechanical behavior is related to frictional angle of joint surface, roughness of joint and the orientation and spacing of joint. The researches on this field can be found in the works by Barton(1971), Barton(1973), Amadei and Saeb(1990), Skinas et al.(1990). The thickness of joint in geologic material is usually considered to be zero. However this is not always true even if the thickness of joint is very small and reasonably to be regarded as zero in macroscopic viewpoint. In some cases, such as direct shear test, shear zone will occur, in which large shear strain may occur and the mechanical behavior of the shear zone can be regarded as discontinuous in macroscopic viewpoint. In jointed geologic material, the joint itself may contain continuous medium. Therefore, it is reasonable to assume that the mechanical behavior of the above mentioned shear zone or joint can still be explained by continuum theory. From this viewpoint, continuum theory is still adopted in this chapter to describe the discontinuous behavior of joint or shear zone. Based on the plasticity theory of Naghdi(1960) and Adachi-Oka's model(Oka, 1985, Oka and Adachi, 1985, Adachi and Oka, 1992) with strain hardening and softening, a new constitutive model is proposed for joint(Adachi et al., 1991).

One of the outstanding characteristics of Adachi-Oka's model with strain-softening is the capability of explaining the dilatancy for over-consolidated materials undergoing shear. It is clear, however, that the Adachi-Oka's model is considered within stress-strain space. Therefore it cannot be directly applied to direct shear test or joint problem in which displacement instead of strain is considered. For this reason, it is necessary to make further investigation of mechanical behavior of material within joint or shear zone occurred in direct shear test.

3-2 Derivation of the model

In order to explain the physical meaning of the variables concerning the discontinued deformation involved in the constitutive model, a new variable which is called as equivalent displacement is introduced based on the assumption that the thickness of joint or shear zone in which large shear strain may occur is not equal to zero. The deformation pattern within a joint is schematically shown in Fig.3-1. From the figure, it is easy to see that the distribution of shear deformation along the direction normal to the shear direction is continuous even if it may change very vigorously. Some components of the equivalent displacement $\bar{\varepsilon}^p_{ij}$ are real displacements that can be seen in following discussion. The equivalent displacement is geometrically related to plastic strain tensor ε^p_{ij} by introducing parameter D which stand for the thickness of joint or the shear zone whose mechanical behavior looks like a joint.

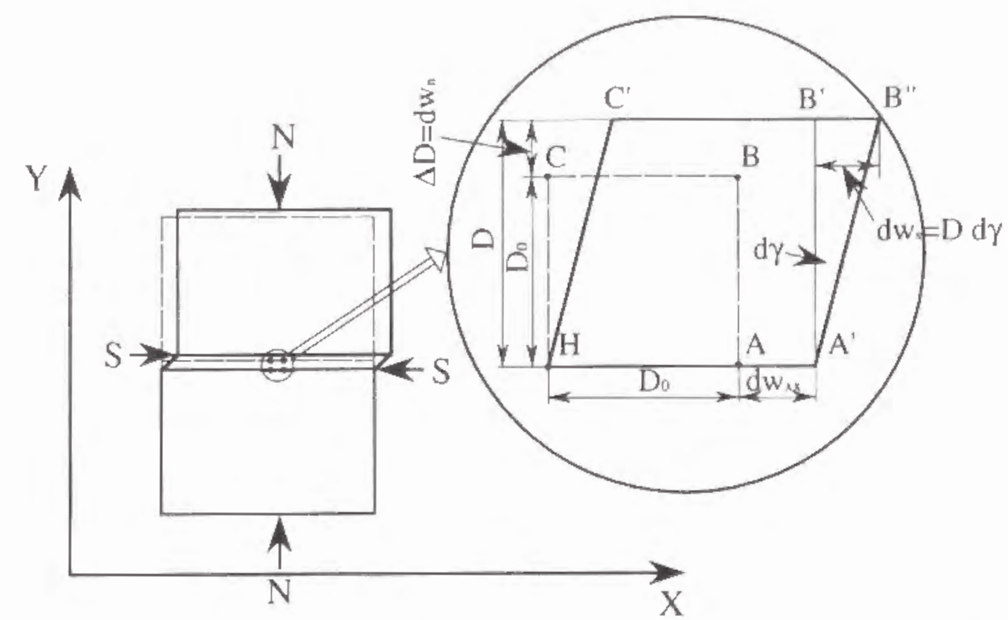

Fig.3-1 Geometry of joint or shear zone in the sample undergone direct shear test

The problem left now is that the thickness D cannot be easily determined because not only it is related to material properties but also to stress state and boundary condition. The parameter D is introduce here, to establish a geometric relation between the shear displacement and the strain in joint or shear zone. The magnitude of D is not necessary to evaluate because, as it can be seen in following inference, by some calculation it can be substituted with other variables which can be measured by experiment.

In present model, non-associated flow law is adopted and takes the same form as the one in Adachi-Oka's model with strain softening,

$$d\varepsilon_{ij}^{p} = A \frac{\partial f_p}{\partial \sigma_{ij}} \frac{\partial \eta^*}{\partial \sigma_{mn}^*} d\sigma_{mn}^* \tag{3-1}$$

The plastic yield function can be written as

$$f = \eta^* - \kappa_s = 0 \tag{3-2}$$

where

$$\eta^* = (s_{ij}^* s_{ij}^* / \sigma_m^{*2})^{1/2} \tag{3-3}$$

is the ratio of second invariant of stress history tensor to mean stress history.

In Eq.3-2, the strain hardening and softening parameter κ_s is different from the one in Adachi-Oka's model. In present case, instead of strain, the equivalent displacement can be expressed in the following equations

$$\bar{e}_{ij}^{p} = \bar{\varepsilon}_{ij}^{p} - \bar{\varepsilon}_{m}^{p} \delta_{ij} / 3 \tag{3-4}$$

$$\bar{\varepsilon}_{ij}^{p} = \int_0^{\varepsilon_{ij}^{p}} D(e_{mn}^{p})\, d\varepsilon_{ij}^{p} \tag{3-5}$$

$$\bar{\gamma}^{p} = \sqrt{\bar{e}_{ij}^{p} \bar{e}_{ij}^{p}} \tag{3-6}$$

where D is the thickness of joint and $\bar{\varepsilon}_{ij}^{p}$ is equivalent displacement and its meaning will be explained later. By introducing these parameters, It is assumed that the strain hardening and softening parameter κ_s takes the form as

$$\kappa_s = \frac{M_f^* \bar{G}' \bar{\gamma}^{p}}{M_f^* + \bar{G}' \bar{\gamma}^{p}} \tag{3-7}$$

It should be pointed out that the Eq.3-7 is similar to the integration of Eq.2-31 only in mathematical form. Its physical meaning is different. In Eq.3-7, it is assumed that the strain hardening and softening parameter is dependent on the equivalent displacement $\bar{\gamma}^{p}$.

Now consider the physical meaning of the equivalent displacement. For the joint problem in the coordinates illustrated in Fig.3-1, it is easy to see from the geometric condition that there exists such relation as

$$dw_s^{p} = D(e_{mn}^{p})\, d\gamma_{xy}^{p} \tag{3-8}$$

and

$$w_s^{p} = \int_0^{\gamma_{xy}^{p}} D(e_{mn}^{p})\, d\gamma_{xy}^{p} \tag{3-9}$$

where dw_s^p and w_s^p are the incremental plastic shear displacement and plastic shear displacement respectively. It is also able to obtain a relation from Fig.3-1 that,

$$dw_n^{p} = D(e_{mn}^{p})\, d\varepsilon_{yy}^{p} \tag{3-10}$$

and

$$w_n^{p} = w_{yy}^{p} = \int_0^{\varepsilon_{yy}^{p}} D(e_{mn}^{p})\, d\varepsilon_{yy}^{p} \tag{3-11}$$

where dw_n^p and w_n^p stand for incremental plastic normal displacement and plastic normal displacement respectively. Similarly, it is able to obtain similar relations along x and z direction as

$$w_{xx}^{p} = \int_{0}^{\varepsilon_{xx}^{p}} D(e_{mn}^{p})\, d\varepsilon_{xx}^{p} \tag{3-12}$$

and

$$w_{zz}^{p} = \int_{0}^{\varepsilon_{zz}^{p}} D(e_{mn}^{p})\, d\varepsilon_{zz}^{p} \tag{3-13}$$

where $w_{zz}{}^{p}$ stands for the plastic horizontal displacement. These variables can be called as equivalent displacement because they do have the meaning of displacement and will affect the volumetric change during shearing in spite of the difficult to measure them in experiment. The parameter $\overline{G}'$ has the dimension of *1/Length* and is the initial tangential modules between the stress historical parameter η' and equivalent displacement γ^{p}.

the boundary surface defining the boundary between normally consolidated region ($f_b \geq 0$) and over-consolidated region($f_b < 0$) is also taken the same form as the one in Adachi-Oka's model

$$f_b = \eta + \overline{M}_m \ln\left(\frac{\sigma_m + b}{\sigma_{mb} + b}\right) = 0 \tag{3-14}$$

where

$$\eta = \left(\frac{S_{ij}}{\sigma_m + b}\,\frac{S_{ij}}{\sigma_m + b}\right)^{1/2} \tag{3-15}$$

and $\overline{M}_m$ is a parameter determining the boundary of over-consolidated region. σ_{mb}, and b are plastic potential parameters

The plastic potential takes the form as

$$f_p = \eta + \overline{M} \ln\left(\frac{\sigma_m + b}{\sigma_{mb} + b}\right) = 0 \tag{3-16}$$

in which

$$\begin{aligned} \overline{M} &= -\frac{\eta}{\ln\left(\dfrac{\sigma_m + b}{\sigma_{mb} + b}\right)} && f_b < 0 \\ \overline{M} &= \overline{M}_m && f_b \geq 0 \end{aligned} \tag{3-17}$$

Combining Eq.3-1,Eq.3-2,Eq.3-7,Eq.3-14,Eq.3-16 and Eq.3-17, it is easily to obtain the constitutive model with strain softening for discontinuous materials. It should be pointed out that the frame-work of Adachi-Oka's model with strain softening remains valid in the present model.

By some arithmetic (See Appendix), it is able to obtain the relation for A as follow,

$$A = \frac{M_f^{*2}}{\overline{G}'(M_f^{*} - \eta^{*})^{2} D(e_{mn}^{p})} (\sigma_m + b) \frac{\dot{\gamma}^{p}\, \eta}{\dot{e}_{ij}^{p}\, \eta_{ij}} \tag{3-18}$$

In the direct shear test, the specific stress-strain state can be given as follow,

$$\begin{gathered} \gamma_{xz}^{p} = \gamma_{yz}^{p} = \gamma_{xz} = \gamma_{yz} = 0 \\ \tau_{xz} = \tau_{yz} = 0 \\ \sigma_{xx} = \sigma_{zz} = 0 \\ \dot{\varepsilon}_{xx}^{p} = \dot{\varepsilon}_{zz}^{p} \end{gathered} \tag{3-19}$$

The stress and strain variables can be given as

$$\sqrt{2J_2} = \sqrt{s_{ij}\, s_{ij}} = \sqrt{2(\tau_{xy}^{2} + \sigma_{yy}^{2}/3)} \tag{3-20}$$

$$\sqrt{2J_2^{*}} = \sqrt{2(\tau_{xy}^{*2} + \sigma_{yy}^{*2}/3)} \tag{3-21}$$

$$\sigma_m = \sigma_{ii}/3 = \sigma_{yy}/3 \tag{3-22}$$

$$\eta^{*} = \sqrt{18(\tau_{xy}^{*2}/\sigma_{yy}^{*2} + 1/3)} \tag{3-23}$$

$$\bar{\gamma}^p = \sqrt{2/3(\bar{\varepsilon}^p_{yy} - \bar{\varepsilon}^p_{xx})^2 + \bar{\gamma}^{p2}_{xy}/2} \tag{3-24}$$

$$C_1 = 2/3\sigma^*_{yy}(\sigma_{yy} - \sigma^*_{yy}) + \tau^*_{xy}(\tau_{xy} - \tau^*_{xy}) \tag{3-25}$$

$$C_2 = \left(\frac{C_1}{\sqrt{2J_2^*}} - \frac{\sqrt{2J_2^*}}{\sigma^*_m}(\sigma_m - \sigma^*_m)\right) \tag{3-26}$$

$$C_3 = \frac{\bar{\gamma}^p\,\eta}{\bar{e}^p_{ij}\,\eta_{ij}} = \frac{\bar{\gamma}^p\sqrt{2J_2}}{2/3\,(\bar{\varepsilon}^p_{yy} - \bar{\varepsilon}^p_{xx})\,\sigma_{yy} + \bar{\gamma}^p_{xy}\,\tau_{xy}/2} \tag{3-27}$$

$$\bar{\gamma}^p_{xy} = w^p_s \tag{3-28}$$

$$\bar{\varepsilon}^p_{yy} = w^p_n \tag{3-29}$$

$$\bar{\varepsilon}^p_{xx} = w^p_{xx} \tag{3-30}$$

$$dw^p_s = D(e^p_{mn})\,d\gamma^p_{xy} = \frac{2M_f^{*2}}{\bar{G}'(M^*_f - \eta^*)^2}\frac{C_3}{\sigma^*_m}C_2\frac{dz}{\tau}\frac{\tau_{xy}}{\sqrt{2J_2}}$$

$$dw^p_n = D(e^p_{mn})\,d\varepsilon^p_{yy} = \frac{M_f^{*2}}{\bar{G}'(M^*_f - \eta^*)^2}\frac{C_3}{\sigma^*_m}C_2\frac{dz}{\tau}\left(\frac{2\sigma_{yy}}{3\sqrt{2J_2}} - \frac{\sqrt{2J_2}}{\sigma_m + b}\frac{1}{3} + \frac{\bar{M}}{3}\right)$$

$$dw^p_{xx} = dw^p_{zz} = D(e^p_{mn})\,d\varepsilon^p_{xx} = \frac{M_f^{*2}}{\bar{G}'(M^*_f - \eta^*)^2}\frac{C_3}{\sigma^*_m}C_2\frac{dz}{\tau}\left(-\frac{\sigma_{yy}}{3\sqrt{2J_2}} - \frac{\sqrt{2J_2}}{\sigma_m + b}\frac{1}{3} + \frac{\bar{M}}{3}\right)$$

(3-31)

In present model, dz takes the form as

$$dz = dw_s \tag{3-32}$$

which means that the stress history takes the equivalent displacement as internal variable.

From Eq.3-20 to Eq.3-31, it can be seen that though the parameter D in the constitutive model can not be solved directly, it can be omited in inferring the expression for the displacement. The total displacements can be given in the follow equations

$$dw_s = dw^e_s + dw^p_s \tag{3-33a}$$

$$dw^e_s = d\sigma_\tau / k_s \tag{3-33b}$$

$$dw_n = dw^e_n + dw^p_n \tag{3-33c}$$

$$dw^e_n = d\sigma_n / k_n \tag{3-33d}$$

There are eight parameters involved in the constitutive model. The determination of these parameters are given as follow,

(1)k_s: the elastic shear stiffness in unit length, is determined by direct shear test under constant normal stresses. The equation to calculate the k_s is as follow,

$$k_s = (\Delta\sigma_\tau / \Delta w_s)_{initial}$$

(2)k_n: elastic normal stiffness, is determined by one-axial compression test.

(3)M^*_f: the strain softening parameter, is determined by the value of η^* at the state at which residual strength is reached.

(4)$\bar{G}'$: strain hardening parameter, is the initial gradient of stress history ratio η^* to shear displacement at the unloading-reloading cycle in residual state.

(5)σ_{mb}: plastic potential parameter, can be determined by isotropic consolidation test and takes the value of pre-consolidated stress

(6)b: plastic potential parameter. The purpose of introducing this parameter is to explain the dilatancy. It can be determined by the assumption that the stress ratio η is kept constant in over-consolidated region along M_m-line as shown in Fig.2-3.

(7)$\bar{M}_m$: parameter determining the boundary of over-consolidated area, is the value of η^* at the state at which the maximum compression takes place.

(8)τ: the stress historical parameter, is determined by the peak stress with curve fitting method.

3-3 Application to direct shear test of sand under constant normal stress

In order to examine the validity of the constitutive model proposed in this chapter, experimental results of direct shear test for Toyoura standard sand are compared with the theoretical ones.

Fig.3-2 is the experimental results of the relationship between shear stress and shear displacement for direct shear test of dense Toyoura standard sand. Material parameters involved in the constitutive model are listed in Table 3-1. Fig.3-3 is the comparison between experimental results and theoretical results. It can be seen from the figures that the constitutive model can well simulate the relation of shear stress-shear displacement. It can also well describe the dilatancy occurred in the direct shearing test of dense sand.

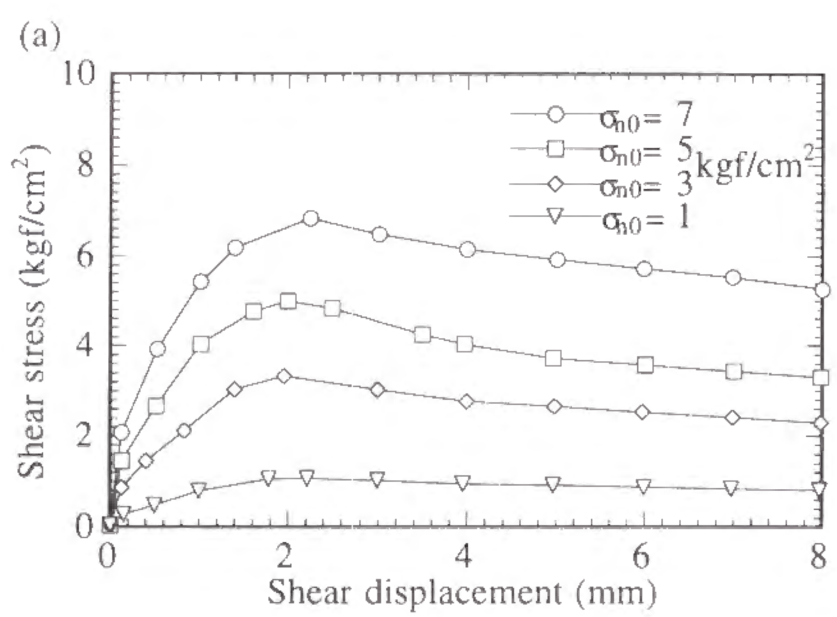

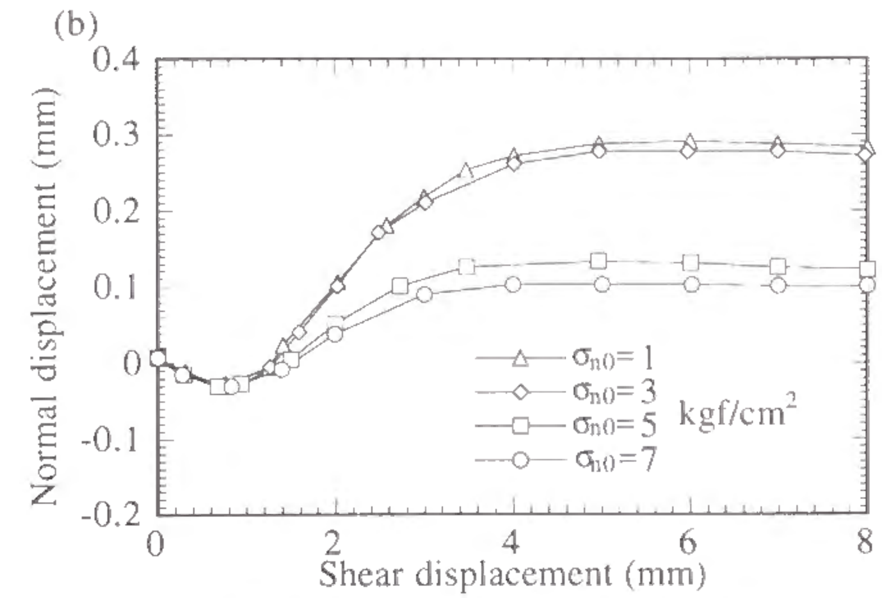

Fig.3-2 Experimental results of dense Toyoura standard sand undergone direct shear test

Table 3-1 Material parameters of Toyoura sand in direct shear test at constant normal stress

Normal stress	I	II	III	VI
σ_{n0}(kgf/cm^2)	1.00	3.00	5.00	7.00
k_s(kgf/cm^3)	18.0	30.0	60.0	60.0
k_n(kgf/cm^3)	110.0	110.0	110.0	110.0
M_f^*	4.25	4.13	3.98	4.26
$\overline{G}$'(1/cm)	500.0	700.0	700.0	700.0
σ_{mb}(kgf/cm^2)	60.0	60.0	60.0	60.0
b(kgf/cm^2)	0.14	0.30	0.74	1.32
$\overline{M}_m$	1.61	1.61	1.61	1.61
τ	0.057	0.087	0.063	0.060

(a) Normal stress(σ_{n0})=1(kgf/cm^2)

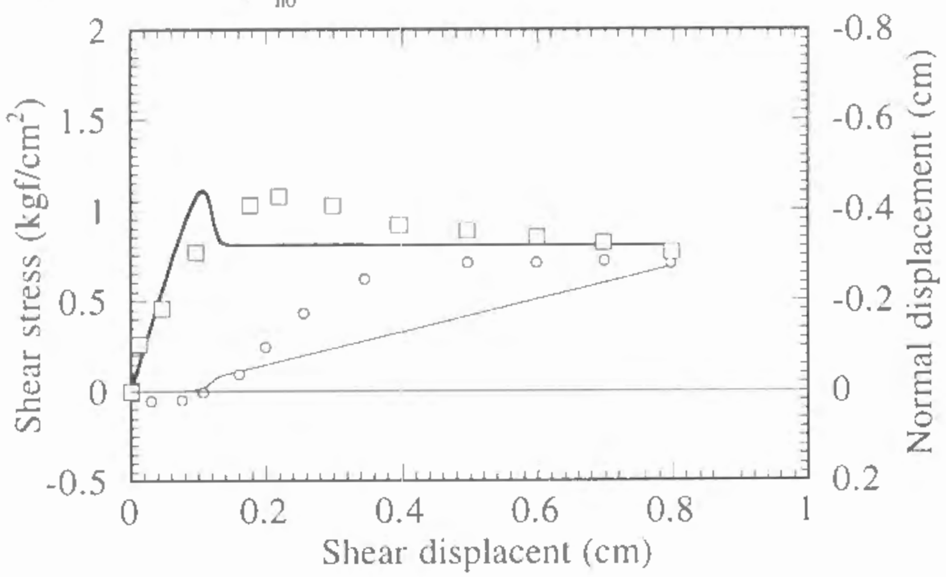

(b) Normal stress(σ_{n0})=3(kgf/cm^2)

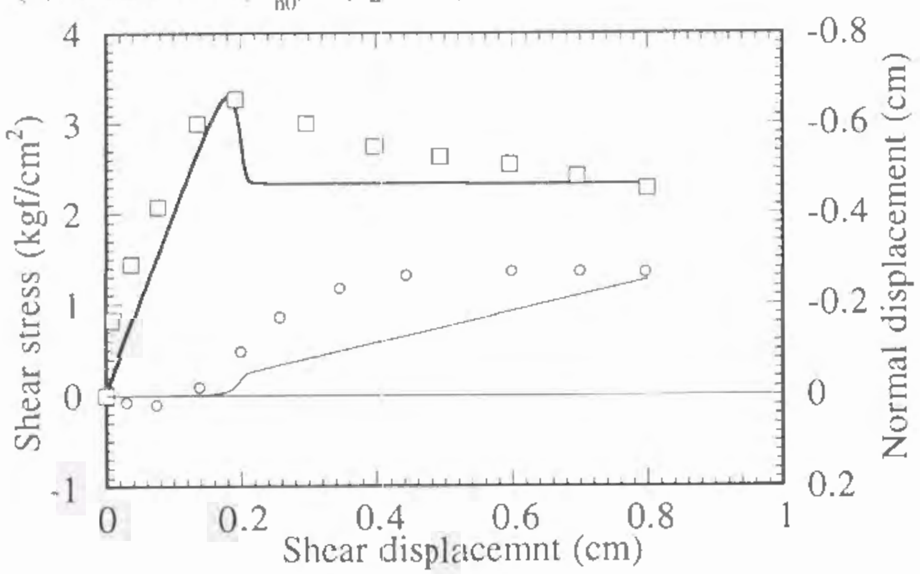

(c) Normal stress(σ_{n0})=5(kgf/cm^2)

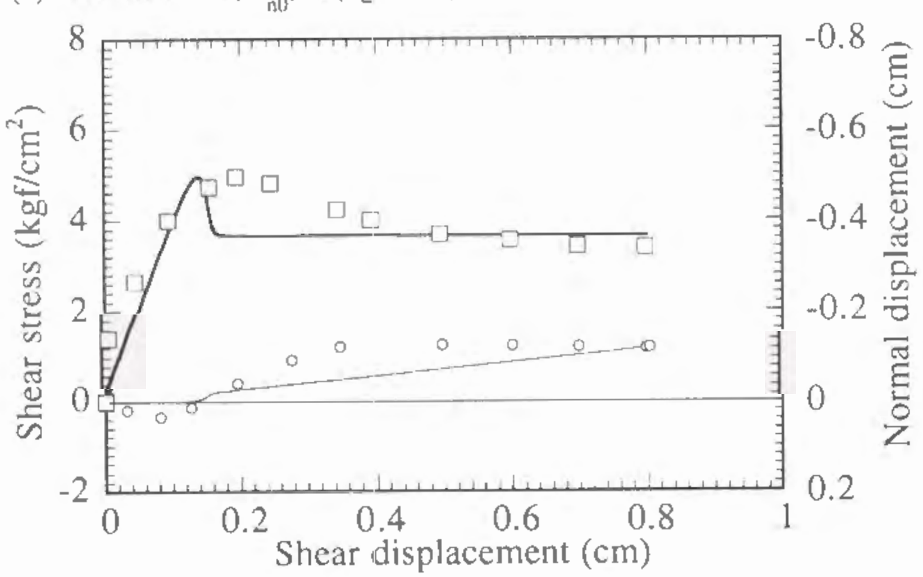

(d) Normal stress(σ_{n0})=7(kgf/cm^2)

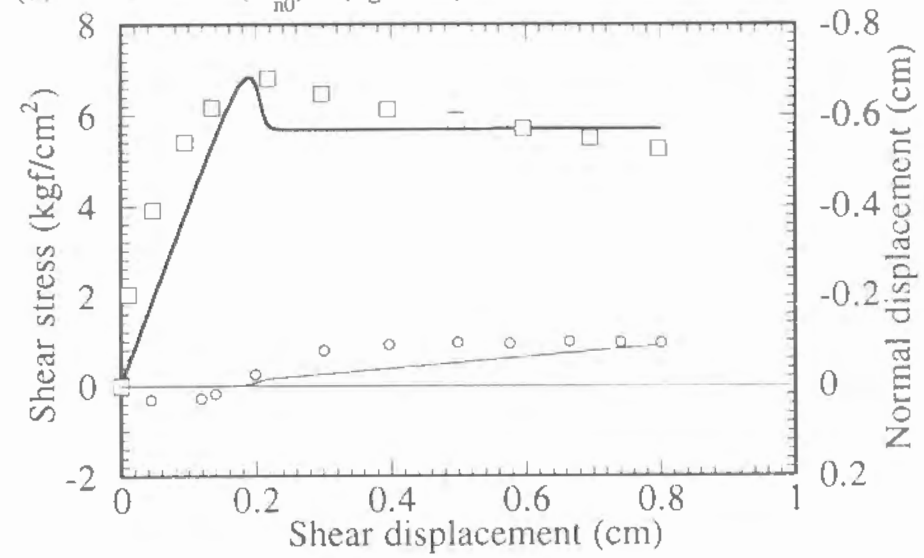

Fig.3-3 Comparison of theoretical and experimental stress-displacement relation and shear displacement-normal displacement relation at different normal stress for dense Toyoura standard sand

3-4 Application to direct shear test of jointed cement under constant normal stress

Experimental results obtained from a series of direct shear tests on jointed specimens(Nishigawa, 1991) are also used to verify the validity of the model proposed in this chapter. A simple description of the experiment will be given next.

Because it is nearly impossible to prepare several natural rock specimens with same stiffness and shape of joint which is necessary to avoid scattered experimental results, cement-mortar specimens with a joint cast from natural jointed surface are used in the experiment. The procedure of preparing the specimens is shown in Fig.3-4. Firstly, a cast-iron form is cast with the same jointed surface as a natural granite rock. Secondly, taking the cast-iron form as the base of a mold with a diameter of 10 cm, mortar is then poured into the mold to form the up part of a specimen as shown in Fig.3-4(b). Finally, taking the up part of the specimen as the base of the mold, mortar is poured into the mold to form the low part of the specimen as shown in Fig.3-4(c).

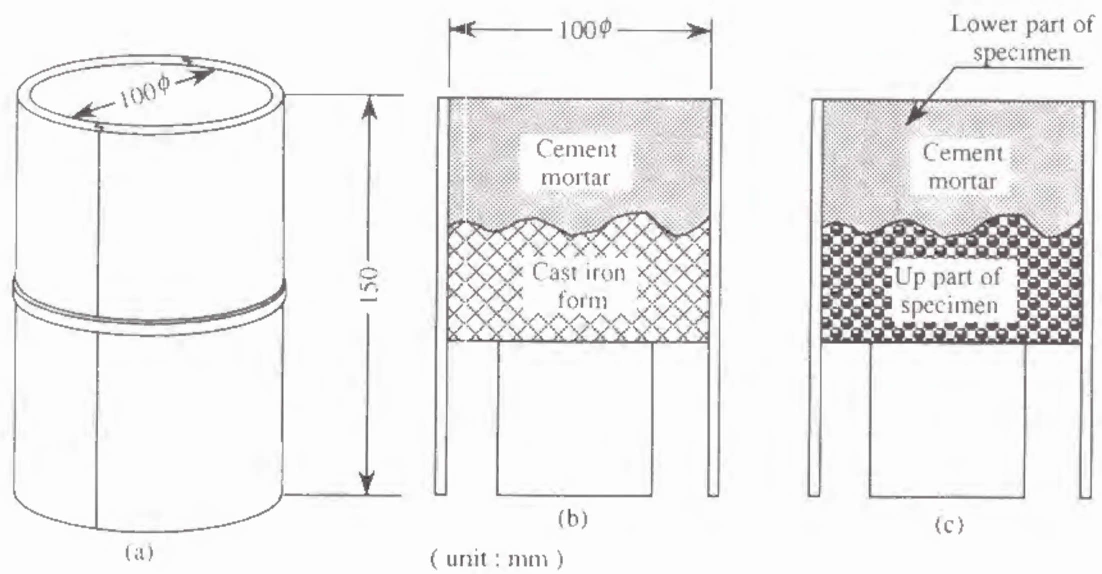

Fig.3-4 Preparation of specimen

The shape of the specimen is cylinder with diameter of 10 cm and height of 12 cm. The ratio of the mortar in cement, standard sand and water is 1:2:0.65. The specimens were tested under constant normal stresses of 5 kgf/cm^2, 10 kgf/cm^2, 20 kgf/cm^2 and 40 kgf/cm^2. The material parameters are listed in Table 3-2.

Table 3-2 Material parameters of jointed mortar in direct shear test at constant normal stress

Normal stress	I	II	III	VI
σ_{n0}(kgf/cm^2)	5.00	10.0	20.0	40.0
k_s(kgf/cm^3)	180.0	180.0	350.0	723.0
k_n(kgf/cm^3)	5190.3	5190.3	5190.3	5190.3
M_f^*	3.48	4.48	3.07	3.19
$\overline{G}'$(1/cm)	2000.0	1500.0	2000.0	2000.0
σ_{mb}(kgf/cm^2)	440.0	440.0	440.0	440.0
b(kgf/cm^2)	0.75	1.53	0.98	2.40
$\overline{M}_m$	1.61	1.61	1.61	1.61
τ	0.031	0.065	0.065	0.090

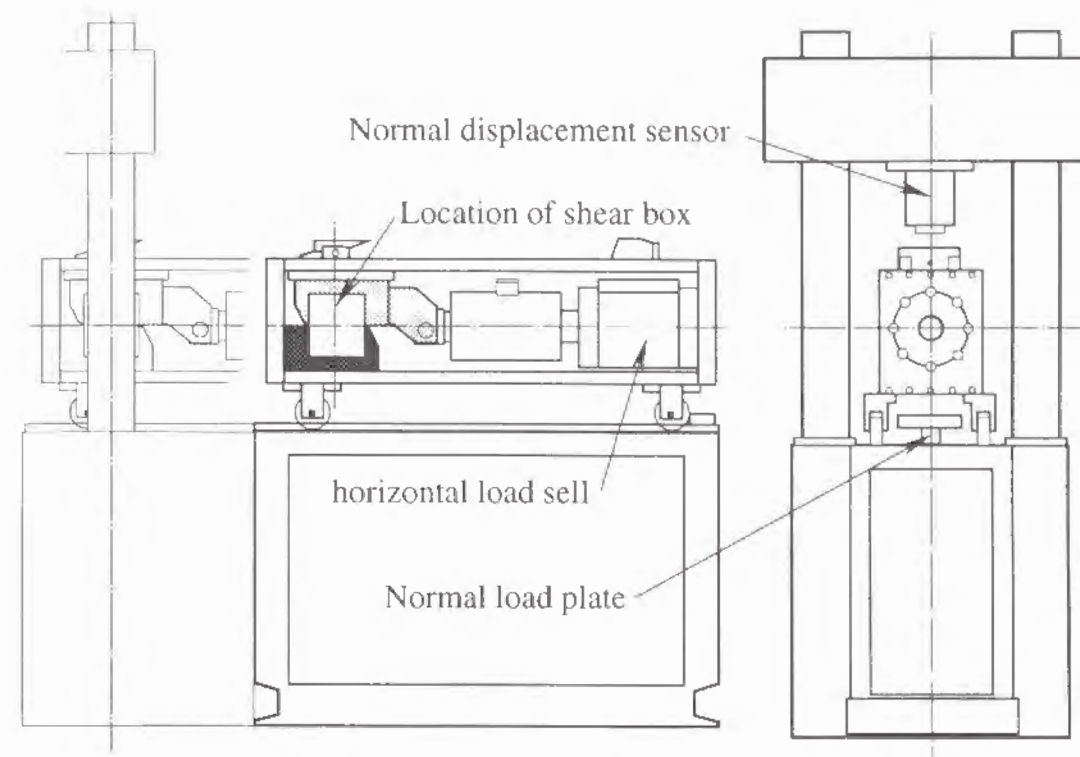

Fig.3-5 General view of the direct shear test apparatus used in the experiment

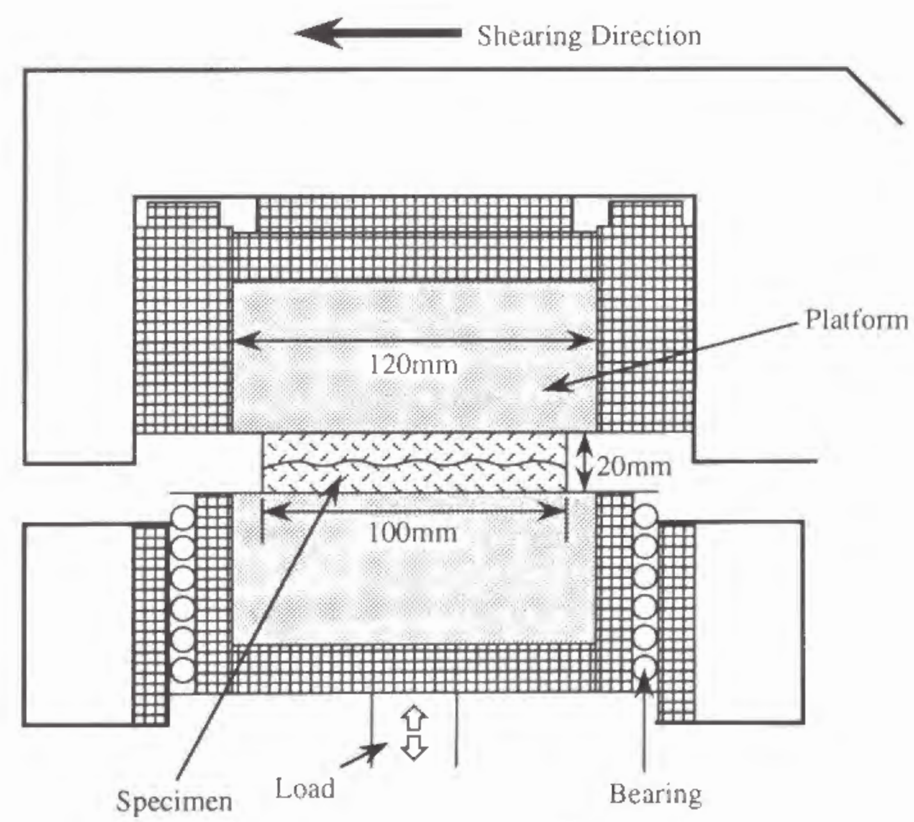

Fig.3-6 Shear box used in direct shear test

Fig.3-5 is a general view of the apparatus of direct shear test used in the experiment. The apparatus has the capacities of 20 tonf and 25 tonf in normal and shear load respectively. It can accommodate joint specimen up to 10cm(D) × 12cm(H) for cylinder and 10cm(L) × 10cm(W) × 12cm(H) for rectangle respectively. The shearing box used in the direct shear test is shown in Fig.3-6. Fig.3-7 shows the system map of shear test.

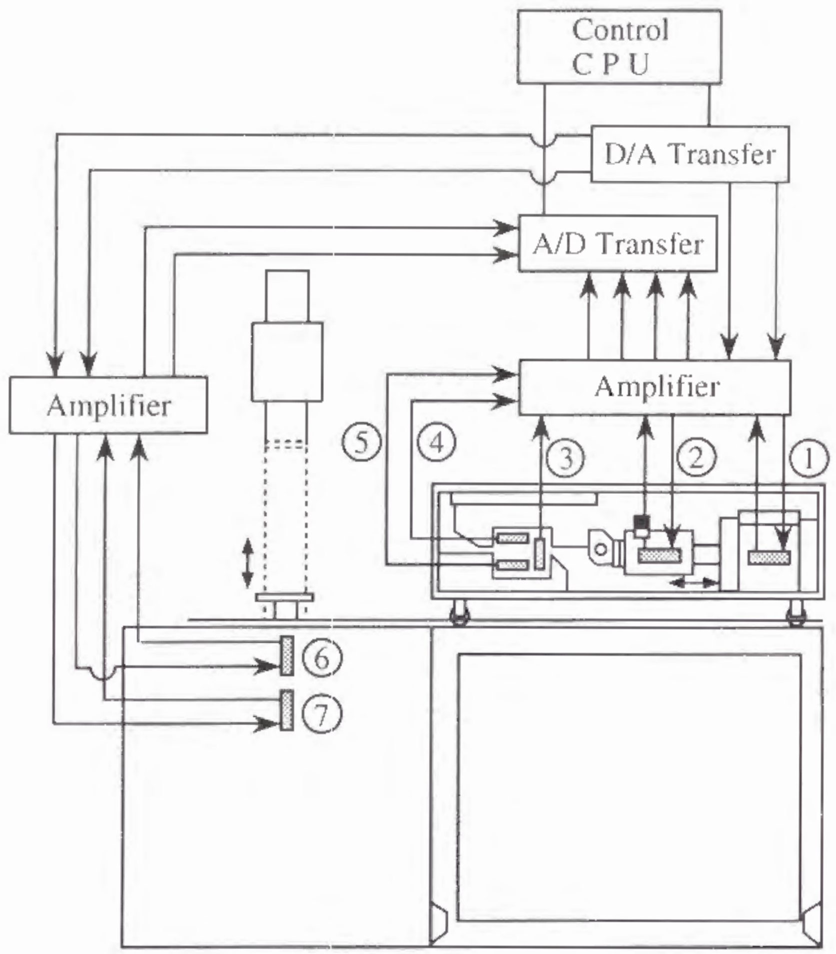

① Horizontal load (± 20tonf)
② Horizontal displacement 1 (± 25mm)
③ Vertical displacement (± 2.5mm)
④ Holizontal displacement 2 (± 2.5mm, ± 5mm)
⑤ Pore-water pressure (± 10kgf/cm²)
⑥ Vertical load (± 25tonf)
⑦ Vertical displacement (± 25mm)

Fig.3-7 System map of shear test

Fig.3-8 shows the experimental results of direct shear test under different normal stresses. Fig.3-9 is the comparison between experimental results and theoretical results. It is evident from the figure that the peak strength and residual strength can be well simulated while for the post-peak stress the theoretic results decrease very rapidly which is not coincide with the experiment ones. This might be caused by the over-rapid change of stress history ratio η' in yielding equation from zero to residual state. The dilatancy occurred in shearing can also be well simulated by the present constitutive model.

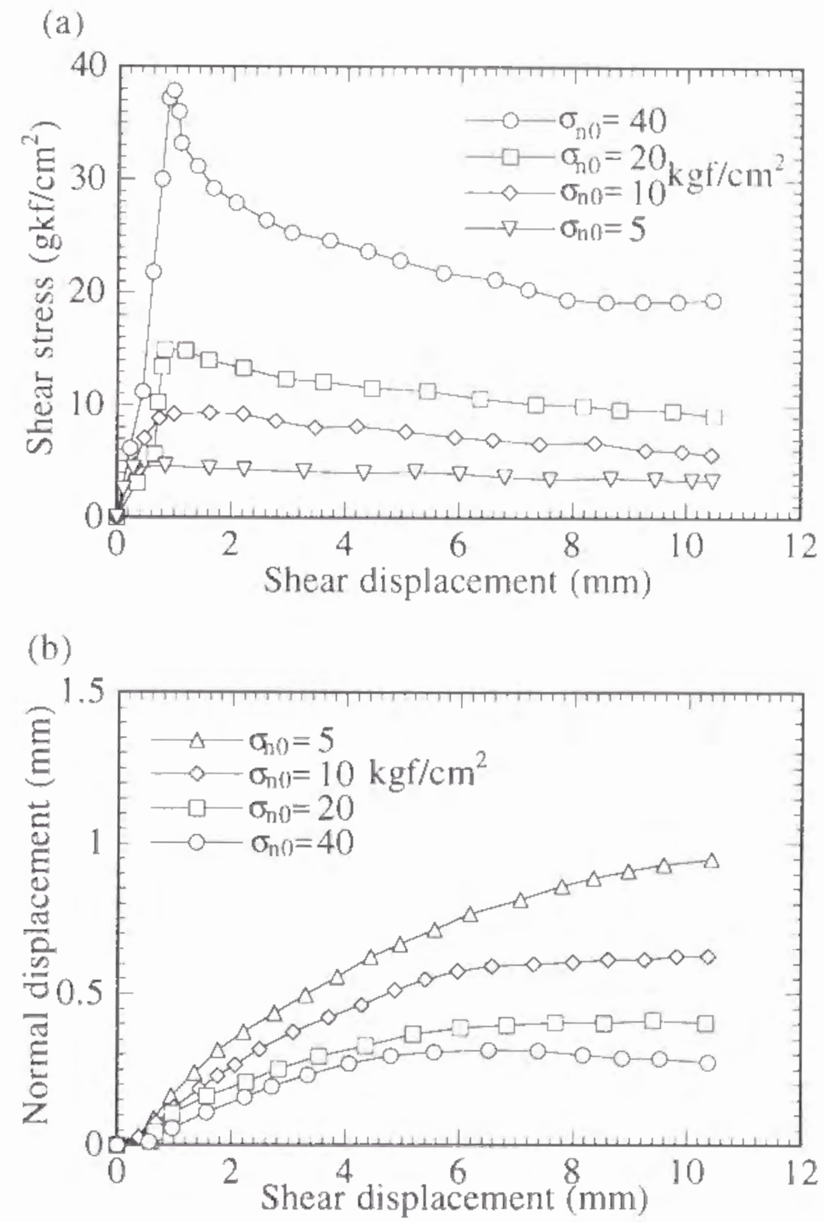

Fig.3-8 Experimental results of jointed cement mortar undergone direct shear test at constant normal stress

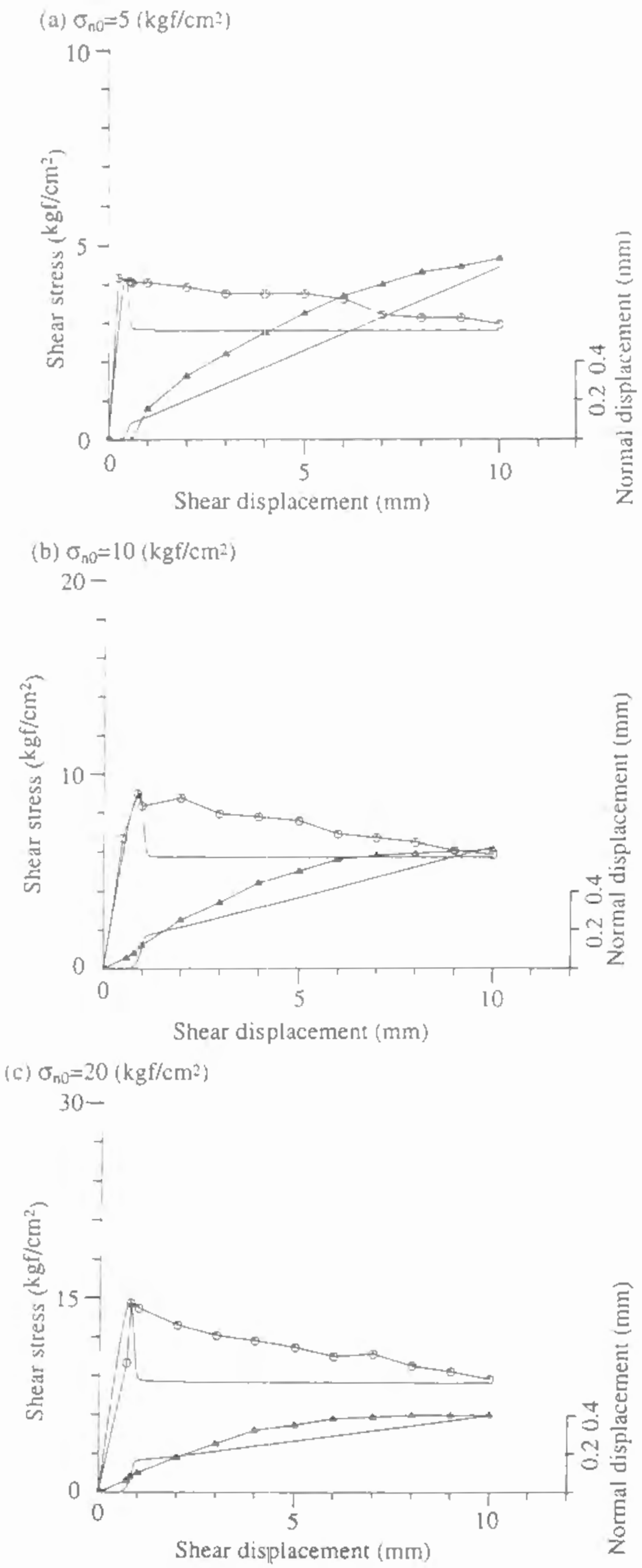

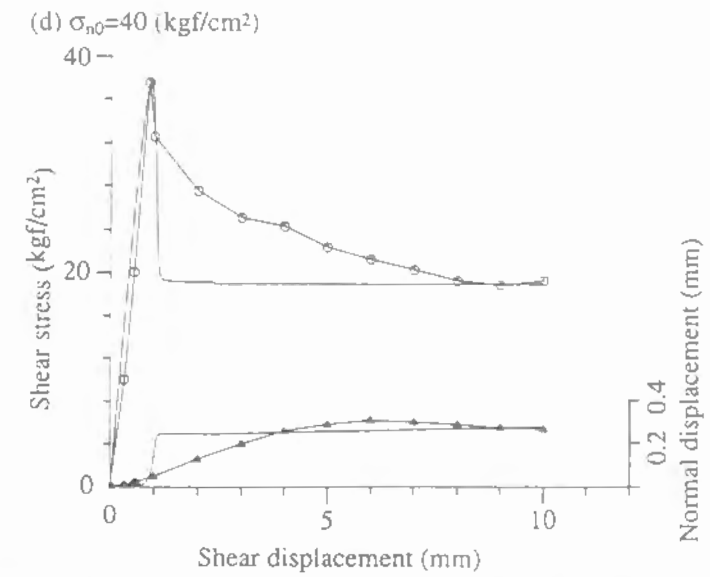

Fig.3-9 Comparison of theoretical and experimental stress-displacement relation and shear displacement-normal displacement relation at constant normal stress

3-5 Application to direct shear test of jointed cement under constant stiffness

The dilatancy of joints undergoing shear may affect greatly the shear strength and stress-displacement relation. For a given joint and boundary condition, the amount of dilatancy depends on the normal stress acting on joint surface, the amount of shear displacement and the roughness of joint. If the material surrounding the joint is deformable enough to absorb the normal displacement associated with dilatancy, shearing may be regarded as being carried out under a constant normal stress. If, on the other hand, the material surrounding the joint is very hard (with low deformablity), the dilatancy occurred in shearing will shows prominent effect. Each increment of dilation will increase the normal stress, which, in turn, will change the shear strength of the joint. Such direct shear test is also called as direct shear test with constant stiffness.

In present study, it is tried to use the constitutive model proposed in this chapter to simulate the mechanical behavior of direct shear test of jointed cement sample under constant stiffness. Such problem can be simulated by a simplification that the tested sample is composed of a jointed mass connected to a spring whose one end is fixed. The simplification can be expressed in a system shown in Fig.3-10.

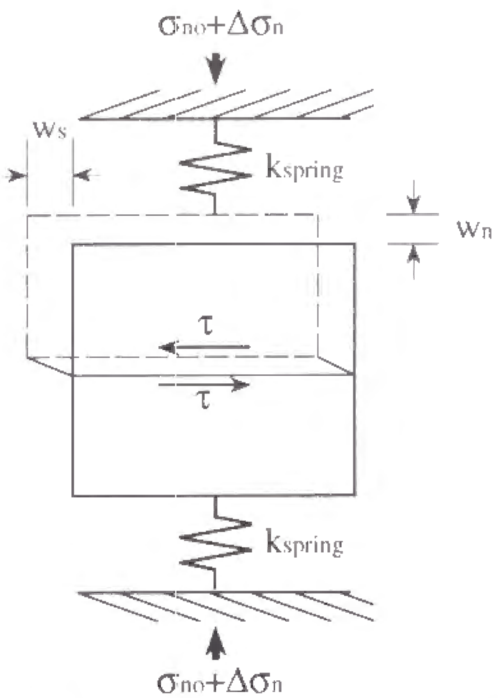

Fig.3-10 Simplified mode of direct shear test under constant stiffness

For jointed mass, there exist such relation

$$\Delta w_n = \Delta w_n^e + \Delta w_n^p = -\Delta w_{spring} \tag{3-34}$$

In Eq.3-34, for convenience, all displacement and stress is assumed to be positive for compression

$$\Delta w_n = \frac{\Delta\sigma_n}{k_n} + \Delta w_n^p = -\frac{\Delta\sigma_n}{k_{spring}} \tag{3-35}$$

In Eq.3-35, k_{spring} is the stiffness of the spring in the simplified model of direct shear test under constant stiffness. Eq.3-35 can be written in another way

$$\Delta\sigma_n = -k\,\Delta w_n^p \tag{3-36}$$

where, k is the stiffness of two series-connected spring and can be evaluated as

$$\frac{1}{k} = \frac{1}{k_n} + \frac{1}{k_{spring}} \quad . \tag{3-37}$$

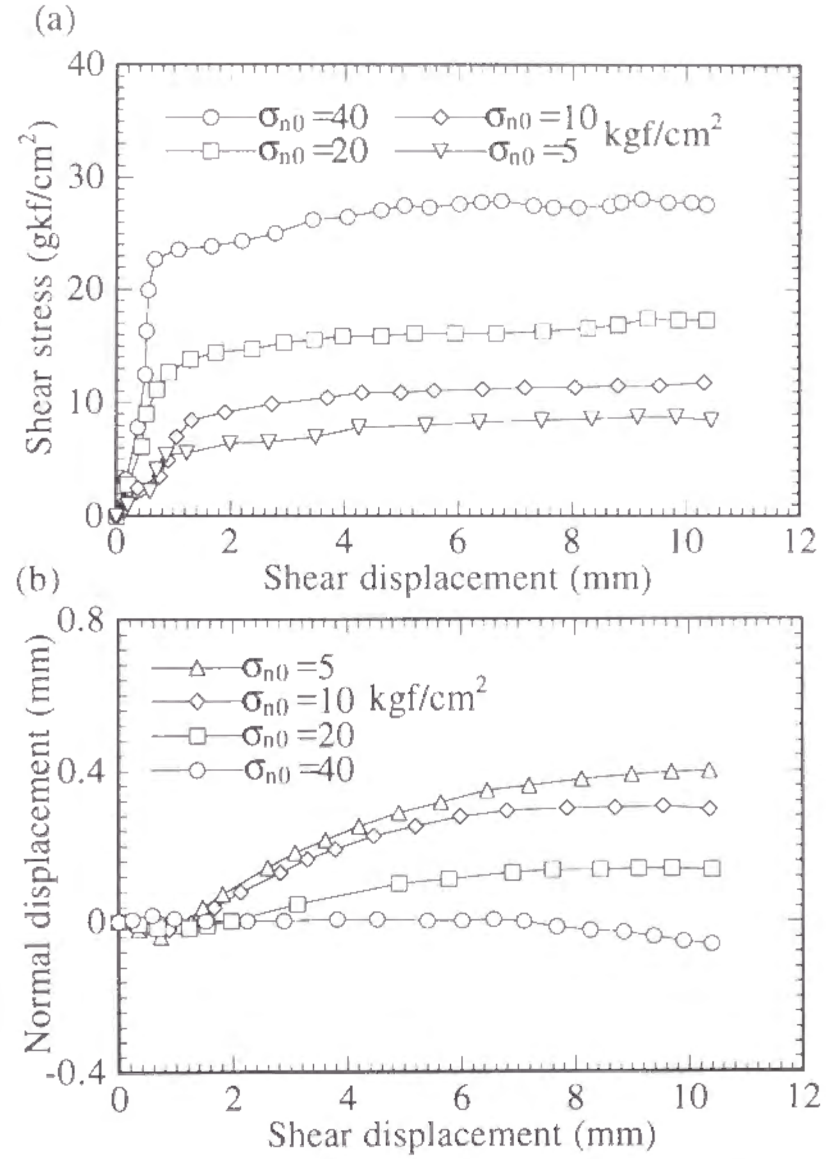

Fig.3-11 Experimental results of jointed cement mortar undergone direct shear test at constant stiffness

Fig.3-11 shows the experimental results of jointed cement mortar undergone direct shear test at constant stiffness. It is clear that the dilation will not increase any more after the shear displacement reach to some value. While the plastic normal displacement is not equal to zero. Based on the above discussion, the following relation exists in large shear displacement:

$$\Delta w_n = \frac{\Delta\sigma_n}{k_n} + \Delta w^p = \frac{-k\,\Delta w^p}{k_n} + \Delta w^p \approx 0 \tag{3-38}$$

which means

$$k \approx k_n \quad . \tag{3-39}$$

On the other hand, it is mathematically easy to show that

$$\frac{1}{k} = \frac{1}{k_n} + \frac{1}{k_{spring}} \approx \frac{1}{k_n} \qquad if\ \ k_n << k_{spring} \quad . \tag{3-40}$$

Based on Eq.3-39 and Eq.3-40, It is reasonable to assume that the elastic stiffness k_n is not a constant and is dependent on shear displacement. The detailed expression for k_n is assumed to be

$$k_n = k_{n0}\exp(\alpha_d\, w_s) \quad , \tag{3-41}$$

where k_{n0}, the initial normal stiffness, is determined by one-axial compression test. α_d, the material parameter, is dependent on the roughness of the joint and be determined by curve fitting method. It has the dimension of *1/Length*.

In order to investigate the validity of the above mentioned assumption, theoretical results are compared with the experimental results shown in Fig.3-11. In the experiment, the shearing is repeated for three time. The results obtained from the first time of direct shear test exhibit unstable discrepancy. While the experiment results shows good stability after the second time of shearing. For this reason, the result obtained from the second time is used as test results to make comparison. The material parameters of the mortar specimens and the spring are listed in Table 3-3.

Fig.3-12 shows the comparison between experimental results and theoretical ones for the relation of shear stress-shear displacement and shear displacement-normal displacement for jointed cement sample undergoing direct shear test at constant stiffness. From the figure, it is

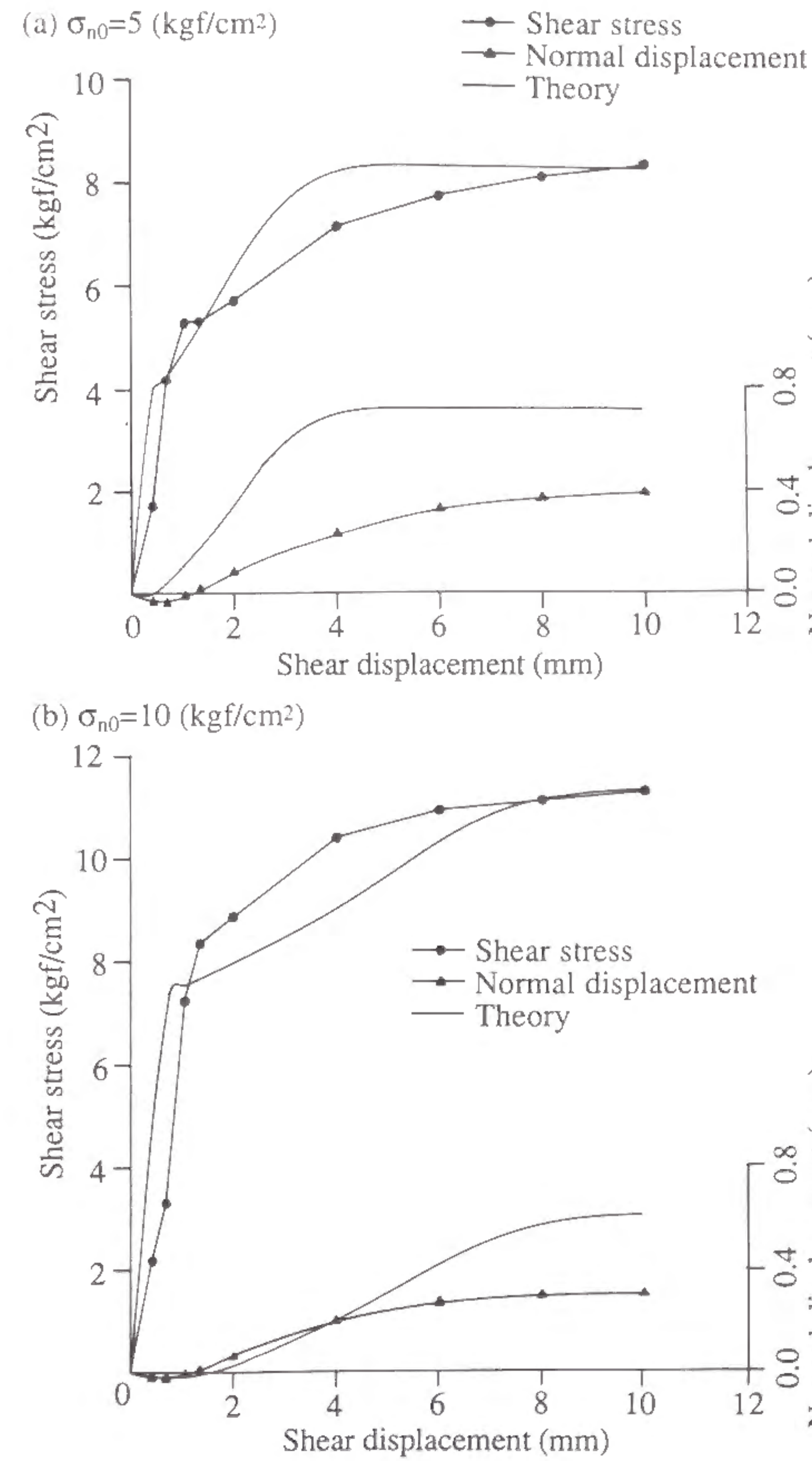

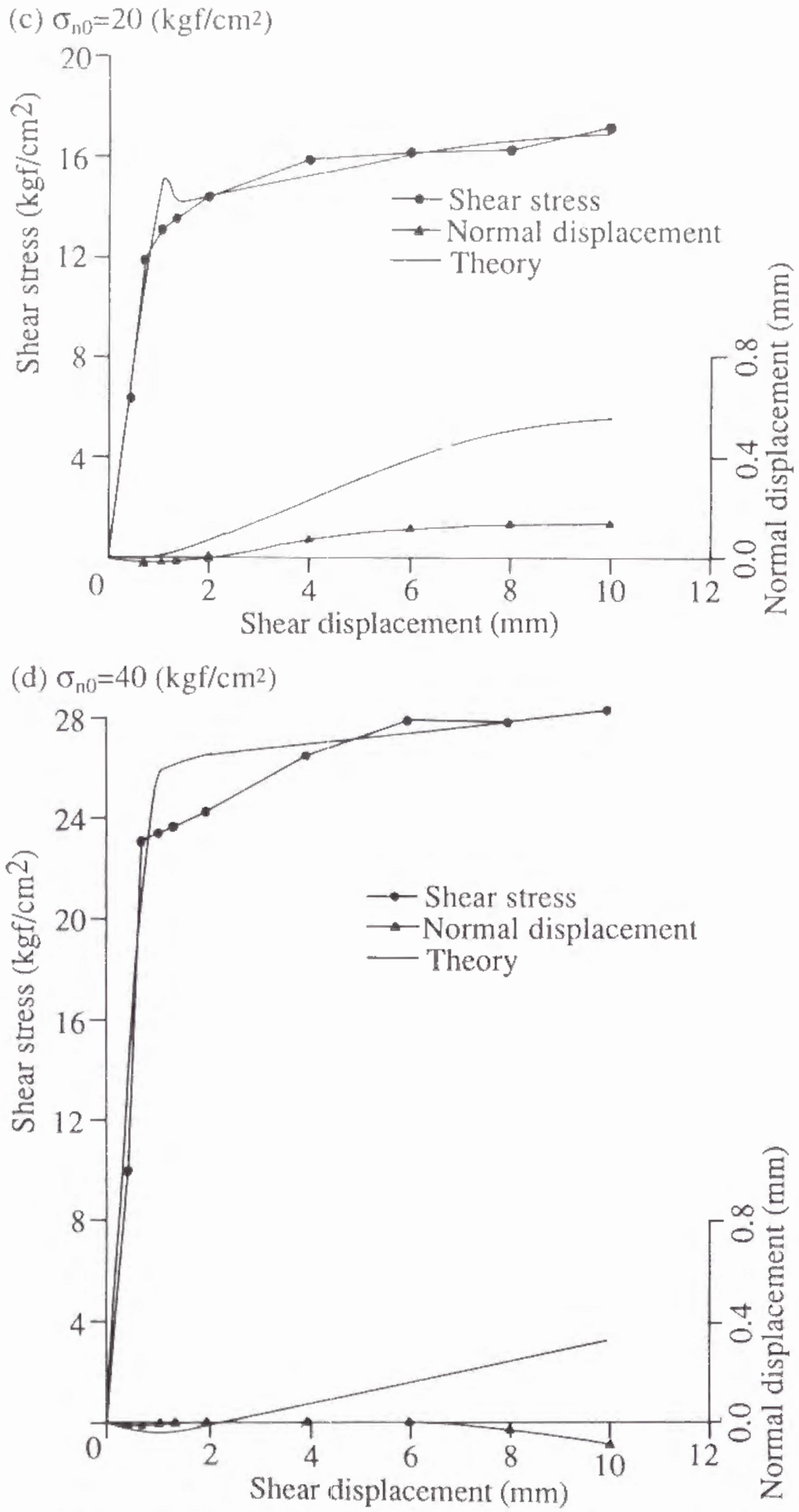

Fig.3-12 Comparison of theoretical and experimental results of direct shear tests at constant stiffness

clear that present theory can well simulate the relation between shear stress and shear displacement for different initial normal stress.

Table 3-3 Material parameters of jointed mortar(constant stiffness)

Normal stress σ_{n0}(kgf/cm^2)	I	II	III	VI
	5.00	10.0	20.0	40.0
k_s(kgf/cm^3)	180.0	180.0	250.0	480.0
k_{n0}(kgf/cm^3)	5190.3	5190.3	5190.3	5190.3
M_f^*	4.29	4.20	3.90	3.82
$\overline{G}'$(1/cm)	2000.0	2000.0	2000.0	2000.0
σ_{mb}(kgf/cm^2)	440.0	440.0	440.0	440.0
b(kgf/cm^2)	1.30	3.20	4.30	6.50
$\overline{M}_m$	1.61	1.61	1.61	1.61
τ	0.013	0.019	0.030	0.065
k_{spring}(kgf/cm^3)	71.94	71.94	71.94	71.94
α_d(1/cm)	60.0	70.0	75.0	90.0

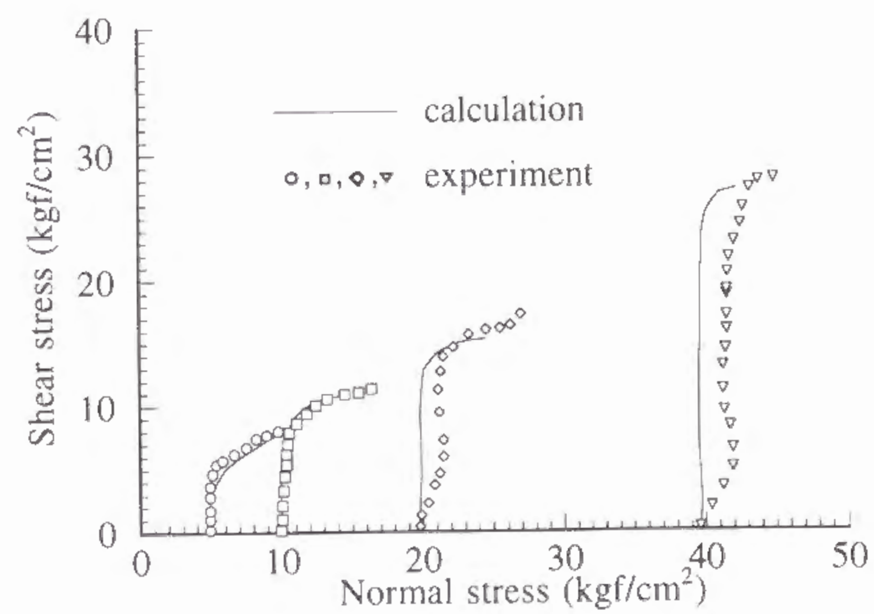

Fig.3-13 Comparison of theoretical and experimental results of stress paths at different initial normal stress under constant stiffness

Fig.3-13 shows the comparison of theoretical results with experimental results on stress paths in different initial normal stress. It is obviously that present study can also well simulate the relation between shear stress and normal stress. For dilatancy, theoretical result is a little bit of exaggeration comparing with experimental result. The reason why such phenomenon occur may be that the increment of normal stress is dependent on the initial normal stiffness and stiffness of the spring in simplified test mode. The larger the normal displacement is, the larger the increment of normal stress will be. Therefore, it is difficult to simulate both the dilation and stresses relation well. As a result, if the stresses relation is well simulated, the dilatancy will take much large value than experimental results.

3-6 Conclusions

Based on Adachi-Oka's model with strain-hardening and strain-softening, a constitutive model is proposed in this chapter to describe the discontinuous behavior of joint materials. By introducing a new strain-hardening and softening function in which the variable describing the discontinuous deformation of joint materials in macroscopic is geometrically related to strain tensors, the model based on continuum theory is able to describe the discontinuous behavior of joint materials. An application of the model to direct shear test of over-consolidated sand and jointed cement mortar under constant normal stress and constant stiffness condition shows good agreement between the experimental and theoretical results.

Appendix

Considering the constitutive equation

$$d\varepsilon_{ij}^{p} = \wedge \frac{\partial f_p}{\partial \sigma_{ij}} df \qquad \text{(a-1)}$$

where

$$\wedge = \frac{\dfrac{\partial \eta^*}{\partial \sigma_{ij}^*} d\sigma_{ij}^*}{\dfrac{\partial k_s}{\partial \bar{\gamma}^p} \dfrac{\partial \bar{\gamma}^p}{\partial \varepsilon_{ij}^p} \dfrac{\partial f_p}{\partial \sigma_{ij}} df} \qquad \text{(a-2)}$$

Substitute Eq.a-2 into Eq.a-1, it is able to obtain

$$d\varepsilon_{ij}^{p} = A \frac{\partial f_p}{\partial \sigma_{ij}} \frac{\partial \eta^*}{\partial \sigma_{mn}^*} d\sigma_{mn}^* \qquad \text{(a-3)}$$

where,

$$A = \frac{1}{\dfrac{\partial \kappa_s}{\partial \bar{\gamma}^p} \dfrac{\partial \bar{\gamma}^p}{\partial \varepsilon_{ij}^p} \dfrac{\partial f_p}{\partial \sigma_{ij}}} \qquad \text{(a-4)}$$

It is easy to show the following relation,

$$\frac{\partial \bar{\gamma}^p}{\partial \varepsilon_{ij}^p} = \frac{\partial \bar{\gamma}^p}{\partial \bar{\varepsilon}_{kl}^p} \frac{\partial \bar{\varepsilon}_{kl}^p}{\partial \varepsilon_{ij}^p} = \frac{\partial \bar{\gamma}^p}{\partial \bar{e}_{kl}^p} \frac{\partial \bar{\varepsilon}_{kl}^p}{\partial \varepsilon_{ij}^p} = \frac{\bar{e}_{ij}^p}{\bar{\gamma}^p} D(e_{mn}^p) \qquad \text{(a-5)}$$

Substitute Eq.a-5 into Eq.a-4, it is easy to obtain,

$$A = \frac{M_f^{*2}}{\bar{G}(M_f^* - \eta^*)^2 D(e_{mn}^p)} (\sigma_m + b) \frac{\bar{\gamma}^p \eta}{\bar{e}_{ij}^p \eta_{ij}}$$

References

(1) Adachi, T. and Oka, F. (1992) : "A elasto-plastic constitutive model for soft rock with strain softening," Proc. JSCE, No.445/III-18, pp.9-16.

(2) Adachi, T., Oka, F., Ohnishi, Y. and Zhang, F. (1991) : "A Constitutive Model for Rock Discontinuity with Strain Softening,"

Journal of Japan Society of Dam Engineering, Vol.3, pp.34-40.(In Japanese)
(3) Amadei, B. and Saeb, S. (1990) : "Constitutive method of rock joints," Barton and Stephansson (eds), pp.584-585.
(4) Barton, N. R. (1971) : "A relationship between joint roughness and joint shear strength," Proc. Int. Symp. on Rock Mech., Nancy, paper 1-8.
(5) Barton, N. R. (1973) : "Review of a new strength criterion for rock joint," Engng. Geol. Vol.4, No.4, pp.287-332.
(6) Naghdi, P. M. (1960) : "Stress-strain in plasticity and thermo-plasticity," Proc. 2nd Symp. on Naval Structural Mechanics, Pergamon Press, pp.121-169.
(7) Nishigawa, N. (1991) : "A experimental study on the strength and deformation of jointed rock," Bachelor Theses, Dept. of Civil Engng., Kyoto University(In Japanese).
(8) Oka, F. (1985) : "Elasto/viscoplastic constitutive equation with memory and internal variables," Computer and Geomechanics, Vol.1, pp.59-69.
(9) Oka, F. and Adachi, T. (1985) : "A constitutive equation of geologic materials with memory," Proc. 5th Int. Conf. on Numerical Method in Geomechanics, Vol.1, pp. 293-300.
(10) Skinas, C. A., Bandis, S. C. and Demiris, C. A. (1990) : "Experimental investigation and modeling of rock joint behavior under constant stiffness," Rock Joints, Barton & Stephansson(eds), A. A. Balkema, pp.301-308.

Chapter 4

Finite and joint element analyses based on the constitutive models with strain softening

4-1 FEM analysis

The finite element method is a powerful tool in solving boundary and initial value problems encountered in geotechnical engineering, especially for nonlinear problem in which few problems exist theoretical solution for boundary and initial value problems. However, for the materials with strain softening, great precaution had to be taken in finite element calculation. As many researchers, such as Bazant(1976), Schreyer et al.(1986), Frantziskonis and Desai(1987), Bazant and Belystschko(1987), Bazant(1988) pointed out that the strain softening is associated with localization. If no precaution is taken, the region of localization will depend on the size of the mesh used for spatial discretization. Inherent in finite element method is the problem that the region of localization that is smaller than the finite element size cannot be accurately represented. As the result, the predicted response will generally depend on the element size that the modeling of actual physical phenomena is lost. Obviously, this mesh-dependency is unacceptable. Many complicated numerical technical have been proposed to avoid such shortcoming. Adachi et al.(1991)[2),3),4)] published their researches that Adachi-Oka's model with strain softening is applicable for the numerical analysis of strain-hardening and strain-softening behavior of geological materials. Based on the model, finite element analysis can lead to a unique solution for initial value problem in Valanis's sense(Valanis, 1985) and the analytical results have very small dependency on mesh size.

In this chapter, the commonly used techniques in FEM for strain hardening material such as initial stress method is examined and compared with the new technique developed in this chapter.

For nonlinear problem, the whole strain increment can be divided into two parts, elastic and plastic strain increment

$$d\varepsilon_{ij} = d\varepsilon_{ij}^{e} + d\varepsilon_{ij}^{p} \tag{4-1}$$

According to Hooke's law

$$d\sigma_{ij} = Dd\varepsilon_{ij}^{e} = Dd\varepsilon_{ij} - Dd\varepsilon_{ij}^{p} \tag{4-2}$$

where D is the elastic stiffness matrix. In plane strain condition, only the whole strain increment $\Delta\varepsilon_z$ is equal to zero, the plastic strain increment $\Delta\varepsilon_z^p$ is not necessary to be zero. Therefore Eq.4-2 in plane strain condition will take the form as

$$\Delta\sigma_z = G\beta(\Delta\varepsilon_x + \Delta\varepsilon_y) - G[\beta(\Delta\varepsilon_x^p + \Delta\varepsilon_y^p) + \alpha\Delta\varepsilon_z^p] \tag{4-3}$$

and

$$\begin{Bmatrix} \Delta\sigma_x \\ \Delta\sigma_y \\ \Delta\tau_{xy} \end{Bmatrix} = G\begin{bmatrix} \alpha & \beta & 0 \\ \beta & \alpha & 0 \\ 0 & 0 & 1 \end{bmatrix}\begin{Bmatrix} \Delta\varepsilon_x \\ \Delta\varepsilon_y \\ \Delta\gamma_{xy} \end{Bmatrix} - G\begin{bmatrix} \alpha & \beta & \beta & 0 \\ \beta & \alpha & \beta & 0 \\ 0 & 0 & 0 & 1 \end{bmatrix}\begin{Bmatrix} \Delta\varepsilon_x^p \\ \Delta\varepsilon_y^p \\ \Delta\varepsilon_z^p \\ \Delta\gamma_{xy} \end{Bmatrix} \tag{4-4}$$

Eq.4-4 can also be written as

$$\{\Delta\sigma\} = [C]\{\Delta\varepsilon\} - \{\Delta\sigma^r\} \tag{4-5a}$$

in which,

$$[C]=G\begin{bmatrix} \alpha & \beta & 0 \\ \beta & \alpha & 0 \\ 0 & 0 & 1 \end{bmatrix} \tag{4-5b}$$

$$\{\Delta\sigma\} = \begin{Bmatrix} \Delta\sigma_x \\ \Delta\sigma_y \\ \Delta\sigma_{xy} \end{Bmatrix} \tag{4-5c}$$

$$\{\Delta\sigma^r\} = G\begin{Bmatrix} \alpha\Delta\varepsilon_x^p+\beta(\Delta\varepsilon_y^p+\Delta\varepsilon_z^p) \\ \alpha\Delta\varepsilon_y^p+\beta(\Delta\varepsilon_x^p+\Delta\varepsilon_z^p) \\ \Delta\gamma_{xy}^p \end{Bmatrix} \tag{4-5d}$$

where $\{\Delta\sigma^r\}$ is called as relaxed stress. The equilibrium equation and geometric equation in finite element analysis can also be expressed in following incremental way

$$\int_v [B]^T\{\Delta\sigma\}dV = \{\Delta F\} \tag{4-6}$$

$$\{\Delta\varepsilon\} = [B]\{\Delta u\} \tag{4-7}$$

where,

$$[B] = [B_1\ B_2 \cdots B_n] \tag{4-8a}$$

$$[B_i] = \begin{bmatrix} N_{i,x} & 0 \\ 0 & N_{i,y} \\ N_{i,y} & N_{i,x} \end{bmatrix} \tag{4-8b}$$

$$\{\Delta u\} = \{\Delta\delta_1\ \Delta\delta_2 \cdots \Delta\delta_n\}^T \ , \ \{\Delta\delta_i\} = \begin{Bmatrix} \Delta u_x^i \\ \Delta u_y^i \end{Bmatrix} \tag{4-8c}$$

Among the Eq.4-8, N_i $(i=1,n)$ is the shape function of finite element and n is the number of nodes in one element. Substituting Eq.4-5 and Eq.4-7 into Eq.4-6 will result in following equation

$$[K]\{\Delta u\} = \{\Delta R\} + \{\Delta R^r\} \tag{4-9a}$$

where

$$[K]=\int_v [B]^T[C][B]\,dV \tag{4-9b}$$

$$\{\Delta R^r\} = \int_V [B]^T \{\Delta\sigma^r\}\, dV \tag{4-9c}$$

$$\{\Delta\sigma^r\} = [C]\{\Delta\varepsilon^p\} \tag{4-9d}$$

In initial incremental stress method, the algorithm of the calculation can be expressed as

$$[K]\{\Delta u_n\}_{j+1} = \{\Delta R_n\} + \{\Delta R_n^r\}_{j+1} \tag{4-9e}$$

$$\{\Delta R_n^r\}_{j+1} = \int_V [B]^T \{\Delta\sigma_n^r\}_{j+1}\, dV \tag{4-9f}$$

$$\{\Delta\sigma_n\}_{j+1} = [C]\{\Delta\varepsilon_n\}_{j+1} - \{\Delta\sigma_n^r\}_{j+1} \tag{4-9g}$$

$$\{\Delta\sigma_n^r\}_{j+1} = [C]\{\Delta\varepsilon_n^p\}_j \tag{4-9h}$$

In Eq.4-9e to Eq.4-9h, n denotes nth incremental step and j denotes jth iteration. The criteria of convergence for this method is that the difference of $\{\Delta\sigma_n^r\}$ between two iterations will be less than any given infinitesimal value.

For the constitutive model with strain softening described in chapter 2, it is easy to show that there exist a relation such that,

$$\{\Delta\sigma^r\} = \left\{h(\sigma_{ij}, \sigma_{ij}^*, \varepsilon_{ij}^p)\ \frac{\Delta z}{\tau}\right\} \tag{4-10}$$

in which the function $\{h(x)\}$ can be easily found out by some algebra. If the stress history tensor take the form as Eq.2-26

$$\sigma_{ij}^* = \frac{1}{\tau}\int_0^z \exp(-\frac{z-z'}{\tau})\sigma_{ij}(z')dz' \tag{2-26}$$

and let $\Delta z \Rightarrow 0$, Eq.4-10 can also be expressed as

$$\left\{\frac{d\sigma^r}{dz}\right\} = \left\{h(\sigma_{ij}(z)\,,\, \sigma_{ij}^*(z)\,,\, \varepsilon_{ij}^p(z))\ \frac{1}{\tau}\right\} = \{F(\{\sigma^r(z)\}\,,\, z)\} \tag{4-11a}$$

By denoting the symbol as

$$\{\sigma^r\} = \boldsymbol{\sigma}^r \tag{4-11b}$$

Eq.4-11a can be rewritten as

$$\frac{d\boldsymbol{\sigma}^r}{dz} = \boldsymbol{F}(\boldsymbol{\sigma}^r(z)\,,\, z) \tag{4-11c}$$

For such kind of ordinary differential equations of first order, Runge-Kutta method seems very suitable in obtaining the numerical solution. The method dose not need any specific condition that the function $\boldsymbol{F}(t,y)$ in Eq.4-12 must satisfied for convergence, if and only if the function $\boldsymbol{F}(t,y)$ has a continuous forth order differential and satisfy the Lipschize condition expressed as

for $\begin{matrix} a \le t \le b \\ -\infty \le \boldsymbol{y} \le \infty \end{matrix}$, there exist a positive L which is independent of $(t, \boldsymbol{y})$

and enable the following relation be valid

$$|\boldsymbol{F}(t, \boldsymbol{y}_1) - \boldsymbol{F}(t, \boldsymbol{y}_2)| \le L|\boldsymbol{y}_1 - \boldsymbol{y}_2| \tag{4-11d}$$

where $|\boldsymbol{y}_1 - \boldsymbol{y}_2|$ denotes the distance between two points $\boldsymbol{y}_1$ and $\boldsymbol{y}_2$ in the norm of $|\bullet|$.

It is obvious that the Adachi-Oka's constitutive model with strain softening and other models proposed in previous chapters satisfy the condition because function h(x) is a combination of simple functions such as exponential and hyperbolic function.

For the associated differential equations expressed in Eq.4-12, the formulas of the Runge-Kutta method can be expressed with Eq.4-13

$$\frac{dy}{dt} = \boldsymbol{F}(t\,,\, \boldsymbol{y}) \tag{4-12}$$

$$K_1 = \Delta t\, F(t_n, y_n) \tag{4-13a}$$

$$K_2 = \Delta t\, F(t_n + \frac{\Delta t}{2}, y_n + \frac{K_1}{2}) \tag{4-13b}$$

$$K_3 = \Delta t\, F(t_n + \frac{\Delta t}{2}, y_n + \frac{K_2}{2}) \tag{4-13c}$$

$$K_4 = \Delta t\, F(t_n + \Delta t, y_n + K_3) \tag{4-13d}$$

$$y_{n+1} = y_n + (K_1 + 2K_2 + 2K_3 + K_4)/6 \tag{4-13c}$$

In order to investigate the validity of the method proposed(the method here is called as generalized Runge-Kutta method) in this study, a boundary value problem depicted in the Fig.4-1 is considered with two different numerical methods. The boundary value problem is under plane strain condition. The body which is pre-consolidated at confining pressure of 2 kgf/cm^2 is subjected to uniform elongation deformation(unloading of σ_1).

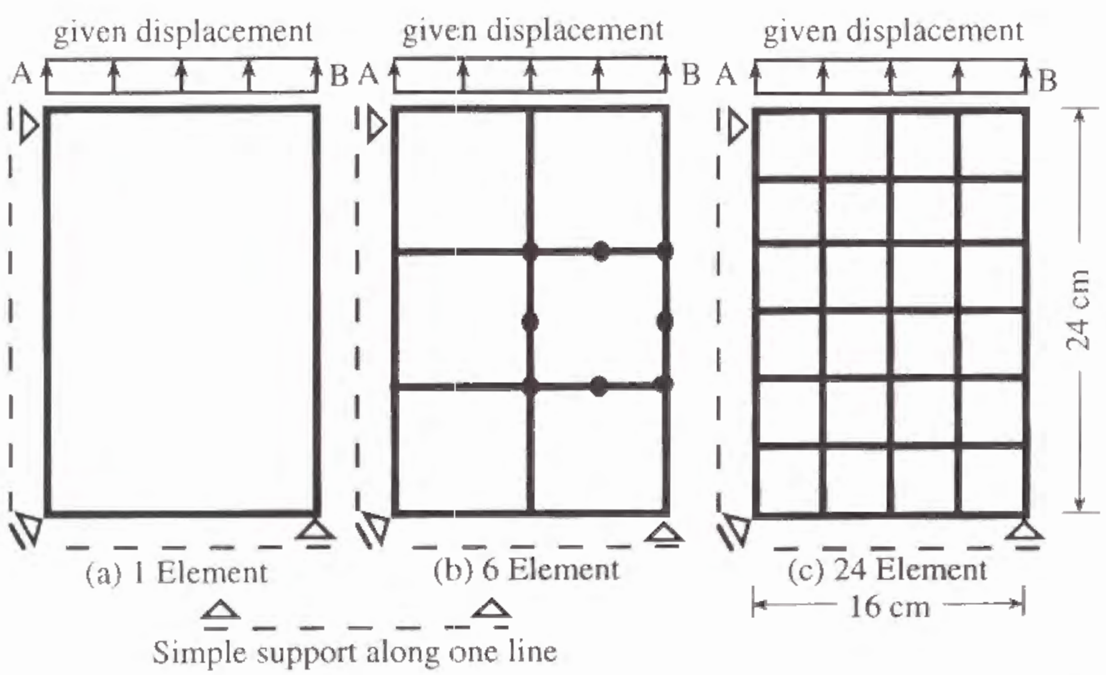

Fig.4-1 Finite element meshes of the specimen undergone elongation in plane strain condition(no restriction)

Because of the symmetric condition, only one forth(with the width of 16 cm and the length of 24 cm) of the specimen is considered. The body is elongated by 2.4 cm, which means that the ε_y experienced a maximum strain of 10.0 %.

Table 4-1 Material parameters of the specimen considered in Fig.4-1,4-5

K(kgf/cm^2)	30.0	σ_{mb}(kgf/cm^2)	20.0
G(kgf/cm^2)	20.0	b(kgf/cm^2)	2.00
α_R (M_f^*)	1.22	$\overline{M}_m$	1.00
β_R	1.00	τ	0.023
G'	100.0		

σ_0=2.00(kgf/cm^2)

The material parameters are listed in Table 4-1. In order to investigate the mesh size effect, three kinds of mesh size, that is, 1, 6 and 24 finite elements are considered for this boundary value problem. It is found that the results obtained from three meshes are the same. The following results concerning this boundary value problem are obtained from the mesh of 24 elements.

(a) Relations of octahedral stress-stress history-strain

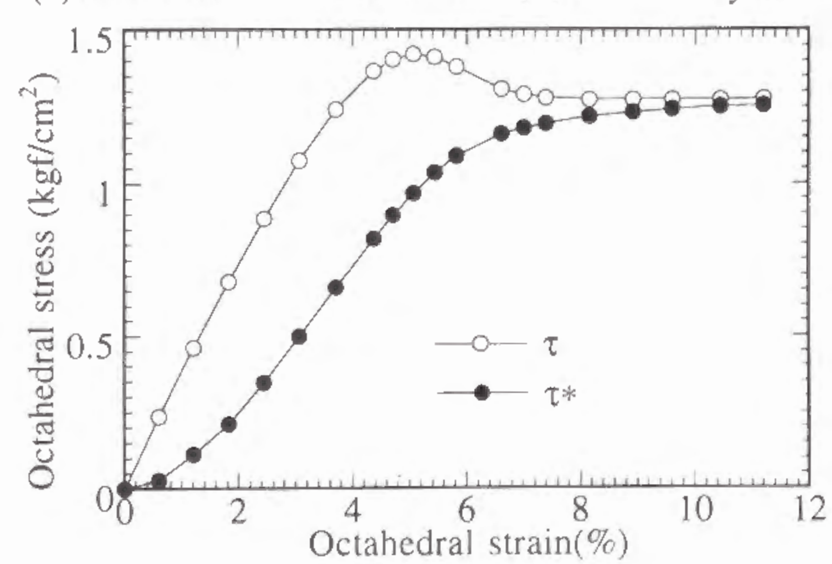

(b) Relation of axial load-displacement

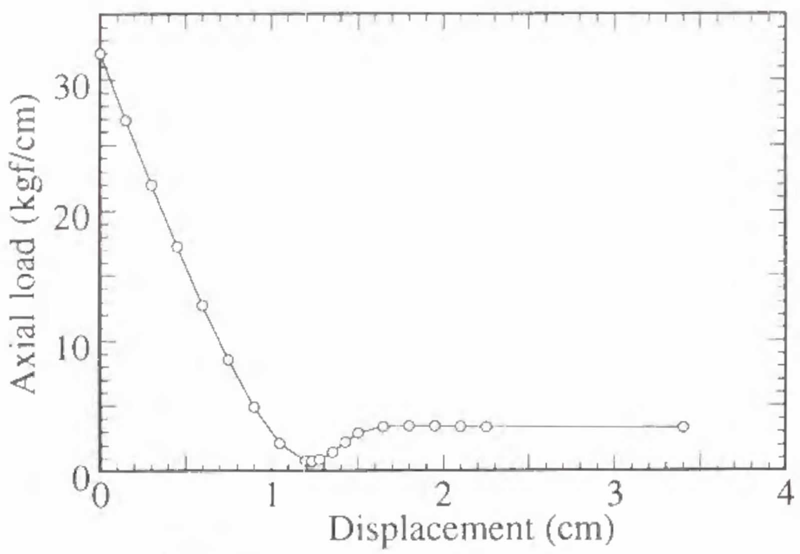

Fig.4-2 Results of the problem shown in Fig.4-1

Fig.4-2 shows the theoretical result(theoretical result here means the convergent result that obtained from no matter what kind of numerical procedures) for the boundary value problem shown in Fig.4-1.

Fig.4-3 shows the calculating results using initial stress method with different incremental steps. From the figure, it is evident that even for such simple case of one dimensional boundary value problem, the minimum steps needed to obtain convergent solution are 160 steps.

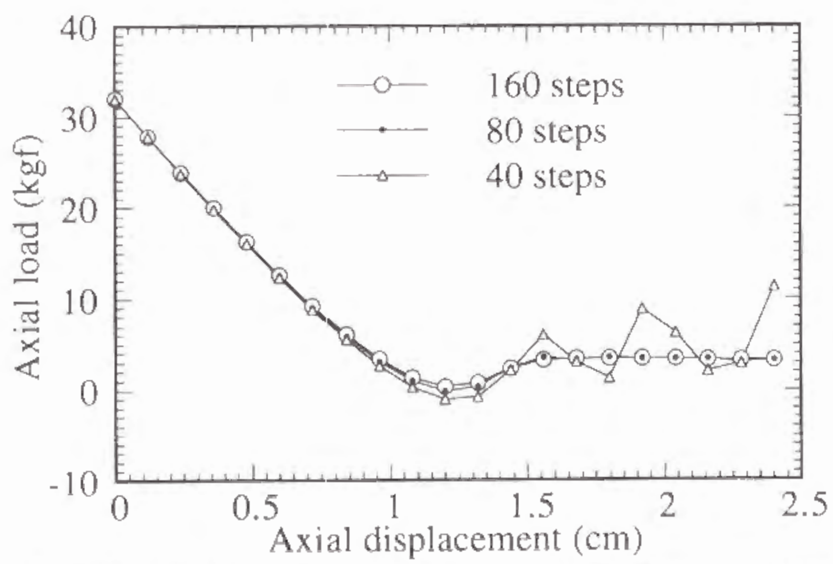

Fig.4-3 Influence of load-steps in initial stress method

Fig.4-4 shows the calculating results with generalized Runge-Kutta method. It can be seen from the figure that the minimum steps to obtain convergent solution are 40 steps.

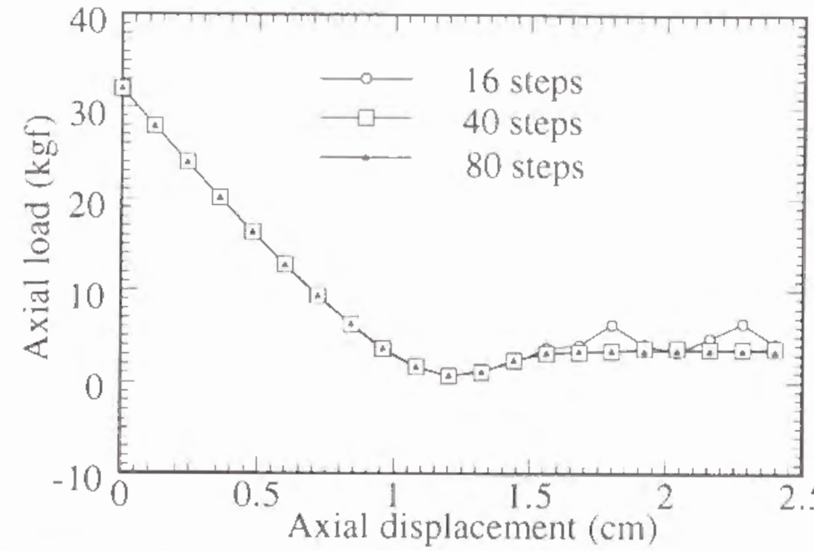

Fig.4-4 Influence of load-steps in generalized Runge-Kutta method

Fig.4-5 shows the body under different boundary condition. It can be seen from the figure that the deformation along horizontal direction at B is restricted. In such case the problem is no longer one dimensional problem.

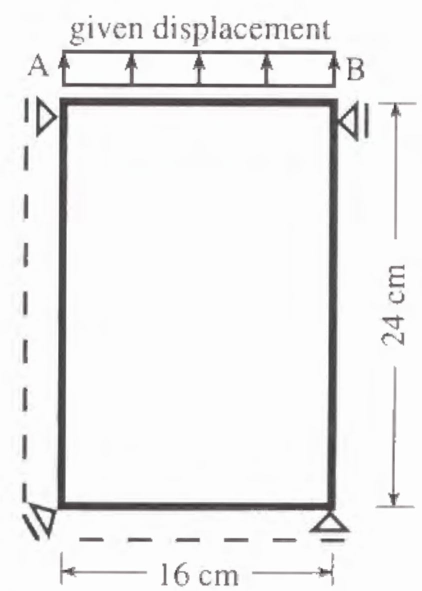

Fig.4-5 Finite element meshes of the specimen undergone elongation (restriction exists)

Fig.4-6 and Fig.4-7 shows the calculating results for the problem with the methods mentioned above. Here it can be seen that the convergent steps for the two methods in present situation is almost the same. In both case, 400 steps are needed for the convergence. If taking into consideration the fact that the generalized Runge-Kutta method needs four iterations for one step. It seems the method has no advantage over the initial stress method. As a matter of fact, which method is better will depend on different problem and different boundary condition. As it can be seen later, the new method can always get a convergent solution though sometimes it may need a large number of calculating steps.

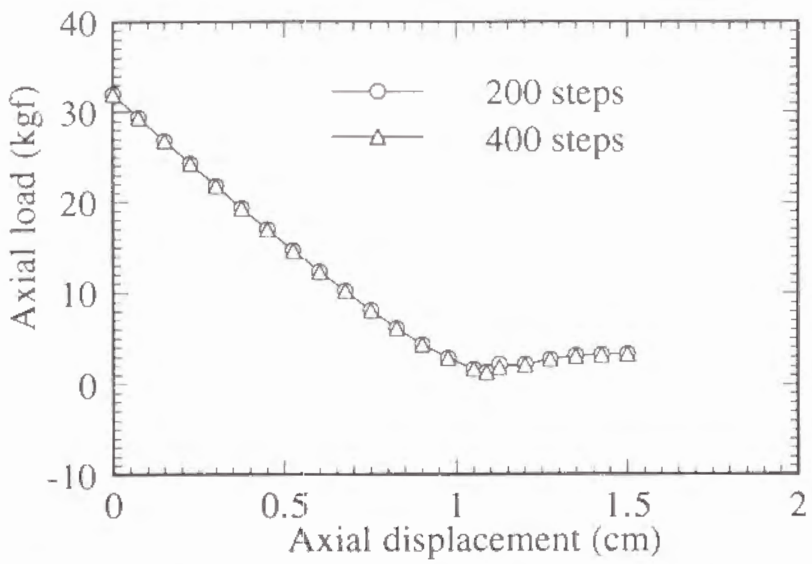

Fig.4-6 Influence of load-steps in generalized Runge-Kutta method

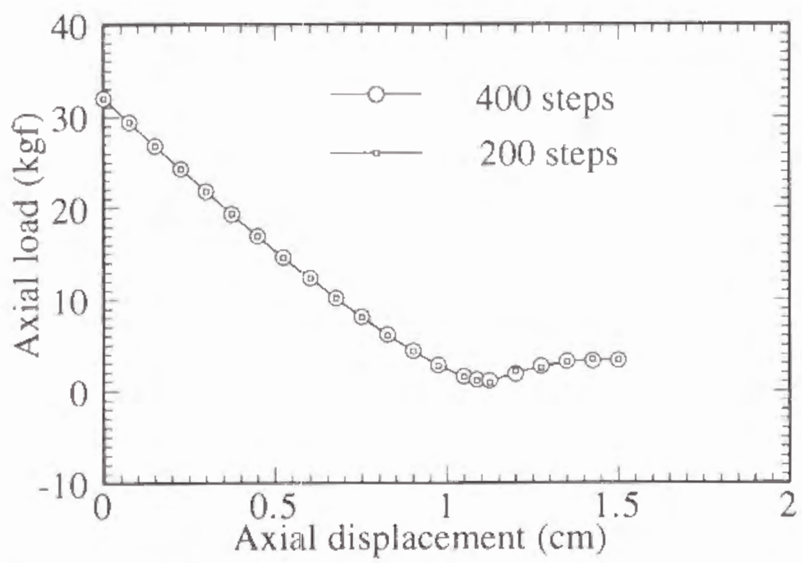

Fig.4-7 Influence of load-steps in initial stress method

4-2 Finite and joint element analysis

In the chapter 3, a new constitutive model of strain softening dealing with discontinued behavior in geological material is proposed. In this section, it is tried to develop a finite and joint element analytical method based on this new model. As for joint element, the following relation is valid between stress and relative displacement

$$\{\sigma\} = [K]\{w^e\} \tag{4-14}$$

where,

$$\{w^e\} = \{w\} - \{w^p\} \tag{4-15}$$

$$\{w\} = \begin{Bmatrix} w_s \\ w_n \end{Bmatrix}, \quad \{w^p\} = \begin{Bmatrix} w_s^p \\ w_n^p \end{Bmatrix}, \quad \{\sigma\} = \begin{Bmatrix} \sigma_s \\ \sigma_n \end{Bmatrix} \tag{4-16}$$

$$[K] = \begin{Bmatrix} k_s & \\ & k_n \end{Bmatrix} \tag{4-17}$$

where

w_s, σ_s: shear displacement and shear stress,

w_n, σ_n: normal displacement and normal stress,

k_s, k_n: shear and normal stiffness which can be determined by direct shear test and one axial compression test.

In joint element analysis, it is usually assumed that k_n takes a very large value when compression takes place and a very small value when expansion takes place. The reason why making such assumption is that joint element is artificially introduced to simulate discontinuous deformation along the direction paralleled to joint and finite elements on both sides of joint cannot penetrate each other when compression. Therefore, the elastic normal displacement will be very small in compression and the relationship between normal stress and relative normal displacement will take the form as

$$\sigma_n = k_n(w_n - w_n^p) \tag{4-18}$$

$$k_n = \begin{cases} k_{nc}(>10^6 kgf/cm^3) & when\ \sigma_n>0 \\ k_{nt}(<1\ kgf/cm^3) & when\ \sigma_n<0 \end{cases} \tag{4-19}$$

where k_{nc} and k_{nt} stand for the normal stiffness when normal stress is compressive and extensive respectively.

However, in present analysis, it is not necessary to make such assumption, because the thickness of the joint element is not necessary to be zero as explained in Chapter 3. When normal stress become minus which means expansion occur, k_n will take a very small value to stand for the state at which there is no interaction between joint surfaces.

If the linear shape function is used in four-node joint element, displacement vector $\{w\}$ will take the form as follow

$$\{w\} = 1/2\begin{bmatrix} A & 0 & B & 0 & -B & 0 & -A & 0 \\ 0 & A & 0 & B & 0 & -B & 0 & -A \end{bmatrix}\{\delta\}^e \qquad (4\text{-}20)$$

where

$$\{\delta\}^e = \{u_1\ v_1\ u_2\ v_2\ u_3\ v_3\ u_4\ v_4\}^T \qquad (4\text{-}21)$$

$$A = 1 - \frac{2x}{L}\ , \quad B = 1 + \frac{2x}{L} \qquad (4\text{-}22)$$

By defining matrix $[D]$ as

$$[D] = \begin{bmatrix} A & 0 & B & 0 & -B & 0 & -A & 0 \\ 0 & A & 0 & B & 0 & -B & 0 & -A \end{bmatrix} \qquad (4\text{-}23)$$

Eq.4-20 can be written as

$$\{w\} = \frac{1}{2}[D]\{\delta\}^e \qquad (4\text{-}24)$$

According to virtual energy theory, it is able to obtain

$$\{\Delta\delta\}^T\{F\}^e = \int_{-l/2}^{l/2}\{\Delta w\}^T\{\sigma\}\,dx \qquad (4\text{-}25)$$

By substituting Eq.4-24 into Eq.4-25, the following equation can be obtained:

$$\{F\}^e = \frac{1}{4}\int_{-l/2}^{l/2}[D]^T[K][D]dx\{\delta\}^e - \frac{1}{2}\int_{-l/2}^{l/2}[D]^T[K]\{w^p\}dx \qquad (4\text{-}26)$$

By defining the following variables as

$$\overline{[K]} = \frac{1}{4}\int_{-l/2}^{l/2}[D]^T[K][D]dx \qquad (4\text{-}27)$$

and

$$\{R\}^e = \frac{1}{2}\int_{-l/2}^{l/2}[D]^T[K]\{w^p\}dx\ , \qquad (4\text{-}28)$$

Eq.4-26 can be expressed as

$$\{F\}^e = \overline{[K]}\{\delta\}^e - \{R\}^e \qquad (4\text{-}29)$$

Using the same way, it is able to obtain the incremental form of Eq.4-29 as

$$\{\Delta F\}^e = \overline{[K]}\{\Delta\delta\}^e - \{\Delta R\}^e \qquad (4\text{-}30)$$

The detailed expression of stiffness matrix in Eq.4-30 is

$$\overline{[K]} = \frac{L}{6}\begin{bmatrix} 2k_s & & & & & & & \\ 0 & 2k_n & & & & \textit{Symmetry} & & \\ k_s & 0 & 2k_s & & & & & \\ 0 & k_n & 0 & 2k_n & & & & \\ -k_s & 0 & -2k_s & 0 & 2k_s & & & \\ 0 & -k_n & 0 & -2k_n & 0 & 2k_n & & \\ -2k_s & 0 & -k_s & 0 & k_s & 0 & 2k_s & \\ 0 & -2k_n & 0 & -k_n & 0 & k_n & 0 & 2k_n \end{bmatrix} \qquad (4\text{-}31)$$

The stiffness matrix of Eq.4-31 is established in local coordinates. In joint element analysis, however, joint element may not be horizontal. In such case, the relation between local and global coordinates is given in following transformation equation

$$\begin{Bmatrix} x \\ z \end{Bmatrix} = \begin{bmatrix} \cos\beta & \sin\beta \\ -\sin\beta & \cos\beta \end{bmatrix} \begin{Bmatrix} X \\ Z \end{Bmatrix} = [t] \begin{Bmatrix} X \\ Z \end{Bmatrix} \tag{4-32}$$

where [X,Z] and [x,z] stand for global and local coordinates respectively. By defining

$$[T] = \begin{bmatrix} t & & & \\ & t & & \\ & & t & \\ & & & t \end{bmatrix} \tag{4-33}$$

the relation between local and whole node-displacement, node-force and stiffness matrix can then be expressed as

$$\{F\}^e = [T]\{\tilde{F}\}^e \tag{4-34}$$

$$\{\delta\}^e = [T]\{\tilde{\delta}\}^e \tag{4-35}$$

$$[\tilde{K}] = [T]^T [\tilde{K}][T] \tag{4-36}$$

$$\{\Delta R\}^e = [T]\{\Delta\tilde{R}\}^e \tag{4-37}$$

Eq.4-30 can be written in global coordinates as

$$\{\Delta\tilde{F}\}^e = [\tilde{K}]\{\Delta\tilde{\delta}\}^e - \{\Delta\tilde{R}\}^e \tag{4-38}$$

In above equations, the symbol '~' is corresponding to global coordinates. The detail expression for Eq.4-37 can be obtained by following reasoning,

$$\{\Delta R\}^e = \frac{1}{2}\int_{-L/2}^{L/2} [D]^T [K] \{\Delta w^p\}^e dx$$

$$= \frac{L}{2} \begin{vmatrix} I_{2\times2} \\ I_{2\times2} \\ -I_{2\times2} \\ -I_{2\times2} \end{vmatrix} [K]\{\Delta w^p\}^e$$

$$= \frac{L}{2}\left\{k_s\Delta w_s^p \; k_n\Delta w_n^p \; k_s\Delta w_s^p \; k_n\Delta w_n^p \; -k_s\Delta w_s^p \; -k_n\Delta w_n^p \; -k_s\Delta w_s^p \; -k_n\Delta w_n^p\right\}^T \tag{4-39}$$

The corresponding expression in global coordinate is

$$\{\Delta\tilde{R}\}^e = [T]^T\{\Delta R\}^e$$

$$= \frac{L}{2}\begin{Bmatrix} k_s\Delta w_s^p\cos\beta - k_n\Delta w_n^p\sin\beta \\ k_s\Delta w_s^p\sin\beta + k_n\Delta w_n^p\cos\beta \\ k_s\Delta w_s^p\cos\beta - k_n\Delta w_n^p\sin\beta \\ k_s\Delta w_s^p\sin\beta + k_n\Delta w_n^p\cos\beta \\ -(k_s\Delta w_s^p\cos\beta - k_n\Delta w_n^p\sin\beta) \\ -(k_s\Delta w_s^p\sin\beta + k_n\Delta w_n^p\cos\beta) \\ -(k_s\Delta w_s^p\cos\beta - k_n\Delta w_n^p\sin\beta) \\ -(k_s\Delta w_s^p\sin\beta + k_n\Delta w_n^p\cos\beta) \end{Bmatrix} \tag{4-40}$$

The expression of the stress at originate of local coordinate is

$$\{\Delta\sigma\}^e_{x=0} = [K]\{\Delta w^e\}^e_{x=0}$$

$$= [K](\{\Delta w\}^e - \{\Delta w^p\}^e)_{x=0}$$

$$= [K](\frac{1}{2}[I_{2\times2}\; I_{2\times2}\; -I_{2\times2}\; -I_{2\times2}]\{\Delta\delta\}^e - \{\Delta w^p\}^e)$$

$$= [K](\frac{1}{2}[t_{2\times2}\; t_{2\times2}\; -t_{2\times2}\; -t_{2\times2}]\{\Delta\tilde{\delta}\}^e - \{\Delta w^p\}^e) \tag{4-41}$$

For the first step, a very simple boundary value problem shown in Fig.4-8a is considered. The joint material considered here is the standard Toyoura dense sand whose material parameters are given in Table 4-2. The finite element is supposed to be elastic and has the material parameters as, E=2000(kgf/cm^2); ν=0.3. A uniform displacement is given along the right side of the upper part. Such boundary value problem is corresponding to direct shear test. Fig.4-8b shows the relationship of shear stress and stress

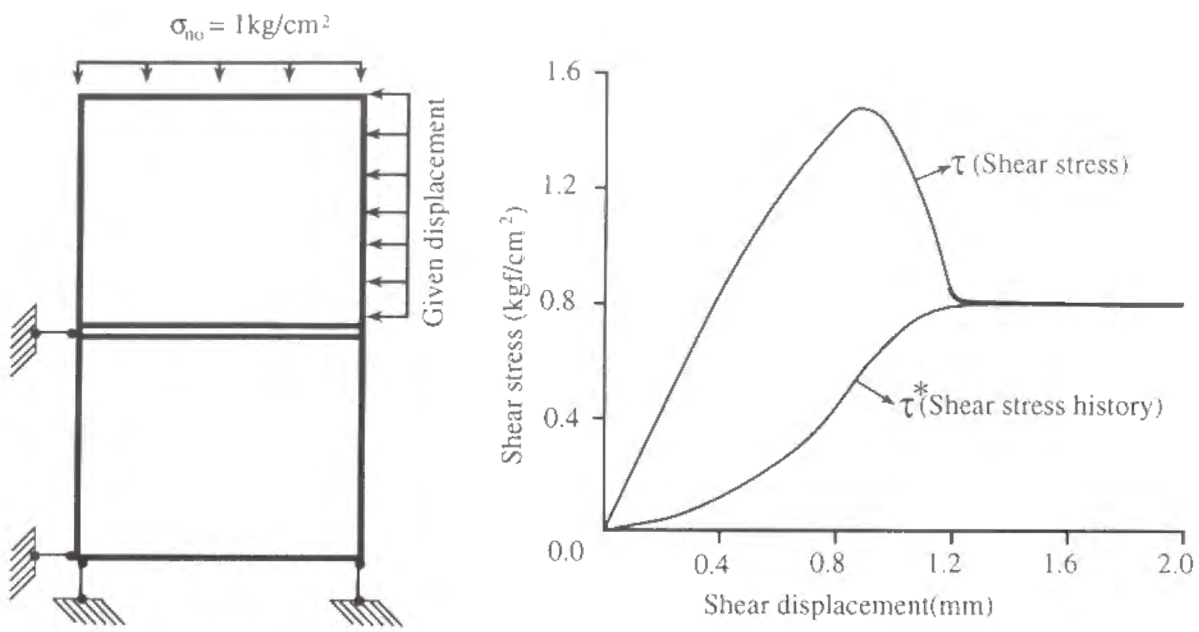

(a)Mesh of FEM and JEM (b) Calculated relation of shear stress-displacement

Fig.4-8 Analysis of direct shear test with JEM and FEM

history vs. shear displacement. Compared with Fig.3-3a, it is easy to see that the calculated result obtained from the boundary value problem with joint element analysis is similar to the theoretic one.

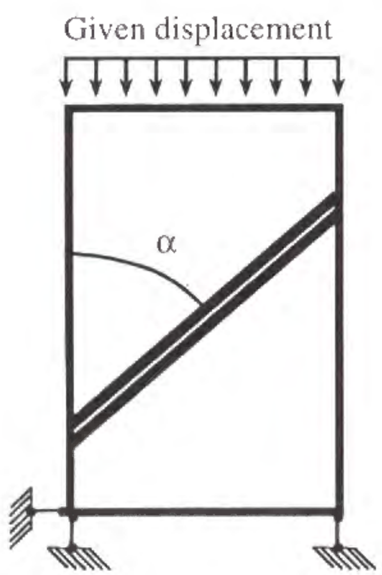

Fig.4-9 Mesh of JEM and FEM used in the boundary value problem of restricted dilatancy

Fig.4-9 shows another boundary value problem considered in present method. The material of the joint is the same as the one shown in Fig.4-8 and its material parameters are given in Table 4-2. Only the angle between x-axis and joint is no longer equal to zero. Being different from the boundary value problem shown in Fig.4-8 that is sheared under constant normal stress, the boundary value problem considered now is the shearing problem that the normal stress is changed during loading. It is still assumed here that the finite element is the same elastic body as shown in Fig.4-8.

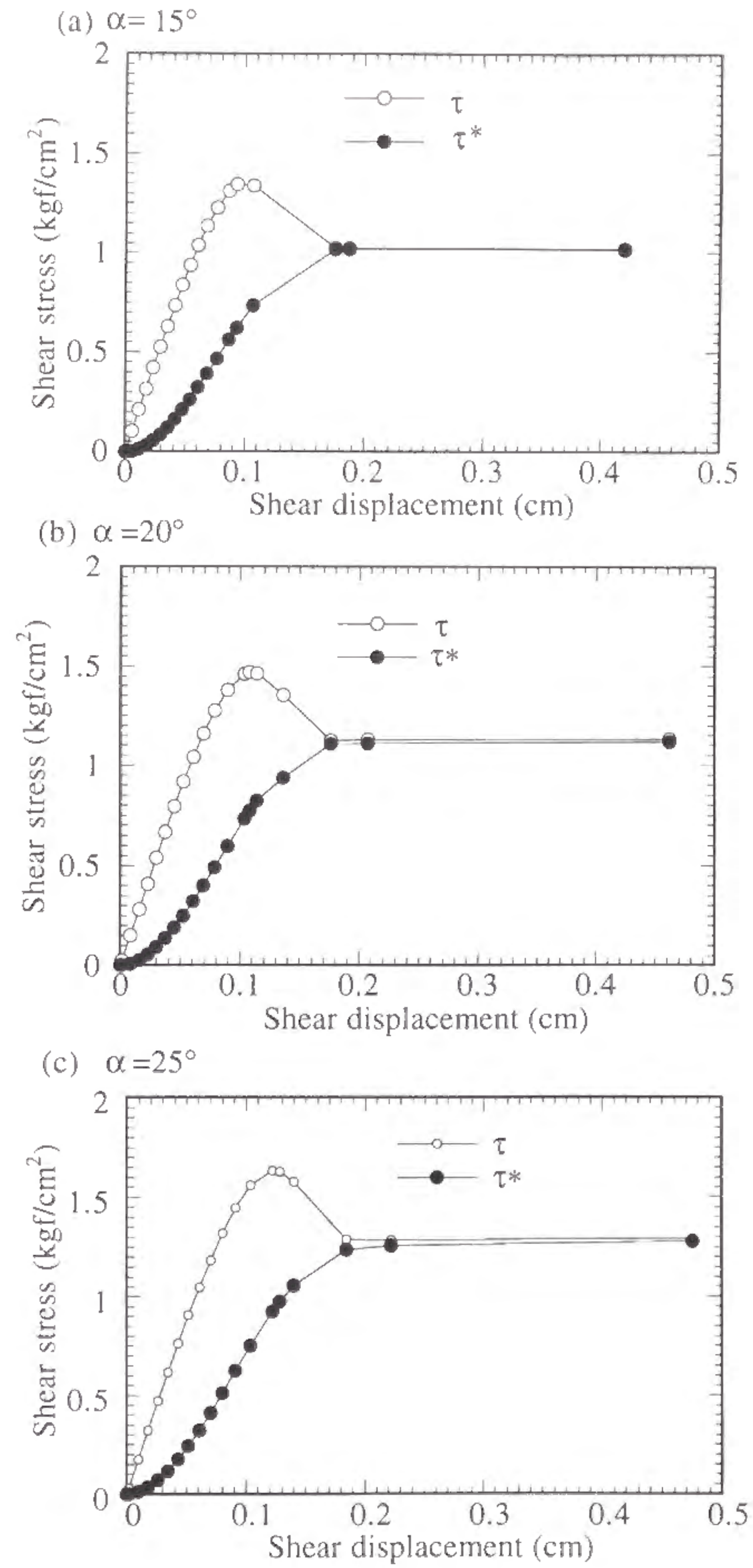

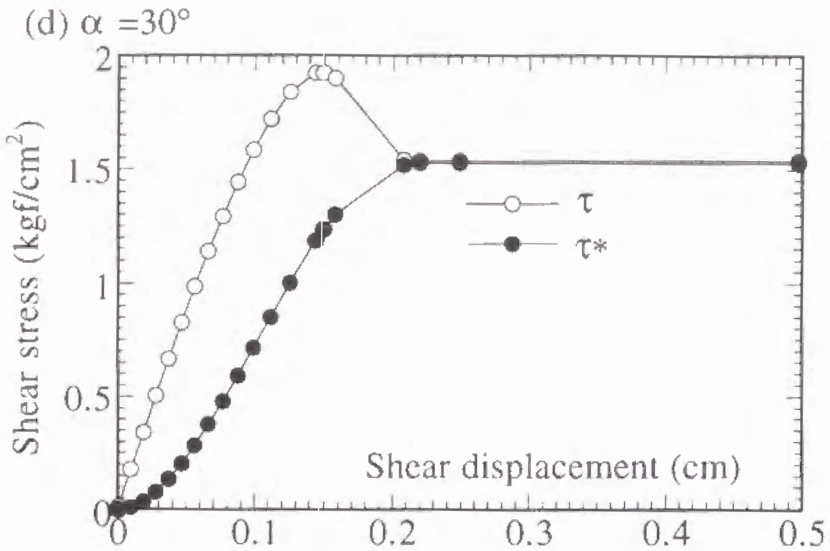

Fig.4-10 Relationships of shear stress and stress history vs. shear displacement at different angles of joint

Table 4-2 Material parameters of the specimen shown in Fig.4-8, 4-9

$k_s(kgf/cm^3)$	18.0	$\sigma_{mb}(kgf/cm^2)$	60.0
$k_n(kgf/cm^3)$	110.0	$b(kgf/cm^2)$	0.14
M_f^*	4.25	$\overline{M}_m$	1.61
$\overline{G}'(1/cm)$	500.0	τ	0.057

Fig.4-10 shows the relationships of shear stress and stress history vs. shear displacement at different angles of joint. In the calculation, the angle α changes from 0° to 45°. When α=0°, it is equivalent to direct shear test under the condition of constant normal stress. Theoretically, the possible range of angle in which the strain softening may occur is from 0°~$tan^{-1}M_f^*$, because of the fact that when the α is larger than $tan^{-1}M_f^*$, the normal stress history σ_m^* increase more rapid than shear stress history τ^* and consequently critical state will never be reached.

Fig.4-11 is the stress paths in σ_m-$(2J_2)^{1/2}$ plane for different angles. In the calculation, the steps need to obtain convergent result is different for different angle. Detailed results obtained from generalized Runge-Kutta method are listed as follow

α=15°: 2400 steps; α=20°: 1200 steps;

α=25°: 2400 steps; α=30°: 4800 steps.

While the initial stress method did not converge when the steps is less than 12000 steps.

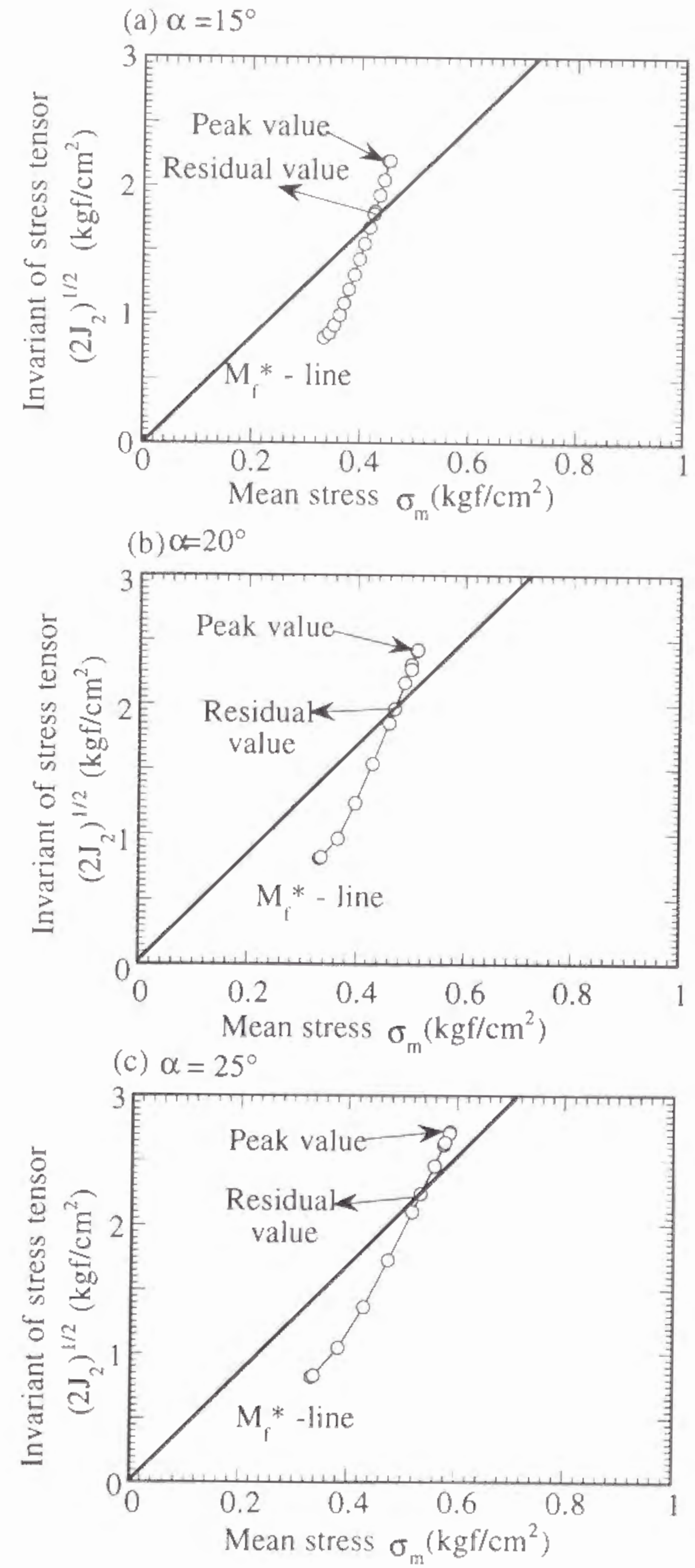

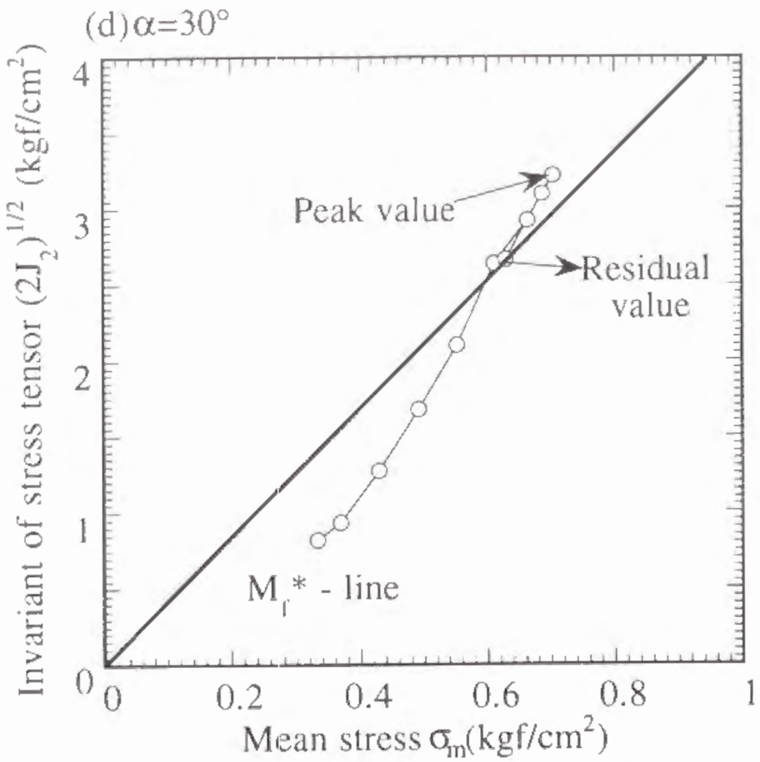

Fig.4-11 Stress paths in σ_m-$(2J_2)^{1/2}$ plane at different angles

4-3 Numerical analysis of conventional triaxial test of sedimentary rock

Many geotechnical engineering projects, such as bridge and tunnel, are often constructed in the ground of soft rock. The great attention has been paid to the research on soft rock. Many researches on this field, including laboratory tests, constitutive model and numerical analysis have been reported. Generally speaking, the mechanical behavior of soft rock such as sedimentary rock is elasto-plastic, dilatant, strain hardening-strain softening and time dependent. In this section, it is tried to simulate the mechanical behavior of sedimentary rock in conventional triaxial test based on constitutive model with strain softening using finite element method.

Saturated samples of Ohya stone(porous tuff) deposited in Miocene Epoch of Tertiary Period were tested in previous study(Adachi and Ogawa, 1980). Physical properties of the material are listed in Table 2-1.

In present finite element analysis, only one case, that is, the confining pressure of 10 kgf/cm^2 is taken under consideration. The comparison between experimental result and theoretical result obtained from the constitutive model with strain-softening is given in Fig.2-4(c).

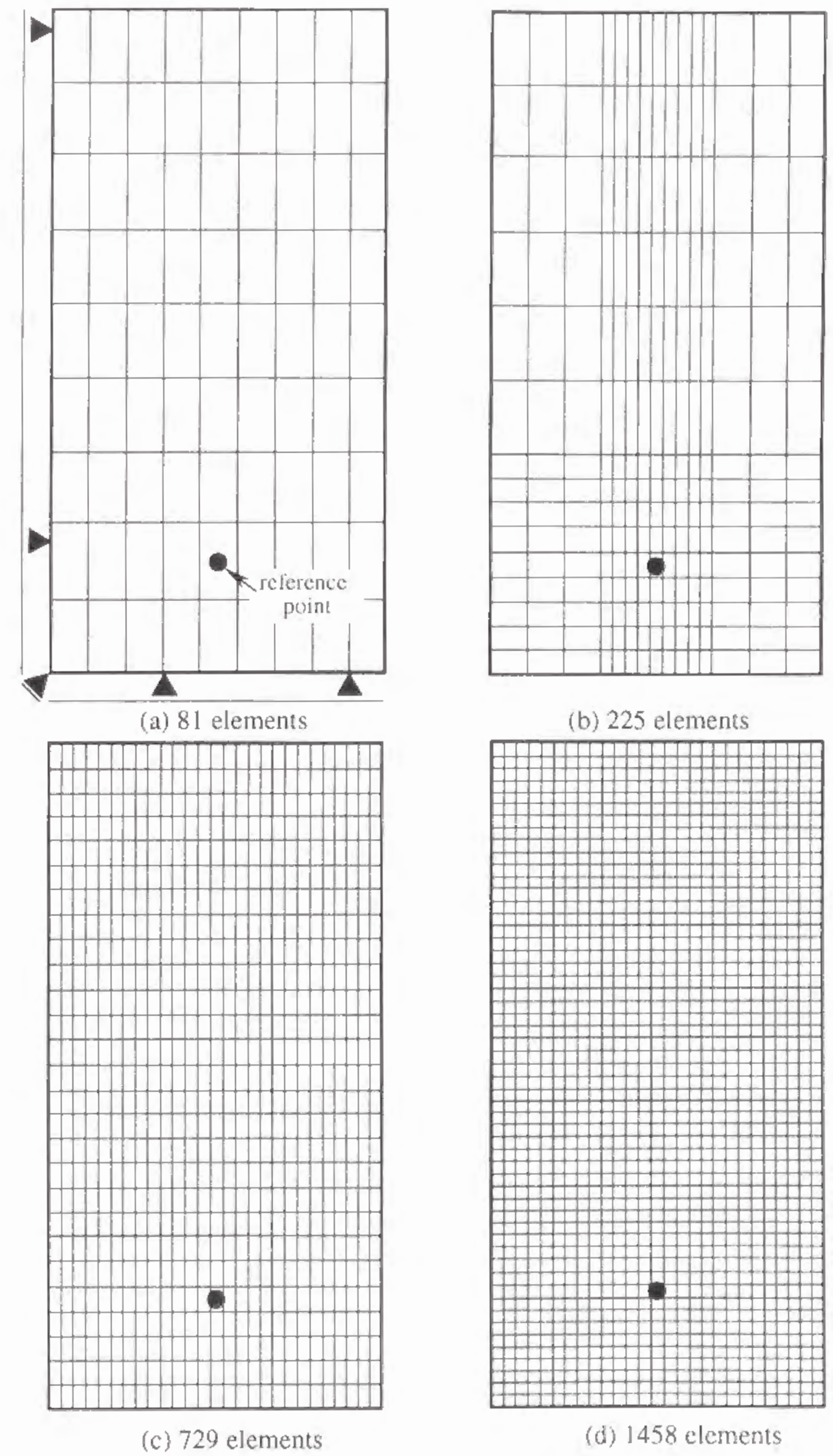

Fig.4-12 Finite element meshes used in calculation

The purpose of the finite element analysis here is to investigate (1) the mesh-size influence in finite element analysis concerning softening materials (2) the influence of the friction between sample and loading cap which is difficult to be free from in conventional triaxial tests.

In present analysis, a finite element program in axisymmetric condition is used to simulate the triaxial tests. Two kinds of boundary condition are considered. One is related to the ideal conventional triaxial test, that is, there exists no friction between testing sample and loading cap. Another is related to the actual conventional triaxial test in which friction exists between testing sample and loading cap.

Because of the symmetric condition, only one fourth of the sample is considered in finite element meshes. For the first kind of boundary condition, only the displacement in y direction along the button line is fixed. For the second kind of boundary condition, in order to simulate the friction, a concentrated force in x direction is applied at the central point of surface line. The loads in both cases are applied with given displacement which corresponds to strain controlled loading in the experiments. Fig.4-12 shows the finite element meshes used in the calculation. In all calculations, axial displacement of 0.4 cm, which corresponds to ε_{axial}=8%, is applied in 800 steps.

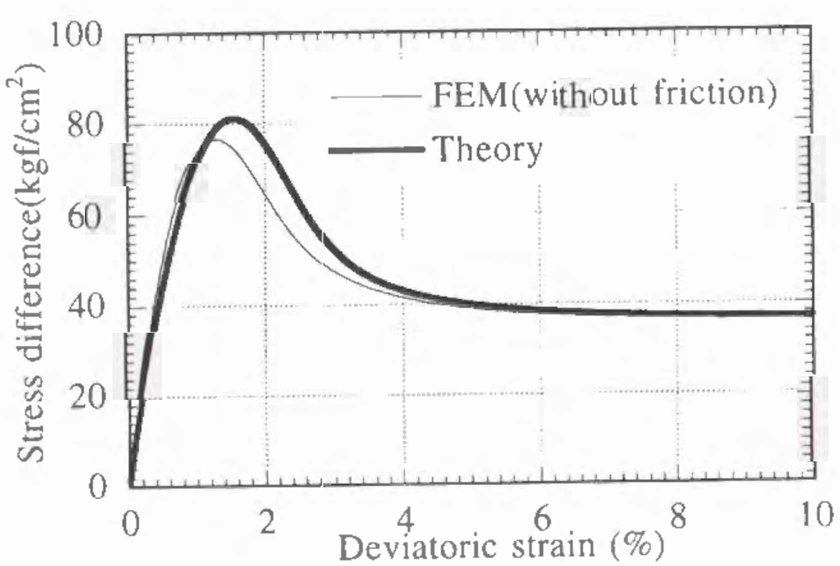

Fig.4-13 Comparison between theoretical and calculated stress-strain relation(without friction)

Case I Without friction

Fig.4-13 shows the comparison between theoretical and finite element analytical results of stress difference-deviatoric strain relation. The peak value obtained from finite element analysis is 5% less than theoretical one while the residual values are the same. Because the contact surface between sample and loading cap is free from friction, the distribution of the displacement and strain in the sample are uniform even in residual state. Fig.4-14 shows the deformation pattern and stress distribution at residual state. Same result can be obtained for different spatial discretization of 81, 225, 729 and 1458 elements. No localization is observed in present boundary value problem. It is evident form the figures that in ideal condition, the present analysis can well simulate the ideal conventional triaxial test.

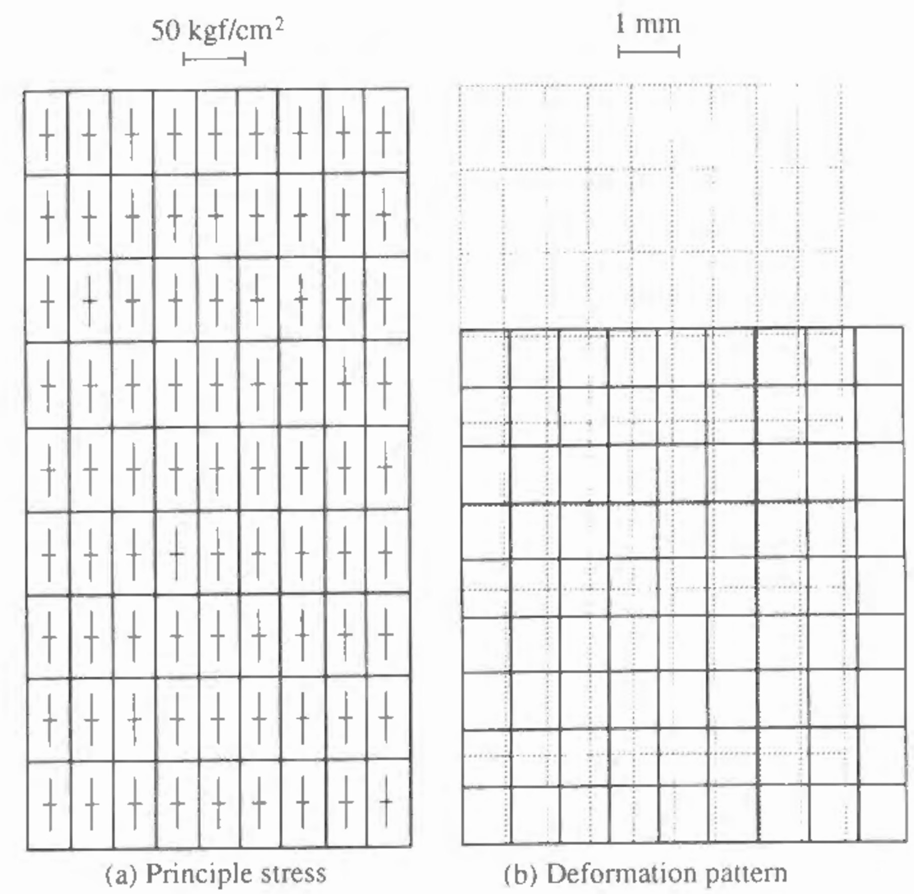

Fig.4-14 Distribution of principal stress and deformation pattern at residual state(without friction)

Case II With friction

Fig.4-15 shows the contours of octahedral strain at different loading stages obtained from finite elements analysis in which the friction between sample and loading cap is considered. The concentrated load acting at the frictional surface is supposed to be a very small value of 0.01 kgf. Such friction probably exists in actual conventional triaxial test. As the same result can be obtained for different spatial discretization of 81, 225, 729 and 1458 elements, only the results from the analysis of 1458 elements are given in Fig.4-15. Before the stress state reaches to peak value which occurs at the state of undergone approximately 1% of axial strain, such little friction shows no evident influence on the uniformly distributed strain. When peak strength is reached and softening occurs, the influence become prominent. In Fig.4-15, (a), (b) and (c) represent the distribution of octahedral strain at the stages at which the sample undergone 2%, 3% and 3.1% axial strain respectively. From the figure, it is quite clear that the larger the axial strain is, the more serious disturbance of strain distribution will occur.

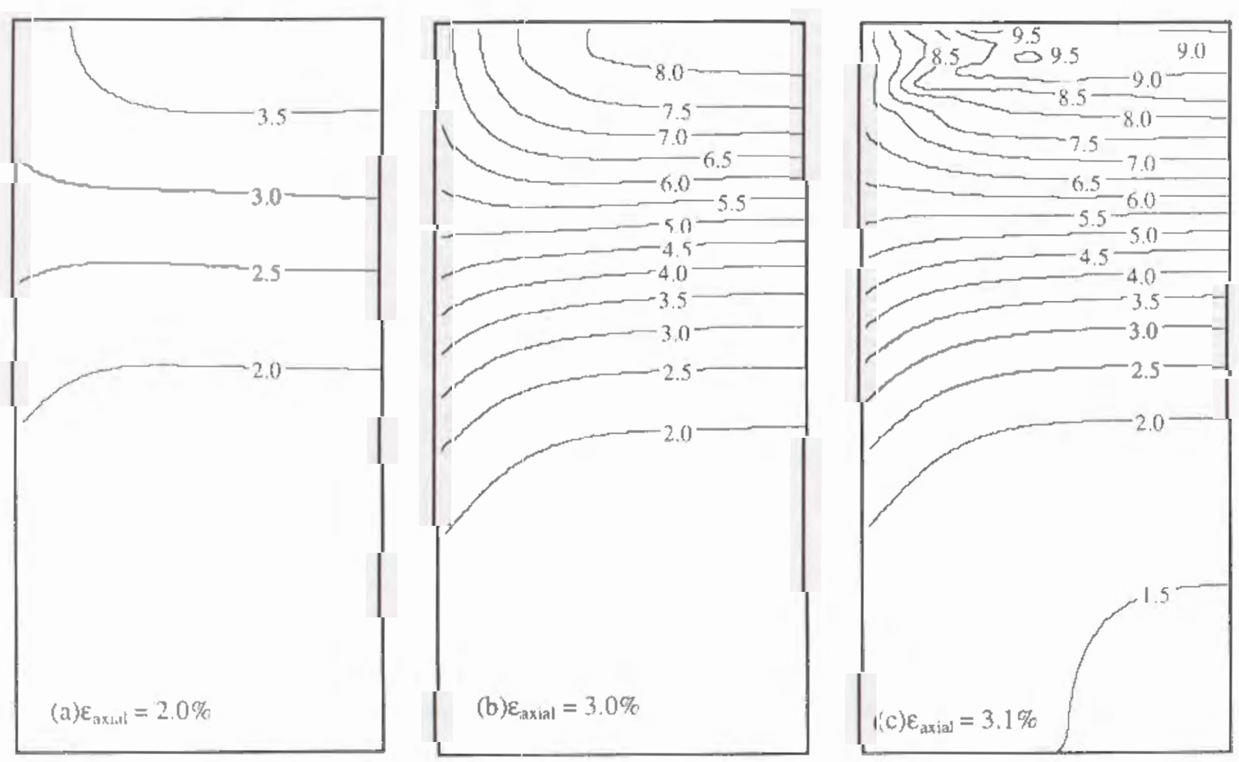

Fig.4-15 Contours of octahedral strain at different strain levels

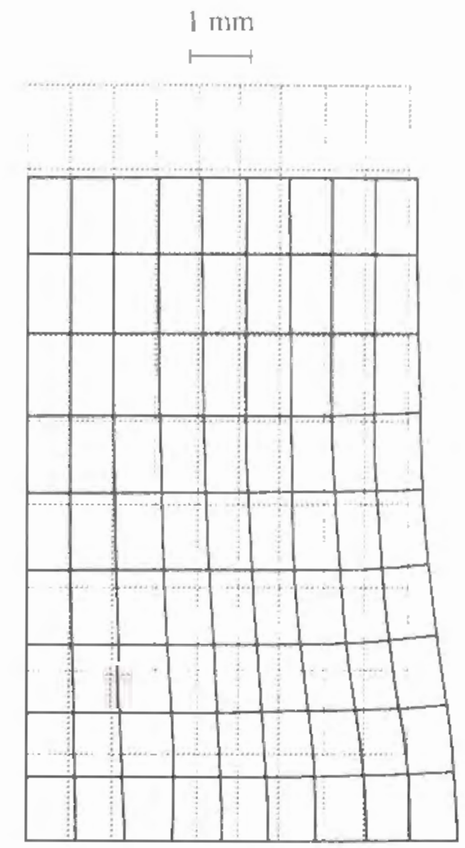

Fig.4-16 Deformation pattern at residual state(friction exists)

Fig.4-16 shows the deformation pattern at residual state. Though the frictional force is very small, the deformation pattern of sample after peak strength shows significant difference from the one for the analysis without friction. The shape of the sample at the residual state looks like a barrel which can also be observed in experiments.

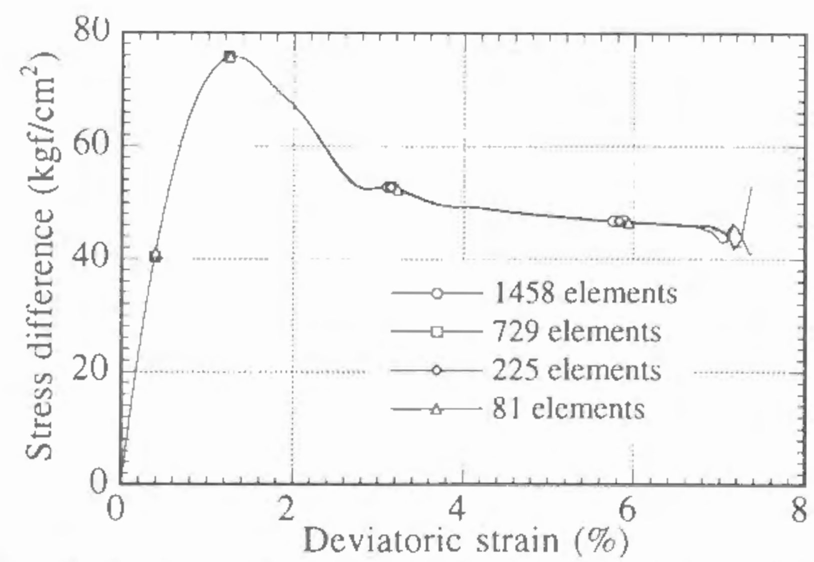

Fig.4-17 Influence of finite element mesh on stress-strain relation

Fig.4-17 shows the relations of stress difference-deviatoric strain obtained from different finite element meshes at a prescribed point. In order to make it possible to compare the result in same position, finite element meshes are arranged in such a way that the point at which the stress-strain relation is picked up is located at same position for different meshes. From the figure, it is clear that when the spatial discretization decreases to a certain size, the results will be the same. In the present case, 81 finite element mesh is sufficient enough to be used to obtain a satisfied results.

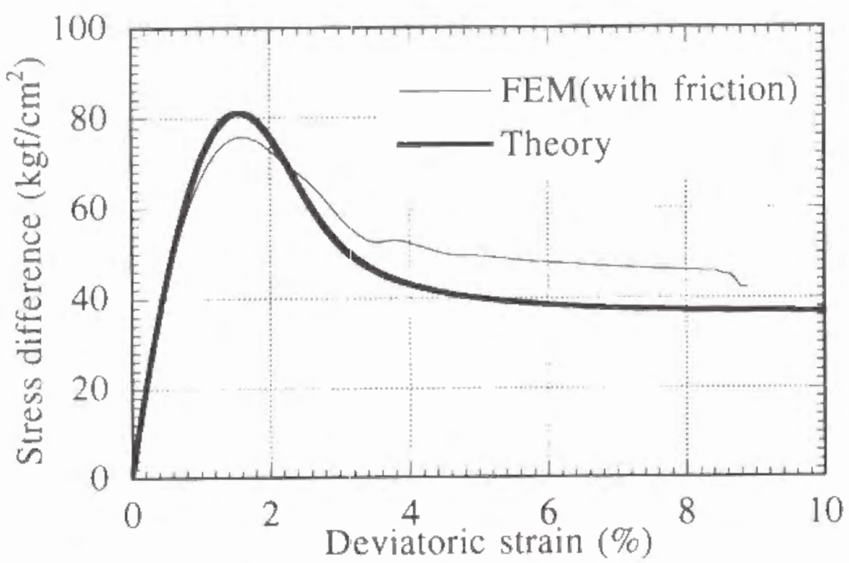

Fig.4-18 Comparison between theoretical and calculated stress-strain relation with friction

Fig.4-18 shows the comparison between theoretical and finite element analytical relations of stress difference-deviatoric strain. The peak value obtained from finite element analysis is 5% less than theoretical one while the residual values of finite element analysis is 20 % larger than the theoretical one.

4-4 Conclusions

In this chapter, FEM and JEM based on the constitutive models with strain softening are used to simulate the mechanical behavior of different boundary value problems related to some laboratory tests such as direct shear test and conventional triaxial tests. In order to make sure that the

numerical procedures used in the analyses are convincing, a new numerical technique is proposed and its capability to obtain a convergent solution for boundary value problems concerning strain softening is proved mathematically. The new technique is also compared and checked with other numerical procedures in two dimensional boundary value problem of plane strain and axisymmetric conditions. It is found that the numerical procedure used in this chapter is capable of treating the boundary value problems relating to the strain softening material. No special precaution is needed to be taken to the region of localization and the analytical results are independent of the mesh size used for spatial discretization. The method proposed in this chapter can provide a powerful tool for the further investigation on the boundary value problems related to geotechnical engineering problems.

References

(1) Adachi, T. and Ogawa, T. (1980) : "Mechanical Properties and failure criteria of soft rock," Proc. JSCE, No.295, pp.51-62(In Japanese).

(2) Adachi, T., Zhang, F., Oka, F. and Yashima, A. (1991) : "Finite element analysis with strain-softening constitutive model," Proc. of 7th Int. Conf. on Computer Methods and Advances in Geomechanics, Cairns, pp.535-540.

(3) Adachi, T., Zhang, F., Oka, F. and Yashima, A. (1991) : "A FEM analysis of strain localization using a non-local strain-softening plasticity," Proc. 3th Int. Conf. on Constitutive Laws for Engineering Materials, Theory and Application, Tucson, USA, pp.83-94.

(4) Adachi, T., Oka, F. and Yashima, A, (1991) : "Finite Element Analysis of Localization for Soft Rock with Strain Softening," Archive of Applied Mechanics, No.61, pp.183-191.

(5) Bazant, Z. P., (1976) : "Instability, Ductility and Size Effect In Strain-Softening Concrete," ASCE, Journal of Engineering Mechanics Division, EM2, pp.331-334.

(6) Bazant, Z. P. and Belystschko, T. B. (1987) : "Strain softening continuum damage: Localization and size effect," Proc. Int. Conf. on

Constitutive Laws for Engineering Materials, Edit by C. S. Desai, et al., Elsevier, Vol.1, pp.11-33.
(7) Bazant, Z. P., (1988) : "Nonlocal continuum damage, localization instability and convergence," J. Appl. Mech. ASME. Vol.55, pp.287-293.
(8) Frantziskonis, G. and Desai, C. S. (1987) : "Constitutive model with strain softening," Int. J. Solid and Structures, Vol.23, No.6, pp.733-750.
(9) Schreyer, H. L. and Chen, Z. (1986) : "One-Dimensional Softening with Localization," ASCE Journal of Engineering Mechanics Division, Vol. 53, pp.791-797.
(10) Valanis, K. C. (1985) : "On the uniqueness of solution of the initial value problem in softening materials," J. Appl. Mech. Vol.52, pp.649-653.

Chapter 5

Analysis of tunnel excavation

5-1 Introduction

In these two decades, NATM (New Austrian Tunneling Method) (Rabcewicz, 1965) has been extensively used all over the world. The method may be characterized by the following three points.

(1) It is based on the basic mechanical principle of tunneling, i.e., "a tunnel should be supported by the surrounding ground as much as possible".
(2) For realizing the basic mechanical principle of tunneling and preserving the strength of surrounding ground, flexible support systems such as shotcrete and/or rock bolts are efficiently applied based on the second principle of tunneling, i.e., "permit elastic deformation in ground, but exclude loosening it".
(3) Field measurements(viz., observational method) are efficiently applied in order to confirm whether the flexible support system is satisfactorily functioning and to indicate the proper timing for operations such as final tunnel lining.

These basic mechanical principles of tunneling stated above are not the original ideas only of NATM, but have been cultivated from experience in tunnel constructions throughout the world, extending over many years. It can be said that the significance of NATM is in the realization of these principles by making the best use of shotcrete and rock bolts.

In any case, it is important to clarify precisely and understand the mechanical behavior of the surrounding ground during tunneling. Therefore, first of all, it is necessary to explain the principle in connection with the stress-strain characteristics of ground materials.

Generally speaking, as schematically illustrated in Fig.5-1a, the stress-strain curves of ground material show a strain-hardening-softening type when the confining pressure is less than the transitional stress of the material. The volume change is compressive in nature at the initial stage of shear deformation before the peak strength is reached and shows remarkable dilatancy, viz., resulting in loosening of the strength. Also, the stress-strain relations of ground materials are affected by the strain rate. Thus, immediately after excavating a tunnel, deformation of the surrounding ground is governed by the stress-strain relation indicated by the strain rate(high) in Fig.5-1b, whereas the stress relaxation from point P to point R will take place later when the ground deformation is restrained by placing tunnel lining.

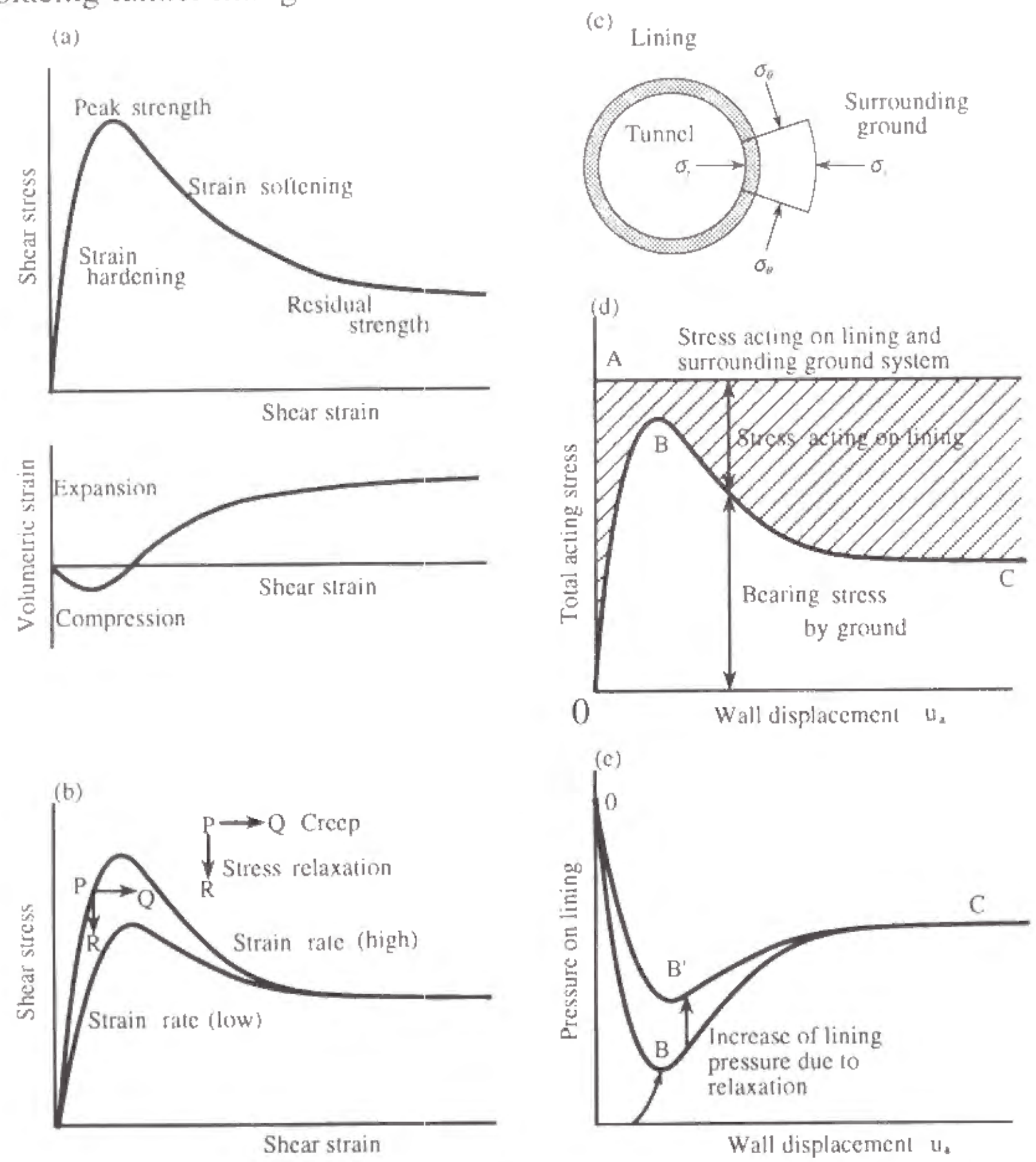

Fig.5-1 Schematic representation of the basic principle of tunneling, (a) Stress-strain relationship of ground material, (b) effect of strain rate on stress-strain relation, (c) lining and ground system against acting stress condition, (d) changes in lining and bearing stresses with tunnel wall displacement, and (e) change of lining pressure with tunnel wall displacement.

Consider the case when the surrounding ground with aforementioned mechanical properties and lining are working together against the shear strength (σ_θ-σ_r) developed by tunnel excavation as shown in Fig.5-1c. It is easily understood that the total bearing strength of both ground and lining is required to be larger than the acting stress, in order to stabilize the tunnel. Since bearing stress of the ground varies with the deformation as given by the curve OBC in Fig.5-1d, the portion of stress which should be taken over by the lining also changes with tunnel wall displacement. The relationship between the bearing stress by lining and the tunnel wall displacement is given in Fig.5-1e. This is Fenner-Pacher curve in NATM. This figure shows that the best way to place lining is to aim at point B where the ground exhibits the maximum strength. Conversely speaking, the acting pressure on the lining becomes the minimum value. This is the explanation for the second principle of tunnel, "permit elastic deformation in ground, but exclude loosening it".

It is also shown in Fig.5-1e that the lining pressure increases with time, because stress relaxation occurs in the ground later when the ground deformation is restrained by placing lining. This is one reason why the tunnel lining pressure increases with time especially for rate sensitive ground materials.

From above discussion, it is very clear that in order to explain the characteristics of tunneling with NATM, such as Fenner-Pacher curve and time dependent behavior, the constitutive model which can not only describe the strain-hardening and strain softening behavior, but also time dependency is absolutely necessary. The aim of this chapter, is to establish a suitable designing method for tunnel construction using a series of finite and joint element analyses based on suitable elasto-plastic constitutive model with strain softening. Researches on this field can be found in the works by Adachi et al.(1985), Adachi et al.(1986), Adachi and Oka(1989), Adachi et al.(1991) and Adachi et al.(1993). The time dependent behavior of tunneling will be discussed in chapter 8.

5-2 Numerical analysis of trapdoor with finite and joint element methods

5-2-1 FEM analysis based on the model with strain softening

Experiment with trapdoor is often performed in order to clarify the mechanical behavior of the ground and lining in a tunnel excavation. The Fenner-Pacher curve in NATM can be seen in the trapdoor test on granular material as shown in Fig.5-2. That is, when a trapdoor is opened the pressure upon the door drops rapidly to its minimum value but increases again gradually as the door is lowered further (Szechy, 1966). Ladanyi and Hoyaux (1969) carried out a series of model trapdoor tests in which the pressure on the trapdoor was measured and the displacement trajectories of the ground mass consisted of aluminum rods with a frictional angle of 25°~26° were photographically recorded. Fig.5-3 shows the experimental results of ground convergence curves.

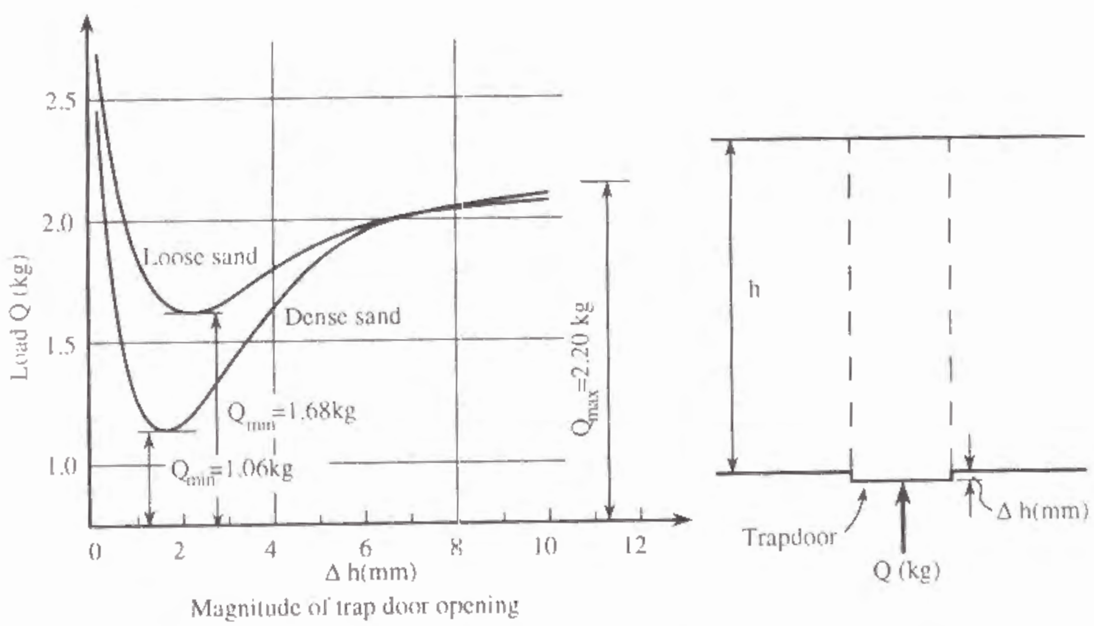

Fig.5-2 Result of trapdoor test in sandy ground(after Szechy ,1966)

In this section, the behavior of trapdoor is simulated with finite element method based on Adachi-Oka's model with strain softening. As a first step, a very simple case is considered, in which the ground is composed of homogeneous material and initial stress is uniform. In FEM analysis, 8-node isoparametric element is used. In order to avoid the excessive stress concentration around the edge of the trapdoors due to the discontinuous decent of the trapdoor, the intermediate area of displacement between the

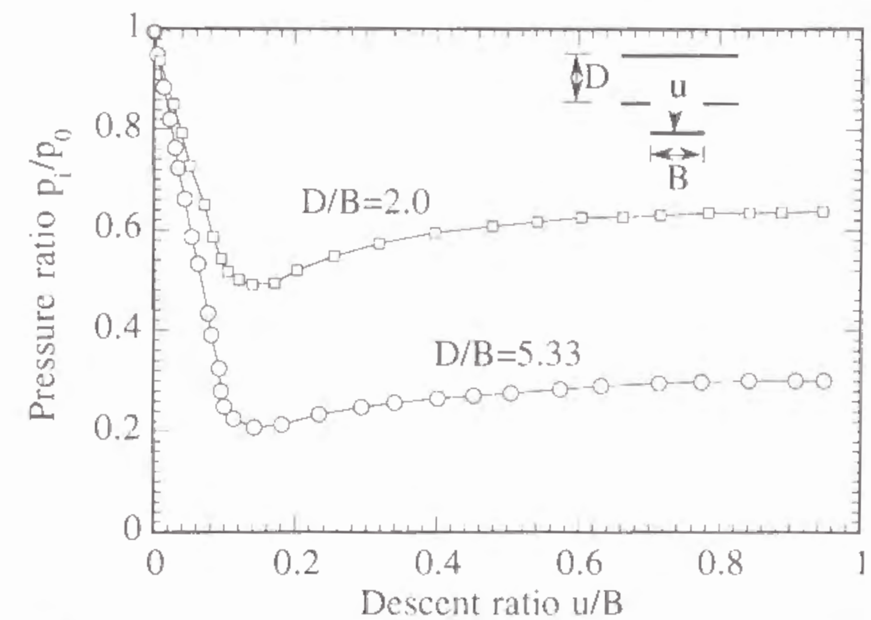

Fig.5-3 Result of trapdoor test in model ground made of aluminum rods(after Ladanyi et al., 1969)

trapdoor and the base of the box is introduced. Finite element mesh, boundary condition and material parameters are shown in Fig.5-4. The initial stress field is a uniform one. Initial stress method is used in the calculation and no iteration is carried out. The trapdoor is simulated by giving displacement to 8 mm in 24 steps. It should be pointed out that the

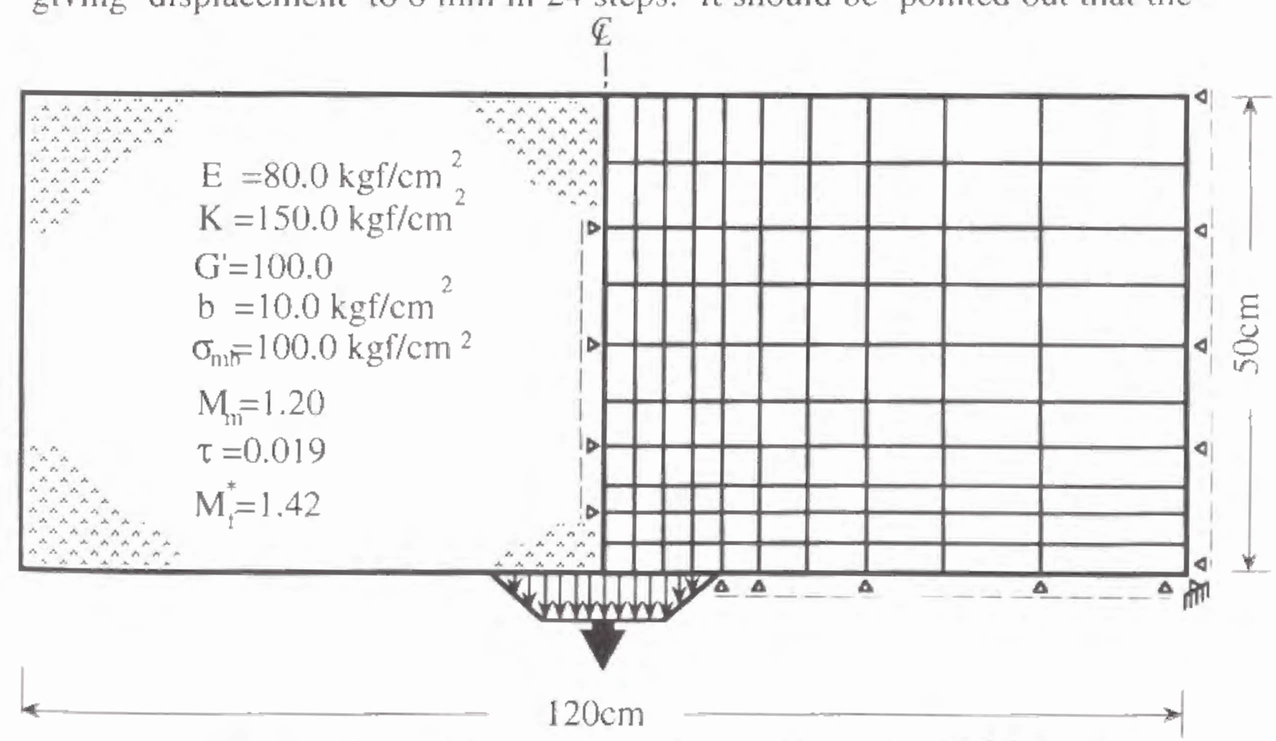

Fig.5-4 Numerical conditions for trapdoor problem in model ground

material parameters and initial stress conditions used for calculation has little relation to real ground material. The ground considered here is only a fictional one. Fig.5-5 shows the relation between earth pressure acting upon the trapdoor and the decent of trapdoor. It is clear that earth pressure decreases very rapidly due to the lowering of trapdoor. However, when the pressure acting upon the trapdoor reaches its minimum value, it again increase. This result is coincide with the empirical phenomena that "if a ground is loosened excessively, the earth pressure to tunnel increase". The contour of octahedral strain at the stage when the trapdoor is lowered down to 8mm is shown in Fig.5-6.

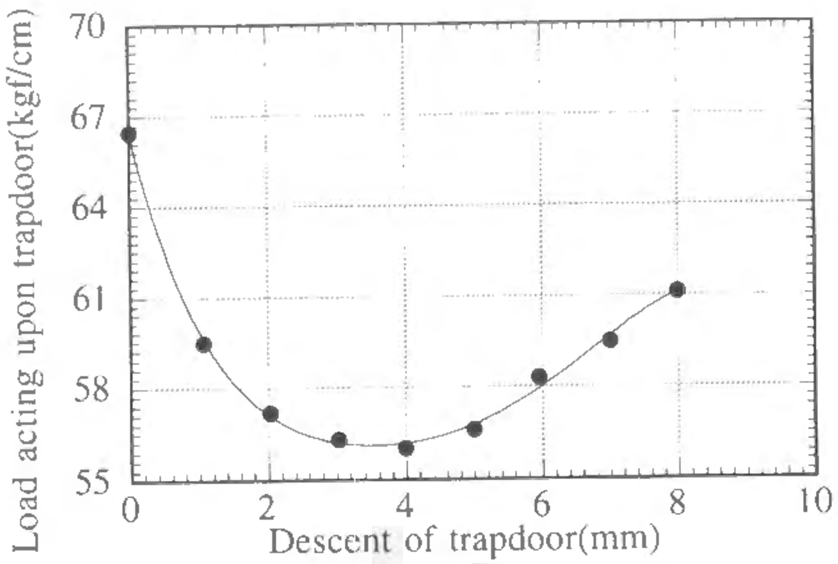

Fig.5-5 Calculated result of load-descent relation of trapdoor

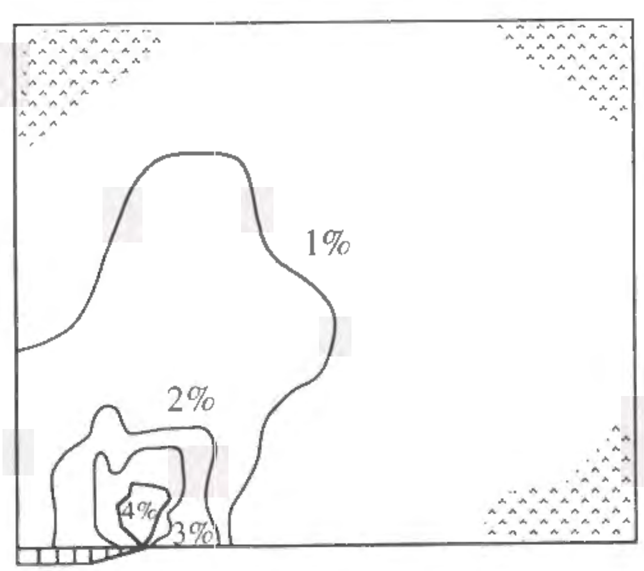

Fig.5-6 Contours of octahedral strain(when descent of trapdoor=8 mm)

Next a trapdoor in model ground is considered. The material of the model ground is assumed to be dense sand. The finite element mesh, boundary condition and material parameters are shown in Fig.5-7. In simulating the decent of trapdoor, there exist two different ways. One is simulated by given displacement. As it can be seen from Fig.5-6, because of the discontinuity of the descent at the corner of trapdoor, a transitional area has to be introduced to avoid the discontinuity which will lead to mathematical problem in finite element analysis. Besides, using given displacement method will cause a tension at the corner of trapdoor, which is contradicted to real situation. Another way of simulating the decent of trapdoor is simulated by releasing the stress along the trapdoor, that is, the stress along trapdoor is first released freely in certain ratio and then a rigid plate is suddenly installed to prevent the further decent. Using this method, no tension nor displacement discontinuity will occur. This method is adopted in present simulation.

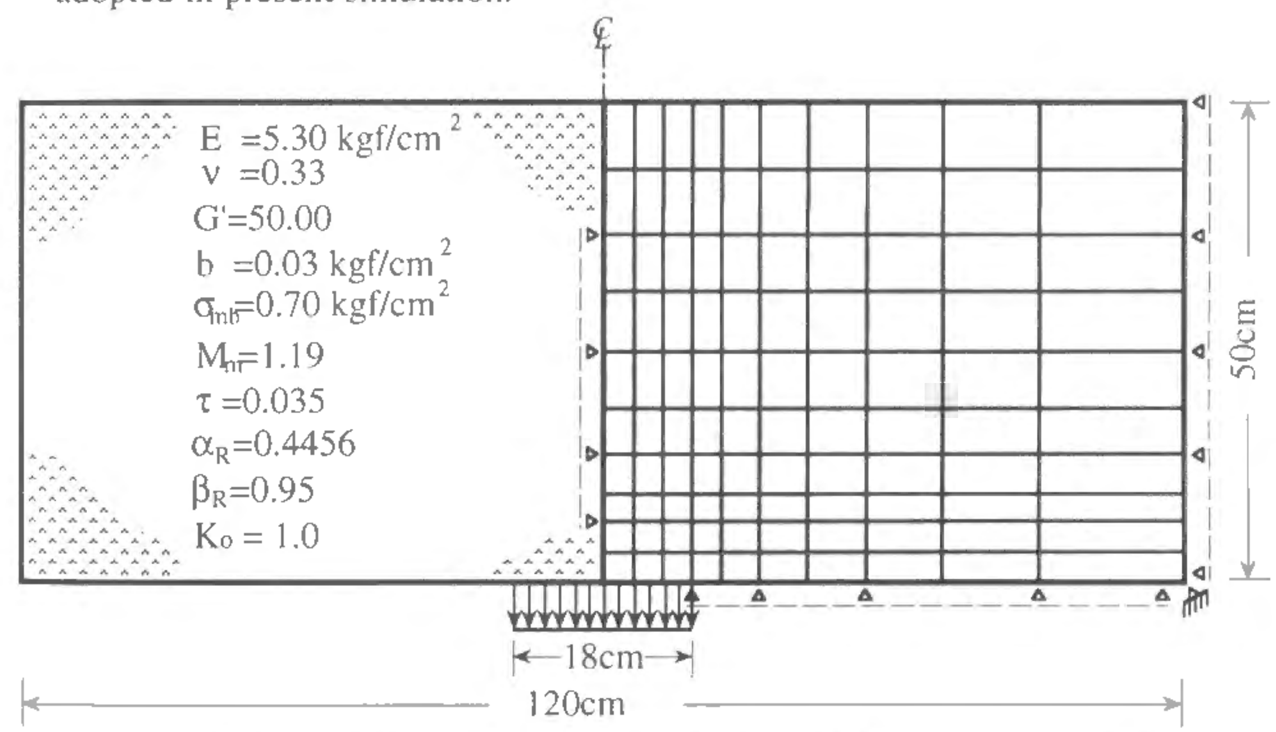

Fig.5-7 Numerical conditions for trapdoor problem in sandy ground

Fig.5-8 shows the theoretical relations of stress difference-deviatoric strain and volumetric strain-deviatoric strain of sand in triaxial compression test.

Fig.5-9 shows the relation of octahedral stress vs. octahedral strain at the corner of trapdoor(the dark area shown in Fig.5-10) during the stress releasing along trapdoor. The octahedral stress firstly increases to peak value and then decreases to residual value, while the stress history increases monotonously and finally reaches to the residual strength of octahedral stress. The residual strength is about 3/4 of the peak strength.

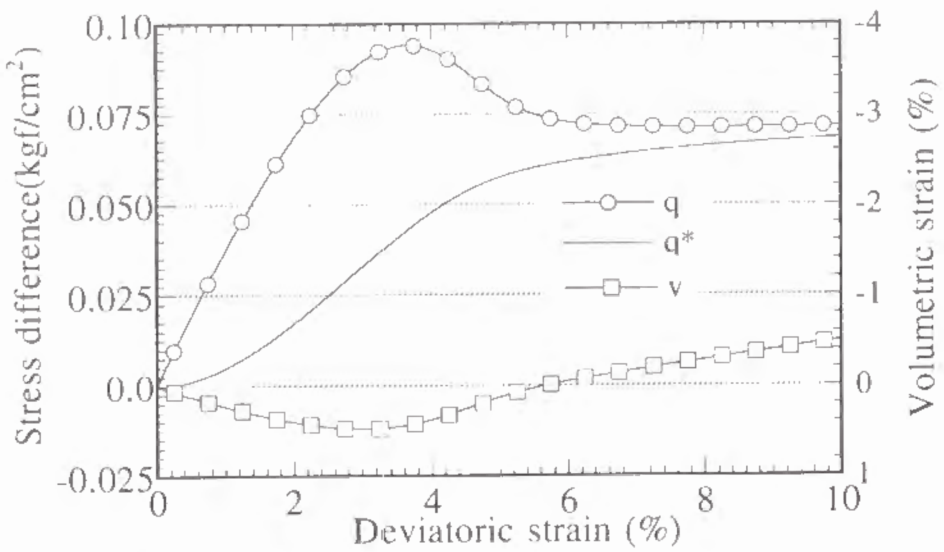

Fig.5-8 Theoretical relations of stress difference-deviatoric strain and volumetric strain-deviatoric strain of sand in conventional triaxial test.

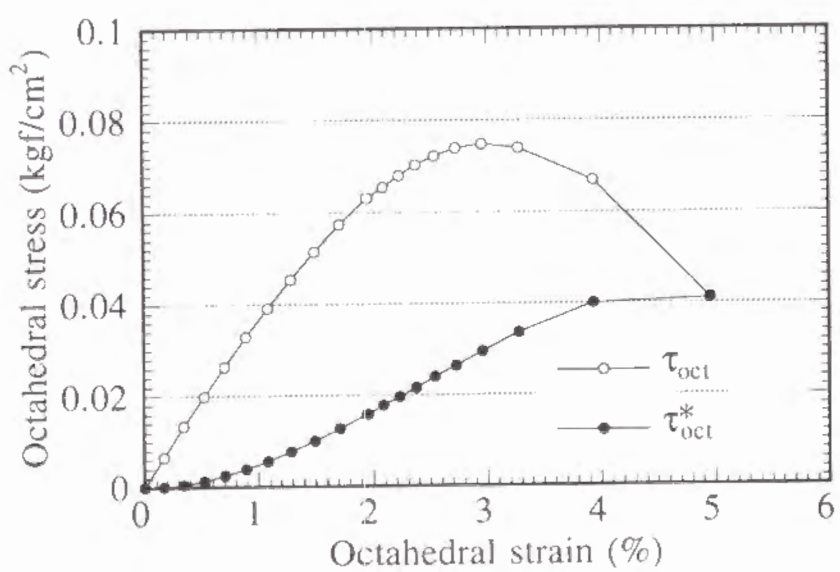

Fig.5-9 Calculated relation of octahedral stress-octahedral strain of element at the corner of trapdoor

Fig.5-10 shows the softening zones occur at different stress released ratio. When the stress released ratio reaches 100% (Equivalent to free decent),

The size of the softening area in vertical direction will almost be equal to the half width of the trapdoor.

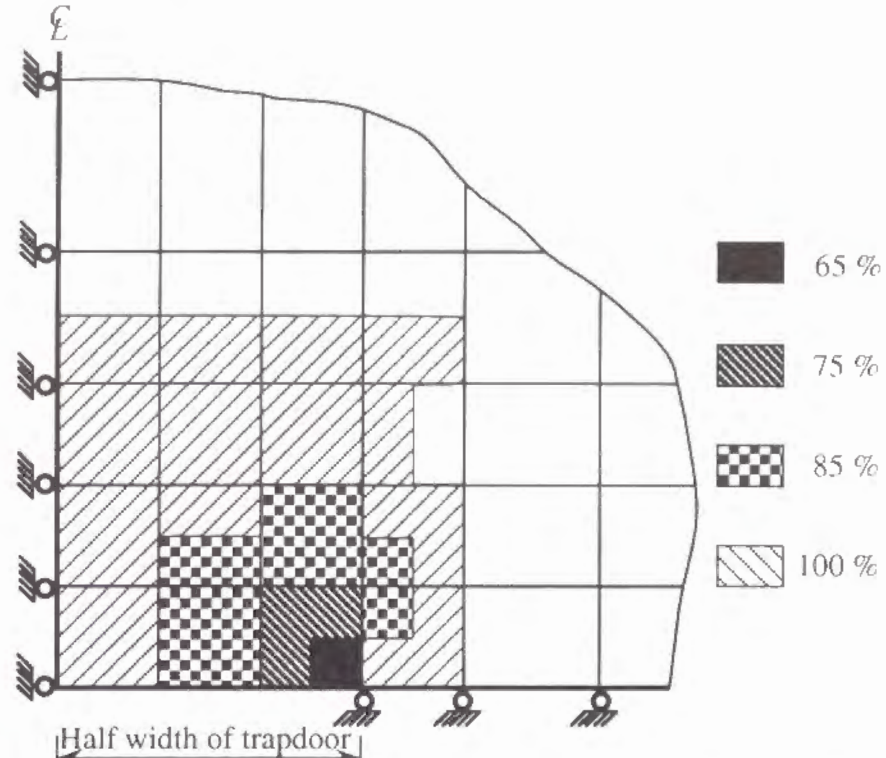

Fig.5-10 Softening zones occurred at different stress released ratio

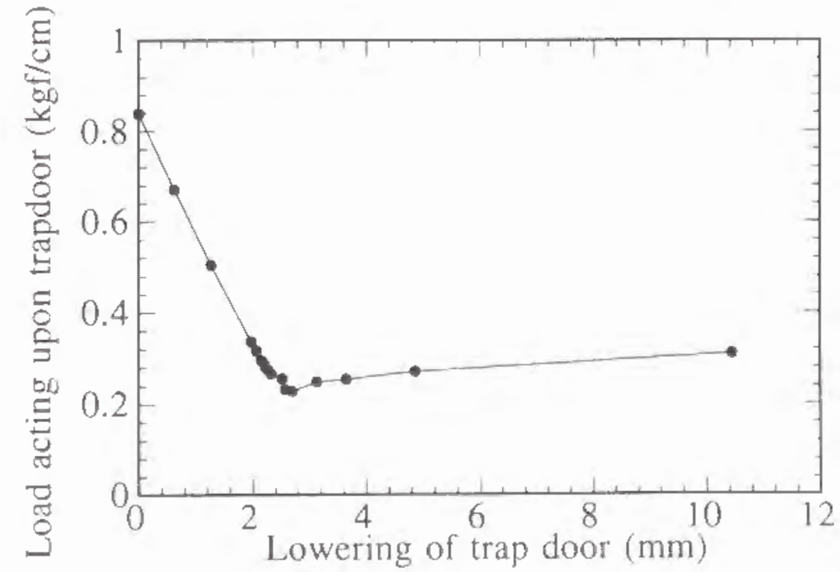

Fig.5-11 Calculated load-decent relation of trapdoor in sand ground

Fig.5-11 shows the calculated results of ground convergence curve of trapdoor. The load firstly decreases with the decent and increases when softening occur in some elements. Compared the figure with Fig.5-3, it can been seen that the shape of the load-displacement curve obtained form numerical analysis is similar to the experimental result. The increase of the load after peak strength, however, is less than the difference between the peak and residual strength. This is the reason that not all the elements above the trapdoor come into softening and some of them can still bear partly the weight of the ground itself.

In order to obtain a convergent solution, calculations with different steps have been done with generalized Runge-Kutta method. It is found that when the steps is taken more than 260, convergent solutions can be obtained.

5-2-2 FEM and JEM analyses based on the constitutive model for discontinuous material

In previous section, two different simulating methods are used in the finite element analysis of trapdoor. The analyses were based on continuum theory. In this section, joint element is introduced in the analysis of trapdoor. The introduction of joint elements at the corner of trapdoor can describe the discontinuous behavior near the corner and avoid the mathematical trouble met in the finite element analysis. Needless to say, the artificial introduction of joint in the ground will result in some problems, among which the effect of arrangement of joints and the determination of the material parameters of joint should be considered. For the first problem, two different arrangements of joint elements are used to investigate the influence. Secondly, in determining the material parameters of joint, the shear stiffness of joint should be determined by direct shear test on the material of ground in which the joints exist.

In present analysis, the mechanical behavior of joint material is described by a strain-softening model for discontinuous material proposed in chapter 3(Adachi et al., 1991). While the finite element is supposed to be elastic body. The model ground considered here is assumed to be a sand. The material parameters of joints are listed in Table 5-1 while the finite element which stands for continuum in the ground, has the material parameters as, E_{ground}= 46.8 (kgf/cm^2) ; ν_{ground}= 0.3. Considering the behavior of sand in extension, it is assumed that the initial normal stiffness k_{n0} take a very little value if $\sigma_n < 0$ in a joint element. In such case, the connection between the

Table 5-1 Material parameters of the joint in the ground* of trapdoor

k_s(kgf/cm^3)	18.0	b(kgf/cm^2)	0.39
k_{n0}(kgf/cm^3)	4.70	M_m	1.61
M_f^*	4.25	τ	0.081
G'(1/cm)	500.0	α_d(1/cm)	90.0
σ_{mb}(kgf/cm^2)	60.0		

* E_{ground}(kgf/cm^2)=46.8, ν_{ground}=0.3

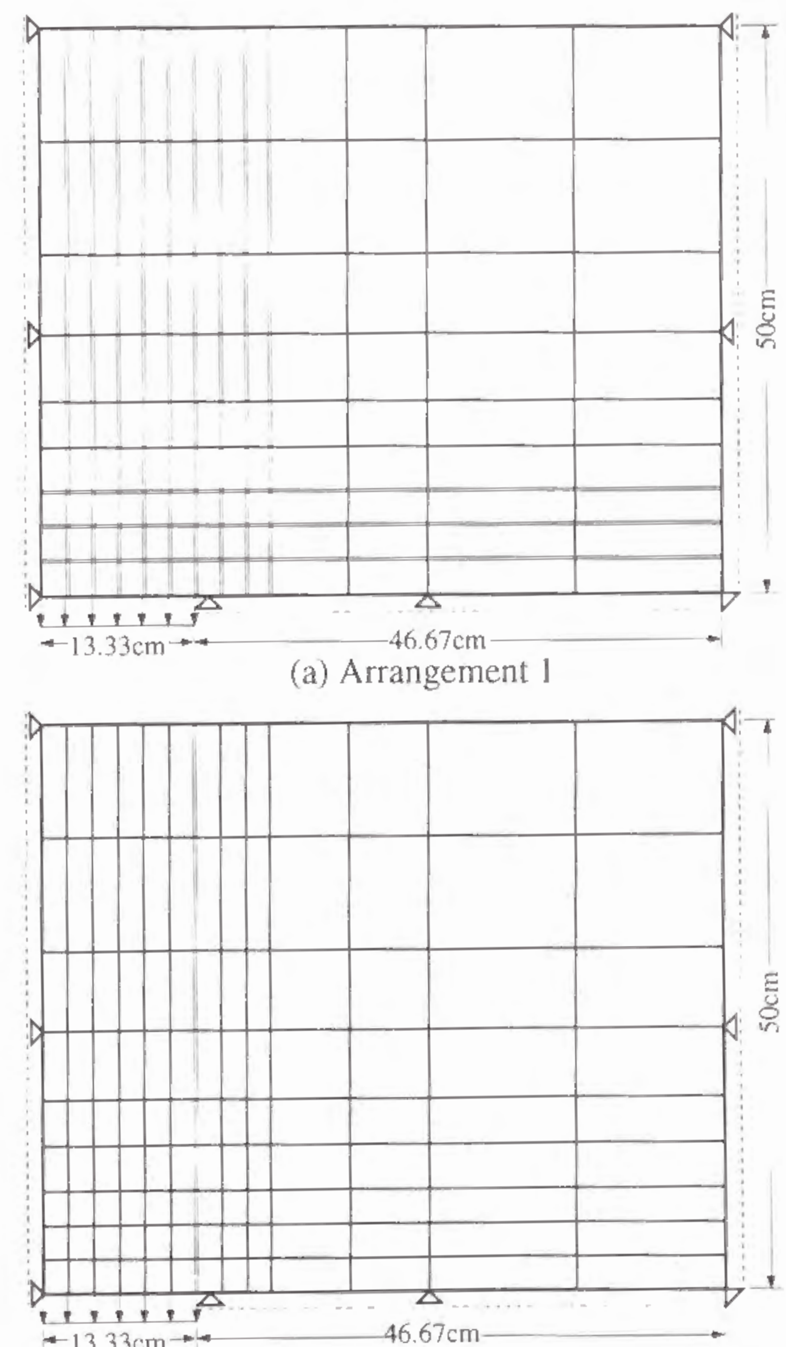

Fig.5-12 Mesh arrangements for trapdoor problem in model ground

two finite elements which are connected by the joint element will be very weak.

Fig.5-12 shows two different arrangements of joint element in the simulation of trapdoor. Double lines in the figure stand for joints. In order to get convergent solutions, the calculations for arrangement 1 and 2 take 300 and 540 steps respectively. The generalized Rung-Kutta method is used in the calculation.

Fig.5-13 shows the calculated results of shear stress-shear displacement for the joint element at the corner of trapdoor in different arrangements. It can be seen that the results for both case is the same.

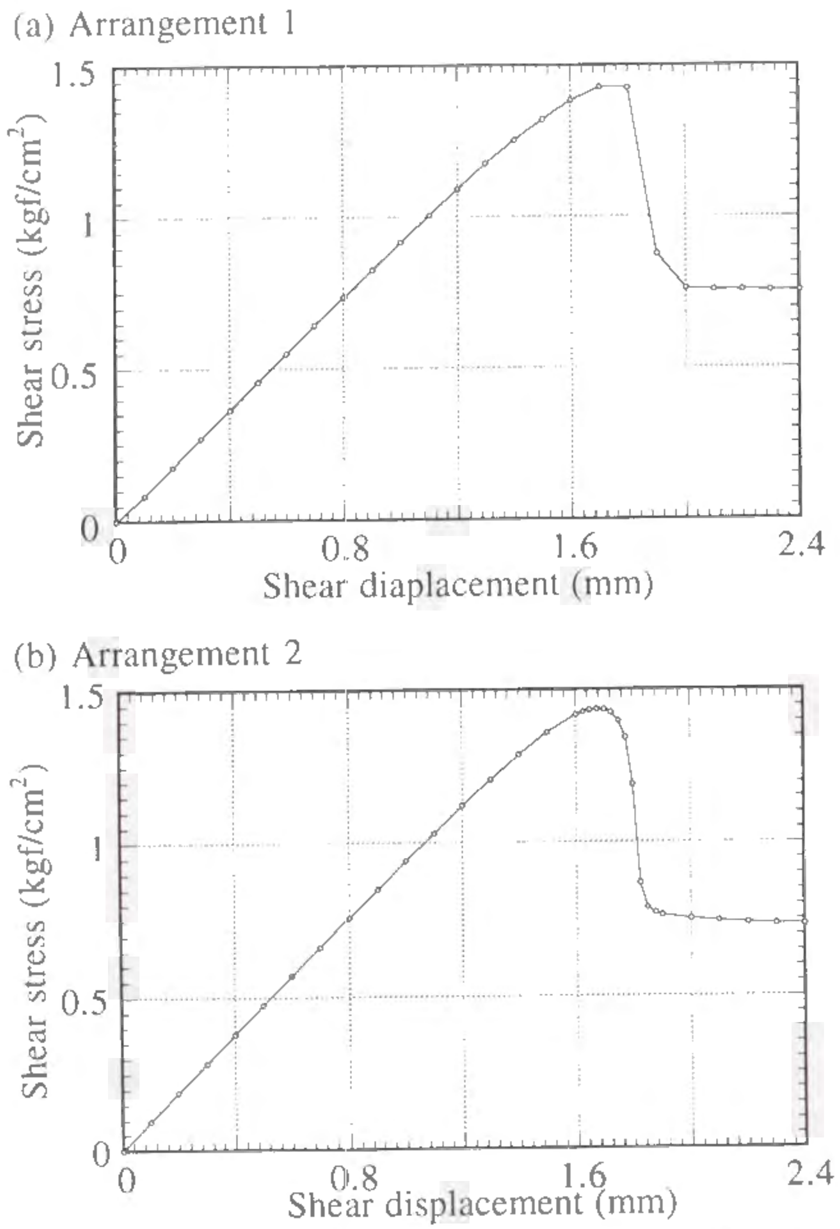

Fig.5-13 Stress-strain relation of the joint element at the corner of trapdoor

Fig.5-14 shows the relation between load acting upon trapdoor and descent of trapdoor. In arrangement 1, joint element is introduced along horizontal lines. It is evident from the Fig.5-14(a) that the load acting upon trapdoor increases to some value and then remains almost constant for a range of descent. While for the arrangement 2, there is no such behavior occurring, due to the fact the connection between finite elements is kept constant even if tensile normal stress occur. However in both case, the loads acting upon trapdoor increase to some value and then decrease again. From above discussion, it can be concluded that the arrangements of joint dose not affect the analytical results too much and the introduction of joint into

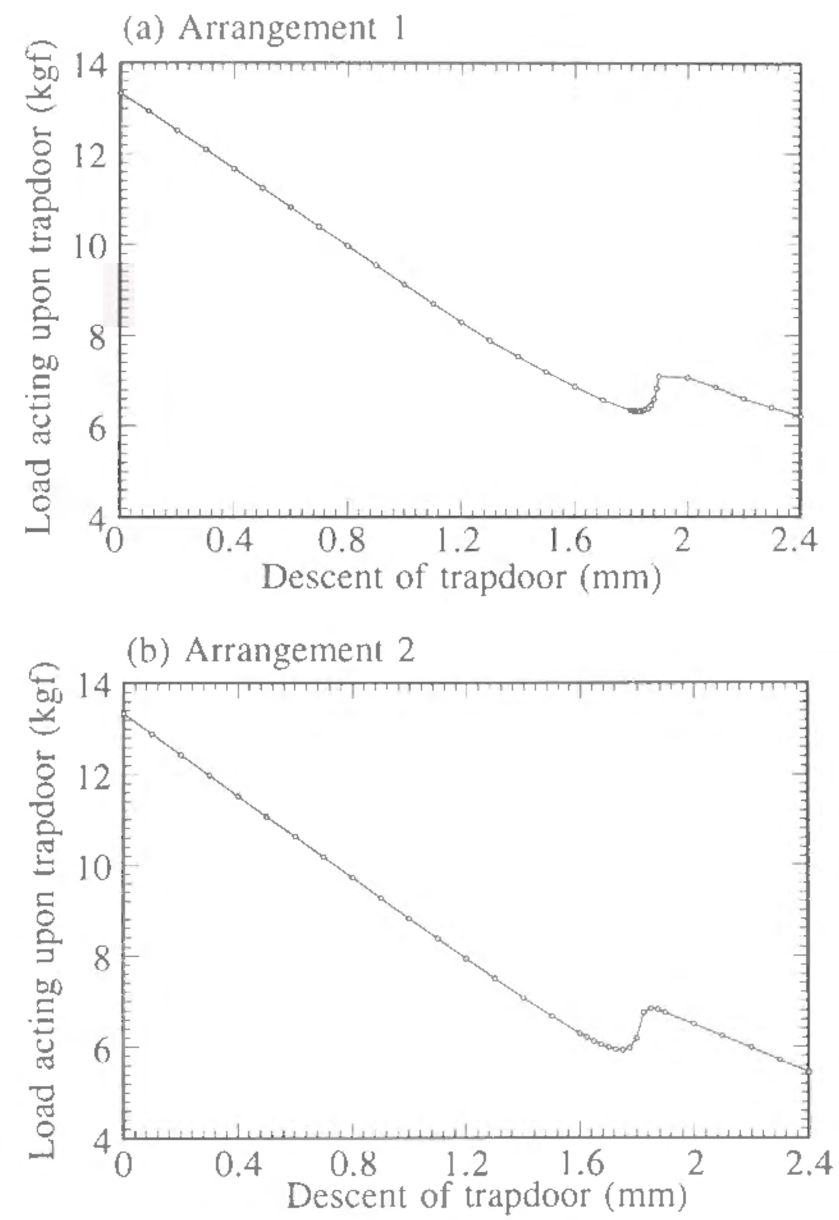

Fig.5-14 Relation of load-descent of trapdoor

intact ground can simulate the mechanical behavior of trapdoor to some extent. The reason why the loads decrease again is that not all the joints along sliding plane come into softening. Therefore the ground can still bear some load by itself and the load acting on decent plate will decrease.

5-3 An analysis of characteristic curve of tunneling with NATM in a model ground with homogeneous stress

In order to establish a applicable analytical method which can simulate the mechanism of the surrounding ground and the interaction between ground and lining when tunnel is excavated, a finite element analysis based on Adachi-Oka's model(Oka and Adachi,1985) with strain softening have been performed in plain strain condition. As a primary step, a model ground with homogeneous stress field is considered

The analysis is focused on the following aspects:

(a) Deformation pattern around tunnel wall,

(b) Typical stress-strain relation in the areas where strain softening occurs in tunneling,

(c) Strain softening area occurred in tunneling,

(d) Relationship between displacement of tunnel wall and load acting upon lining.

5-3-1 FEM analysis

Eight parameters involved in Adachi-Oka's model with strain softening for the model ground are listed in Table 5-2a. Beam element is introduced to simulate primary lining used in tunnel excavation. The material parameters of the lining are listed in Table 5-2b. The initial stress fields are supposed to be uniform stress fields in which the mean stresses take the values of the vertical stress at the centers of tunnel in gravitational stress field.

The finite element mesh is shown in Fig.5-15. Different ratios of overburden to diameter of tunnel (*H/D*) are considered. The distances from the center to fixed boundary along horizontal and vertical direction are taken as 69 meters and 40 meters respectively so as to diminish the influence of artificial boundary condition. Because of the symmetrical

Table 5-2a Material parameters of ground

E(kgf/cm^2)	1000.0	σ_{mb}(kgf/cm^2)	10.00
ν	0.30	b(kgf/cm^3)	1.42
$\alpha_R(M_f^*)$	0.85	$\bar{M}_m$	1.194
β_R	1.00	τ	0.0031
G'	450.0		

(γ_s=2.00 gf/cm^3)

Table 5-2b Material parameters of lining

EA_{beam}(kgf)	2.0×10^7	EI_{beam}(kgf·cm^2)	6.67×10^8
E_{beam}(kgf/cm^2)	1.0×10^5		

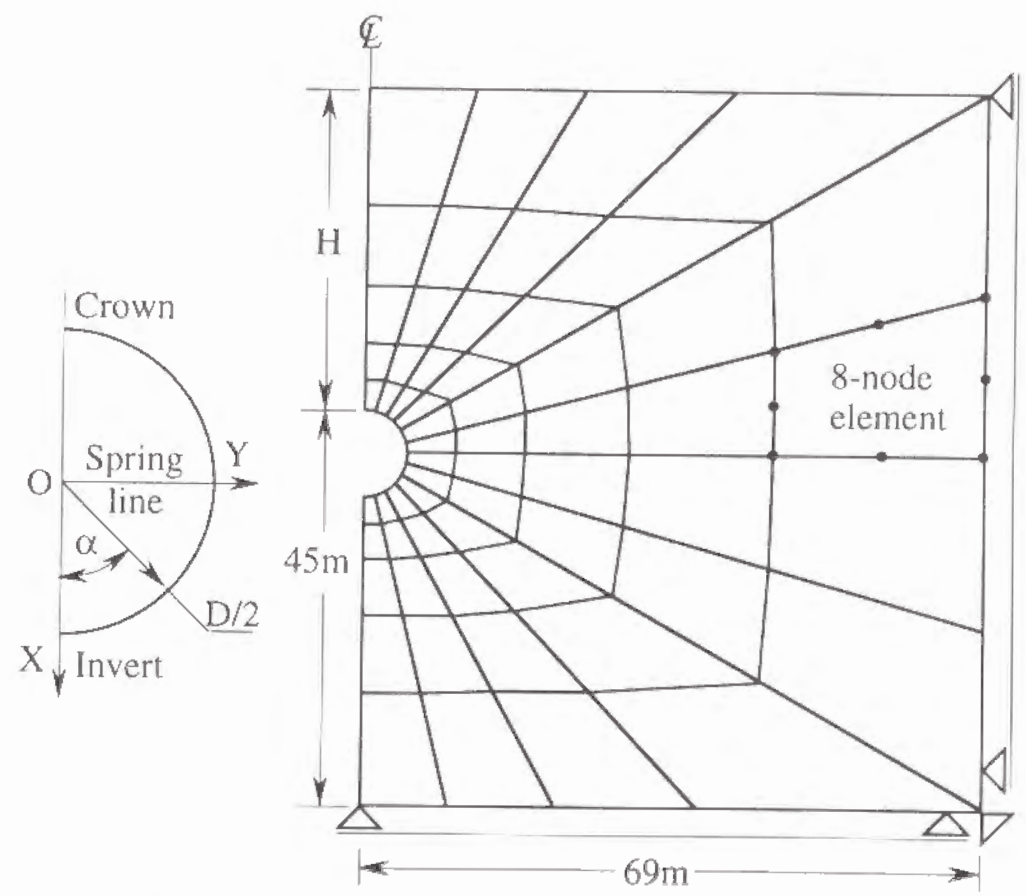

Fig.5-15 Finite element mesh of tunnel excavation in model ground

condition, only right half of the tunnel is considered. In the FEM analysis, 8-node isoparametric element is used. Tunnel excavation is simulated by releasing the initial stress along the periphery of tunnel step by step. For convenience, in the following section, the initial stress released ration is expressed as ISRR.

5-3-2 Results and analysis

Deformation Pattern

Fig.5-16 shows the deformation ratios of ground surface to crown (δ_g/δ_c) and spring line to crown (δ_s/δ_c) due to tunneling at different ratio of H/D. It can be seen from the figure that the ratios (δ_g/δ_c) in different overburden are quite different. For relative deep tunnel(H/D=2.0 and H/D=3.5), the vertical displacement ratio decreases with the increase of load released ratio and accelerates after softening occurs, which means that the deformation is only restricted to the vicinity of tunnel periphery because of the arch-effect of ground. While for shallow tunnel(H/D=1.0), the vertical displacement ratio changes little at first and increases very rapidly after softening occurs, which means that the deformation direct reaches to ground surface and the ground above tunnel crown subsides on the whole. The deformation ratio of spring line to crown (δ_s/δ_c) shows that for deep tunnel, the ratio decreases rapidly after softening occurs while for shallow tunnel, the ratio increases rapidly after softening occurs.

Fig.5-17 shows the patterns of settlement along ground surface. For the tunnel with deep overburden(H/D=3.5), the vertical displacement along ground surface is quite exaggerated at distant place, which is contrary to the recognized fact in real tunneling in which the ground far from tunnel is almost kept unmoved. This is caused by exaggerated stress released ratio and absence of lining. For shallow tunnel, there is no such behavior even if lining is absent.

Stress-Strain Relation in Tunneling

Fig.5-18 shows the octahedral stress-strain relation of the elements at crown where strain softening occur during tunneling. It can be seen from

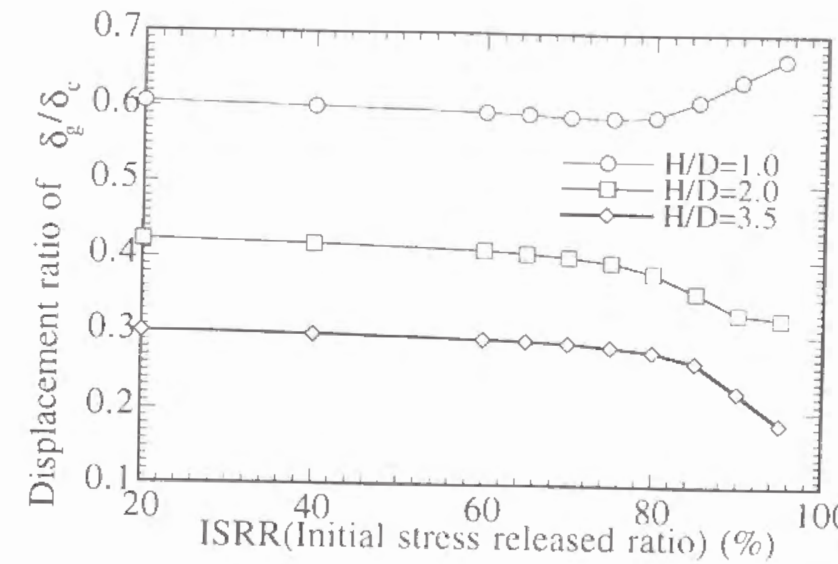

Fig.5-16a Relation between vertical displacement ratio of ground surface to crown and ISRR

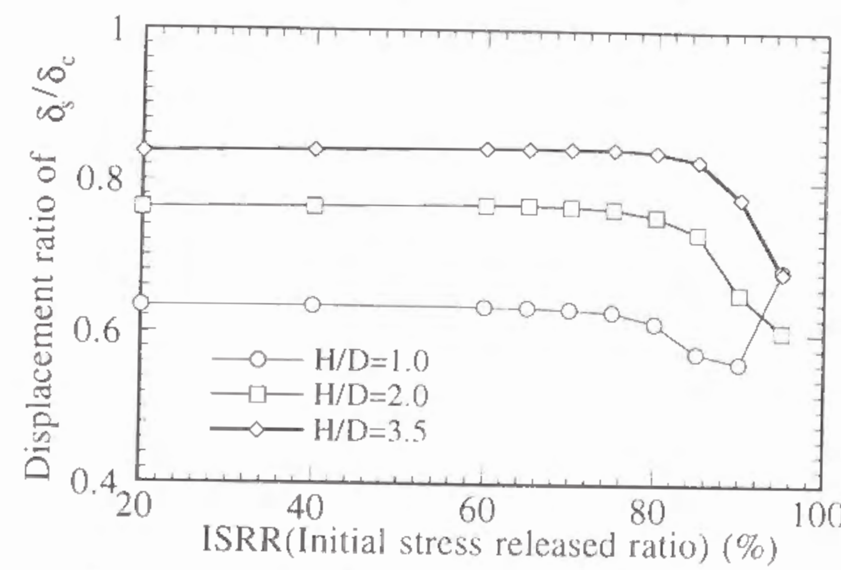

Fig.5-16b Relation between deformation ratio of spring line to crown and ISRR

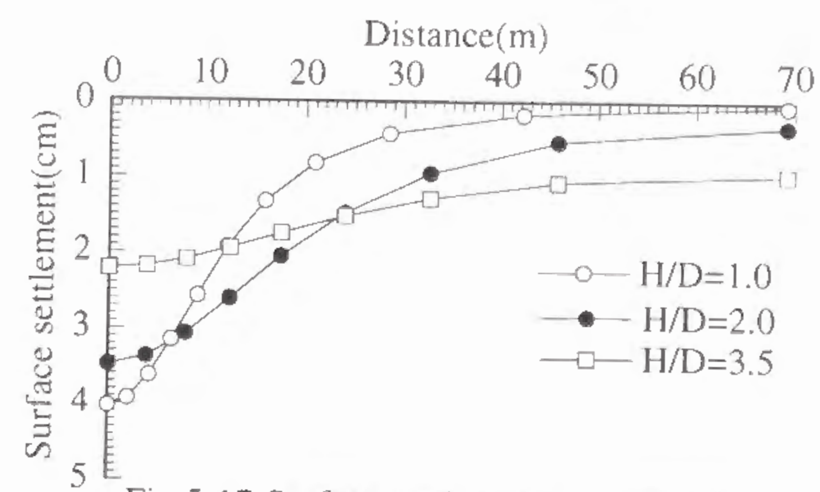

Fig.5-17 Surface settlements in different overbudern(ISRR=100%)

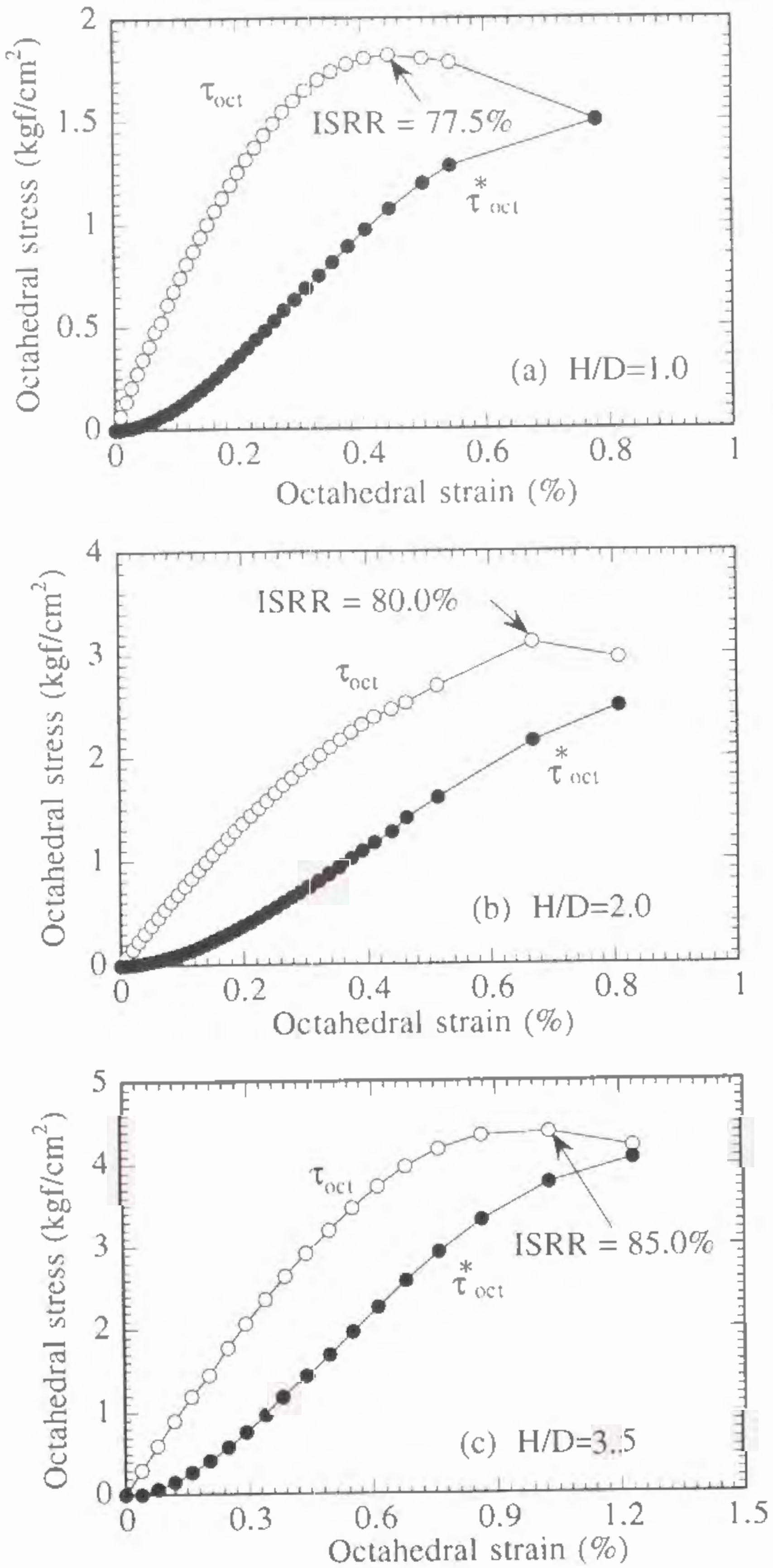

Fig.5-18 Octahedral stress-strain relation at crown for different overburdens

the figure that in all cases, strain softening occurs and happens in different stress released stages. The more shallow the ground cover is, the earlier strain softening will occur. For the ratio of *H/D*=1.0, it occurs when the 77.5% of the stress along the wall of tunnel is released. For *H/D*=2.0 it will occur when the 80.0% of stress is released and 85.0% for *H/D*=3.5. In the areas in which strain softening occur, stress reaches its peak value at first and then decreases. As a consequence, the strain increases rapidly and the ground begins to loose.

Strain Softening Area

Fig.5-19 shows the strain softening areas in different ratio of *H/D*. It is found that the softening areas are quite different for different overbudern ratio. In all cases, only those areas close to the tunnel periphery come into softening. The figure also shows that for shallow tunnel (*H/D*=1.0), the strain softening occurs in two layers of elements, the first layer ranging from 60° to 180° and the second layer ranging from 110° to 180° along tunnel periphery. For the tunnel of *H/D*=2.0, the strain softening occurs in two layers of elements, the first layer ranging from 0° to 180° and the second layer ranging from 150° to 180° along tunnel periphery. For deep tunnel(*H/D*=3.5), only the first layer of elements in the tunnel periphery comes into softening.

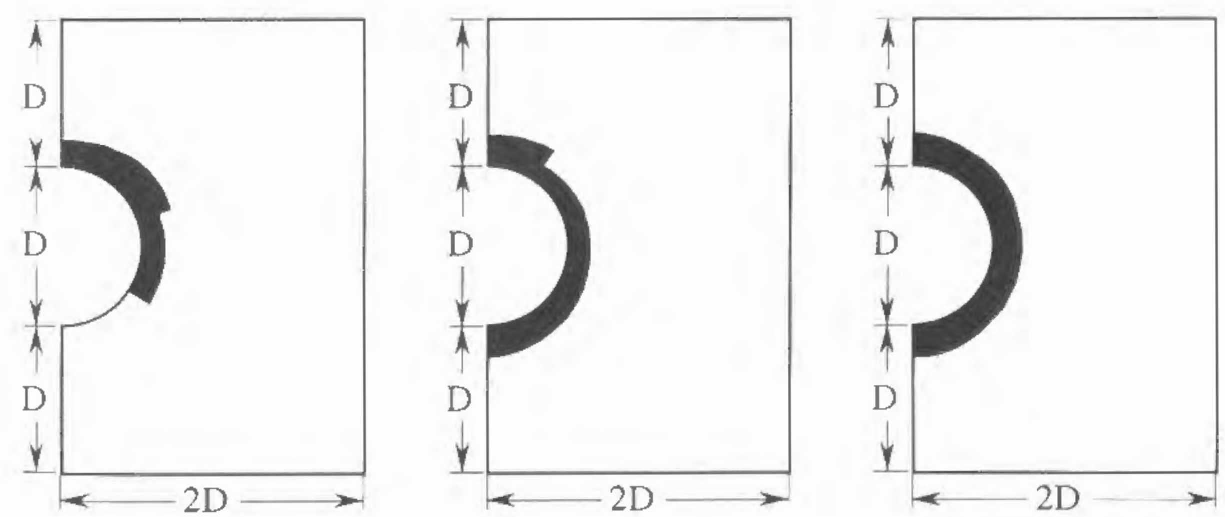

(a) Softening zone when ISRR=100.0% (H/D=1.0)   (b) Softening zone when ISRR=100.0% (H/D=2.0)   (c) Softening zone when ISRR=100.0% (H/D=3.5)

Fig.5-19 Softening zones for different ratios of overburden to diameter(H/D)

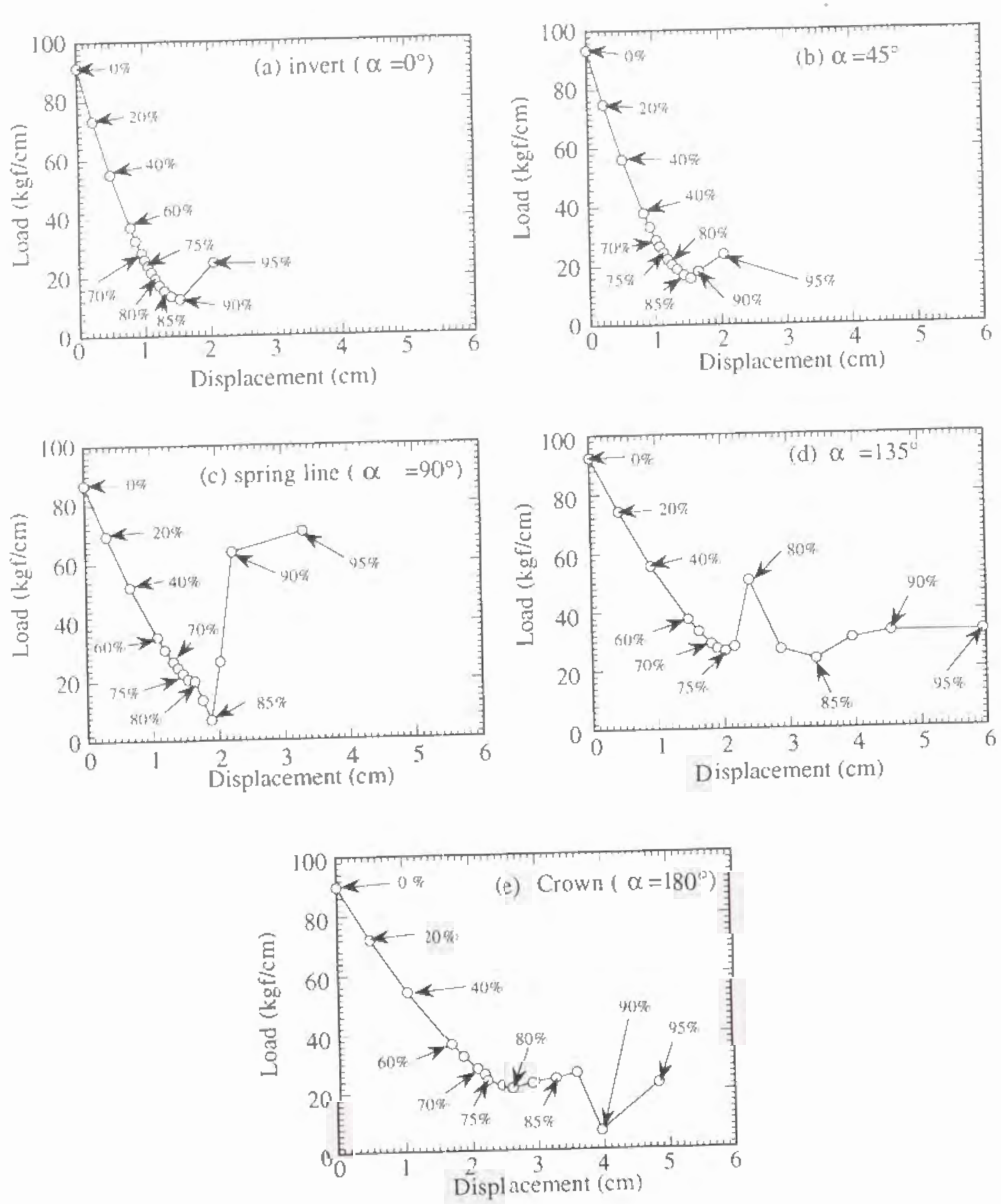

Fig.5-20 Characteristic curves of tunneling with NATM in model ground (H/D=1.0)

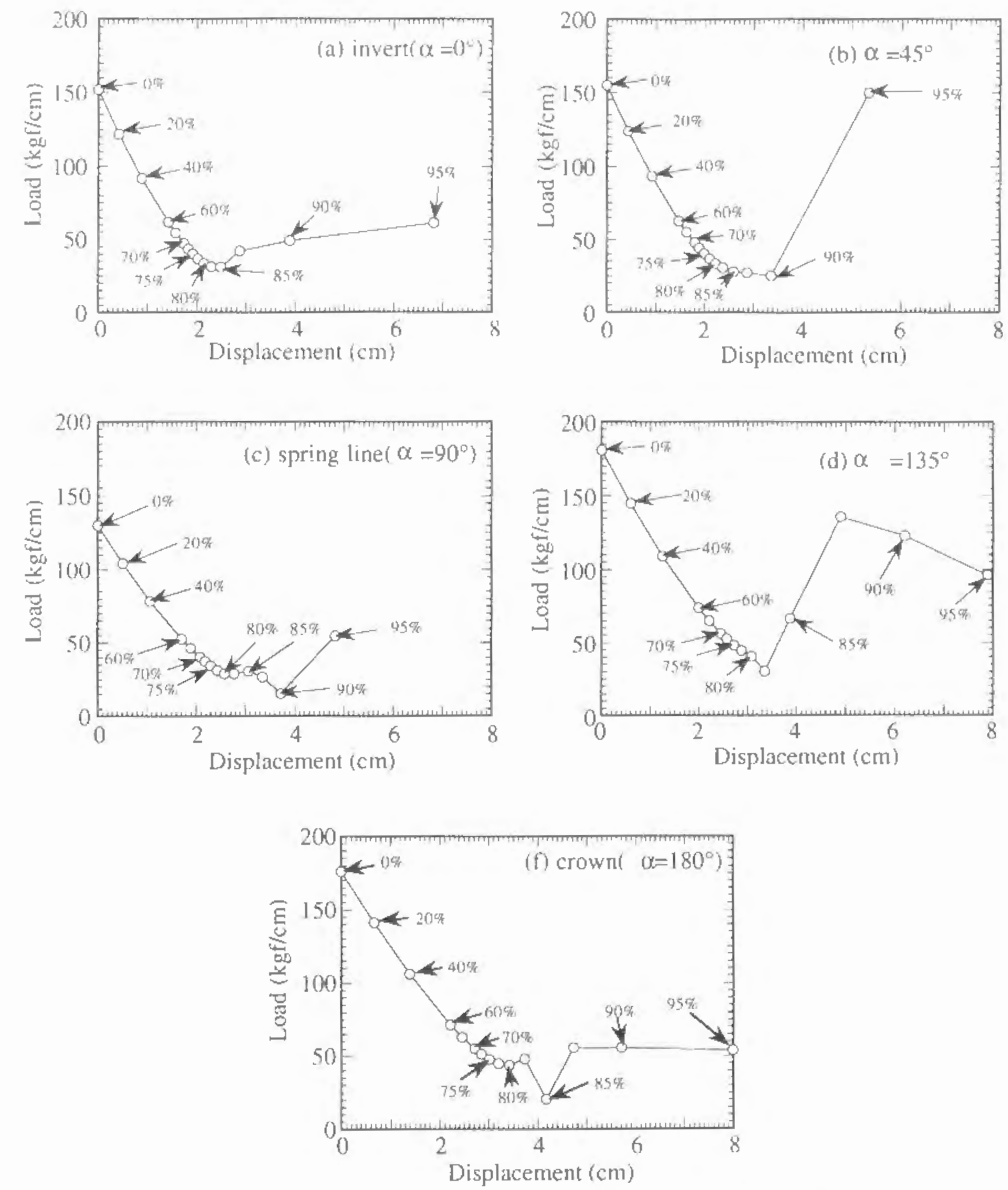

Fig.5-21 Characteristic curves of tunneling with NATM in model ground (H/D=2.0)

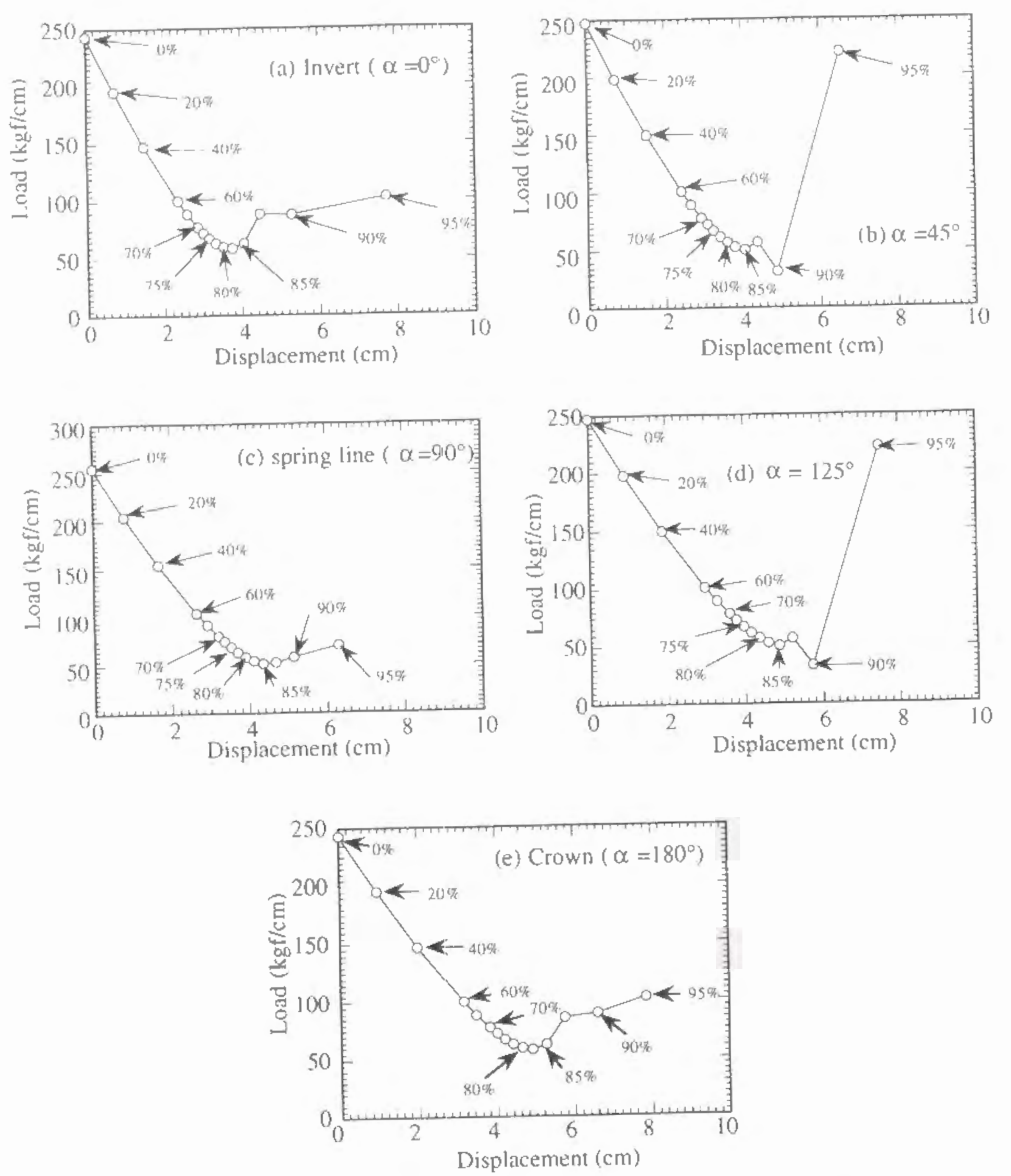

Fig.5-22 Characteristic curves of tunneling with NATM in model ground (H/D=3.5)

Ground Convergence Curve

In tunnel excavation with NATM, engineers are interested in when is the most suitable time to install the lining so that the ground will bear maximum load itself and do not lose stability. Needless to say, the most favorite thing is that lining is installed just at the point B as shown in Fig.5-1(e). Therefore it will be of great significance if it is able to simulate the characteristic curve and to know the exact position of point B by suitable numerical analysis. Fig.5-20, Fig.5-21 and Fig.5-22 show such kind of curves for different overbudern ratios respectively. In FEM analysis, lining is installed at different stress released stages. From above figures, it can be seen that the load acting upon lining decreases at first as the deformation increase and when it reaches its minimum value it increases again. In the figures, the points marked percentages are corresponding to the stages at which the lining is installed. It can be seen from the figures that for different ratio of *H/D*, the minimum point B is different from each other. In all the cases of *H/D*, the ground convergence curves are different at different points along tunnel periphery. It is noticeable that in the ground convergence curves, there exist some vibration after minimum value of load reaches. This is caused by the influence of neighboring elements in which strain softening occur in different ISRR.

5-4 Case study I-deep tunnel

5-4-1 Constitutive Model

Generally speaking, real ground was historically undergone anisotropy consolidation (K_0 consolidation). For such stress induced anisotropy, the constitutive model describing the mechanical behavior of normally consolidated materials should be modified to account for the effect caused by the anisotropy.

In Adachi-Oka's constitutive model with strain softening, the stress-history tensor σ^*_{ij} is introduced to account for the influence on mechanical behavior by stress history and strain history. For isotropic consolidated material, stress-history tensor was defined as,

$$\sigma^*_{ij} = \frac{1}{\tau}\int_0^{z} \exp(-\frac{z-z'}{\tau})\sigma_{ij}(z')dz' \qquad (5\text{-}1)$$

In which, the initial consolidation history is not considered. Therefore, it can only be suitable to isotropic consolidated materials. In order to account for the influence of anisotropy consolidation, the initial stress history should be considered. The stress-history tensor is generalized here as follow,

$$\sigma^*_{ij} = \frac{1}{\tau}\int_0^{z} \exp(-\frac{z-z'}{\tau})[\sigma_{ij}(z')-\sigma_{ij}(0)]\,dz' + \sigma_{ij}(0) \qquad (5\text{-}2)$$

In the equation, $\sigma_{ij}(0)$ is initial stress tensor and is equal to initial stress history tensor $\sigma^*_{ij}(0)$, It is evident that the physical meaning of stress-history tensor defined by Eq.5-2 is much clearer than the one defined by Eq.5-1 because Eq.5-2 not only consider current stress but also initial stress history condition.

As mentioned in chapter 2, stress history parameter τ is dependent on confining stress, a generalized expression for τ is proposed based on over-consolidation ratio OCR. Detail expression for the τ can be given as

$$\tau = \alpha_\tau OCR^{\beta_\tau} = \alpha_\tau(\frac{\sigma_{mc}}{\sigma_{m0}})^{\beta_\tau} \qquad (5\text{-}3)$$

here, α_τ, β_τ are material parameters which can be determined by conventional triaxial compression test combined with curve fitting method. σ_{m0} and σ_{mc} are initial consolidated mean stress and pre-consolidated mean stress that the undisturbed samples undergone once upon a time.

5-4-2 Results and analysis of FEM simulation

Maiko testing tunnel is taken under consideration in this section(Adachi, et al., 1994). The finite element analysis is carried out in plane strain

condition. The longitudinal section of the tunnel is given in Fig.5-23. As shown in the figure, the gradient of the slope is 11.4%. In this study, only the section A-A is considered. The ratio of overburden to tunnel diameter is 3.2, therefore it is reasonable to regard it as a deep tunnel. Table 5-3 gives the in situ test results for the materials of ground in section A-A. Because of the scattered experimental result of Young's modules E, the expression of E in the calculation is given as

$$E = E_0\,(\sigma_{m0})^{E_1} \qquad (5\text{-}4)$$

Here, E_0, E_1 are constants and can be determined by in situ measurement result with least square method.

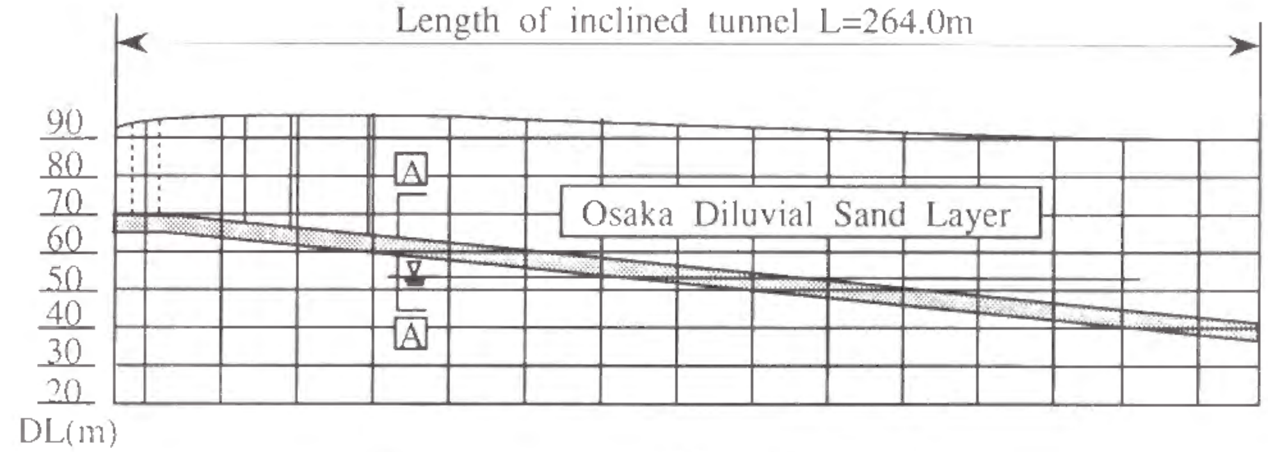

Fig.5-23 Alignment of Maiko testing tunnel

Table 5-3 Material parameters of ground

Geological profile	unit weight γ_t (g/cm^3)	Young modules E(kg/cm^2)	Poisson ratio ν
B	1.90	300.	0.35
Og_2	2.10	500.	0.30
Oc_2	2.10	950.	0.30
Og_4	2.10	1059.	0.30
Ko	2.20	1500.	0.28

Table 5-4 Material parameters involved in the constitutive model used in FEM

Geological profile	B	Og_2	Oc_2	Og_4	Ko
$\alpha_R(M_f^*)$	1.30	1.30	1.35	1.35	1.40
β_R	-0.10	-0.10	-0.10	-0.10	-0.12
G'	100.0	100.0	100.0	130.	200.
σ_{mb}(kgf/cm^2)	40.0	80.0	80.0	100.0	120.
b(kgf/cm^2)	4.0	6.0	8.0	10.0	10.0
M_m	1.20	1.08	1.08	1.08	1.30
α_τ	0.022	0.014	0.011	0.009	0.002
β_τ	-0.10	-0.10	-0.10	-0.10	-0.10

Table 5-5 Material parameter of lining

EA_{beam}(kgf)	$2.0\text{x}10^7$	EI_{beam}(kgf.cm^2)	$6.67\text{x}10^8$
E_{beam}(kgf/cm^2)	1.0×10^5		

Table 5-4 lists the material parameters involved in Adachi-Oka's model with strain softening. The material of the ground in the section is sand with fine grained soil. Because of the different geological condition along the whole tunnel, different tunneling method are used at different positions. In section A-A, multi-stage cutting method was adopted. As the tunnel section is located above ground water, no special water drainage method was used. The geometry of tunnel in section A-A and finite element mesh used in the analysis are given in Fig.5-24. 8-element isoparametric finite element is used in calculation. Beam element is introduced to simulate the lining. Table 5-5 lists the material parameters of lining in section A-A.

Investigation of ground behavior caused by tunnel excavation without lining

At first, the behavior of ground during tunnel excavation without lining is investigated. Fig.5-25 shows the relations among the octahedral stress τ_{oct}, stress history $\tau*_{oct}$ and strain γ_{oct} for the element at the spring line of

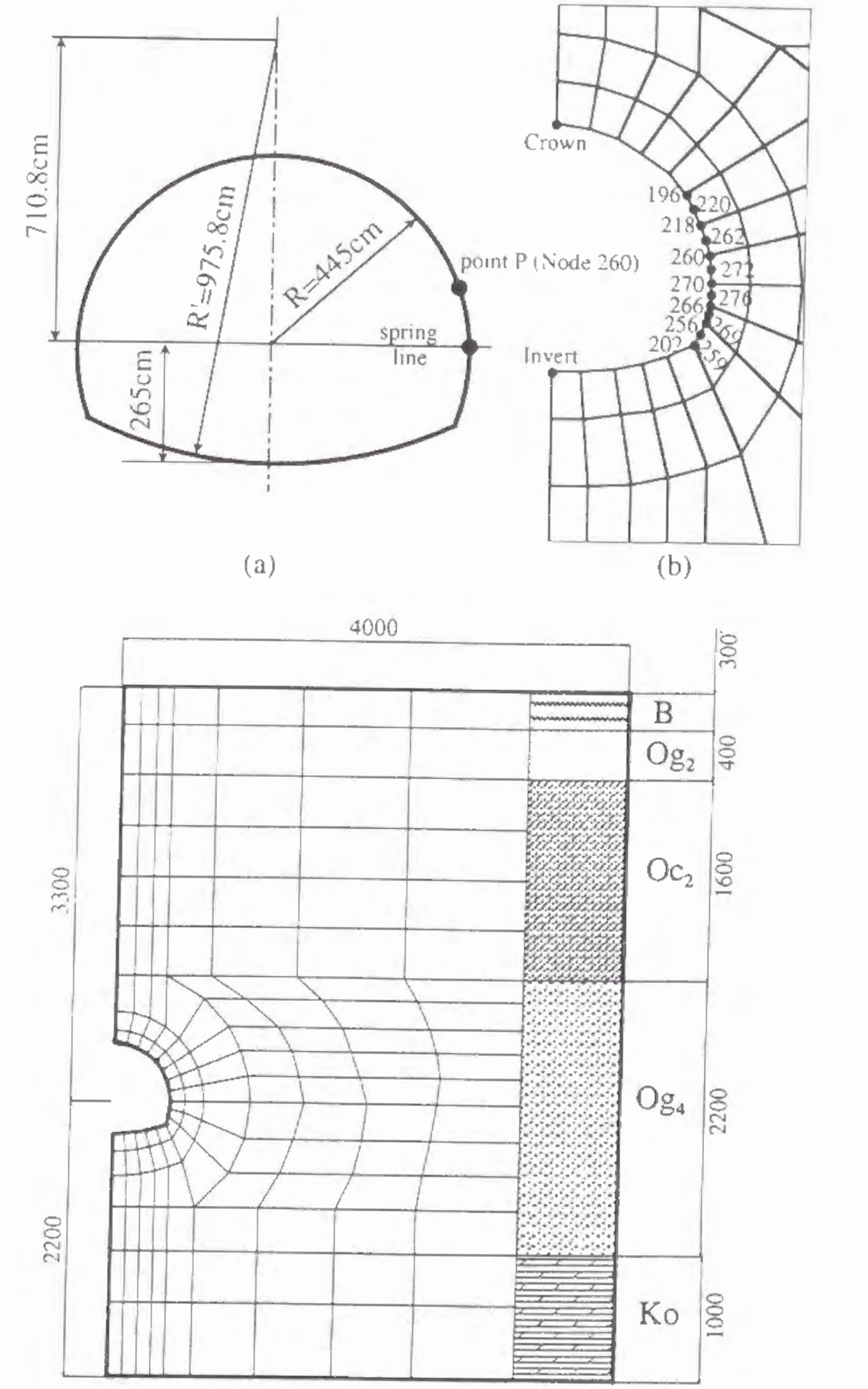

(c) (unit : cm)

Fig.5-24 Geometry of tunnel in section A-A and finite element mesh used in analysis tunnel when ISRR equals to 90%. It is found in previous chapter that Adachi-Oka's model has the features of satisfying the uniqueness of the solution in initial and boundary value problems (Adachi et al., 1991) and less mesh-size-dependency in FEM analysis. In order to obtain convergent solutions, the influence of loading steps on calculated result is investigated and it is found that when the steps are more than 40, convergent solutions can be obtained.

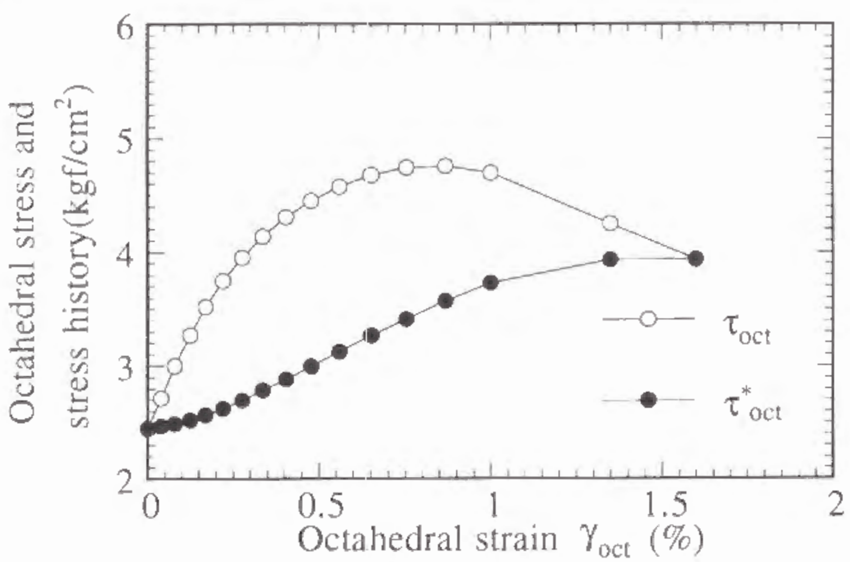

Fig.5-25 Calculated stress-strain relation

Fig.5-26 shows the displacement vectors when ISRR equals to 90% in the case of without linings. The settlements of crown and upright ground surface are 4.80cm and 1.97cm respectively. By comparing this result with observed data, it is found that the analytical results are much larger than the observed data, that is, 0.79cm at crown and 0.0cm at upright ground surface. It is also clear from the figure that even in those points far from the tunnel, the surface settlement is still very large. The reason why this discrepancy occurs is that lining is not installed in present analysis.

Fig. 5-27 gives the softening area and displacement pattern around tunnel periphery when ISRR equals to 90% in the case of without linings. Softening occurred in one layer of finite elements around tunnel periphery. The displacements of crown and invert are 4.80cm and 3.81cm respectively. From this analysis, it can be seen that if lining is not installed in tunnel excavation, large deformation will occur and tunnel wall may lose stability.

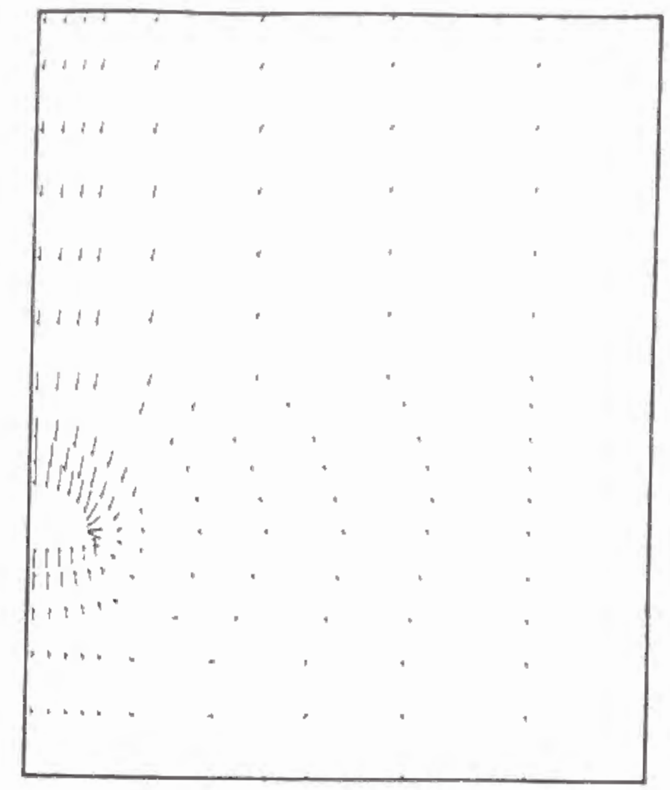

Fig.5-26 Displacement vectors when ISRR=90%(without lining)

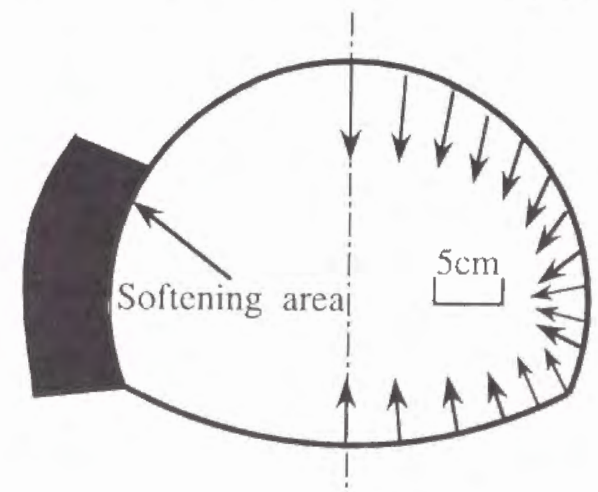

Fig.5-27 Softening zone

Investigation of ground behavior caused by tunnel excavation with lining installed at different stress released ratio

Now consider the case when tunnel lining is placed in tunnel excavation. In the analysis, the installation of primary lining is simulated as follows; beam elements, which stand for primary lining, are introduced at a prescribed initial stress released ratio and subsequently the remained initial stress is removed with the existence of lining.

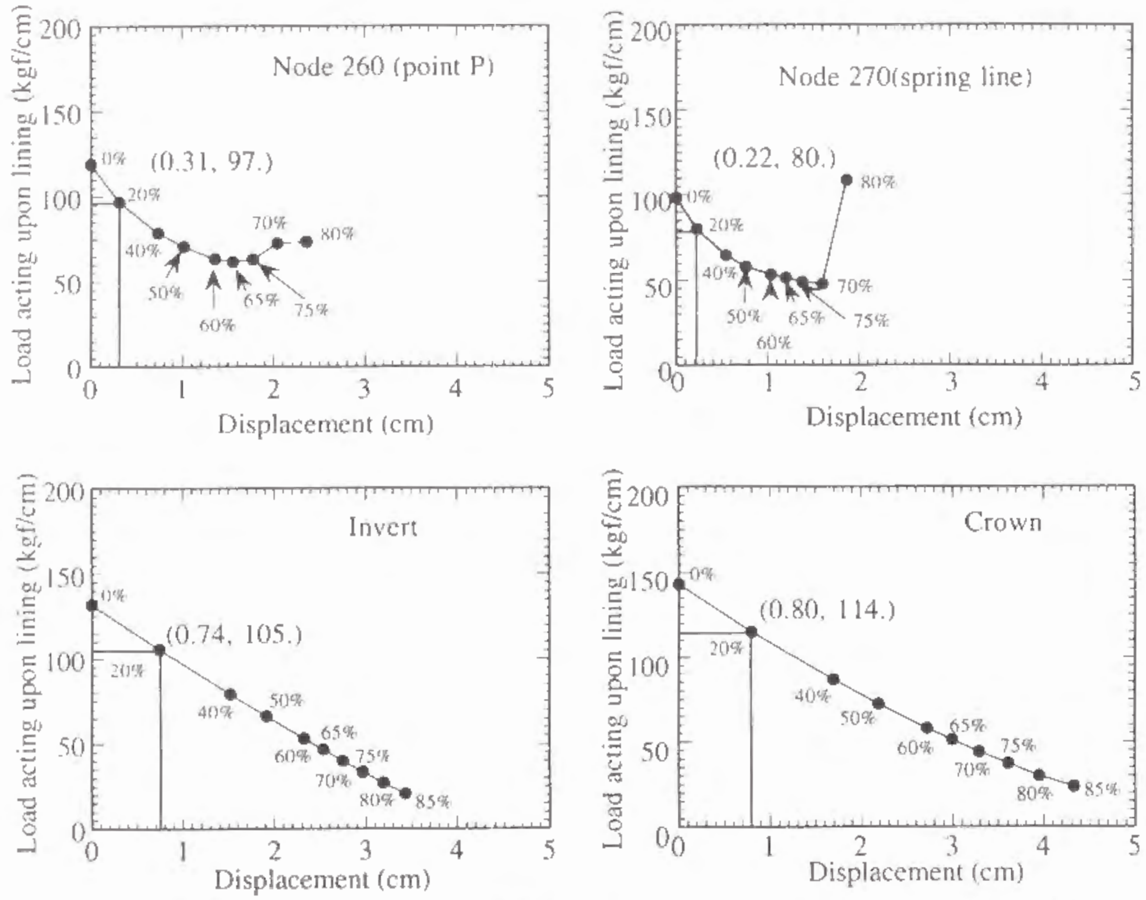

Fig.5-28 Relationships between the load acting upon lining and the displacement of tunnel lining

Fig.5-28 shows the relationship between the load acting upon the lining and the displacements of tunnel lining at point P shown in Fig.5-24. It can be seen from the figure that, if lining is installed too late and the deformation of ground become too large, the ground adjacent to tunnel periphery will lose its stability and the load acting upon lining will convert to increase along with deformation. For the test tunnel, such case did not occur and the deformation of point P ceased at 0.31 cm and consequently the load acting at point P is 97.0 kgf/cm as given by the figure, from which ISRR can be judged as 20%. It is also found in the calculation that at the invert and crown of the tunnel, the loads acting upon lining decrease almost linearly with the increase of deformation in both locations at which no prominent plastic strain occurs. The shapes of load-displacement curves in the softening area, however, show much difference. In some locations on

the tunnel lining, the load may even increase to such value that the final load is greater than the initial one. The reason of such phenomena occurring is that when strain softening occur, the stress within the softening area will redistribute to compensate for the loss of shear strength in softening area. It is also found in present calculation that strain softening takes place at different stress released stage at different locations. At any rate, it is reasonable to say that the ground convergence curve known as Fenner-Pacher curve in real tunnel excavation can be simulated by a fitting constitutive model with strain softening.

Fig.5-29 is a comparison between the observed and the calculated results of displacement when lining is installed at the time of ISRR being equal to 20%. The settlements of crown and upright ground surface are calculated as 0.80cm and 0.25cm, and the spring line is 0.37cm. The observed and the calculated results of deformation in the ground are also in good agreement.

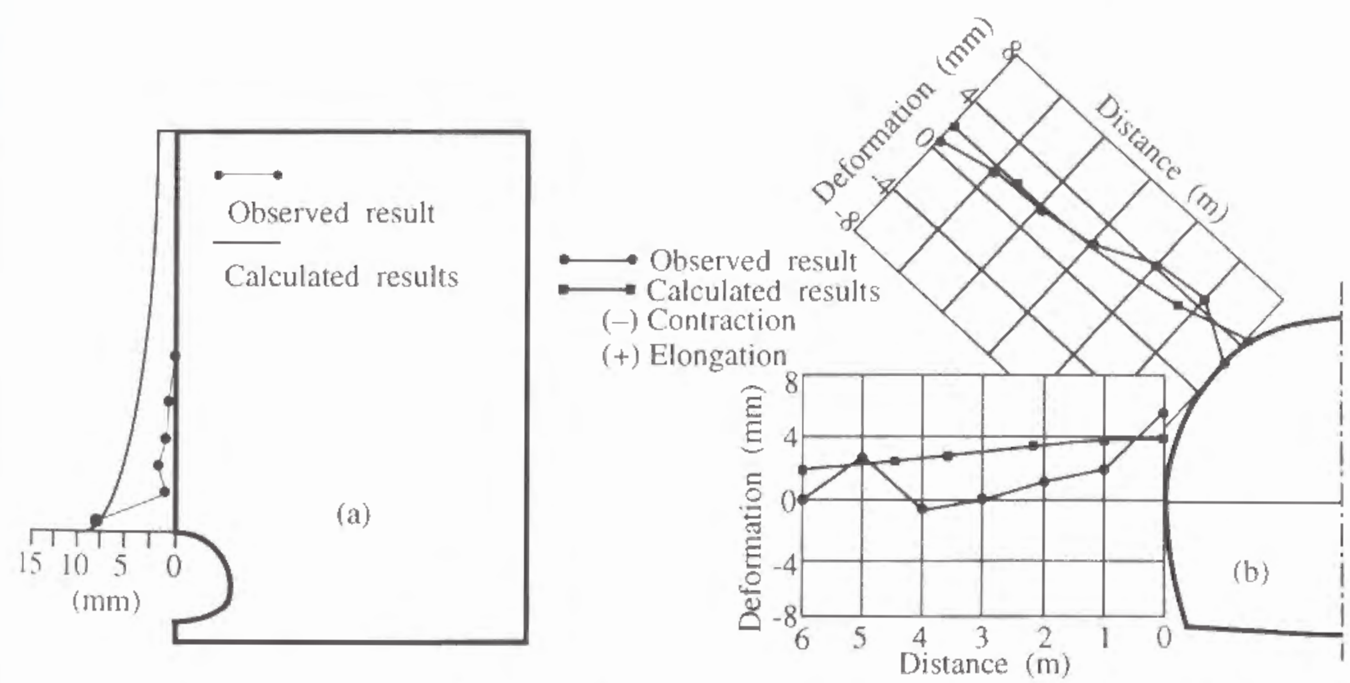

Fig.5-29 Comparison between calculated and observed displacement when ISRR=20%

Fig. 5-30 is a comparison between observed and calculated results of axial stress in lining when the lining is installed when ISRR equals to 20%. The calculated results agree well with the observed ones at crown. But at the spring line, there exists big difference between calculated and observed data. This might be due to the difficulty of simulating properly the interaction, particularly the shear force transmission, between lining and surrounding ground at the invert of tunnel. In real tunnel construction, lining especially shotcrete is installed separately in upper and lower part. While in numerical analysis, it is installed simultaneously, which will exaggerate the restriction of deformation at invert and consequently overestimate the stress in lining.

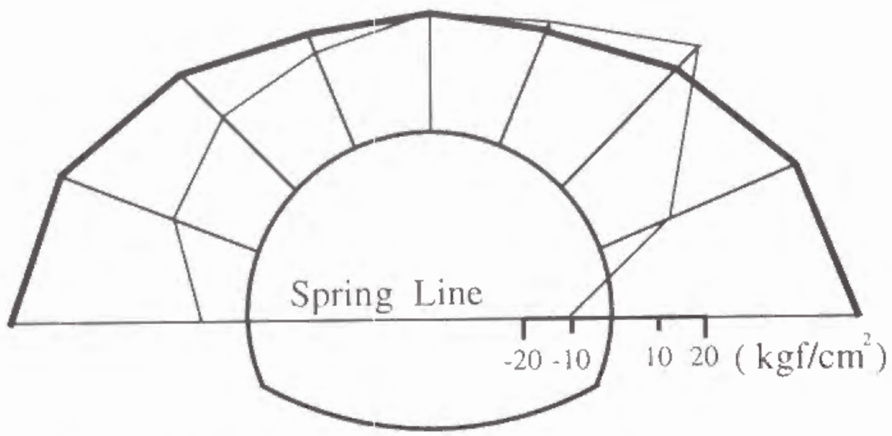

(━) : Calculating results "+": Compression
(—) : Observed results "-": Extension

Fig.5-30 Comparison between calculated and observed axial stress in lining when ISRR=20%

5-5 Case study II-shallow tunnel

5-5-1 Introduction

In shallow tunnel excavation, large surface subsidence may occur, which will greatly affect the adjacent structures. In this section, a shallow tunnel in soft rock with NATM was studied with a series of finite element analyses. Because of the fact that the ground arching effect cannot be fully achieved in such shallow tunnel with a thin overburden, discontinuous ground movement was observed in tunnel excavation. Therefore, the analysis of boundary value problem with continuum theory cannot well described this behavior.

The tunnel excavation investigated here(Adachi et al., 1993) is Subway No.1 of Fukuoka city in Japan, at the place marked by 10^k 280^m. Fig.5-31 is the geological profile and geometry of the tunnel under investigation. The

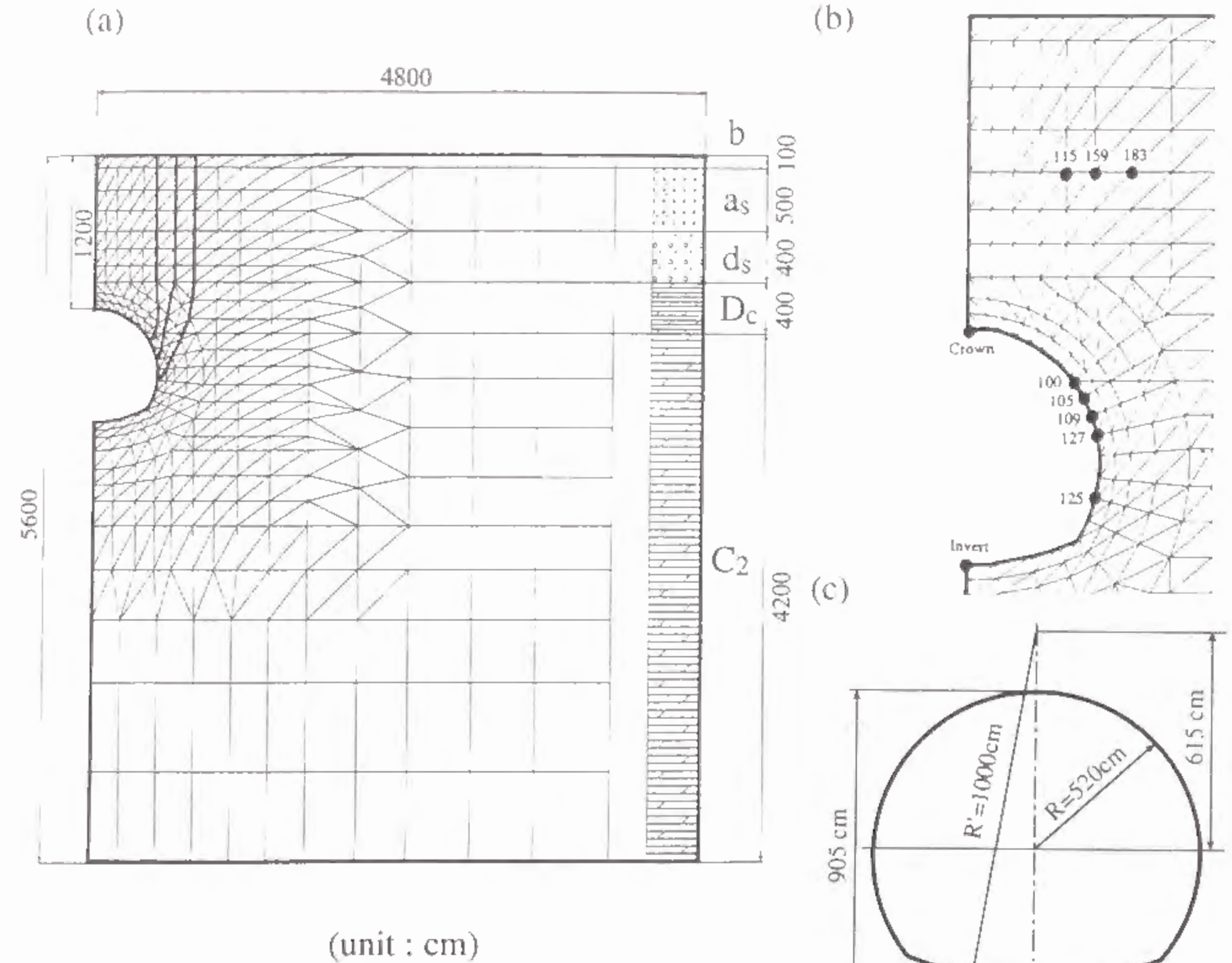

Fig.5-31 Geological profile and geometry of tunnel

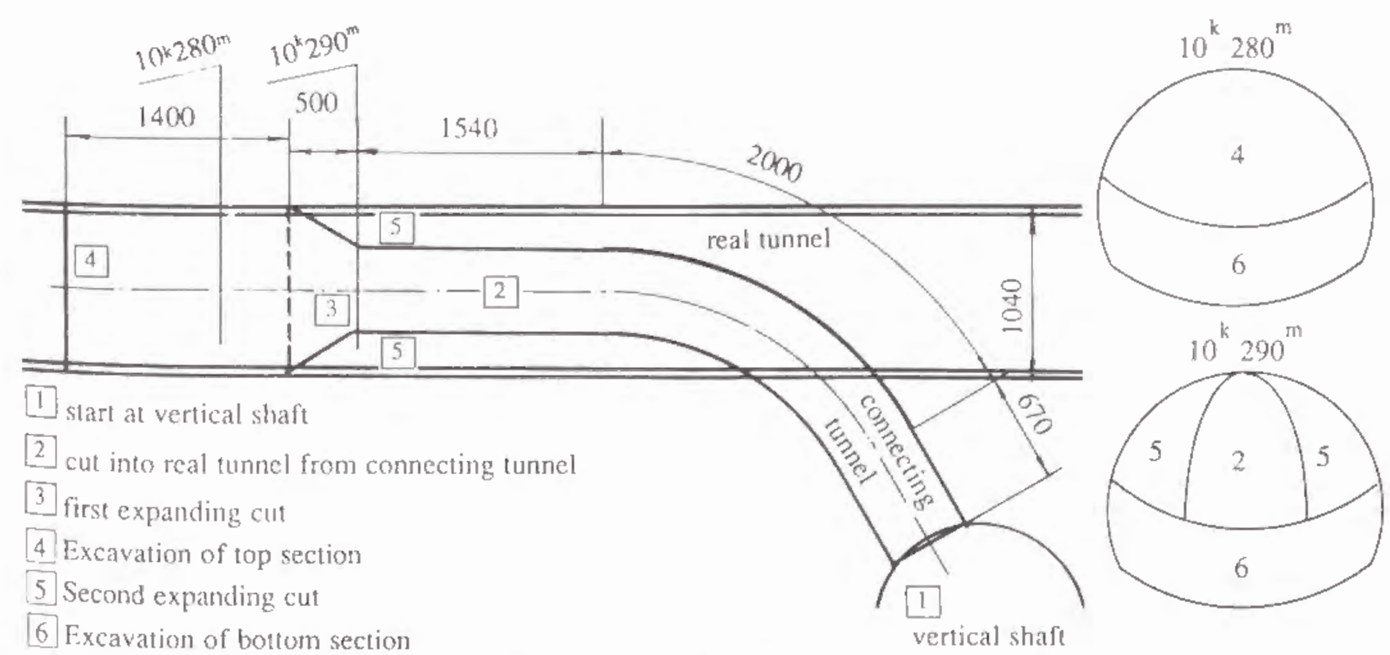

Fig.5-32 Procedure of tunnel excavation

ground is composed of topsoil b, alluvial sand with sandy silt a_s, diluvial sand d_s, strongly weathered shale D_c and weathered shale C_2. The material parameters of the ground are listed in Table 5-6.

Table 5-6 Parameters of ground material

Geological profile		Unit weight γ_t(g/cm^3)	Young modules E(kgf/cm^2)	Poisson ratio	Cohesion C (kgf/cm^2)	Friction angle ϕ (degree)
b		1.7	15.	0.4	0.	20.
a_s		1.8	30.	0.4	0.	20.
d_s		1.9	100.	0.4	0.	30.
Tr	D_c	1.9	300.	0.3	1.	0.
	C_2	2.2	1000.	0.25	10.	35.

Fig.5-32 is the demonstration of the tunnel excavating procedure. The tunnel is firstly started cutting from connecting tunnel in small scale and then start first expanding cut at section 10^k 290^m. After the excavation of top part of section 10^k 280^m, start second expanding cut at section 10^k 290^m

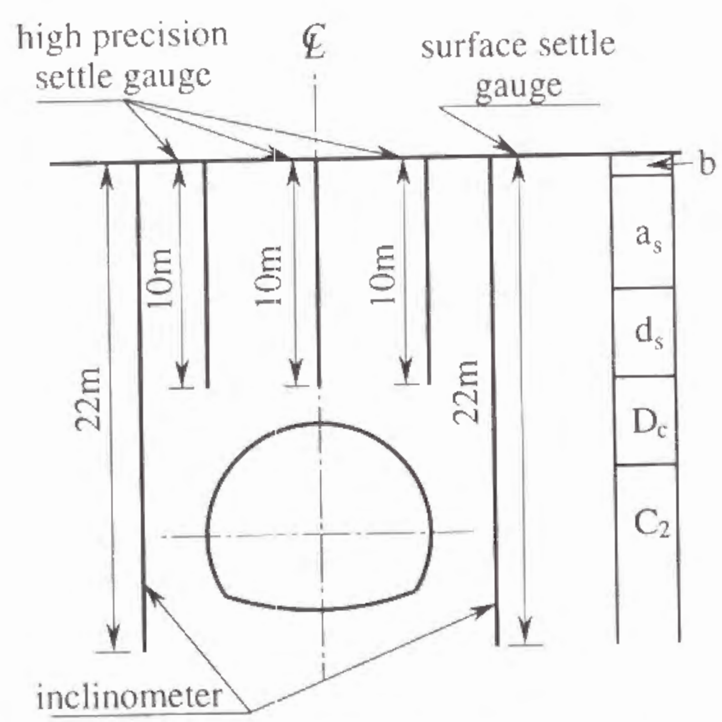

Fig.5-33 Layout of the settle gauge used in observation

and finally excavate the tunnel to full scale. During the excavation, shotcrete, steel arch and rock bolt were installed continually to avoid over release of the stress in the ground around tunnel.

In order to take close observation of ground movement during tunneling, settle gauges with high precision of 1/100 (mm) were set up in the ground adjacent to tunnel. The observed data were automatically read and put into microcomputers within the interval between 1 minute to 10 minutes. Therefore the ground movement can be monitored and controlled in microcomputer in real time. The layout of the settle gauges is illustrated in Fig.5-33.

5-5-2 Numerical study

In this section, a series of finite element analyses were carried out to establish a useful numerical analytical method which can suitably describe the mechanical behavior of shallow overburden tunnel with NATM. Four kinds of analyses are listed as follow,

Case-1 elastic finite element analysis
Case-2 elasto-plastic finite element analysis with strain softening
Case-3 elastic finite element and elasto-plastic joint element analysis
Case-4 elasto-plastic finite element with strain softening and elasto-plastic joint element analysis

All these analyses are considered in plane strain condition. Adachi-Oka's model with strain softening was used in finite element analysis. The finite element mesh used in present analysis is shown in Fig.5-31(a).

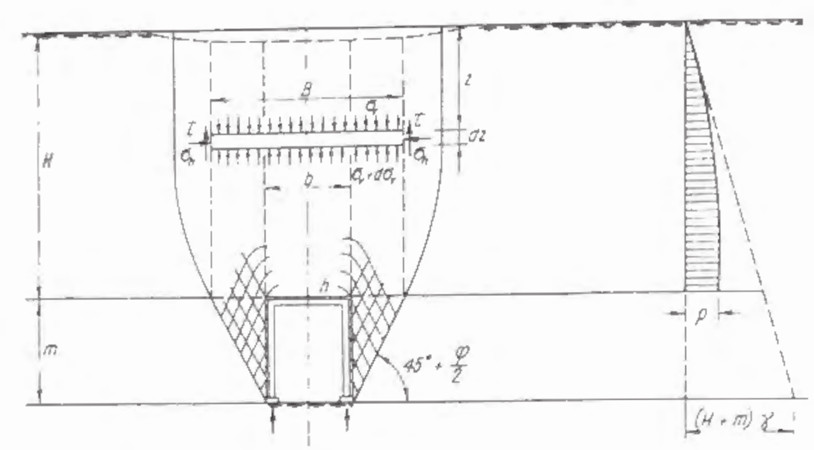

Fig.5-34 Basic assumption of Terzaghi's rock pressure theory

In shallow tunnel, because of the fact that the ground arching effect cannot be fully achieved, discontinuous deformation may occur. Such phenomenon was observed in Fukuoka Tunnel. In order to describe the behavior, joint element is introduced in the ground adjacent to the tunnel. According to Terzaghi's rock pressure theory for tunnel excavation, the displacement caused by tunneling may be sufficient to lead to develop a set of sliding planes characterizing the state of imminent rupture in the ground mass. The displacement of the earth mass is counteracted by friction developed on the vertical shear plane as shown in Fig.5-34. Based on the assumption, a group of joint elements are introduced in finite element mesh shown in Fig.5-31, in which the joint elements are marked by coarse lines. The shear strength acting along these joints in resisting displacement is expressed by Mohr-coulomb yielding rule,

$$\tau_i = c_i + \sigma_{ni} \tan \phi_i \qquad (5\text{-}5)$$

Here i represents the ith layer of geological profile. c_i, ϕ_i are the cohesion and friction angle of joint respectively and their values are equal to those of earth mass in which the joints locate.

The shear stiffness k_s of joint element is assumed to be elasto-perfectly plasticity while normal stiffness k_n takes the value of 105 kgf/cm³ when $\sigma_n > 0$ and 0.1 kgf/cm³ when $\sigma_n < 0$.

Table 5-7 Parameters of the constitutive model with strain softening

	shale	sand
$\alpha_R(M_f^*)$	1.30	1.35
β_R	-0.17	-0.10
G'	200.	100.
σ_{mb} (kgf/cm^2)	100.	20.
b (kgf/cm^2)	10.	4.2
$\overline{M}_m$	1.126	1.126
α_τ	0.009	0.026
β_τ	1.00	1.00

Numerical simulation and material parameters used in numerical analyses

The initial stress field of the ground in the analyses is gravitational field and can be expressed with overburden and K_0 , the coefficient of static earth pressure. The tunnel excavation is simulated by releasing the initial stress around tunnel periphery. The initial stress is released to zero by 100 steps in calculation.

The material parameters E, v, c, ϕ used in the analyses are listed in Table 5-6. For elasto-plastic analysis with strain softening, there are additional parameters needed for the analysis. Table 5-7 lists the values of these parameters which can be determined by conventional triaxial tests. The shear stiffness of the joint is given in the following equation

$$k_{si} = \left\{ \begin{array}{ll} E_i / (1+v)/2/cm & \tau < \tau_i \\ 0.1 \ \ (kg/cm^3) & \tau \geq \tau_i \end{array} \ i = 1,\ldots 5 \right\} \qquad (5\text{-}6)$$

where τ_i is the shear strength of ith layer and can be determined by Eq.5-5

5-5-3 Results and discussion

The following problems were investigated in the numerical analyses:

(1) deformation pattern around the tunnel,

(2) softening area developed during tunneling,

(3) investigation of characteristic curve with NATM.

The parameters of ground material used in numerical analyses are determined from laboratory tests and in-situ measurements

Deformation pattern around the tunnel

Fig.5-35 is the deformation pattern observed in Fukuoka Tunnel and the analytical result at IRSS=44% (In Case-4) for different horizontal levels. From the figure, it is clear that the discontinuous deformation can be well simulated.

Fig.5-36 shows the deformation patterns around the tunnel obtained from different analyses at ISRR=44%. In the figure, dash lines represent the

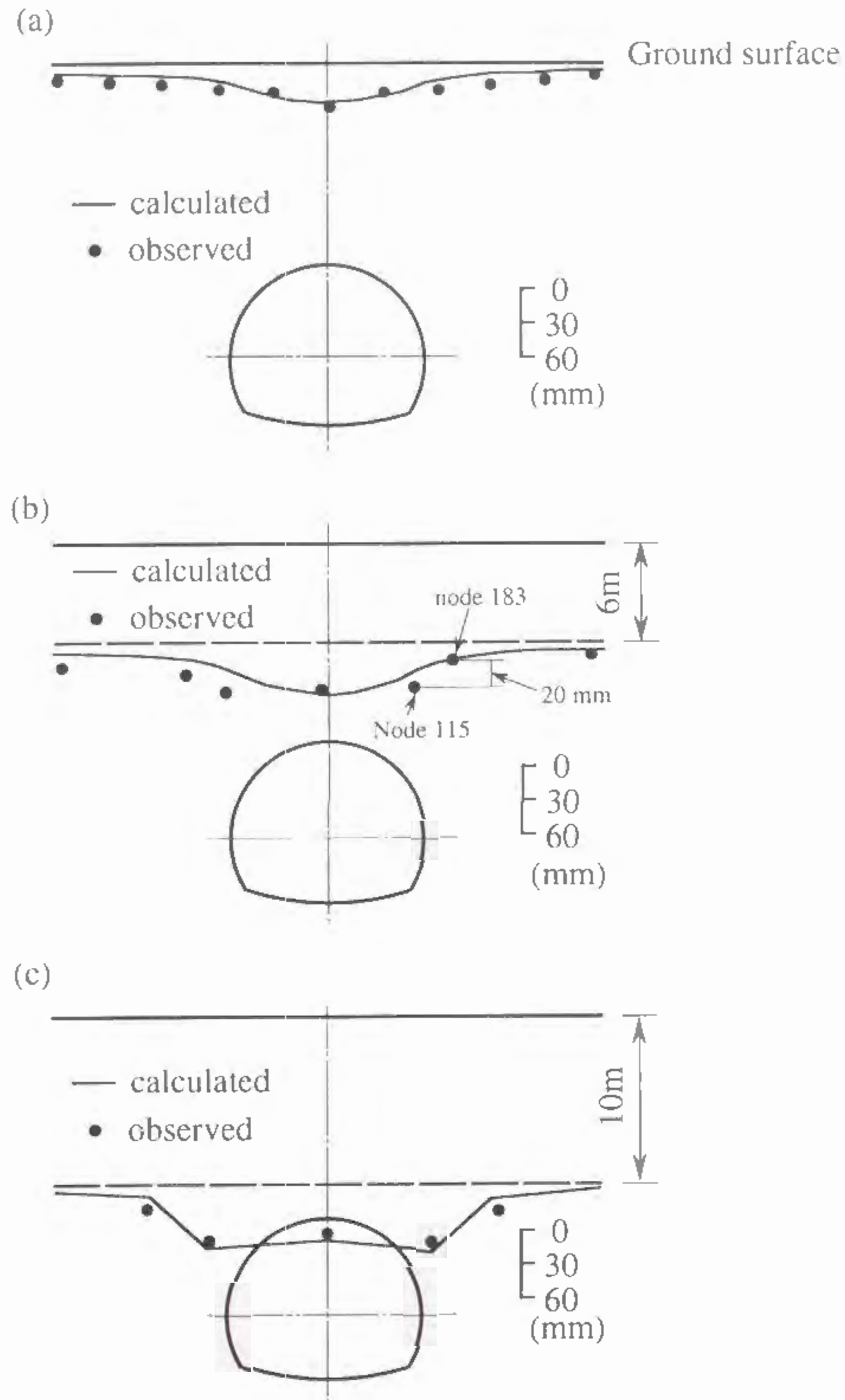

Fig.5-35 Comparison between observed and calculated deformation patterns along different horizontal lines (Case-4)

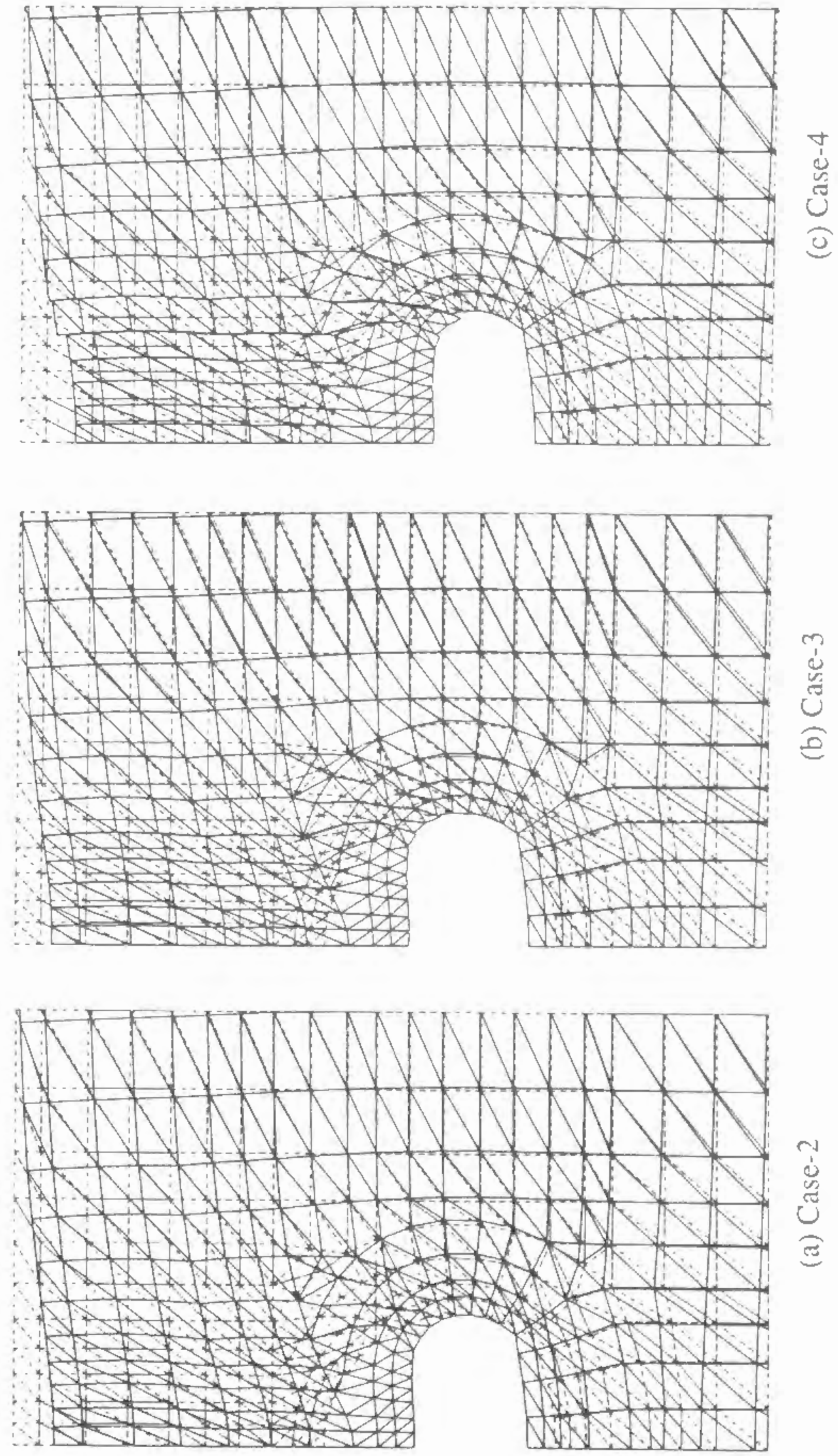

Fig.5-36 Deformation patterns around tunnel periphery when ISRR=44%

ground undergoing no deformation and real lines represent the ground undergoing deformation. It is found, though not given in the figures here, that when the ISRR is less than 35%, the deformation patterns obtained from different analyses show no much difference while at large value of ISRR, results are quite different. It can be seen from the figure that for the surface subsidence, the results from elasto-plasticity without joint (Case-2) show no discontinuous deformation while the results from Case-3 and Case-4 do show the discontinuous deformation along sliding planes.

It is evident that the analyses with joint introduced in possible sliding plane in tunnel excavation are more suitable in describing discontinuous deformation of ground in tunnel excavation than the analyses without joint. In the Case-4, because the stress strain relation of ground (finite element) is elasto-plasticity with strain hardening and softening, the joints come into yielding state earlier than in the Case-3. In Case-3 , the joints yield at ISRR=44% while in Case-4 the joints yield at ISRR=39%.

Table 5-8 Subsidence at crown and surface

	δ_{crown} (cm)		$\delta_{surface}$ (cm)	
ISRR	45%	50%	45%	50%
case 1	4.82	5.12	1.86	1.91
case 2	5.16	5.88	2.15	2.50
case 3	4.67	5.91	2.01	2.84
case 4	5.86	7.34	3.02	4.31
observation	3.8		3.3	

Table 5-8 gives the subsidence at crown and ground surface obtained from observation and analyses. In the table, 45% means that the primary lining is installed immediately after ISRR reached 45% and the remained stress is then released with the existence of lining. For the surface settlements far from tunnel, it shows no much difference. In all cases, the ground away 2D (D: tunnel diameter) from the center of tunnel almost remains unmoved. In Fig.5-35, the observed difference of deformation between node 115 and 183 as shown in Fig.5-31(c) is about 12.0mm while for the analytical result, it is 20.0mm at ISRR=50% and 8.74mm at ISRR=44%. The settlement of crown obtained from the analyses and observation shows much difference. This indicates that the simplification of

whole-face-cutting in the analyses is not so suitable to describe the crown convergence which is prevented by primary lining installed in early stage of excavation in real tunnel construction with multi-stage cutting method.

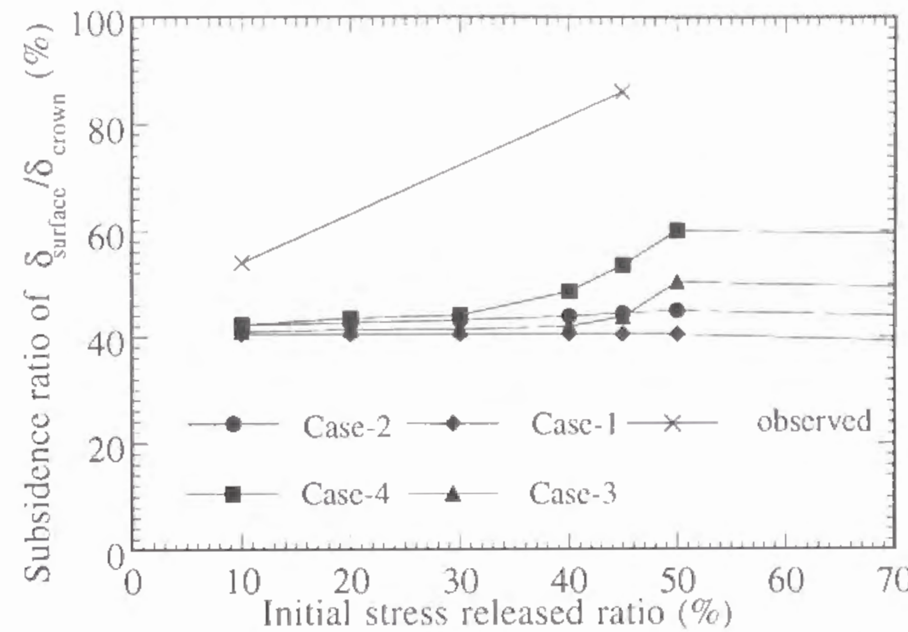

Fig.5-37 Subsidence ratios obtained from different analyses

Fig.5-37 shows the change of subsidence ratios of $\delta_{surface}/\delta_{crown}$ during tunnel excavation. Because of the fact that the arching effect cannot be fully achieved in such shallow tunnel, the subsidence ratio of $\delta_{surface}/\delta_{crown}$ will increases gradually to *100 %* when discontinuous displacement along sliding planes takes place. From the figure, it can be seen that the ratio increases very quickly when the joints come into yielding. This means that the subsidence of crown affects directly the surface settlement and consequently the ground above tunnel settles uniformly. The observed ratio of $\delta_{surface}/\delta_{crown}$ in present case, however, is larger than all calculated results. This discrepancy may be caused by the simplification in the analyses, for example, the assumption of plane strain condition and whole face cutting. In spite of this, the analyses with joint is more suitable in describing the mechanical behavior of ground related to tunnel excavation than the analyses without joint. The analyses without joint cannot describe discontinuous deformation. For this reason, it is better to avoid using the analyses of finite element only to simulate the tunnel excavation in shallow tunnel in which discontinuous deformation will probably occur.

Softening area developed during tunneling

Fig.5-38 is calculated relationship between octahedral stress and strain in softening area. The curve in the figure is not so smooth. This might be caused by the bad precision of triangle finite element in which the differential of the displacement is discontinuous.

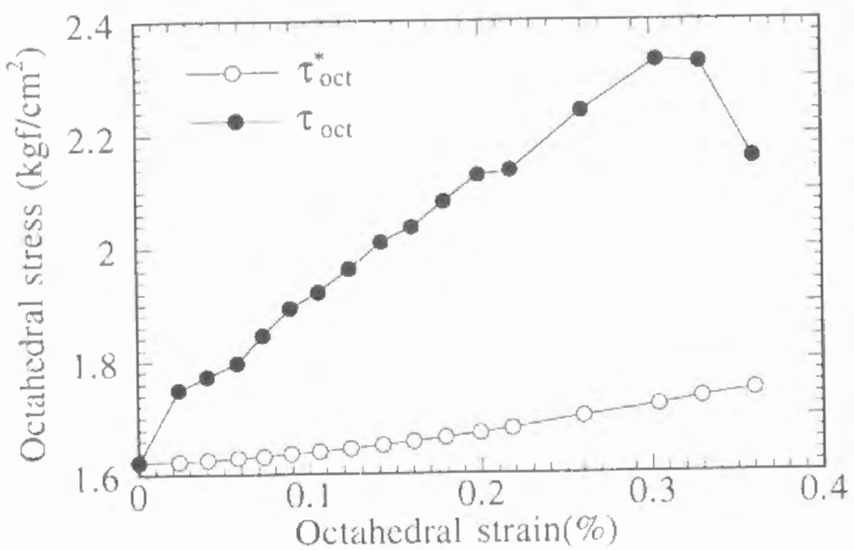

Fig.5-38 Relation between octahedral stress and strain in softening area

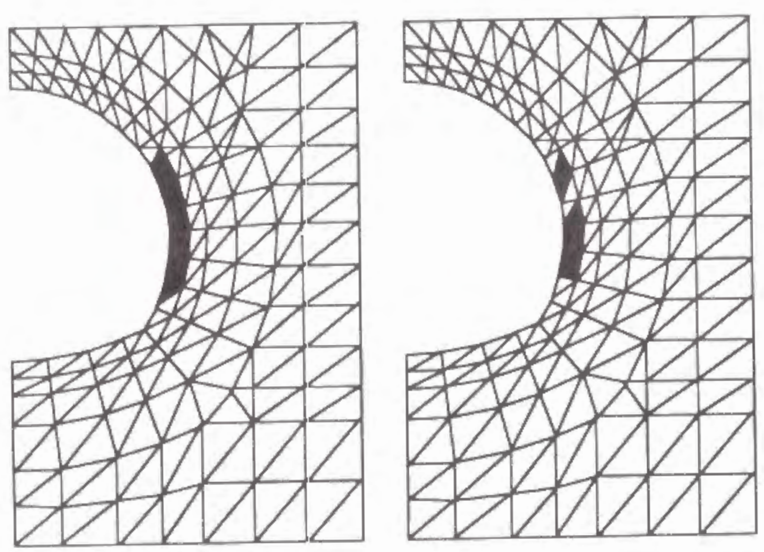

(a) case 3 (a) case 4

Fig.5-39 Softening zones in the ground caused by tunnel excavation (ISRR=50%)

Fig.5-39 shows the softening area of the ground occurred in tunnel excavation. The analyses with joint and without joint show no much

difference for the softening area. In both cases, the softening occurs in the area close to the tunnel periphery.

Investigation of characteristic curve with NATM

The characteristic curve known as Fenner-Pacher in NATM is also discussed in connection with the strain hardening and strain softening of ground materials. Needless to say, within plane strain condition, it is not easy to simulate the three dimensional excavation of tunnel. The primary lining used in the tunnel excavation consists of shotcrete, steel arch and rock bolt. However, in the analysis, the installation of primary lining is simply simulated in the way that the beam elements, which stand for the primary lining, are introduced at the prescribed value of ISRR and subsequently the remained stress is removed with the existence of lining. The material parameters of beam element are estimated from total effects of shotcrete, steel arch and rock bolt and are listed in Table 5-9.

Table 5-9 Material parameters of lining

E_{beam} (kgf/cm^2)	EI_{beam} (kgf·cm^2)	EA_{beam} (kgf)
1.0×10^5	6.67×10^8	2.0×10^7

Fig.5-40 shows the relation between the load acting upon the lining and the displacement of the lining. It can be seen that at the invert and crown of the tunnel, the load acting upon lining decrease almost linearly with the increase of deformation in both points at which no prominent plastic strain occur. Strain softening takes place at different initial stress released steps at different position. When the softening occurs, the load acting upon lining will increase as the convergence of tunnel periphery develops. As in the case study I, the ground convergence curve known as Fenner-Pacher curve can be simulated in shallow tunnel excavation by using suitable constitutive model with strain softening. In Fig.5-40, the black point stands for the point at which lining is installed when ISRR equals to 44%. It is found that if the tunnel excavation is simulated at such condition that lining is installed at ISRR=44% and then the remained stress is released with the existence of lining, the calculated displacements are most fitted to observed data. Therefore, the stress released ratio in Fukuoka Tunnel can be estimated to be 44%. Based on Fig.5-40, it is able to estimate how much the load acting upon lining if lining is installed at prescribed displacement. For example, if lining is installed at the time when the Node 105 undergone 1.75cm of displacement, then the load acting on Node 105 can be estimated to be 63.0 kgf/cm.

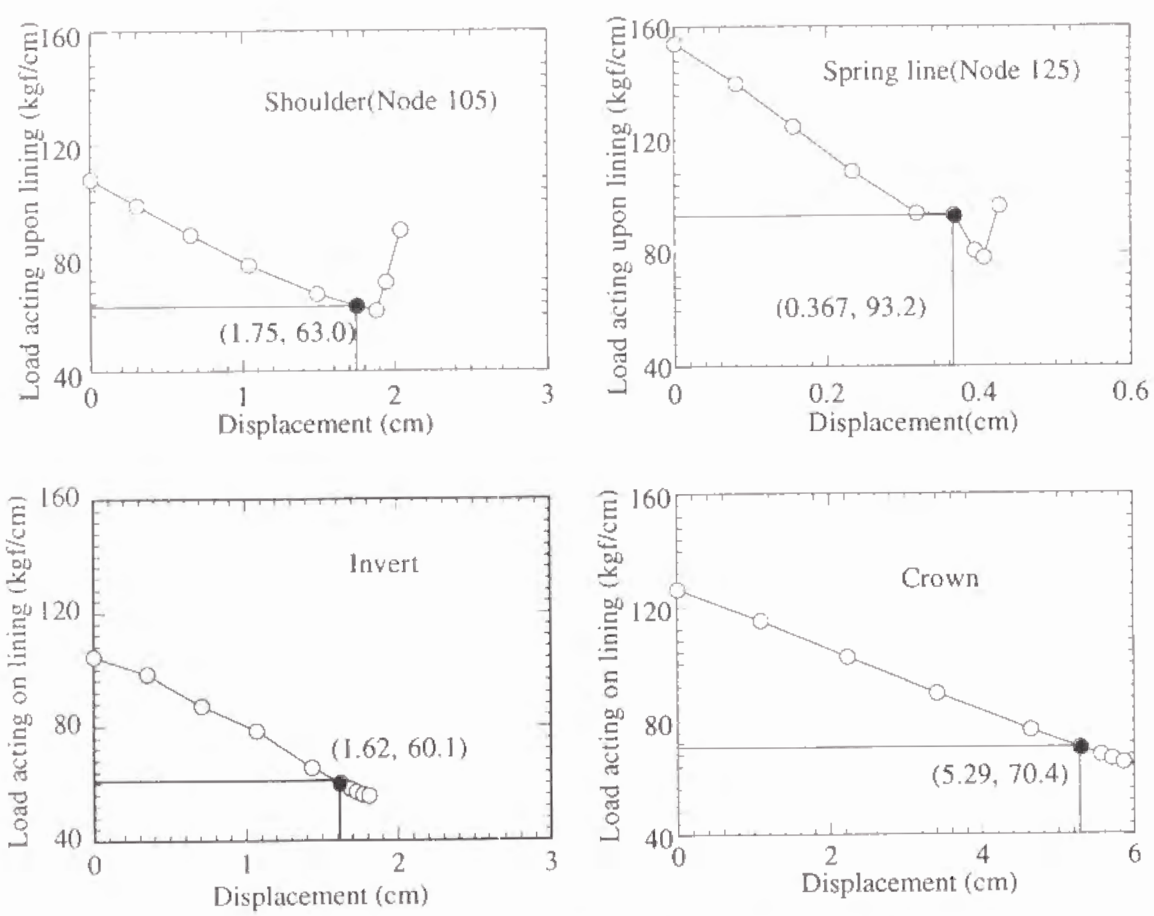

Fig.5-40 Relationships between the load acting upon lining and the displacement of tunnel lining

Fig.5-41 shows the comparison of ground convergence curves of lining obtained from elasto-plasticity with strain softening and elasticity. For the result from elasticity, the load acting upon lining will decrease monotonously while for the result from elasto-plasticity with strain softening, the load acting upon lining will increase with the increase of displacement if softening occurs.

Fig. 5-42 shows the comparison between the observed and calculated results of axial stress in lining when the lining is installed at the time ISRR= 44%. The calculated results agrees well with the observed ones at crown.

But at the spring line, there exists big difference between calculated and observed data. The reason may be as follow. Firstly, the primary lining which consists of shotcrete, steel arch and rock bolt is simply simulated as beam elements whose mechanism is close to shotcrete and steel arch. However, the rock bolt cannot be suitably simulated in this way. If the suspending effect of rock bolt be take into consideration in the analyses, the

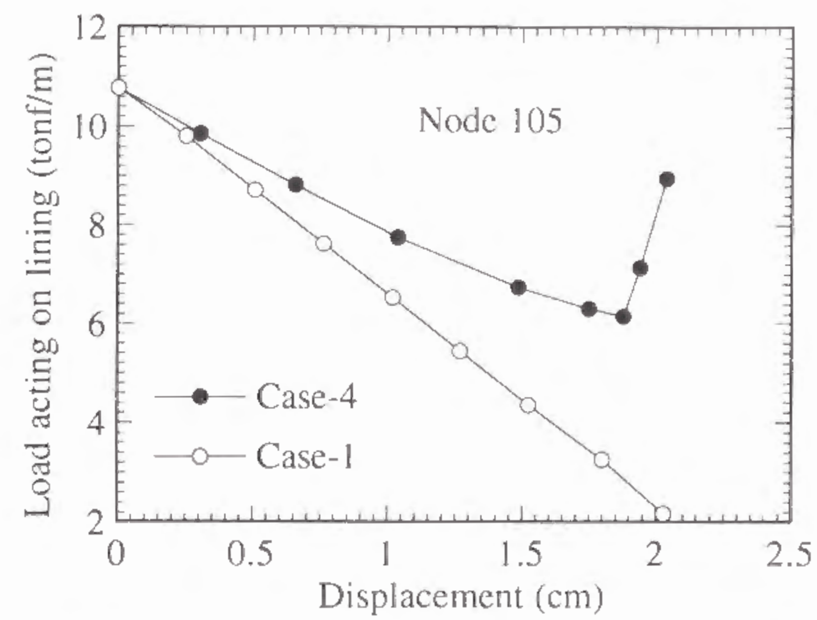

Fig.5-41 Comparison of load-deformation curve of lining obtained from Case-1 and Case-4

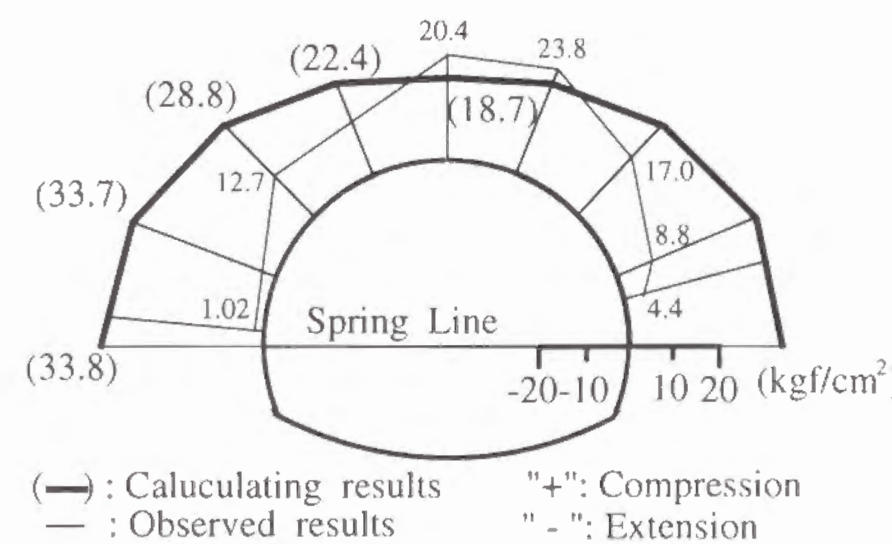

Fig.5-42 Comparison between observed and calculated results of axial stress in lining when ISRR=44%(Case-4)

analytical results of axial stress should be much less in the spring line. Secondly, in the present analysis, the beam elements are introduced all around tunnel periphery at the same time, while in practice, the linings in upper part and invert are installed at different time. Therefore, it is difficult to simulate properly the interaction, particularly the shear force transmission, between lining and surrounding ground at invert.

5-6 Conclusions

In this chapter, the mechanical behavior of ground and lining in tunnel construction is investigated using a series of finite element and joint element analyses based on Adachi-Oka's model with strain softening. As a fundamental study, a trapdoor problem in model ground is investigated with FEM and JEM. The ground convergence curve of trapdoor can be simulated with either of the methods. It is found that in simulating the decent of trapdoor, load method is more suitable than displacement method . Then the mechanism of tunnel excavation in model ground with a homogeneous stress field in different ratios of the overburden to tunnel diameter is investigated. The capability of present analysis to simulate the Fenner-Pacher characteristic curve in tunneling with NATM is confirmed. It is found that the mechanical behaviors of shallow and deep tunnel are quite different and should be dealt with distinctively. In simulating tunnel excavation in real ground, two different types of case studies are carried out. One is related to a relatively deep tunnel excavation and another one is concerned with a shallow tunnel construction in which discontinuous deformation was observed during excavation. A series of finite element and joint element analyses are carried out in order to verify which method is the best in simulating tunnel construction. In the analyses, the parameters involved in the constitutive model are based on in-situ measurement and laboratory tests. The influence of anisotropic consolidation is also taken into consideration in the analyses. The following conclusion from the case studies can be given,

(1) The deformation patterns around tunnel show great difference for different analyses when the ground comes into softening and joints become yielding. The discontinuous deformation observed in shallow tunnel excavation can be well simulated by the analyses with joint. On the contrary, it is better not to use finite element method without joint to simulate shallow tunnel construction. In deep tunnel, such restriction is not necessary.

(2) The analyses based on the constitutive model with strain hardening and softening show that at the geological condition of Fukuoka Tunnel and Maiko tunnel, softening will occur if lining is installed too late and the initial stress released ratio reaches a certain value. The softening area is limited to the ground close to tunnel periphery.

(3) The analyses based on the constitutive model with strain softening can well describe the ground convergence characterized by so called Fenner-Pacher curve in tunneling with NATM.

Though the finite element analyses carried out in this chapter are only referred to two examples of tunnel construction and the material parameters are determined from in-situ measurement and laboratory tests for the special cases, it can also be applied to general situation. The simulation of primary lining used in tunneling with NATM should be improved to be able to describe the real mechanism more precisely.

References

(1) Adachi, T. and Oka, F. (1989) : "A FEM analysis of strain localization for soft rock using a constitutive equation with strain softening," Workshop on Numerical method for localization and bifurcation of granular bodies, Gdansk(Poland), September, 25-30.

(2) Adachi, T., Tamura, T., Yashima, A. and Ueno, A. (1985) : "Behavior and simulation of sandy ground tunnel," Proc. JSCE No.358 /III-3, pp. 129-136(In Japanese).

(3) Adachi, T., Tamura, T., Yashima, A. and Ueno, A. (1986) : "Surface subsidence above shallow sandy ground tunnel," Proc. JSCE No.370 /III-5, pp. 85-91(In Japanese).

(4) Adachi, T., Oka, F., Yashima, A. and Zhang, F. (1994) : "Analysis of earth tunnel by strain softening constitutive model," Proc. 13th ICSMFE, India, Vol.2, pp.879-882

(5) Adachi, T., Zhang, F., Oka, F. and Yashima, A. (1993) : "Finite element analysis for constitutive model with strain softening," Computational Mechanics, A. A. Balkema, pp.325-330.

(6) Adachi, T., Zhang, F., Oka, F. and Yashima, A, (1991) : "A FEM analysis of strain localization using a non-local strain-softening plasticity," Proc. 3th Int. Conf. on Constitutive Laws for Engineering Materials, Theory and Application, Tucson, USA.
(7) Adachi, T., Oka, F., Ohnishi, Y. and Zhang, F. (1991) : "A Constitutive Model for Rock Discontinuity with Strain Softening," Journal of Japan Society of Dam Engineering, Vol.3, pp.34-40.(In Japanese)
(8) Adachi, T., Zhang, F., Matushita, Y. and Hashimoto, T. (1993) : "Shallow tunnel in soft rock with NATM," Proc. of Int. Symp. Geotechnical Engineering of Hard Soils-Soft Rocks, Athens, Greece, A. A. Balkema, pp.1365-1372.
(9) Ladanyi, B. and Hoyaux, B. (1969) : "A study of trap-door problem in a granular mass," Canadian Geotech. J., Vol.6, No.1, pp.1-15.
(10) O. C. Zienkiewicz : "The Finite Element Method," McGRAW-Hill Book Company Third Edition.
(11) Oka, F. and Adachi, T. (1985) : "An elasto-plastic constitutive equation of geologic materials with memory," Proc. of 5th Int. Conf. on Numerical Methods in Geomechanics, Nagoya, pp. 1-5.
(12) Rabcewicz, L. V., (1965) : "The New Austrain Tunneling Method," Part III, Water Power, Jan., pp. 19-24.
(13) Rlph, B., Peck (1969) : "Deep Excavation and Tunneling in Soft Ground," State of the Art Report, 7th Int. Conf. on Soil Mechanics and Foundation, Mexico.
(14) Szechy, K., (1966) : "The Art of Tunnel," Akademiai, Kiado Budapest, Printed in Hungary.

Chapter 6

An elasto-viscoplastic constitutive model with strain softening

6-1 Introduction

It is found that some geologic materials, such as soft rock, are strain-hardening-softening and time dependent materials with dilatancy. As for the time dependent behavior, it involves three aspects, namely, the strain rate effect, creep and stress relaxation. Many models have been proposed to describe the time dependency of geologic materials. They are found in the studies by Andersland and Al-Nouri(1970), Ting(1983). Singh and Mitchell(1968) clarified the mechanism of creep for soil under undrained condition; Saito and Uezawa(1961) gave an empirical prediction of creep failure time. Oka(1985) proposed a viscoplastic model with memory and an internal variable based on the generalized theory of Wang(1969) and Perzyna(1980). Adachi et al.(1990) proposed a viscoplastic model which can describe both the strain rate effect and strain softening of frozen sand. As for the strain softening behavior, Oka and Adachi(1985) proposed an elasto-plastic model for soft rock, taking into consideration the strain-hardening-softening effect.

Most of the above studies focused only on one aspect of the strain-softening and the time dependency of geologic materials. A more general model which can describe both of the above-mentioned behaviors is desirable in geotechnical engineering. Based on the model proposed by Oka(1985) with memory and an internal variable, a new type of elasto-viscoplastic model is proposed in this chapter to describe not only strain softening but also strain rate dependency, creep and stress relaxation.

6-2 Elasto-viscoplastic model with strain softening

Adachi et al.(1990) proposed an elasto-viscoplastic model for frozen sand exhibiting strain softening, using a time measure which is similar to that proposed by Valanis(1971). In present paper, however, the definition of a new incremental time measure is introduced in following form:

$$dz = C \exp\left(-\frac{z-z_1}{C}\right) dt \qquad (6\text{-}1)$$

where dz is an incremental time measure, t is the real time and C is the parameter of time dependency which will be discussed later in detail. z_1 is the initial time measure. In the present study, the stress history tensor is expressed by introducing a single exponential type of kernel function similar to that in a previous work by Adachi and Oka(1990), namely,

$$\sigma^*_{ij} = \frac{1}{\tau}\int_0^z \exp(-(z-z')/\tau)\sigma_{ij}(z')dz' \qquad (6\text{-}2)$$

where τ is a material parameter which expresses the retardation of stress with respect to the time measure. The total strain increment tensor is composed of the elastic and plastic components:

$$d\varepsilon_{ij} = d\varepsilon^e_{ij} + d\varepsilon^p_{ij} \qquad (6\text{-}3)$$

The viscoplastic strain increment is assumed to be given by the non-associated flow rule,

$$d\varepsilon_{ij}{}^p = H\frac{\partial f_p}{\partial \sigma_{ij}} df_y \ , \qquad (6\text{-}4)$$

where f_p is the plastic potential function, f_y is the yield function and H is the loading index describing the hardening-softening characteristics.

The subsequent yield function is defined by

$$f_y = \eta^* - \kappa = 0 \qquad (6\text{-}5)$$

$$\eta^* = \sqrt{S^*_{ij} S^*_{ij}} / (\sigma^*_m + b) \qquad (6\text{-}6)$$

where S^*_{ij} is the deviatoric stress history tensor, b is the plastic potential parameter, σ^*_m is the mean stress history and κ is the strain hardening-softening parameter. The parameter κ is assumed to be given by the following evolution equation for strain hardening and softening:

$$\dot{\kappa} = \frac{G'(M^*_f - \kappa)^2}{M^{*2}_f} \dot{\gamma}^p \qquad (6\text{-}7)$$

where $\dot{\gamma}^p = (\dot{e}^p_{ij} \dot{e}^p_{ij})^{1/2}$. In the case of proportional loading, it can be integrated as

$$\kappa = \frac{M^*_f G'\gamma^p}{M^*_f + G'\gamma^p} \qquad (6\text{-}8)$$

where γ^p is the second invariant of the deviatoric plastic strain, that is, $\gamma^p = (e_{ij}{}^p e_{ij}{}^p)^{1/2}$. G', and M^*_f are strain hardening-softening parameters. M^*_f was supposed to be constant, in the previous study by Adachi et al. (1992), while it is assumed to change according to the time measure in the present study. M^*_f takes the form of

$$M^*_f = M^*_{f\infty} + (M^*_{f0} - M^*_{f\infty})\, e^{-A(z-z_1)} \qquad (6\text{-}9)$$

where $M^*_{f\infty}$ is the residual value of $\eta = \sqrt{2J_2}/(\sigma_m + b)$. A is a material parameter and can be determined by triaxial drained creep tests. M^*_{f0} is dependent on the initial stress state and can be expressed as

$$M^*_{f0} = \begin{cases} \sqrt{2J_2}/\sigma_m\big|_{\text{at } t=0} & if\ \sqrt{2J_2}/\sigma_m\big|_{\text{at } t=0} > M^*_{f\infty} \\ M_{f\infty} & if\ \sqrt{2J_2}/\sigma_m\big|_{\text{at } t=0} \le M^*_{f\infty} \end{cases} \qquad (6\text{-}10)$$

Eq.6-9 shows that the shear strength of a given material decreases with the time measure due to the aging effect. Fig.6-1 shows schematically how the failure line changes in accordance with time measure in stress history space.

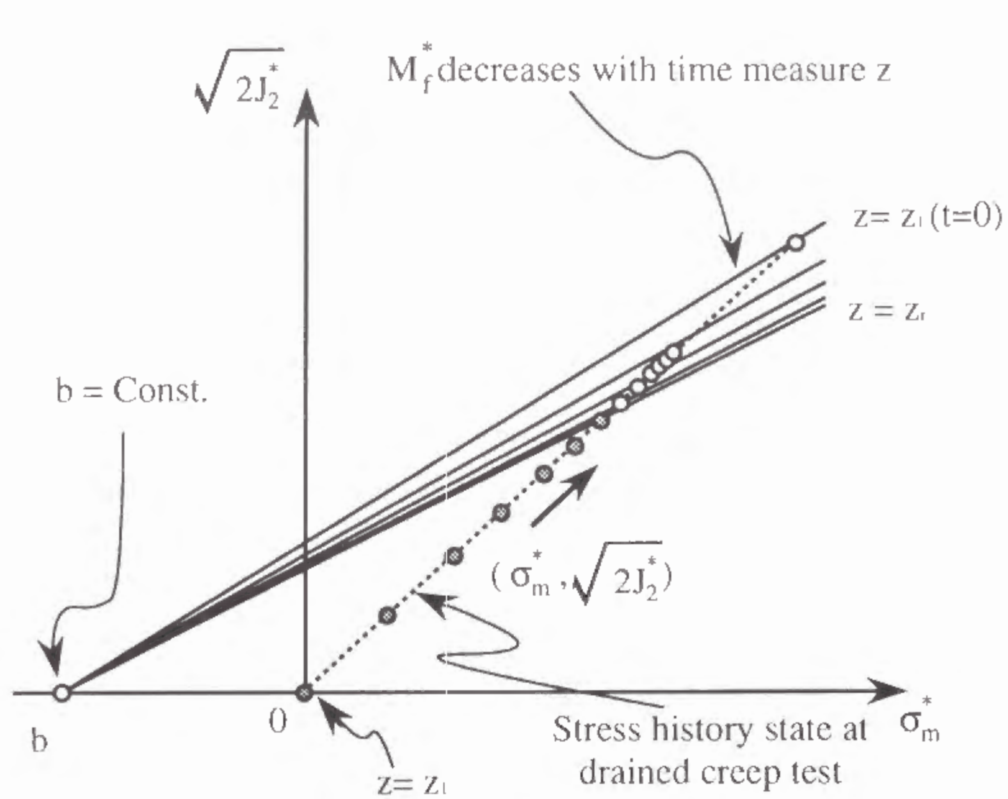

Fig.6-1 Variation of M^*_f with time measure

The loading conditions are given by the following relations:

$$d\varepsilon^p_{ij}\left\{\begin{array}{ll} \neq 0 \ if\ f_y=0,\ df_y>0 & loading \\ =0 \ if\ f_y=0,\ df_y=0 & neutral \\ =0 \ if\ f_y=0,\ df_y<0 & unloading \end{array}\right. \tag{6-11}$$

It is assumed that plastic potential function is expressed by the relation as

$$f_p=\bar{\eta}+\bar{M}\ln\left[(\sigma_m+b)/(\sigma_{mb}+b)\right]=0 \tag{6-12}$$

where $\bar{\eta}=(S_{ij}S_{ij}/(\sigma_m+b)^2)^{1/2}$, in which S_{ij} is the deviatoric stress tensor, σ_m is the mean stress and $\bar{M}$ is the parameter that controls the development of the volumetric strain.

The concept of boundary surface, introduced in previous studies, is expressed by the following relation:

$$f_b=\bar{\eta}+\bar{M}_m\ln\left[(\sigma_m+b)/(\sigma_{mb}+b)\right]=0\ . \tag{6-13}$$

Based on this relation, the value of $\bar{M}$, can be determined by considering the following condition:

$$\left\{\begin{array}{ll} \bar{M}=-\bar{\eta}/\ln\left[(\sigma_m+b)/(\sigma_{mb}+b)\right] & f_b\le 0 \\ \bar{M}=\bar{M}_m & f_b>0 \end{array}\right\}. \tag{6-14}$$

Combining Eq.6-4, 6-5, 6-12, 6-13 and 6-14, it is easy to derive the following equation for the viscoplastic strain increment tensor:

$$d\varepsilon^p_{ij}=\Lambda\left[\frac{\bar{\eta}_{ij}}{\bar{\eta}}+(\bar{M}-\bar{\eta})\frac{\delta_{ij}}{3}\right]d\eta^*$$

or

$$d\varepsilon^p_{ij}=\Lambda\left[\frac{\bar{\eta}_{ij}}{\bar{\eta}}+(\bar{M}-\bar{\eta})\frac{\delta_{ij}}{3}\right]\left[\frac{\eta^*_{kl}}{\eta^*}-\eta^*\frac{\delta_{kl}}{3}\right]\frac{d\sigma^*_{kl}}{\sigma^*_m+b} \tag{6-15}$$

where

$$\Lambda=\frac{M_f^{*2}}{G'(M_f^*-\eta^*)^2}\ ,\quad \bar{\eta}_{ij}=S_{ij}/(\sigma_m+b)\ ,$$

$$\eta^*_{kl}=S^*_{kl}/(\sigma^*_m+b)\ . \tag{6-16}$$

Finally, the elastic strain increment is evaluated by

$$d\varepsilon^e_{ij}=ds_{ij}/2G+d\sigma_m\delta_{ij}/3K\ . \tag{6-17}$$

6-3 Application to drained creep tests on soft rock

In drained triaxial creep tests, the stress is kept constant, that is, $\Delta\sigma_{ij}=0$, $\sqrt{J_2}=const.$ and $\sigma_m=const.$. By integrating Eq.6-1, the expression for the time measure can be given in Eq.6-18 if taking into consideration the fact that the initial time measure, $z\,|_{t=0}=z_I$, is usually not equal to zero, namely,

$$z - z_1 = C\ln(1+t) \quad . \tag{6-18}$$

Here z_1 is the time measure for the time at which the creep tests begin. In drained creep tests, the stress is not applied all at once to the specimens. The loading process from zero to a certain stress state usually takes some time. It is reasonable, therefore, to conclude that the initial time measure is not equal to zero, which means that the stress history will also not be equal to zero. Its value is dependent on the loading rate and the loading path. Here, it can be assumed that the load increases proportionally to time measure z during the interval $[0, z_1]$. The stress history can then be calculated in the following manner:

$$\sigma^*_{ij} = \sigma^*_{ij1} + \sigma^*_{ij2} \tag{6-19}$$

where

$$\sigma^*_{ij1} = \frac{1}{\tau}\int_0^{z_1} \exp(-(z-z')/\tau)\sigma_{ij}(z')dz$$

$$=\sigma_{ij}\frac{e^{-z/\tau}}{z_1}\int_0^{z_1} e^{z'/\tau}\frac{z'}{\tau}dz' = \sigma_{ij}e^{-(z-z_1)/\tau}\ \frac{\tau}{z_1}(\frac{z_1}{\tau} - 1 + e^{-z_1/\tau}) \quad , \tag{6-20}$$

while in creep tests, stress is kept constant, namely,

$$\sigma^*_{ij2} = \frac{1}{\tau}\int_{z_1}^{z} \exp(-(z-z')/\tau)\sigma_{ij}(z')dz = \sigma_{ij}(1 - e^{-(z-z_1)/\tau}) \tag{6-21}$$

$$\sigma^*_{ij} = \sigma^*_{ij1} + \sigma^*_{ij2} = \sigma_{ij}[1 - e^{-(z-z_1)/\tau}g(z_1)] = \sigma_{ij}f(z) \tag{6-22}$$

$$f(z)=1 - e^{-(z-z_1)/\tau}g(z_1) \quad , \quad g = g(z_1) = \frac{\tau}{z_1}(1 - e^{-z_1/\tau}) \ . \tag{6-23}$$

In axisymmetric condition, the detailed expression for the deviatoric and the volumetric components of viscoplastic strain can be given as(See **Appendix**)

$$de^p_{11} = \frac{2}{3G}\frac{M_f^{*2}}{(M_f^*-\eta^*)^2}\, g(z_1)\, \frac{bqe^{-(z-z_1)/\tau}}{(\sigma^*_m+b)^2}\, \frac{dz}{\tau} \tag{6-24}$$

$$dv^p = \Lambda(\bar{M} - \frac{\sqrt{2/3}\,q}{\sigma_m+b})\,d\eta^* = (\bar{M} - \frac{\sqrt{2/3}\,q}{\sigma_m+b})\sqrt{3/2}\,de^p_{11} \tag{6-25}$$

Eq.6-24 can be rewritten as

$$\dot{e}_{11} = \dot{e}^p_{11} = \frac{2bq}{3G'\tau}\, g(z_1)\, \frac{M_f^{*2}}{(M_f^* - \eta^*)^2}\, \frac{e^{-(z-z_1)/\tau}}{(\sigma^*_m+b)^2}\, \dot{z}(t) \quad . \tag{6-26}$$

Substituting Eq.6-18 into Eq.6-26, the following relation can be obtained:

$$\ln\dot{e}_{11} = \ln\frac{2qC\,g(z_1)}{3G'b\tau} - \frac{C}{\tau}\ln(1+t) + 2\ln(\frac{M_f^*}{M_f^* - \eta^*}\,\frac{b}{\sigma^*_m+b}\,\frac{1}{\sqrt{(1+t)}}) \quad . \tag{6-27}$$

In Eq.6-27, the first term of the right-hand side is constant with respect to time and can be regarded as the initial strain rate. The second and third terms correspond to steady creep and accelerating creep, respectively.

Fig.6-2 shows schematically the general process of creep failure. From the figure, parameter α, the initial value of the gradient of strain rate to time, can be defined as

$$\alpha = \frac{d\ln\dot{e}_{11}}{d\ln(1+t)}\Big|_{at\ t=0} \ . \tag{6-28}$$

On the other hand, from Eq.6-27, the initial condition are

$$\frac{C}{\tau} = \frac{d\ln\dot{e}_{11}}{d\ln(1+t)}\Big|_{at\ t=0} \tag{6-29}$$

$\Rightarrow$

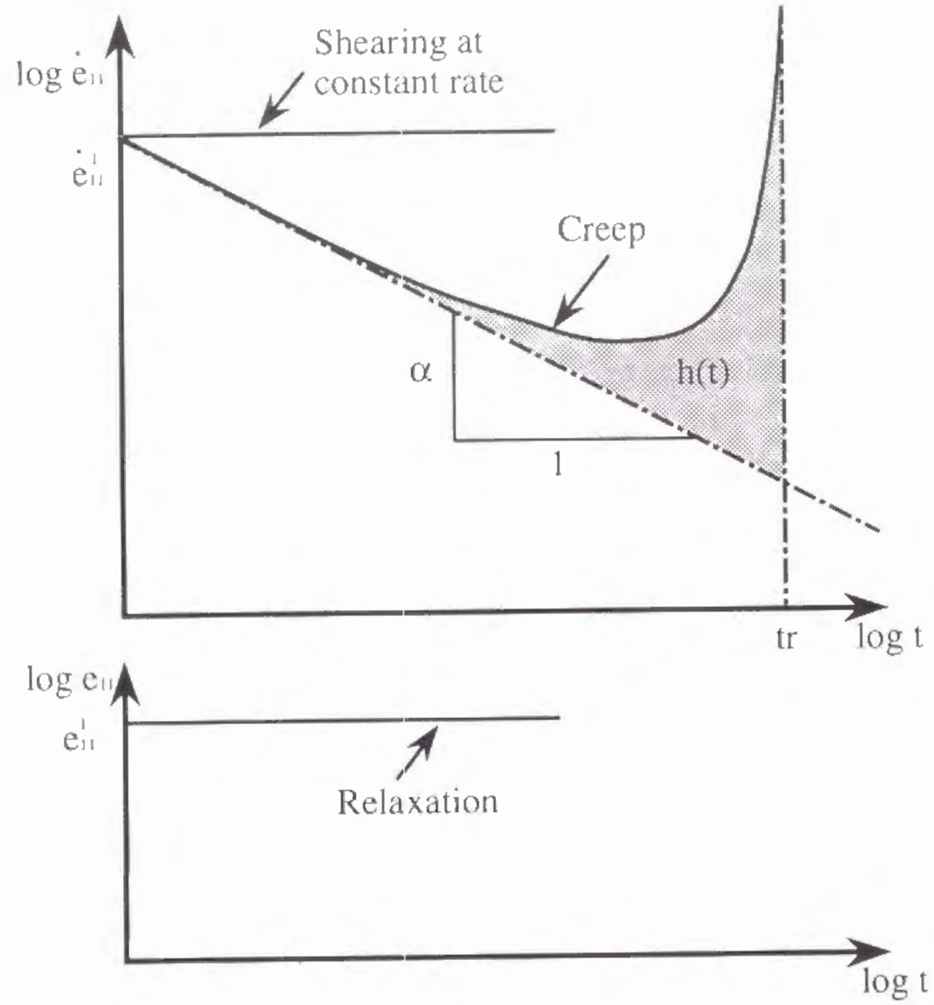

Fig.6-2 The illustration of time dependent behavior

$$\alpha=\frac{C}{\tau}\quad\Rightarrow C=\alpha\tau \tag{6-30}$$

and

$$\dot{e}_{11}^{0}=\frac{2q\alpha}{3G'b}g\frac{M_f^{*2}}{(M_f^{*}-\eta_0^{*})^2}\frac{b^2}{(\sigma_{m0}^{*}+b)^2}\ . \tag{6-31}$$

In Eq.6-31, $\dot{e}_{11}^{0}=\dot{e}_{11}|_{t=0}$, and

$$\eta_0^{*}=\frac{\sqrt{2J_2}\,(1-g)}{\sigma_m(1-g)+b}\ ,\quad \sigma_{m0}^{*}=\sigma_m(1-g) \tag{6-32}$$

$$\frac{M_f^{*2}}{(M_f^{*}-\eta_0^{*})^2}\frac{b^2}{(\sigma_{m0}^{*}+b)^2}=\{\frac{M_f^{*}b}{M_f^{*}b+(\sigma_m M_f^{*}-\sqrt{2J_2})(1-g)}\}^2\ . \tag{6-33}$$

In creep tests, if initial stress ratio $\sqrt{2J_2}/\sigma_m|_{\text{at }t=0}$ is greater than $M_{f\infty}^{*}$, Eq.6-10 becomes

$$M_{f0}^{*}=\frac{\sqrt{2J_2}}{\sigma_m}\ . \tag{6-34}$$

Based on Eq.6-30~6-34, the expression for the initial creep rate is obtained as

$$\dot{e}_{11}^{0}=\frac{2q\alpha\, g(z_1)}{3G'b}\quad\Rightarrow g(z_1)=\frac{3G'b}{2q\alpha}\dot{e}_{11}^{0} \tag{6-35}$$

Based on Eq.6-35, parameter $g(z_1)$ can be determined by triaxial drained creep tests. Eq.27 can be rewritten as

$$\ln\dot{e}_{11}=\ln\dot{e}_{11}^{0}-\alpha\ln(1+t)+\ln h(t) \tag{6-36}$$

In Eq.6-36, the first term at the right-hand side of the equation represents the initial deviatoric strain creep rate. Because it is difficult to measure the strain rate immediately after the creep stress is applied, the initial deviatoric strain creep rate here is determined in such a way that the rate measured at one minute after the creep stress is applied should be coincident with the correspondent calculated results. The second term stands for the steady creep strain in the decreasing stage, which can also be called as the secondary consolidation. The third term can be regarded as the acceleration of creep strain at rupture. The expression for the accelerating creep strain is

$$h(t)=(\frac{M_f^{*}}{M_f^{*}-\eta^{*}}\frac{b}{\sigma_m^{*}+b}\frac{1}{\sqrt{1+t}})^2 \tag{6-37}$$

It is noticeable that when the stress is at such a low level that the initial stress ratio $\sqrt{2J_2}/\sigma_m|_{at\,t=0}$ is less than $M^*_{f\infty}$,

$$\eta^* = \frac{\sqrt{2J_2^*}}{\sigma_m^* + b} < \frac{\sqrt{2J_2^*}}{\sigma_m^*} = \frac{\sqrt{2J_2}}{\sigma_m} < M^*_{f\infty} = M^*_f \qquad (6\text{-}38)$$

This means that the third term at the right-hand side of Eq.6-38 will never become infinite. In other words, creep failure will never occur when the initial stress ratio $\sqrt{2J_2}/\sigma_m|_{at\,t=0}$ is less than $M^*_{f\infty}$.

In application, the drained creep test results(Adachi and Takase, 1981) for a saturated sample of Ohya stone(porous tuff) deposited in the Miocene Epoch of Tertiary Period is analyzed with the present model. The physical properties of the material are listed in Table 6-1, while the material parameters of the model are listed in Table 6-2.

Table 6-1 Physical properties of Ohya stone

Void ratio e	0.72
Porosity n(%)	41.8
Dry density γ_d(gf/cm^3)	1.44
Wet density γ_t(gf/cm^3)	1.86
Water content w(%)	29.2
Specific gravity of soil Gs	2.48

Table 6-2 Material parameters of Ohya stone

K(kgf/cm^2)	4403.0	$\overline{M}_m$	1.694
G(kgf/cm^2)	5029.0	τ	14.15
b(kgf/cm^2)	20.0	α	0.614
σ_{mb}(kgf/cm^2)	110.	a	-0.101
$M^*_{f\infty}$	0.392	g	0.924
G'	1563.		

In the present study, the results of drained creep tests under confining pressure of 1.0 kgf/cm^2 are considered. Fig.6-3 shows the comparison between the theoretical and the experimental results of deviatoric and volumetric creep strain rates at a confining pressure of 1 kgf/cm^2. It is found that the general characteristics of creep behavior, such as the initial creep rate, the steady creep stage and the creep rupture, can be simulated well.

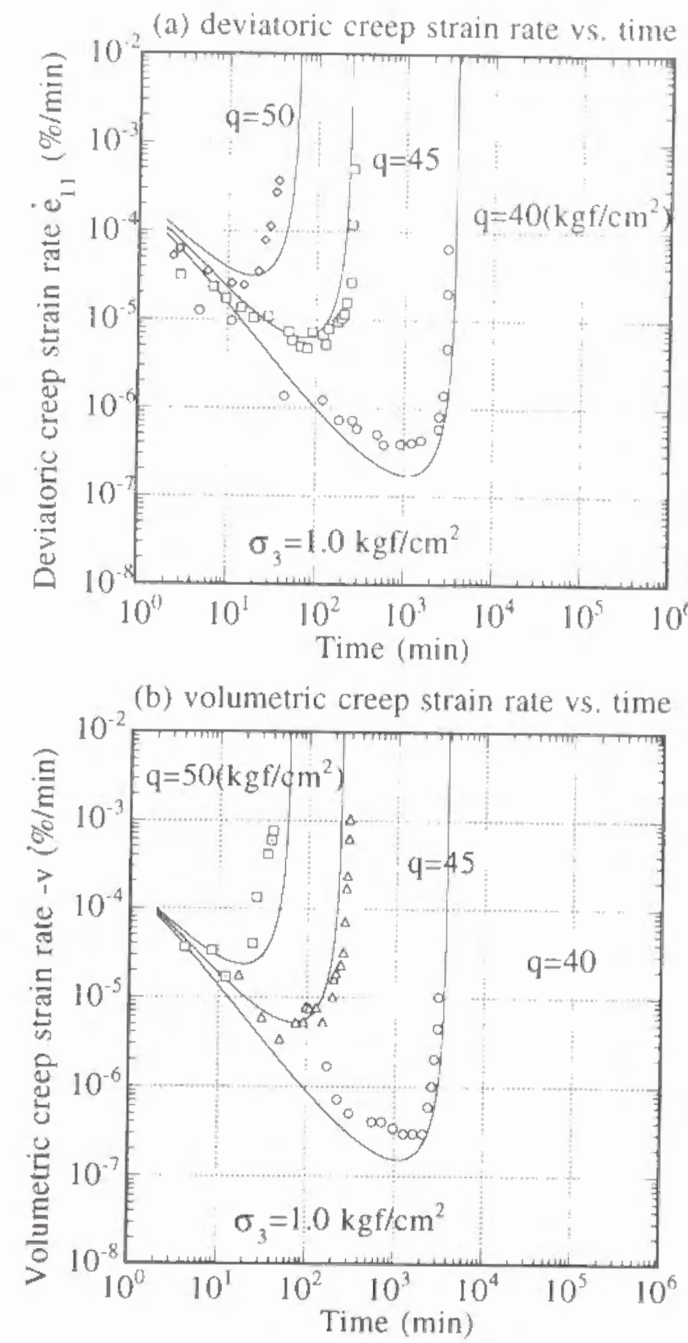

Fig.6-3 Comparison between theoretical and experimental result for deviatoric creep strain rate

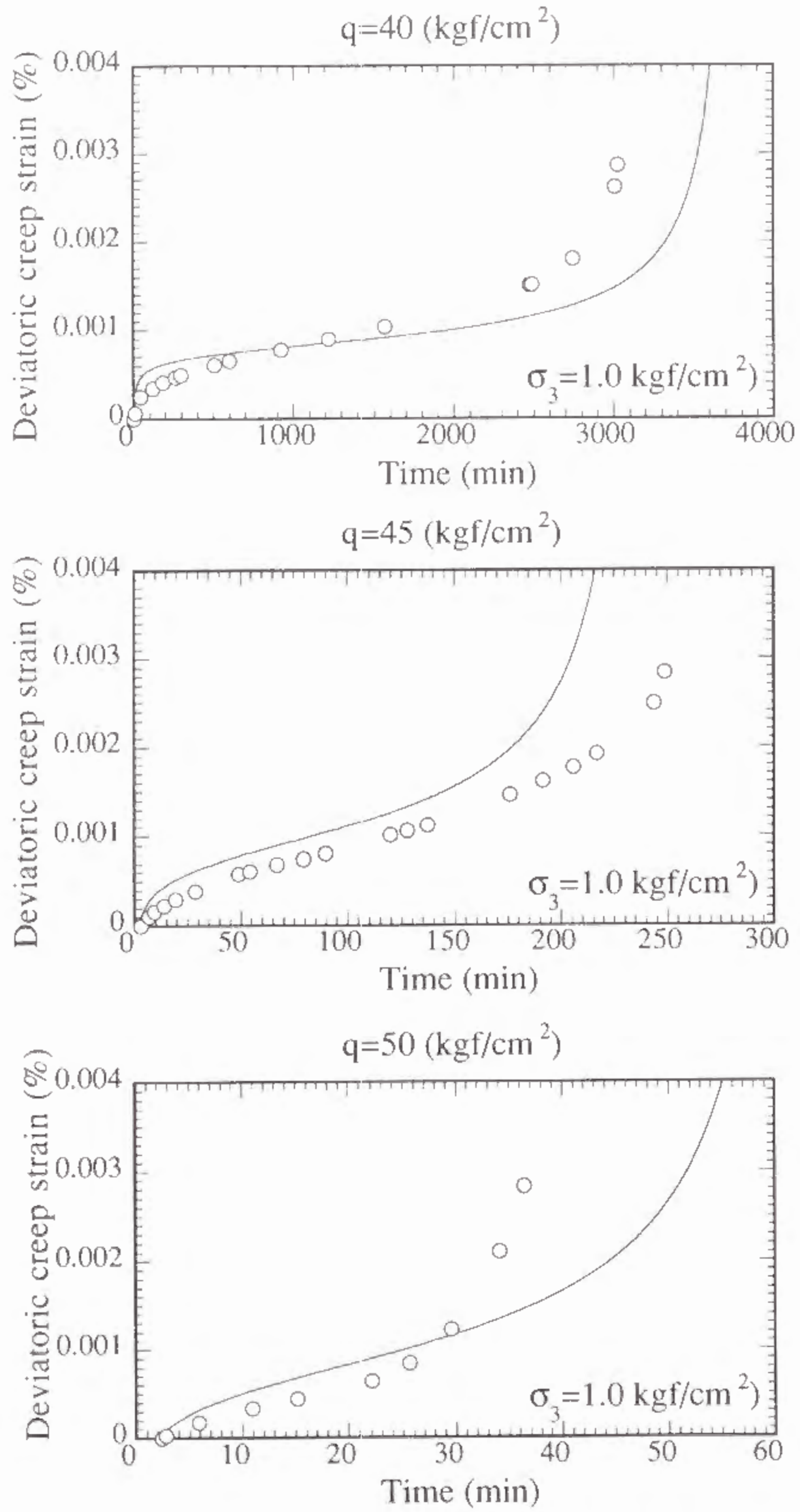

(a) deviatoric creep strain vs. time

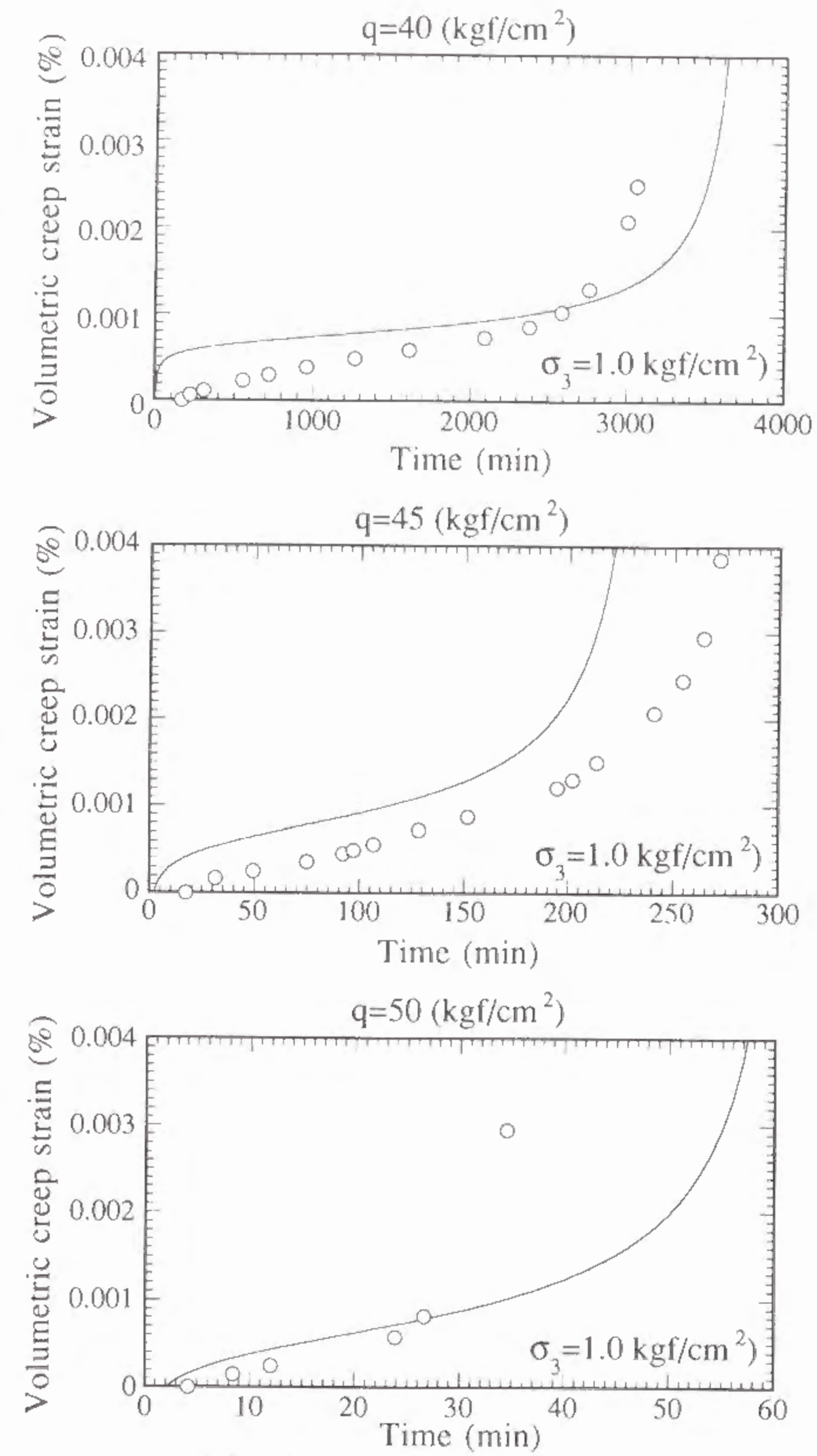

(b) volumetric creep strain vs. time

Fig.6-4 Comparison between theoretic and experimental results

Fig.6-4 shows the comparison between theoretic and experimental results of deviatoric and volumetric creep strains. It can be seen from the figure that the theoretical results are on the whole coincident with the experimental ones. Table 6-3 lists the results of the theoretical and the experimental results of creep failure times and minimum strain rates.

Table 6-3 Comparison between theoretical and experimental results

q (kgf/cm^2)	Creep failure time t_r (min)		minimum strain rate(%) (10^{-6} % / min)		Strain acceleration at steady state α($\%/min^2$)	
	experiment	theory	experiment	theory	experiment	theory
40	2923	3765	0.410	0.17	0.730	0.614
45	253	242	6.0	9.33	0.586	0.614
50	40	64	26.0	31.5	0.703	0.614

6-4 Application to triaxial shear tests on soft rock

Drained triaxial shear tests at a constant strain rate is considered now. In such a case, the initial time measure is equal to zero. Therefore Eq.6-18 can be expressed in another way as

$$z = z_1 + C\ln(1+t) = C\ln(1+t) \quad . \qquad (6\text{-}18)$$

In strain-controlled conventional triaxial tests at a constant strain rate, the following relations exist:

$$\dot{\varepsilon}_{ij} = \dot{\varepsilon}^e_{ij} + \dot{\varepsilon}^p_{ij} = const \qquad (6\text{-}39)$$

$$\dot{e}^e_{ij} = \frac{\dot{s}_{ij}}{2G}, \quad \dot{\varepsilon}^e_v = \frac{\dot{\sigma}_m}{K}, \quad \dot{\varepsilon}^e_{ij} = \dot{e}^e_{ij} + \delta_{ij}\dot{\varepsilon}^e_v \qquad (6\text{-}40)$$

$$d\varepsilon^p_{ij} = \Lambda[\frac{\bar{\eta}_{ij}}{\bar{\eta}} + (\bar{M} - \bar{\eta})\frac{\delta_{ij}}{3}][\frac{\eta^*_{kl}}{\eta^*} - \eta^*\frac{\delta_{kl}}{3}]\frac{d\sigma^*_{kl}}{\sigma^*_m + b} \quad . \qquad (6\text{-}15)$$

The detailed expression of the plastic incremental strain tensor can be evaluated by considering the relation of $d\sigma^*_{ij} = (\sigma_{ij} - \sigma^*_{ij})\,dz/\tau$. The following equation is obtained:

$$d\varepsilon^p_{ij} = \Lambda[\frac{\bar{\eta}_{ij}}{\bar{\eta}} + (\bar{M} - \bar{\eta})\frac{\delta_{ij}}{3}][\frac{\eta^*_{kl}}{\eta^*} - \eta^*\frac{\delta_{kl}}{3}]\frac{1}{\sigma^*_m + b}(\sigma_{kl} - \sigma^*_{kl})\frac{dz}{\tau} \quad . \qquad (6\text{-}41)$$

By substituting Eq.6-18 into Eq.6-41, it is easy to obtain

$$\dot{\varepsilon}^p_{ij} = \Lambda[\frac{\bar{\eta}_{ij}}{\bar{\eta}} + (\bar{M} - \bar{\eta})\frac{\delta_{ij}}{3}][\frac{\eta^*_{kl}}{\eta^*} - \eta^*\frac{\delta_{kl}}{3}]\frac{1}{\sigma^*_m + b}(\sigma_{kl} - \sigma^*_{kl})\frac{C}{1+t} \quad . \qquad (6\text{-}42)$$

In the present case, unlike the creep, the stress history cannot be integrated explicitly and should be solved by the associated differential equations found in Eq.6-39~6-42.

The parameter of time dependency C in the present case is determined in the following way. By differentiating the Eq.6-18, the following relation is found

$$dz = \frac{C}{1+t}dt \quad . \qquad (6\text{-}43)$$

It is known from experimental results that parameter C here is dependent on the shear strain rate. As a reference, the stress history parameter τ is firstly determined under the conditions of $\dot{\varepsilon}_{11} = \dot{\varepsilon}_0 = 1\%$ / min, assuming that C=1. The value of τ here is denoted by τ_0. Secondly, by using the curve fitting method, the values of τ is evaluated at different shearing strain rates with the same assumption of C=1. τ is evaluated in such a way that the peak strength in the theoretical results is the most suitable to the experimental results. Through the above analysis, the following relation is obtained:

$$\tau = (\dot{\varepsilon}_{11}/\dot{\varepsilon}_0)^a\,\tau_0 \quad . \qquad (6\text{-}44)$$

a is called the parameter of strain-rate-dependency here. On the other hand, the change in stress history defined by Eq.6-2 is determined by dz/τ

which can be expressed in the following equation:

$$\frac{d\sigma^*_{ij}}{(\sigma_{ij} - \sigma^*_{ij})} = \frac{dz}{\tau} \quad . \qquad (6\text{-}45)$$

In order to make it easy for comparison, the values of dz/τ in different strain rate are listed in following equation

$$\frac{dz}{\tau_0} = \frac{1}{1+t}\frac{dt}{\tau_0} \quad , \quad \frac{dz}{\tau} = \frac{C}{1+t}\frac{dt}{\tau} \qquad (6\text{-}46)$$

From Eq.6-46, it is found that if the parameter of time dependency C takes the form expressed in Eq.6-47, the values of dz/τ will become independent of the strain rate.

$$\frac{C}{\tau} = \frac{1}{\tau_0} \Rightarrow C = \left(\frac{\dot{\varepsilon}_{11}}{\dot{\varepsilon}_0}\right)^a \qquad (6\text{-}47)$$

The proposed model is applied to a triaxial shear test of Ohya stone under constant axial strain rate(Adachi and Ogawa, 1980).

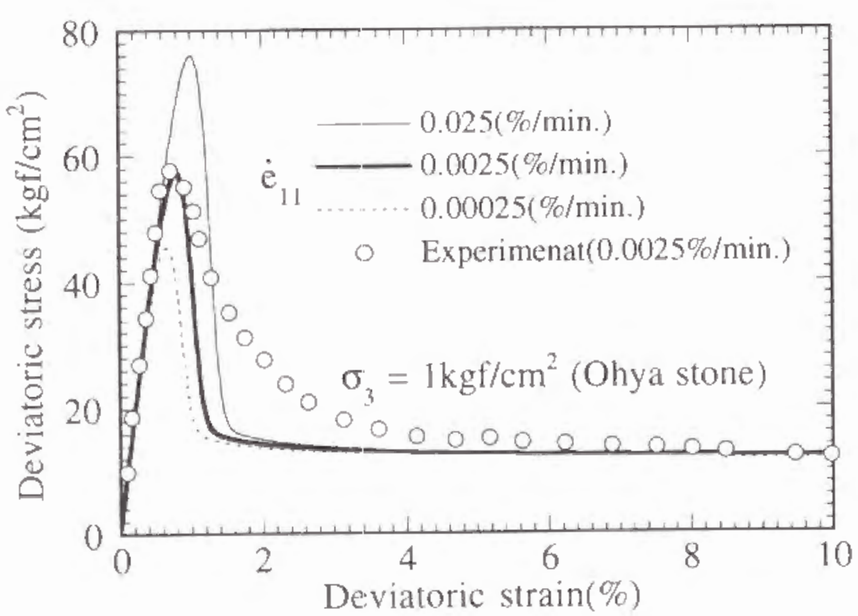

Fig.6-5 Strain rate dependency

The physical properties and the material parameters of Ohya stone are listed in Table 6-1 and Table 6-2. Fig.6-5 shows the relations of deviatoric stress($q=\sigma_{11}-\sigma_{33}$) vs. deviatoric strain. It is found from the figure that the rate dependency of sediment soft rock can be simulated well. Both the peak value of strength and the residual value of strength can be simulated. The theoretical result is also compared with the experimental result at a constant strain rate of 0.0025%/min. It is found that the theoretical result is in good agreement with the experimental one.

6-5 Application to drained triaxial stress relaxation tests

In drained triaxial stress relaxation tests, strain is kept constant. Therefore, the following relation exist:

$$\dot{\varepsilon}_{ij} = 0 \Rightarrow \dot{\varepsilon}^p_{ij} = -\dot{\varepsilon}^e_{ij} \quad . \qquad (6\text{-}48)$$

There also exists the relations as

$$\dot{e}^e_{ij} = \frac{\dot{s}_{ij}}{2G}, \quad \dot{\varepsilon}^e_v = \frac{\dot{\sigma}_m}{K}, \quad \dot{\varepsilon}^e_{ij} = \dot{e}^e_{ij} + \delta_{ij}\dot{\varepsilon}^e_v \qquad (6\text{-}40)$$

$$d\varepsilon^p_{ij} = \Lambda\left[\frac{\bar{\eta}_{ij}}{\bar{\eta}} + (\bar{M} - \bar{\eta})\frac{\delta_{ij}}{3}\right]\left[\frac{\eta^*_{kl}}{\eta^*} - \eta^*\frac{\delta_{kl}}{3}\right]\frac{1}{\sigma^*_m + b}(\sigma_{kl} - \sigma^*_{kl})\frac{dz}{\tau} \qquad (6\text{-}41)$$

$$\dot{\varepsilon}^p_{ij} = \Lambda\left[\frac{\bar{\eta}_{ij}}{\bar{\eta}} + (\bar{M} - \bar{\eta})\frac{\delta_{ij}}{3}\right]\left[\frac{\eta^*_{kl}}{\eta^*} - \eta^*\frac{\delta_{kl}}{3}\right]\frac{1}{\sigma^*_m + b}(\sigma_{kl} - \sigma^*_{kl})\frac{C}{1+t} \quad . \qquad (6\text{-}42)$$

In the present case, being similar to the drained triaxial shearing tests at a constant strain rate, the stress history cannot be integrated explicitly and should be solved by associated differential equations. Because the stress is not applied all at once to the specimen, the loading process from zero to a certain stress state will take some time. Therefore, in calculating the stress history, the time spent on the loading process should be considered. In present case, the stress history σ^*_{ij} cannot be integrated explicitly. It has to be evaluated by solving the above mentioned associated differential equations. Being similar to the drained triaxial shearing tests at a constant strain rate, the initial time measure z_i is equal to zero and $g(z_i) = 1$.

By solving the above differential equations, it is found that parameter C is dependent on the strain rate in the process where the specimen is loaded to the prescribed stress state. C can be determined by drained triaxial stress tests.

The proposed model is used to simulate drained triaxial stress relaxation tests. As drained triaxial stress relaxation tests were not conducted on Ohya stone, only a theoretical estimation of the stress relaxation can be given.

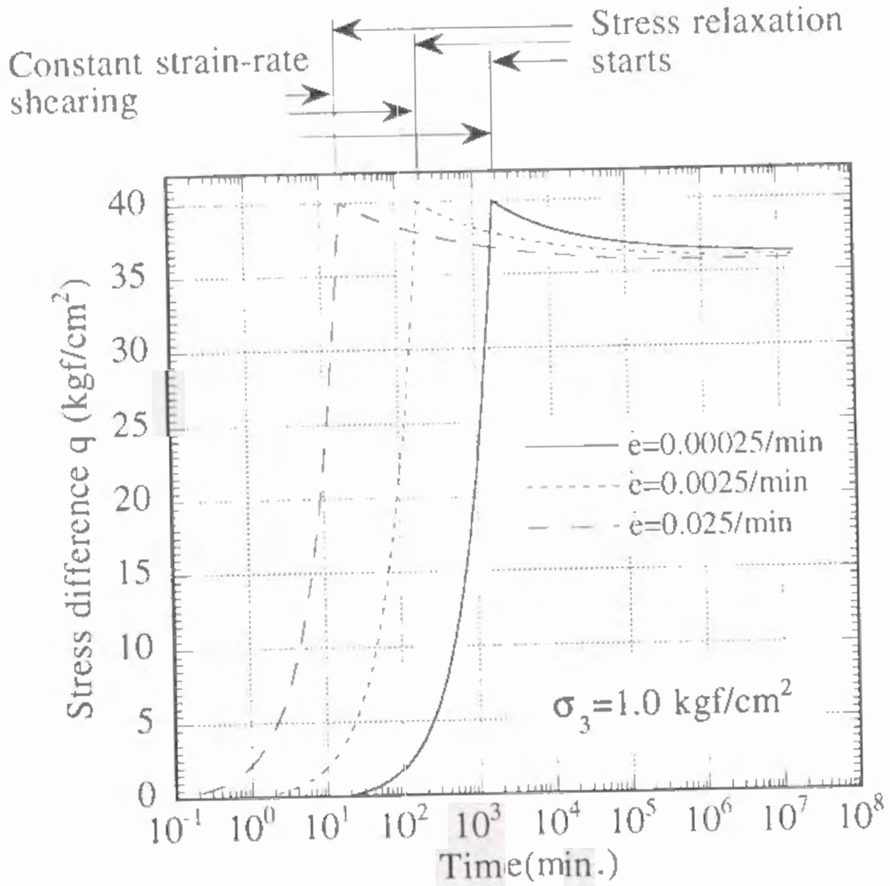

Fig.6-6 Stress relaxation

Fig.6-6 shows the estimated stress relaxation behavior of Ohya stone using the present model. The sample is first loaded to a deviatoric stress state of 40 kgf/cm2 with a confining pressure of 1 kgf/cm2, the strain ε_{11}

at the moment being 0.415%. In order to investigate the influence of the initial strain rate, stress-time relations at three different values of C were evaluated, that is, C = 2.29, 2.88 and 3.63, which correspond to the strain rates of 0.025%/min., 0.0025%/min. and 0.00025%/min. at constant strain-rate shearing respectively, based on the equation $C = (\dot{\varepsilon}_{11}/\dot{\varepsilon}_0)^a$. It is found from the figure that at shearing process, the stress-time relations show no much difference for different strain rates, with only one-order shift in time axis. Such behavior is thought to be reasonable if comparing it with Fig.6-5 in which the stress-strain relations before peak strength also show no much difference. In the process of stress relaxation, the stresses decreases almost linearly at the beginning in stress-logarithmic time axes. After decreased to a certain value, the stress almost remain unchanged. If the value is called as relaxed stress, then the higher the initial strain rate is, the lower the relaxed stress will be. Under the present conditions, the stress relaxation will almost be completed within 10^4 minutes after the relaxation starts and the stress will decrease from 40.0 kgf/cm2 to 36.0 kgf/cm2 after 10^7 minutes.

6-6 Determination of the parameters in the model

Eleven material parameters are involved in the model, that is, G, K: Young's modules; b, σ_{mb}: plastic potential parameters; G', A, $M^*_{f\infty}$ strain hardening-softening parameters; τ: stress history parameter; $\overline{M}_m$: parameter of over-consolidated boundary; C : parameters of time dependency and g: parameter of the initial time measure.

Young's modules and the bulk modules are determined directly by measuring the tangent to the deviatoric stress-strain curve and the tangent to the volumetric stress-strain curve at the initial stage of loading.

The parameter of the over-consolidated boundary, $\overline{M}_m$, takes the value of stress ratio $\sqrt{S_{ij}S_{ij}}/(\sigma_m+b)$ at the point where the maximum contraction occurs in the shearing process. Plastic potential parameter σ_{mb} is determined by isotropic consolidation tests and takes the value of the pre-consolidated stress. Plastic potential parameter b can be determined by the assumption that the stress ratio η is kept constant in the over-consolidated region along the M_m- line.

Stress history parameter τ is determined by a process of trial and error using the peak shearing strength.

Strain hardening-softening parameter $M^*_{f\infty}$ is determined as the value of η^* at the residual state. G' can be determined as the initial gradient of the stress-strain curve in the unloading-reloading process at the residual state. As for parameter A, it is found from creep tests that it increases linearly with stress ratio η and can be given as

$$A = A_0 + \bar{\eta} A_1 \qquad (6\text{-}49)$$

where, the value of A_0 is evaluated to be -0.664 and A_1 to be 0.854 based on creep tests at a confining pressure of 1 kgf/cm^2.

In Eq.6-1, an incremental time measure dz is defined. For time dependent constitutive model, the influence on the time measure from creep, strain rate dependency and stress relaxation of geologic materials should be considered synthetically. Based on previous discussions, the expression for parameter C can be given as

$$C = C(\dot{\varepsilon}_{ij}) \quad . \qquad (6\text{-}50)$$

This means that parameter C is dependent on strain rate tensor ε_{ij}.

In drained triaxial shearing tests at a constant strain rate, Eq.6-50 can be expressed in a more detailed expression as Eq.6-47.

In drained triaxial stress relaxation tests, the strain is kept constant. Therefore, instead of estimating the value of C directly by present strain rate, it is estimated based on the strain rate in the process during which the specimen is loaded to the prescribed stress state.

In drained triaxial creep tests, it is found that the parameter of time dependency is directly related to the gradient of the strain rate at the steady state of drained creep test and stress-history parameter τ in such a way that $C = \alpha\tau$, where τ and α are also dependent on the strain rates in the process during which the specimen is loaded to the prescribed creep stress. Parameter α can be determined by triaxial drained creep tests.

Fig.6-7 shows the possible values of parameter C for Ohya stone in creep, constant-strain shearing and relaxation.

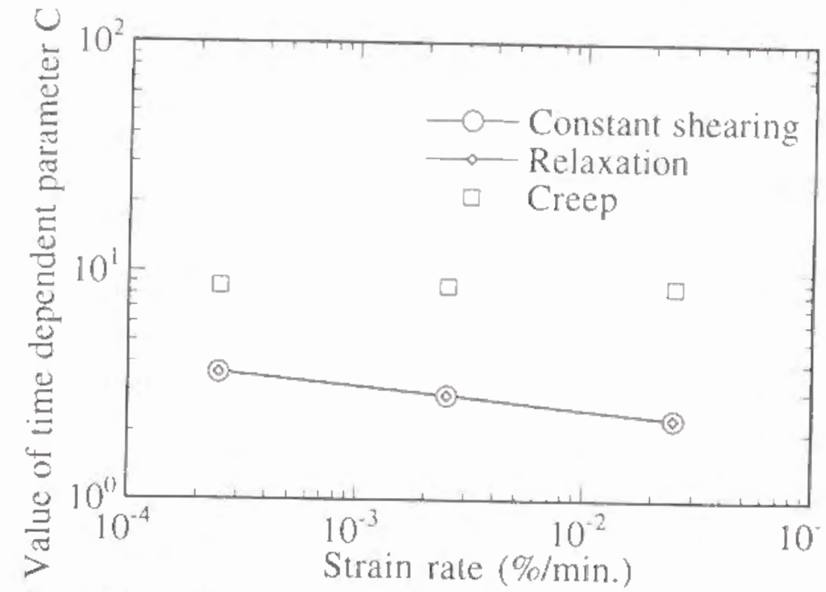

Fig.6-7 Possible value of C in creep, constant shearing and relaxation

6-7 Conclusions

In this chapter, an elasto-viscoplastic model with memory is proposed for geologic materials. A comparison of the analytical results and the experimental results indicates that it is not only able to describe all the aspects of time dependency, such as strain rate dependency, creep and stress relaxation, but also the strain softening behavior of geologic materials. Due to the fact that this model is based on a previous work by Oka and Adachi(1985), most of the parameters involved in the model can be determined in the same way as those in the previous work. The new parameters introduced in this model can be accurately determined by triaxial and drained creep tests.

Appendix

According to the definition of η^*, the following equations can be obtained by some algebraic:

$$d\eta^* = \frac{\partial \eta^*}{\partial \sigma^*_{ij}} d\sigma^*_{ij} = \left(\frac{S^*_{mn}}{(\sigma^*_m + b)\sqrt{2J^*_2}} - \frac{\sqrt{2J^*_2}}{(\sigma^*_m + b)^2}\frac{\delta_{mn}}{3}\right) d\sigma^*_{mn}$$

$$= \frac{1}{(\sigma_m^* + b)^2} \left(\frac{(\sigma_m^* + b) S_{mn}^* dS_{mn}^*}{\sqrt{2J_2^*}} - \sqrt{2J_2^*}\, d\sigma_m^* \right)$$

$$= \frac{1}{(\sigma_m^* + b)^2} \{ b\sqrt{2J_2}\, d(1 - e^{-(z-z_1)/\tau} g(z_1)) \}$$

$$= \frac{b}{(\sigma_m^* + b)^2} g(z_1) \frac{dz}{\tau} \sqrt{2J_2}\, e^{-(z-z_1)/\tau} \quad . \qquad \text{(A-1)}$$

In axisymmetric condition, the following relation exists:

$$\sqrt{2J_2} = \sqrt{\frac{2}{3}} (\sigma_{11} - \sigma_{22}) = \sqrt{\frac{2}{3}}\, q \quad . \qquad \text{(A-2)}$$

Substituting equation A-2 into equation A-1,

$$d\eta^* = \sqrt{\frac{2}{3}} \frac{1}{(\sigma_m^* + b)^2} g(z_1) bq e^{-(z-z_1)/\tau} \frac{dz}{\tau} \qquad \text{(A-3)}$$

Based on Eq.6-13, 6-15, 6-16 and A-3, the detailed expression for the deviatoric and volumetric components of viscoplastic strain can be obtained as found in Eq.6-24 and 6-25.

References

(1) Adachi, T. and Ogawa, T. (1980) : "Mechanical Properties and failure criteria of soft rock," Proc. JSCE, No.295, pp.51-62(In Japanese).

(2) Adachi, T., Oka, F. and Poorooshasb, H. B. (1990) : "A Constitutive Model for Frozen Sand," Trans. ASME, Vol.112, pp.208-212.

(3) Adachi, T. and Takase, A. (1981) : "Prediction of long term strength of soft sedimentary rock," Proc. Int. Symp. Weak Rock, Tokyo, pp.99-104.

(4) Andersland, O. B. and Al-Nouri, I. (1970) : "Time Dependent Strength Behavior of Frozen Soils," Journal of Mechanics and Foundation Division, ASCE, 96SM(4), pp.1249-1265.

(5) Oka, F., 1985, "Elasto/viscoplastic constitutive equation with memory and internal variables," Computer and Geomechanics, Vol.1, pp.59-69.

(6) Oka, F., and Adachi, T. (1985) : "A constitutive equation of geologic materials with memory," Proc. 5th Int. Conf. on Numerical Method in Geomechanics, Vol.1, pp.293-300.

(7) Perzyna, P. (1980) : "Memory Effects and Internal Changes of a Material," International Journal of Nonlinear mechanics, Vol.6, pp.707-716.

(8) Saito, M. & Uezawa, H. (1961) : "Failure of soil due to creep," Proc. 5th ICSMFE, Paris, pp.315-318.

(9) Singh, A. and Mitchell, J. K. (1968) : "General stress-strain-time function for soils," Proc. ASCE, Vol. 94, No.SM1, pp. 21-46.

(10) Ting, J. M. (1983) : "Tertiary Creep Model for Frozen Sands," ASCE Journal of Geotechnical Engineering, 109(7), pp.932-945.

(11) Valanis, K. C. (1971) : "A Theory of Viscoplasticity without a Yielding Surface," Arch. Mech. Stos. Vol.23, No.4, pp.517-533.

(12) Wang, C. C. (1969) : "Generalized Simple Bodies," Arch. Rational Mech. Analysis, Vol.32, pp.1-30.

Chapter 7

Numerical analysis of progressive failure in cut slope on model ground

7-1 Introduction

It is commonly known that soft sedimentary rock can be linked to many geotechnical engineering problems, such as the instability of cut slopes and foundations. Generally speaking, the mechanical behavior of soft sedimentary rock is elasto-plastic, dilatant, strain hardening-strain softening and time dependent. Physically, soft sedimentary rock has an unconfined compressive strength of 10~100 kgf/cm^2 and its mechanical behavior is between the behavior of soil and rock. Its cementation plays an important role in its shearing strength. Compared to other geological materials formed in the same epoch, the void ratio is relatively large and a special structure formed during sedimentation. Its mechanical behavior during shearing is largely dependent on the confined stress and the pore-water pressure. The cementation existed in the structure, deteriorates due to the breakdown of the structure . Such a breakdown is caused by various processes, such as large shearing deformation, cyclic drying-wetting or stress release. The softening behavior of soft sedimentary rock becomes a very important factor in the long-term stability of cut slopes

Yoshida et al.(1991), Adachi and Yoshida(1993) discussed the softening behavior of soft sedimentary rock in detail and concluded that the instability of cut slopes may be caused by three factors, namely, (a) the deterioration of the structure due to swelling and weathering which occurs in excavation, (b) progressive failure, (c) a reduction in the apparent shear strength due to the dissipation of negative pore-water pressure caused by speedy excavation of the cut slope.

In chapter 6, an elasto-viscoplastic model is proposed which can not only describe all the aspects of time dependency, such as strain rate dependency, creep and stress relaxation, but also the strain softening of geologic materials. Based on the model, a finite element analysis is carried out to

investigate the instability of a cut slope, taking into consideration strain softening, time dependency and progressive failure.

As a foundation study, a progressive failure in a cut slope on a model ground is considered(Adachi et al., 1994).

7-2 Finite element analysis

In present finite element analysis, the model ground is supposed to be a kind of strong-weathered soft rock. For simplicity, the ground is assumed to be composed of one kind of material whose material parameters involved in the elasto-viscoplastic model are listed in Table 7-1. As mentioned previously, the strength of the ground decreases with time because of the structural deterioration of materials caused by weathering

Table 7-1 Material parameters of model ground

K(kgf/cm^2)	847.2	M_m	1.194
G(kgf/cm^2)	484.1	τ	24.15
b(kgf/cm^2)	2.0	α	0.614
σ_{mb}(kgf/cm^2)	29.0	a	-0.10
$M_{f\infty}^*$	0.528	g	1.0
G'	150.0	γ (gf/cm^3)	2.1

(a) Stress-strain relations

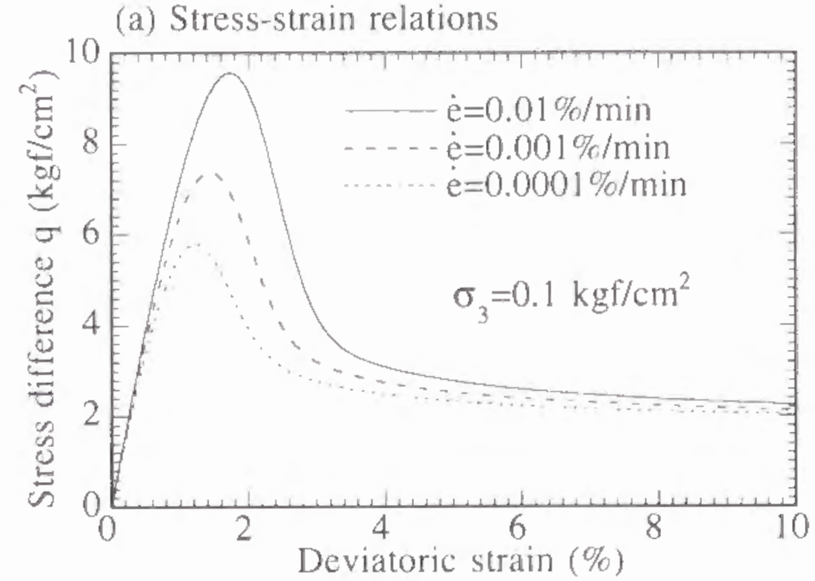

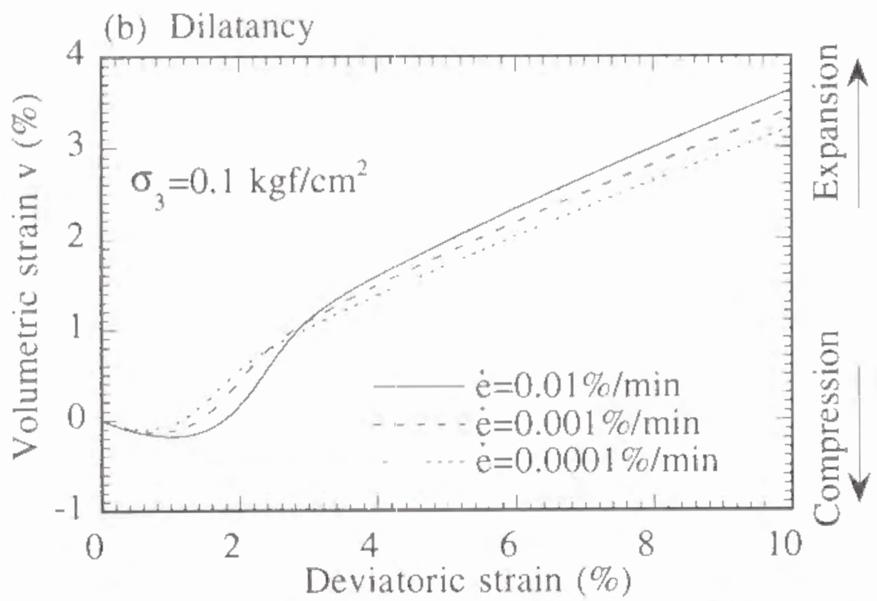

Fig.7-1 Strain softening and rate dependency of model ground

and the dissipation of negative pore-water pressure caused by rapid unloading in slope excavation or natural land sliding. In present analysis, only the effect of structural deterioration is considered. Drained conditions are supposed throughout the analysis. Figure 7-1 shows the stress-strain relation of the model ground based on the elasto-viscoplastic model with the strain softening model proposed in this paper. From the figure, it is seen that the strain softening and strain rate dependent behaviors of the model ground are clearly explained by the model.

Figure 7-2 shows the finite element mesh used in the analysis of the progressive failure problem on the cut slope in the model ground. The gradient of the cut slope is 4/3. The height and the width of the slope are 20 m and 15 m respectively. 8-node isoparametric elements are used in finite element calculation. The number of nodes and elements is 1817 and 570, respectively.

In simulating the mechanical behavior of the cut slope with the finite element method, the gravitational stress field is first evaluated with an initial stress analysis based on elasticity. Then the slope is excavated instantly. As main attention is paid to the instability of the cut slope after excavation, the time needed for the slope excavation is supposed to be zero. In other words, the deterioration of the ground starts immediately after the slope excavation is completed.

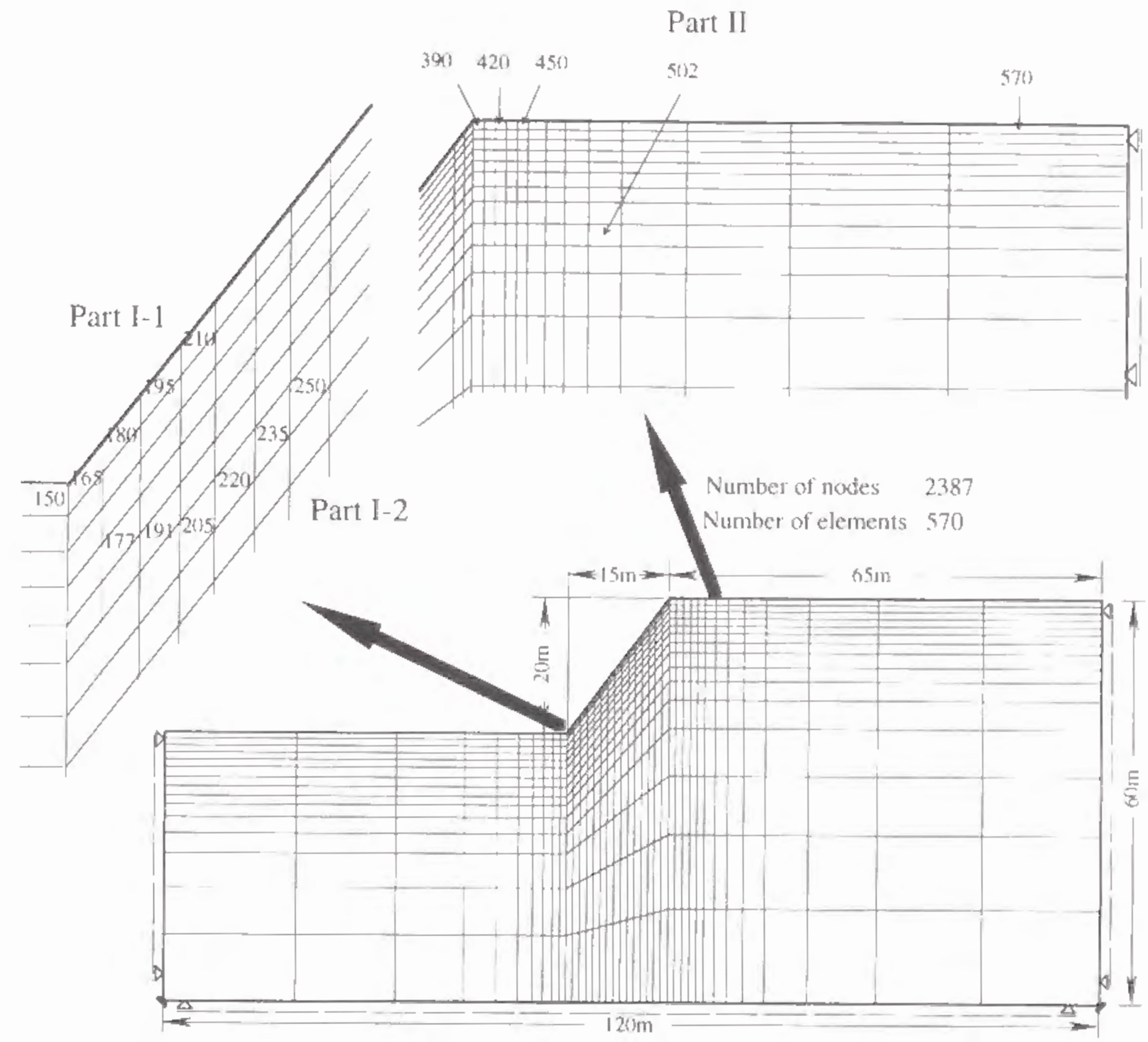

Fig.7-2 Finite element mesh

7-3 Result and consideration

In present analysis, the creep failure of a element is defined as a state at which the stress tensor of the element approaches to residual value and the value of stress history approaches to the value of stress. Fig.7-3 shows the development of the creep failure zones in the model ground. It can be seen from the figure that the creep failure occurs first at the toe of the slope and then gradually expands to other regions. The progressive failure mechanism is well simulated in the present analysis.

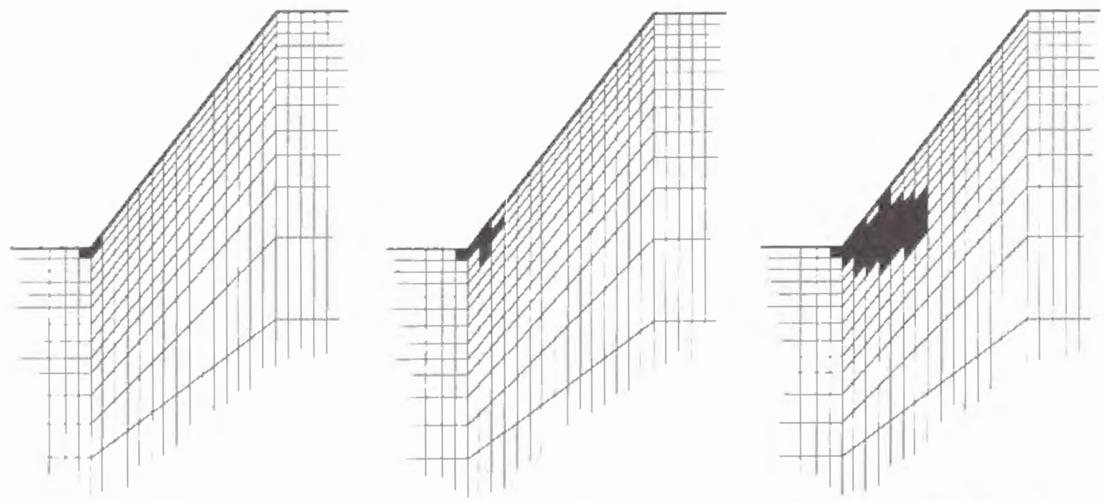

t=156.30(min.) t=4687.4(min.) t=5554.8(min.)

Fig.7-3 Development of creep failure zones

Fig.7-4 shows the changes in the principle stress field with time. In the figure, (a) shows the stress field immediately after the slope excavation is complete. It can be seen from the figure that the principle stress far from the slope is not seriously disturbed by the slope excavation and that the direction of the principle stress is parallel to the x and y axes. The ratio of horizontal stress to vertical stress is about to be K_0. Fig.7-4(b) shows the stress field 156.3 minutes after the slope excavation has been completed. Compared with Fig.7-4(a), the stress field changed a great deal. Especially in the area close to the toe of the slope, the direction of the maximum principle stress rotated clockwise almost 40°. The ratio of horizontal stress to vertical stress increased prominently in the ground. In some places, it even became greater than 1.0. The reason for this change is considered to be the flowing tendency of the ground at the crest of the slope towards the toe of the slope.

Fig.7-5 shows the displacement vectors of ground in different times. The displacement occurred in the initial stress analysis and the slope cutting process is not included in the total displacement. Therefore, the displacement shown in Fig.7-5 is only the one caused by the deterioration of the ground in the cut slope. It is very clear from the figure that an arc-shaped sliding tendency exists in the ground near the slope. Moreover, when the creep failure zone develops to some extent, a large localized deformation is observed in the calculation. It should be pointed that the displacement at the position far from the toe of the slope is also relatively

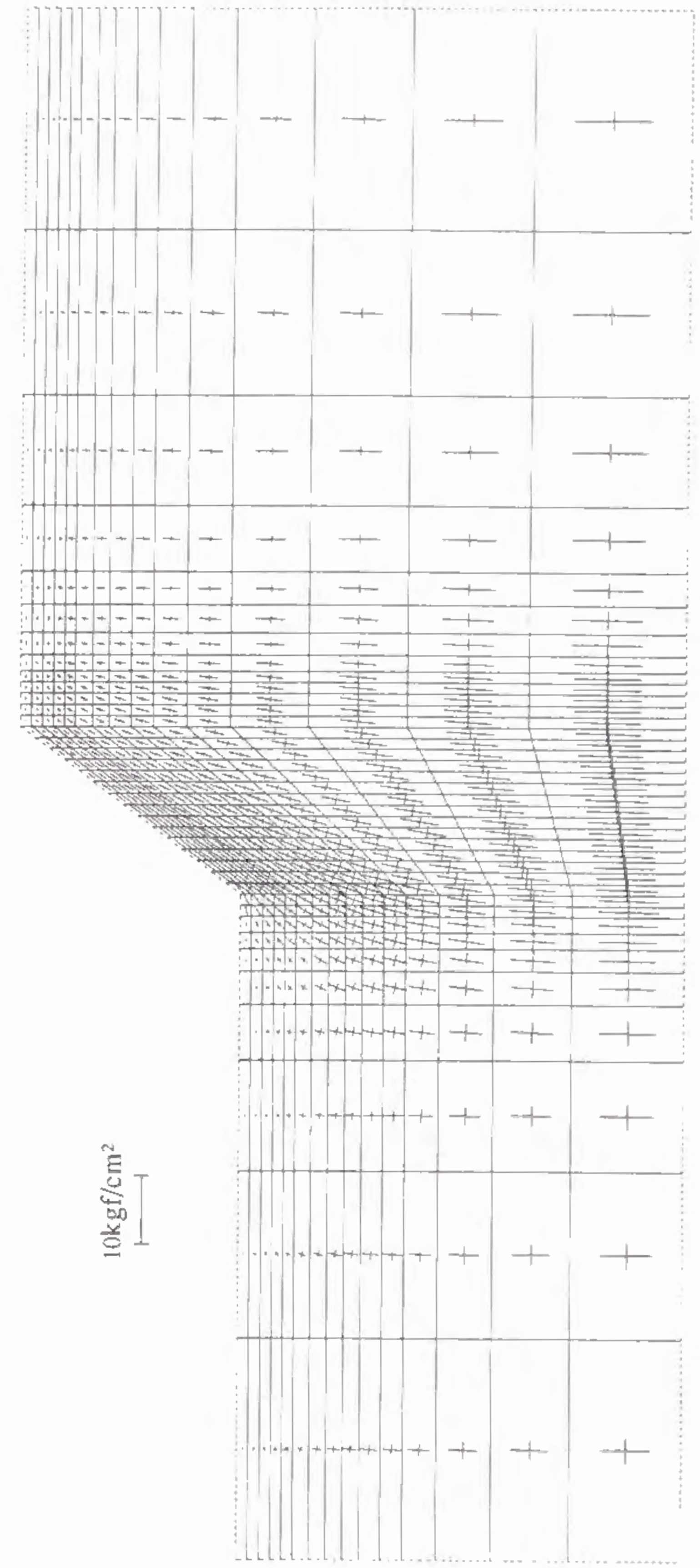

Fig.7-4a Principal stress field(immediately after excavation, time=0.0 min.)

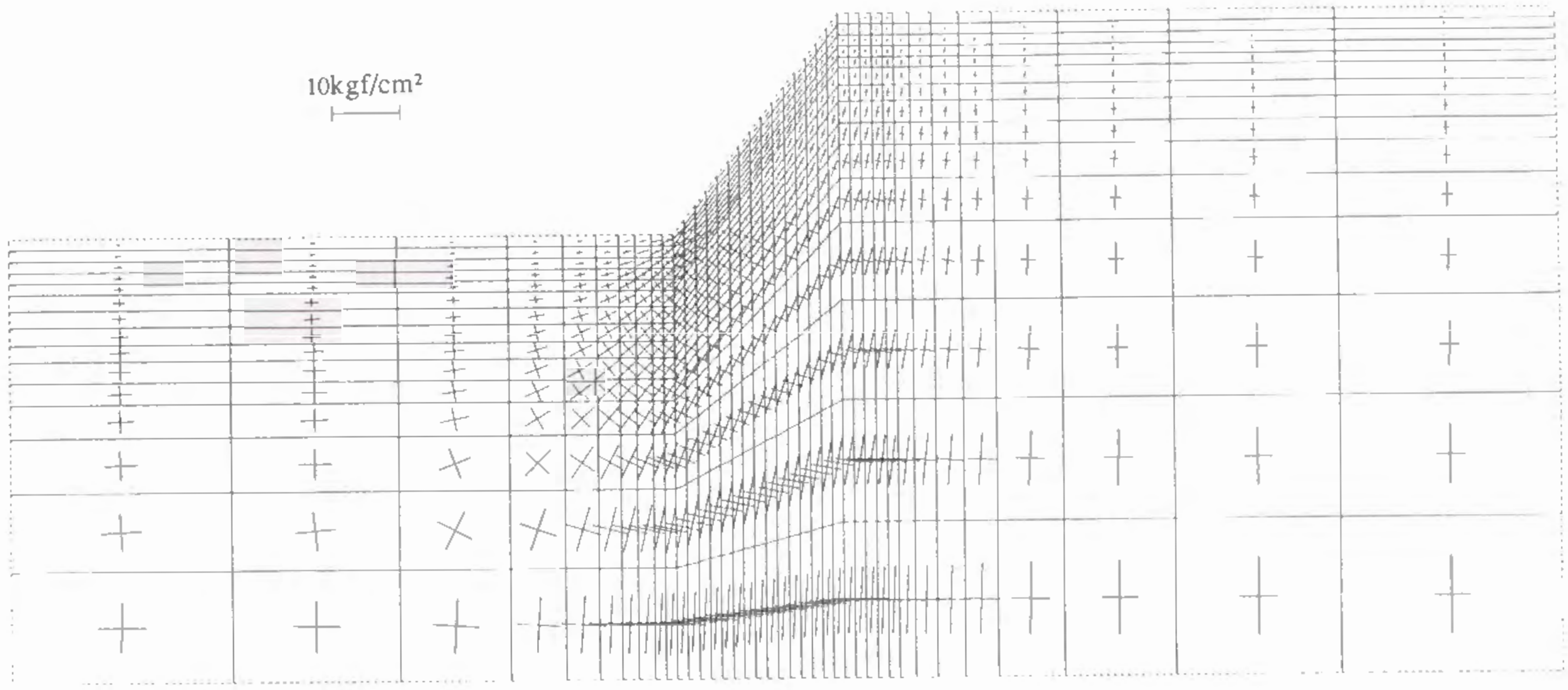

Fig.7-4b Principal stress field(time=156.3 min.)

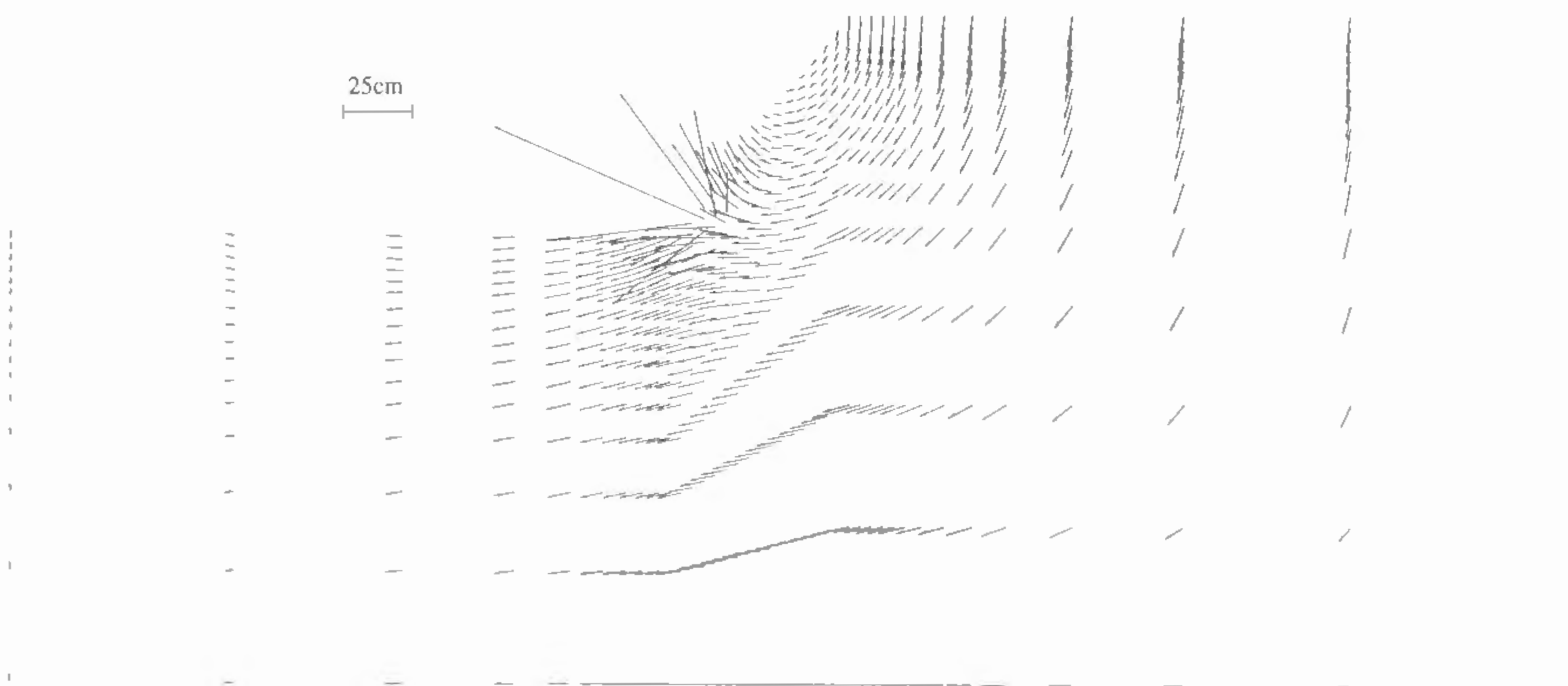

Fig.7-5 Displacement vector(time=5554.8min.)

large. The reason why such phenomenon occurs is that the model ground is assumed to be a uniform material and its material parameters involved in the elasto-viscoplastic model takes the same value in whole ground. As a consequence, the initial strain rates at these place are exaggerated.

In order to find out the changes of stresses at particular positions, the stress paths in the ground are also investigated in the positions which are mainly divided into two parts, creep-failure-zone(Part I) and no-failure-zone(Part II), as shown in Fig.7-2. Fig.7-6 shows the stress paths in these position. As shown in the figure, along the slope surface near the toe of the slope, although the stress in element 150 has already exceeded the residual strength line immediately after the completion of the slope excavation, it still has not reached the peak strength of the ground. The shear stress increases until it reaches the peak strength. When the peak strength is reached, the stress starts to decrease and gradually reaches the residual state. Similar result can be observed in element 165. On the other hand, the changes in stress for element 180 are quite different from those of element 150. At the beginning, the ground at element 150 is strong enough to prevent the ground from sliding. Therefore the stress state in element 180 is in stress relaxation. It decreases at first. When the shear strength in elements 150 and 165 decrease to a residual value and creep failure occurs, however, the stress in the ground close to the failure zone has to be redistributed. As a result, the stress in element 180 starts to increase at some point in time. It is noticeable that element 195 which is surrounded with failed elements at the moment of t=5554.8min still remains unfailed. The reason why this phenomenon occurs is that as the surrounding elements failed and came into residual state, the shearing interaction between element 195 and other elements will not be greater than its shearing strength. The element looks like a isolated hole.

In no-failure-zone, the stresses decrease at first and then turn to increase at final stage because of the large deformation at creep-failure-zone, with the only exception of element 570 in which strain softening is observed. The stresses in the zone are far less than the failure stress.

From above discussion, it is clear that the mechanism of progressive failure, in which the failure first occurred at a local position and gradually extended to other areas, can be simulated well by the present analysis based on the elasto-viscoplastic model with strain softening.

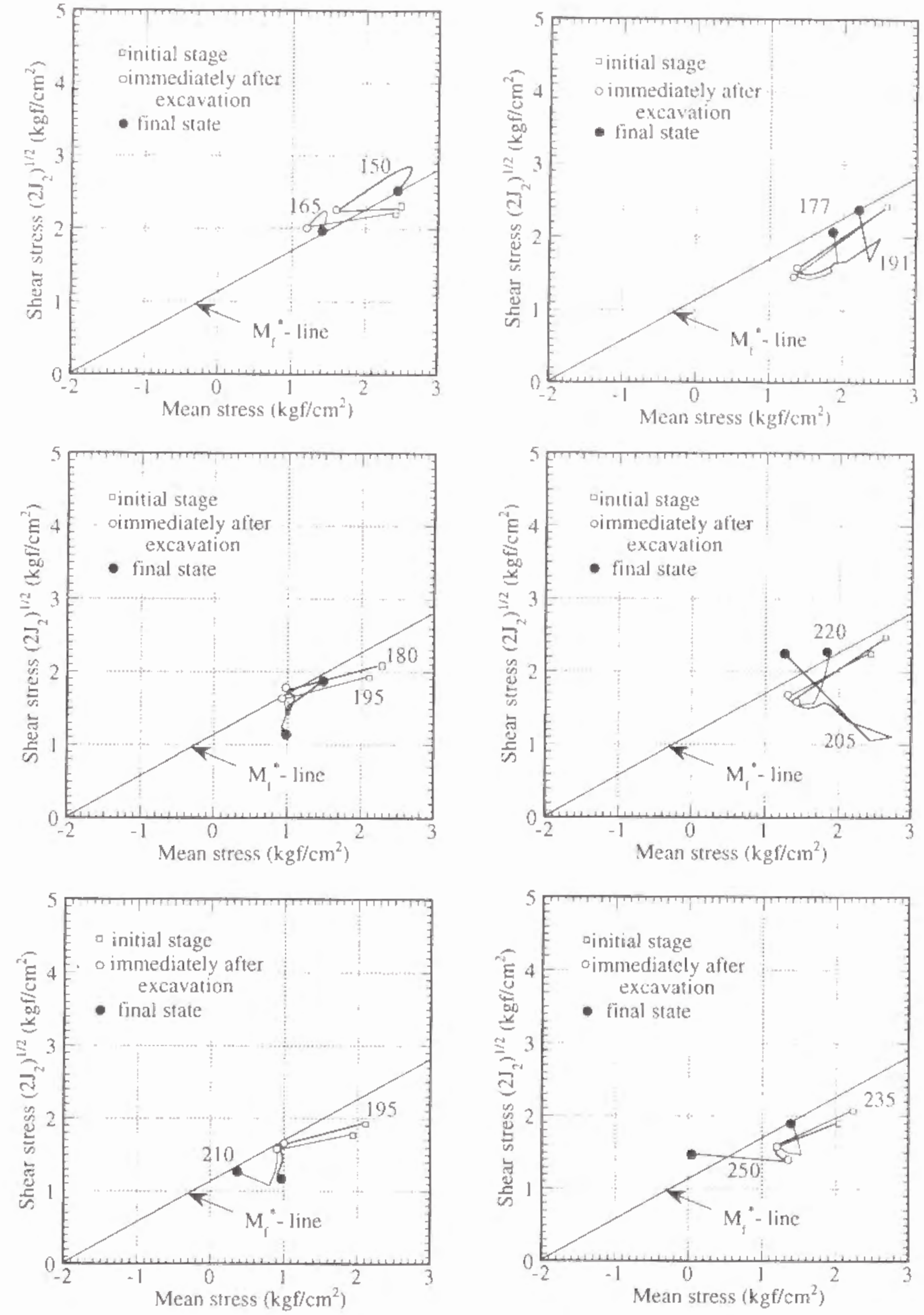

(a) Part I(creep-failure-zone)

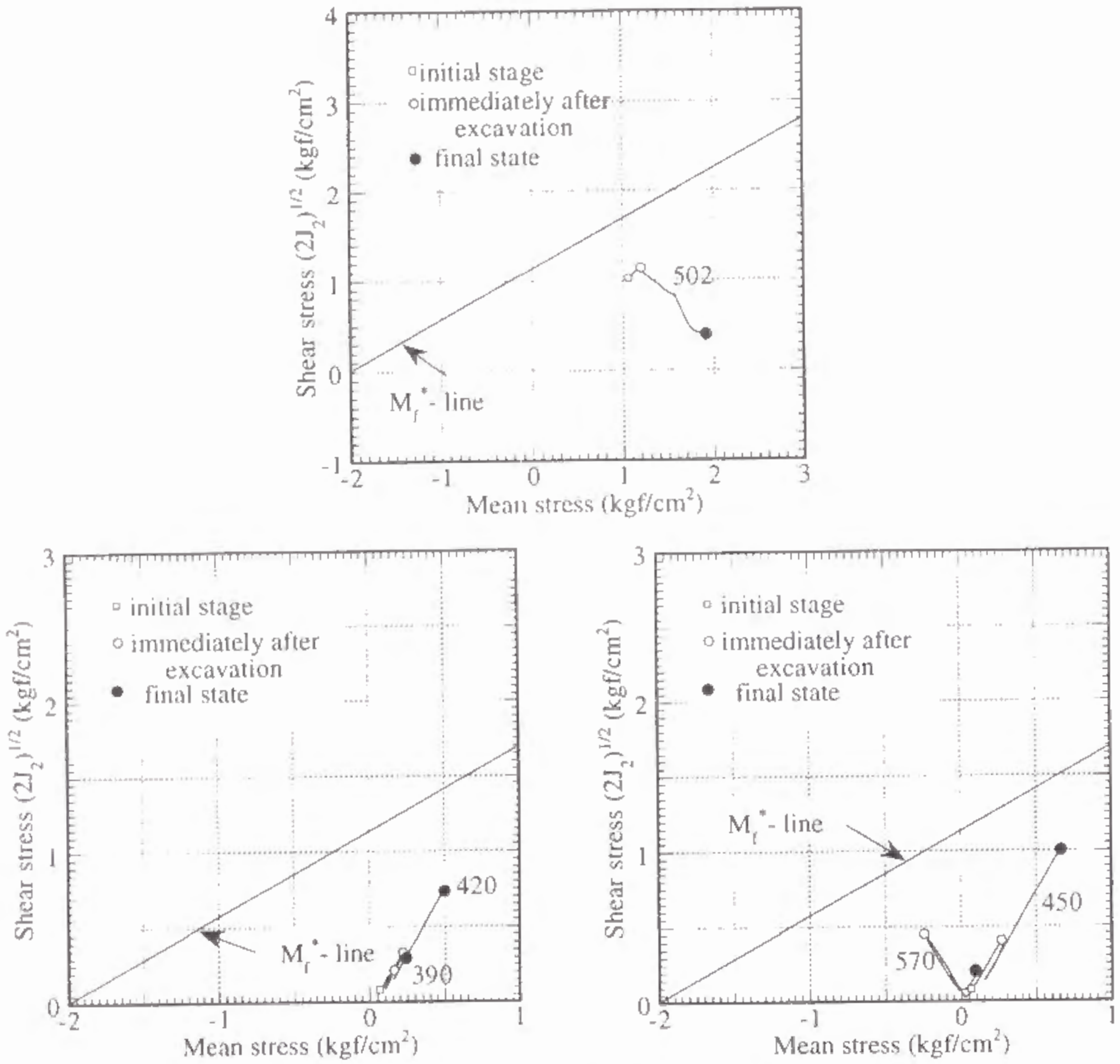

(b) Part II(no-failure-zone)

Fig.7-6 Stress paths of the elements in the model ground

Fig.7-7 shows the relation between shear strain rate and time in some elements. For example, in element 150, the whole creep failure behavior, that is, the migration from the steady creep state to the accelerating creep state with time can be clearly simulated in a boundary value problem with the present finite element analysis. In elements 165 and 180, the relation between shear strain rate and time also shows similar tendency, that is, the migration from a steady creep state to an accelerating creep state. It is found that the relation of strain rate vs. time in these elements are affected by neighboring areas where creep failure have already occurred and a vibration is observed in strain relation. However, the general tendency of the creep strain rates is mainly dependent on the overall behavior of

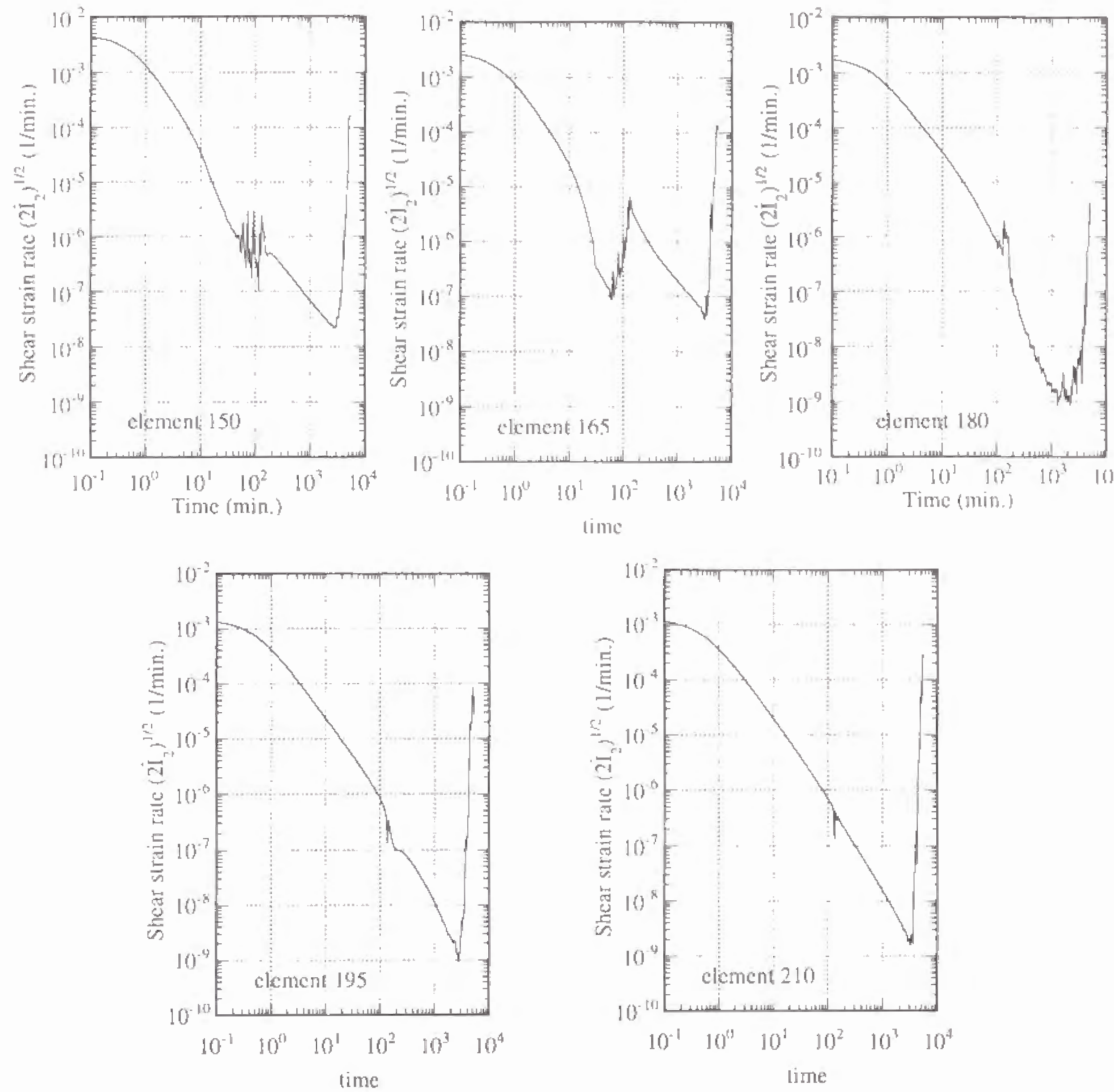

(a) Part I-1(creep-failure-zone)

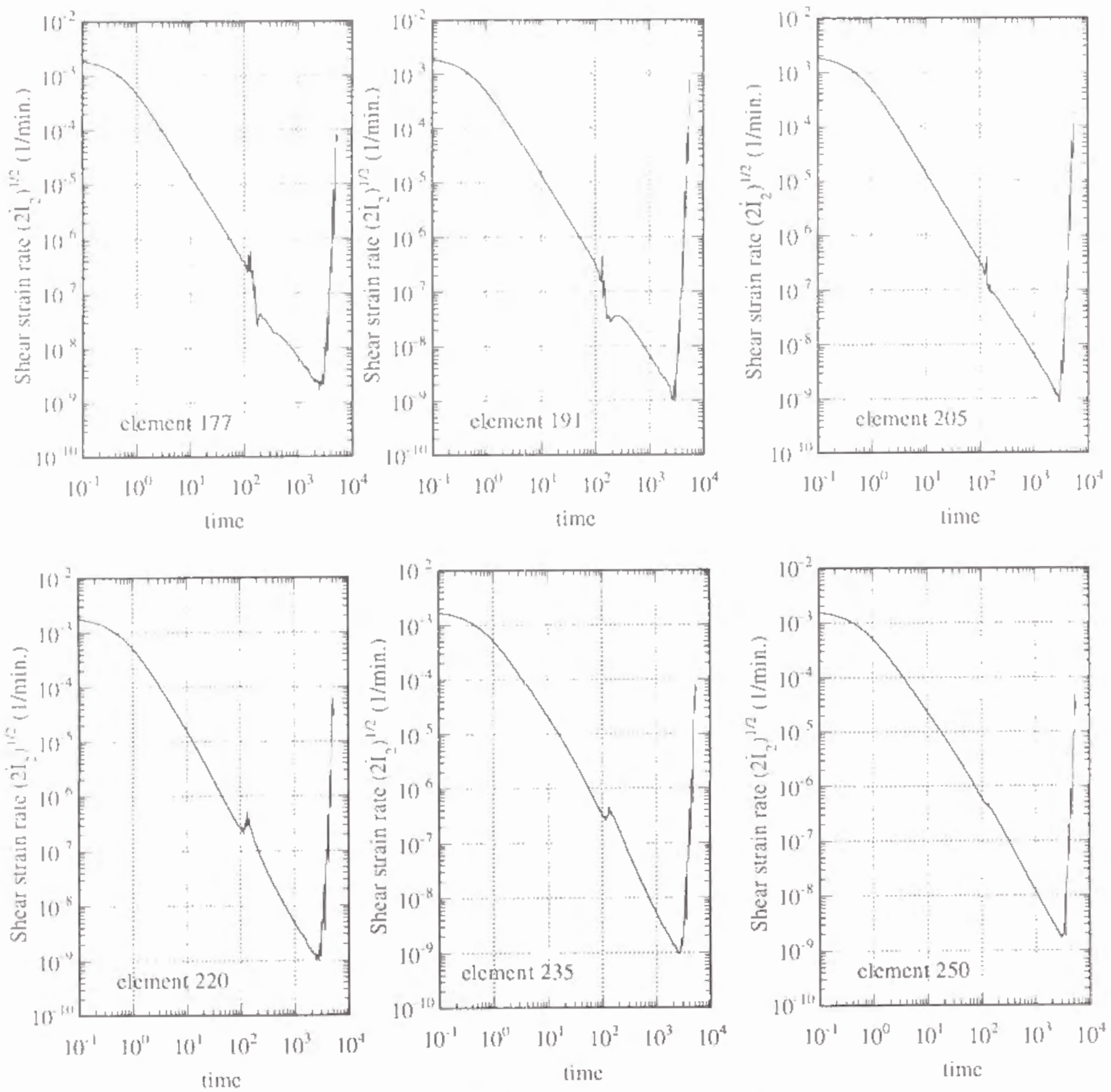

(b) Part I-2(creep-failure-zone)

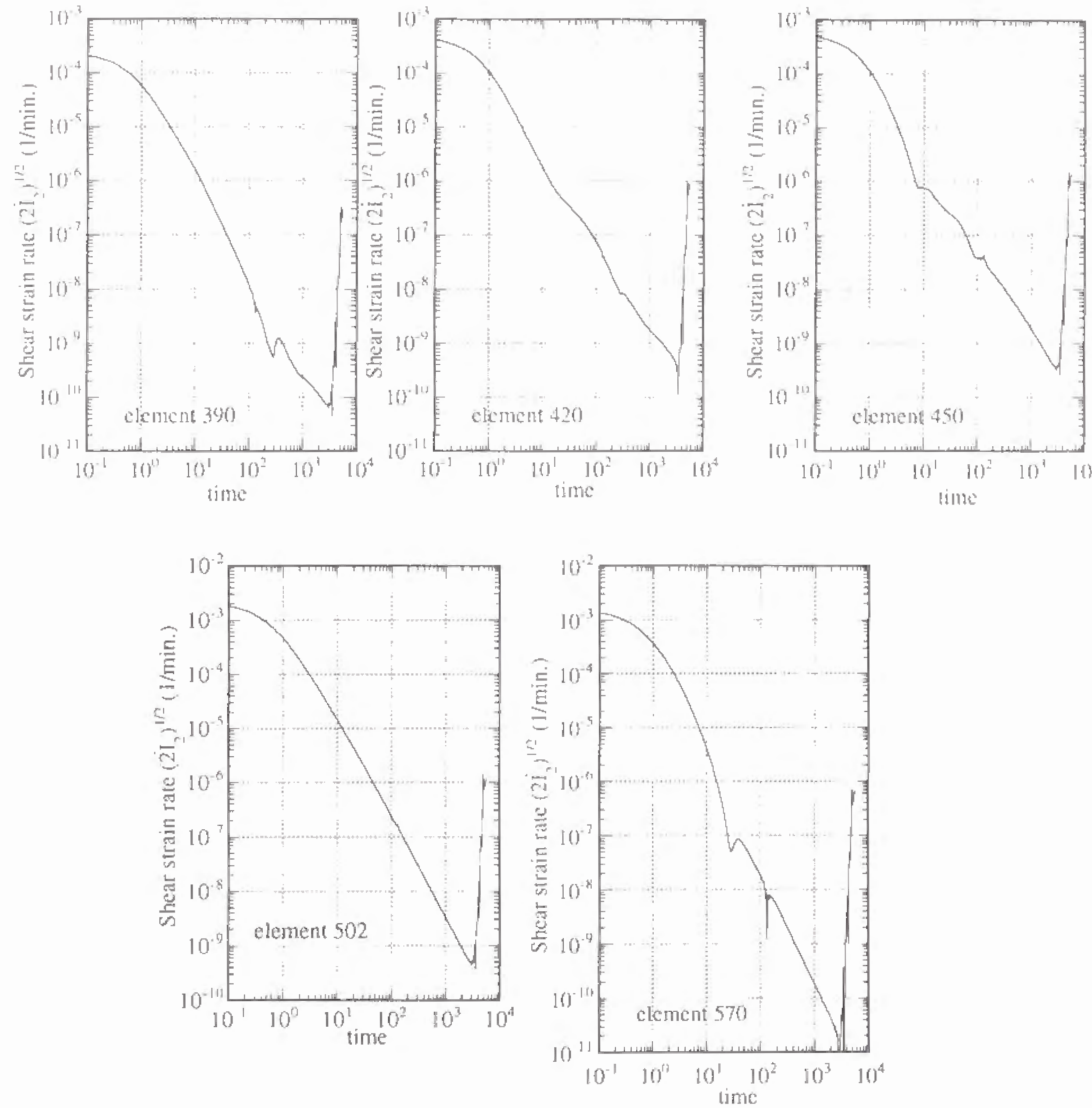

(c) Part II(no-failure-zone)

Fig.7-7 Relation between strain rate and time

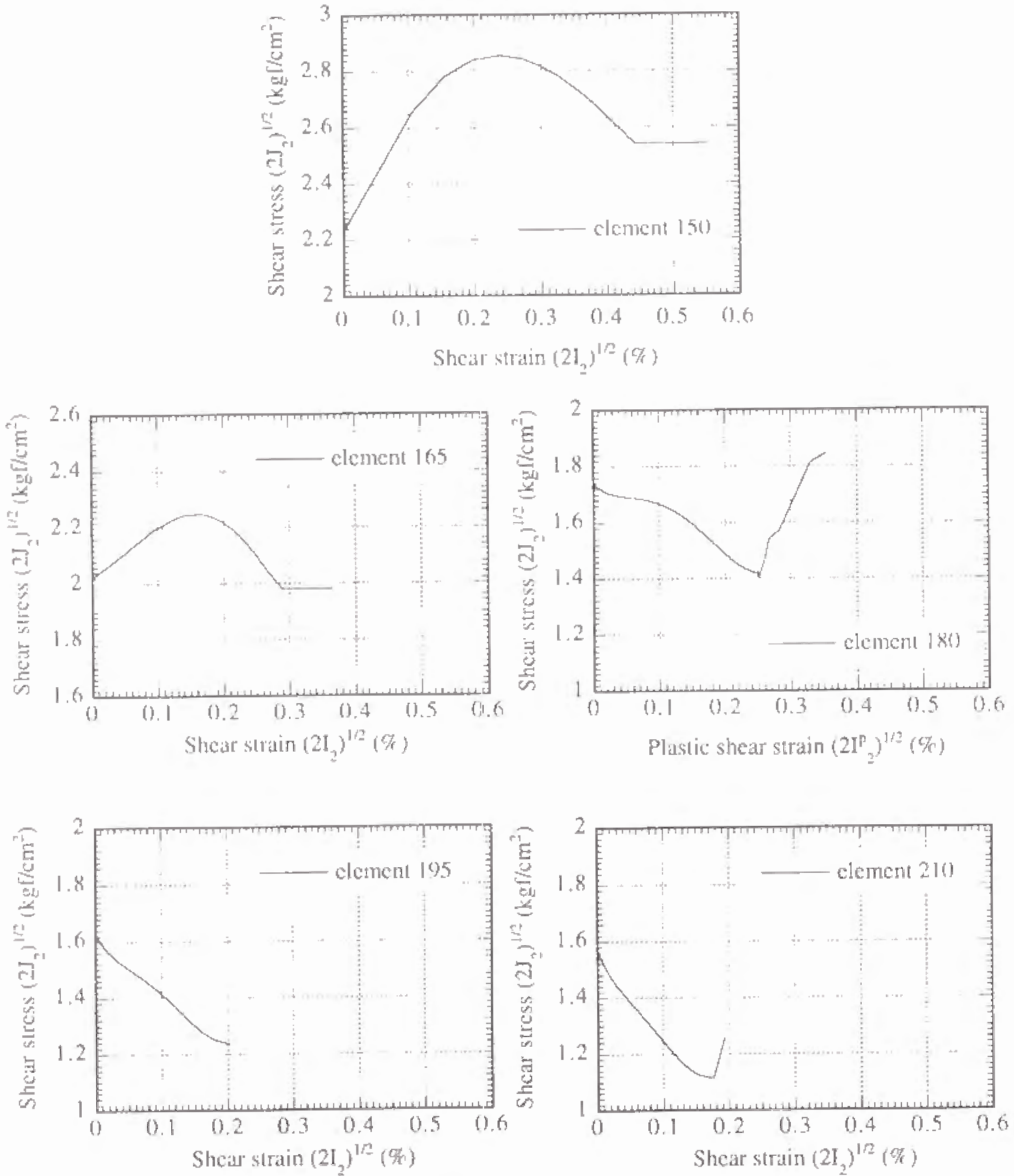

(a) Part I-1(creep-failure-zone)

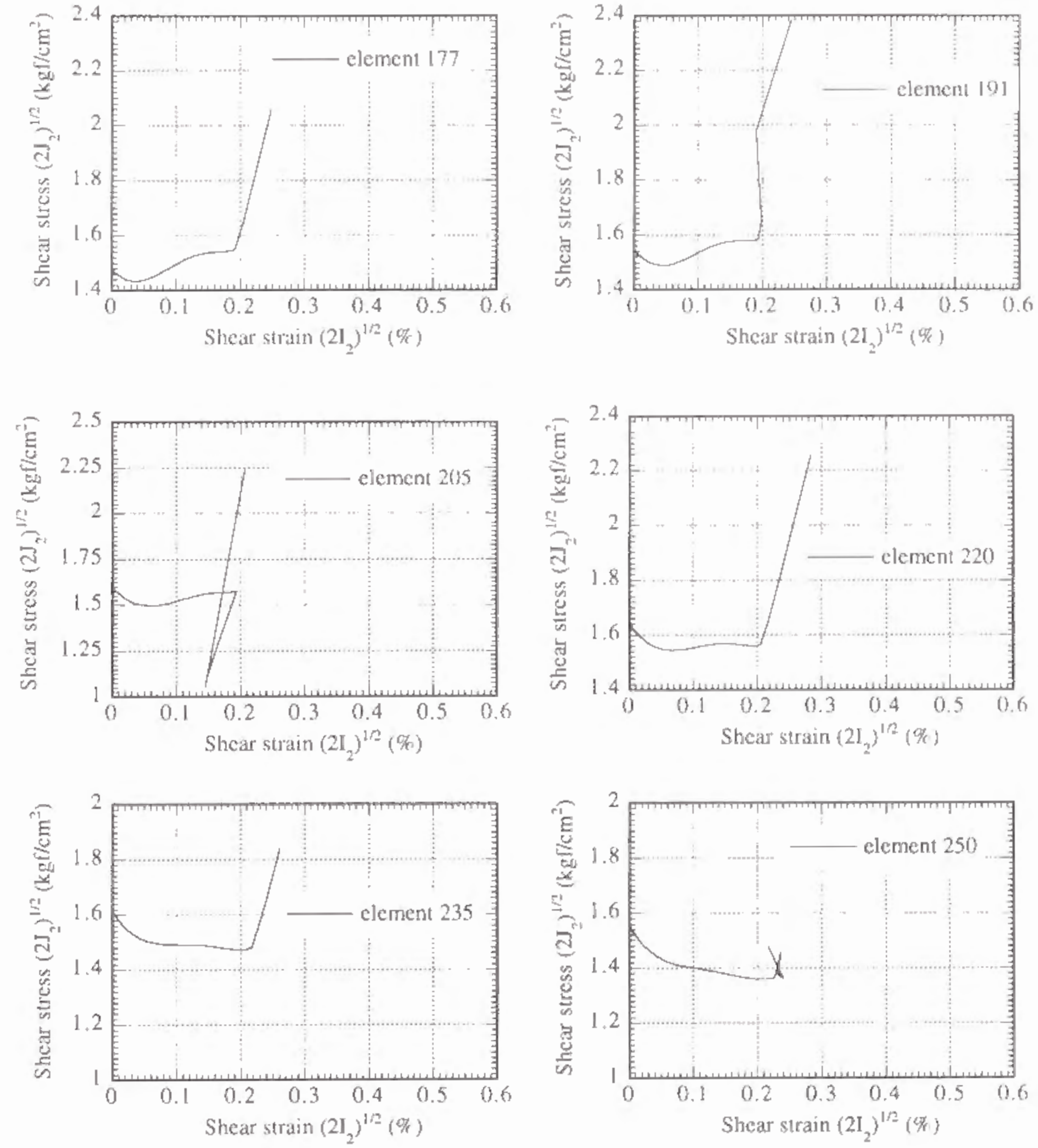

(b) Part I-2(creep-failure-zone)

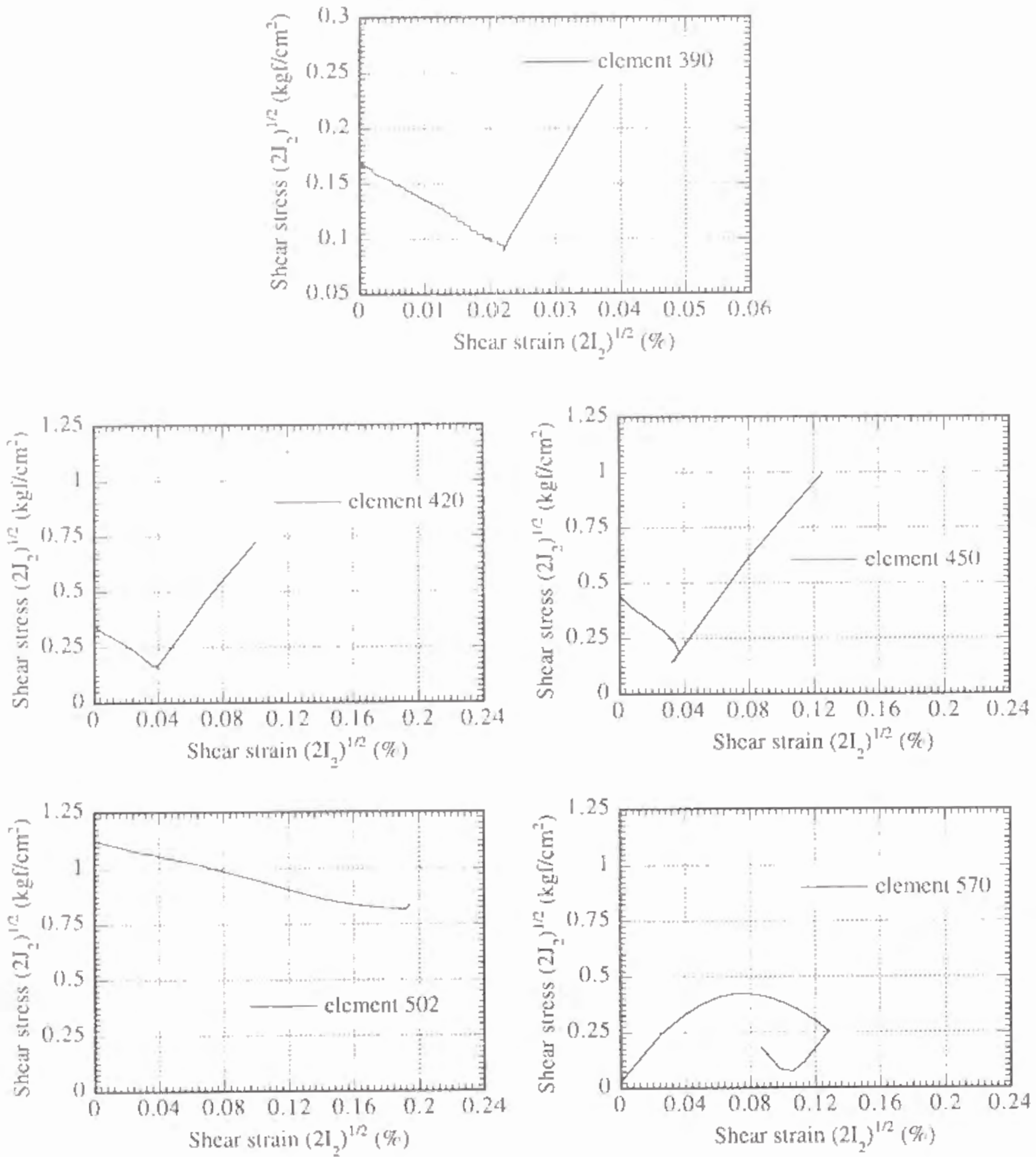

(c) Part II(no-failure-zone)

Fig.7-8 Relationship between shear stress and strain

ground instead of individual element even if it has already failed. For example, in element 165, the creep strain rate increased very quickly when it failed. However, as the surrounding ground still remains unfailed, the strain rate decreased again until overall failure in the toe of the slope. The relations of creep strain rate vs. time are also plotted at no-failure-zone. It is found that even in these elements, the migration from steady creep state to accelerating creep state occurs. It is found that the maximum creep strain rate at no-failure-zone is about 10^{-6}/min., being two orders less than the one at creep-failure-zone. It is found from above discussion that instead of being dependent on the stress state of individual element, the overall deformation of the cut slope, especially the acceleration of creep rate is dependent on the size of failure zone. Once the acceleration of creep rate occur, the tendency of the creep deformation in the ground will be the same, no matter whether the stress of element is in failure state or not.

Fig.7-8 shows the relations of the shear stress-strain in model ground. For example, in creep-failure-zone, element 150 shows a typical stress-strain relation with strain softening. On the other hand, the stress-strain relation in element 180 is quite different from the relation in element 150. It is found that in the beginning, the stress state in element 180 is almost in stress relaxation and the stress decreases as the plastic strain increases. When creep failure occur in neighboring areas, however, it turns out to be in shearing state and the stress increases until failure occurs. It is also found that the stress-strain relations in no-failure-zone, such as element 390, 420 and 450, are similar to that of element 180. However, the stress states in these elements are absolutely different. The strains in element 390, 420 and 450 are mainly elastic while the strain in element 180 is mainly plastic.

7-4 Comparison with classical method in soil mechanics

In soil mechanics, the Mohr-Coulomb failure criteria is most commonly used. It can be expressed as

$$\sigma_1 - \sigma_3 = 2c\cos\varphi + (\sigma_1 + \sigma_3)\sin\varphi \qquad (7\text{-}1)$$

or

$$\sigma_1 = \sigma_3 \tan^2(\frac{\pi}{4} + \frac{\varphi}{2}) + 2c \tan(\frac{\pi}{4} + \frac{\varphi}{2}) \tag{7-2}$$

where c and ϕ are cohesion and the frictional angle of soil respectively. In the present study, the finite element analysis is based on the elasto-viscoplastic model with strain softening in which the residual strength is defined at axisymmetric condition by

$$\tan\Phi = M_f^* = \frac{\sqrt{2/3}\ (\sigma_1 - \sigma_3)}{(\sigma_1 + 2\sigma_3)/3 + b} \tag{7-3}$$

or

$$\sigma_1 = \frac{\sqrt{2/3} + 2/3 \tan\Phi}{\sqrt{2/3} - 1/3 \tan\Phi}\sigma_3 + \frac{\tan\Phi}{\sqrt{2/3} - 1/3 \tan\Phi} \tag{7-4}$$

Comparing Eq.7-2 with Eq.7-4, the following equations are obtained for c and ϕ :

$$\varphi = 2\{\tan^{-1}[(\frac{\sqrt{2/3} + 2/3 \tan\Phi}{\sqrt{2/3} - 1/3 \tan\Phi)})^{1/2}] - \frac{\pi}{4}\} = 16.97^\circ \tag{7-5}$$

$$c = \frac{b \tan\Phi}{2(\sqrt{2/3} - 1/3 \tan\Phi) \tan(\frac{\pi}{4} + \frac{\varphi}{2})} = 0.61(\mathrm{kgf/cm^2}) \tag{7-6}$$

The classical method in soil mechanics was also used to evaluate the safety factor of the slope failure in the model ground. slope, The angle of the cut slope is larger than 53°. Therefore, slope failure would occur at the toe of the slope. By using the values of c = 6.1 tonf/m^2 and γ_s = 2.1 tonf/m^3, a safety factor of about 1.3 is obtained for the slope failure, which means that the present cut slope will not fail according to classical method. In the present finite element analysis based on the model proposed in this paper, however, localized failure dose occur in the cut slope of the model ground. One numerical difficulty is that the calculation has to be stopped 5554.8 minutes after the excavation of the cut slope is complete. Whether the slope fails on the whole could not be verified by the present analysis.

7-5 Conclusions

In this chapter, based on the elasto-viscoplastic model which can not only describe all the aspects of time dependency, such as strain rate dependency, creep and stress relaxation, but also the strain softening of geologic materials, a finite element analysis is carried out to investigate the mechanism of progressive failure in a cut slope on a model ground. It is found from the analysis that the main factors related to the instability of the cut slope, such as the deterioration of the ground and progressive failure, can be simulated in relation to the boundary value condition. The acceleration of creep rate is dependent on the size of failure zone instead of the stress state of individual element. The numerical results are compared with those obtained with the classical method in soil mechanics. It is found that a cut slope in a model ground will not fail with the classical method, while a localized failure does occur in the cut slope of the model ground with the finite element analysis.

References

(1) Adachi, T., and Yoshida, N. (1993) : "Analysis of excavation in clay shales with high K_0 stress states," Proc. Int. Symp. on Application of Comp. Meth. in Rock Mech. and Engng., Xian, China, pp835~842.

(2) Adachi, T., Oka, F. and Zhang, F.(1994) : "An elasto-viscoplastic constitutive model with strain softening and its application to the progressive failure of a cut slope," AMD-Vol.183/MD-Vol.50, Material Instabilities: Theory and Applications, ASME, pp.203~217.

(3) Bjerrum, L. (1967) : "Progressive failure in slopes of over-consolidated plastic clay and clay shales," Proc., ASCE, Vol.93, No. SM5, Sep..

(4) Yoshida, N., Morgenstern, N., and Chan, D. H. (1991) : "Finite-element analysis of softening effects in fissured, overconsolidated clays and mudstones," Canadian Geotech. Jour., Vol.28, pp.51~61.

Chapter 8

Numerical analysis of time dependent behavior in tunnel excavation

8-1 Introduction

Under ground water is thought to be one of the most important problems in relation to constructing tunnel in soft rock and many researches on this field have being reported. The time dependent behavior of tunneling in soft rock ground is also a very important problem(Adachi, 1979). For example, when tunnel is excavated in swelling ground, the deformation of tunnel section and the change of earth pressure on lining with time are also needed to be investigated.

The time dependent behavior of tunnel excavation in saturated soft rock is mainly caused from three reasons. That is,

(1) the inherent property of ground with time dependency,
(2) the change of pore-water pressure caused by tunnel excavation,
(3) The change of boundary condition along with the advancement of cutting face.

In this chapter, only the inherent property of ground with time dependency in tunnel excavation is considered. In chapter 6, an elasto-viscoplastic model is proposed which can not only describe all the aspects of time dependency as strain rate dependency, creep and stress relaxation but also the strain softening of geologic materials. Based on the model, a finite element analysis is carried out to investigate the time dependent behavior of tunnel excavation, taking consideration of strain softening and time dependency.

In chapter 5, as a case study, Maiko testing tunnel is investigated based on elasto-plastic model with strain softening, in which main attention was paid to the stress-strain relation, characteristic curve of NATM and softening zone occurred in tunnel excavation. In this chapter, as a fundamental study, we mainly focus on the time dependent behavior after the tunnel excavation is completed.

8-2 Finite element analysis

The purpose of the present analysis is to investigate the deformation of tunnel section and the change of earth pressure on lining with time. In chapter 5, it is found that the initial stress released ratio in Maiko testing tunnel(Adachi et al., 1994) is about 20% and softening zone did not occur. The stress-strain condition is usually regarded as elasticity at the moment when the lining was installed in the case of Maiko testing tunnel. As the same in chapter 5, the finite element analysis in this chapter is carried out in plane strain condition. The geometrical and physical condition of the tunnel are also the same in chapter 5. Table 5-3 shows the in situ test results for the materials of ground in section A-A. Table 8-1 lists the material parameters involved in elasto-viscoplastic model with strain softening proposed in chapter 6. Compared with Table 5-4, about half of the material parameters are remained unchanged. Only the stress history parameter τ, the strain hardening parameter G' and M^*_f are changed because of the definition of stress history ratio and time measure are changed. The determination of the parameters in Table 8-1 is based on the rule illustrated in chapter 6.

Table 8-1 Material parameters of elasto-viscoplastic model used in FEM

Geological profile	B	Og_2	Oc_2	Og_4	Ko
E(kgf/cm^2)	300.0	500.0	950.0	1270.0	1500.0
ν	0.35	0.30	0.30	0.35	0.28
b(kgf/cm^2)	4.0	6.0	8.0	10.0	10.0
σ_{mb}(kgf/cm^2)	40.0	80.0	80.0	100.0	120.0
$M^*_{f\infty}$	0.220	0.335	0.622	0.502	0.868
G'	200.0	200.0	500.0	1500.0	2000.0
$\bar{M}_m$	1.20	1.08	1.08	1.08	1.30
τ	3.10	3.10	3.30	3.30	3.50
α	0.614	0.614	0.614	0.614	0.614
a	-0.11	-0.11	-0.11	-0.11	-0.11
g	1.0	1.0	1.0	1.0	1.0

The geometry of tunnel in section A-A and finite element mesh used in the analysis are given in Fig.5-24. 8-element isoparametric finite element is used in calculation. Beam element is introduced to simulate the lining. The numbers of nodes and elements are 565 and 160 respectively.

In simulating the mechanical behavior of tunnel excavation, the gravitational stress field is first evaluated with initial stress analysis based on elasticity and then the tunnel is excavated instantly to a prescribed stress released ratio according to the result obtained from chapter 5. In present case, stress released ratio is 20%. The remained 80% of initial stress is then removed with the existence of lining which is simulated by beam element. As main attention is paid to the time dependent behavior of tunnel after excavation completed, the time needed for tunnel excavation and installation of lining is supposed to be zero. Taking a review on Fig.5-28, it can be seen that in such condition, the tunnel construction is completed within the stage at which no prominent plastic strain develops and the lining is installed in the linear region of characteristic curve known as Fenner-Pacher curve.

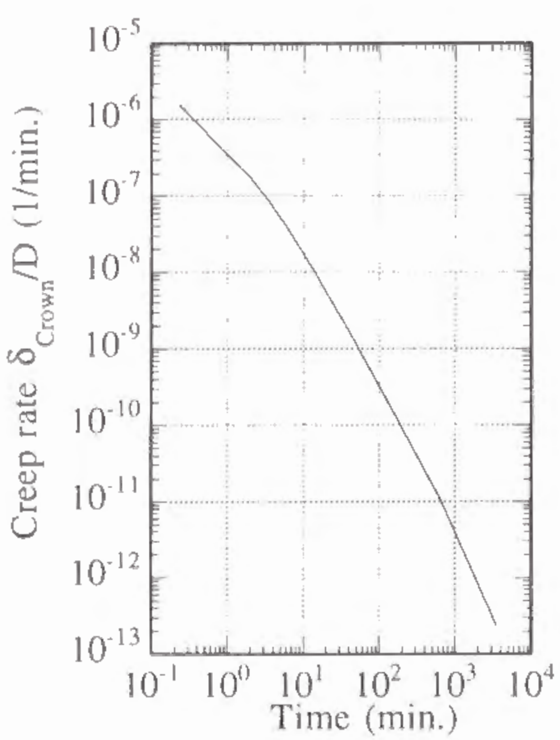

Fig.8-1 Relationship of creep deformation rate vs. time at crown

Fig.8-1 shows the change of creep rate at crown with elapsed time. It can be seen from the figure that the creep rate decreased very quickly and shows almost linear relation with elapsed time in logarithmic coordinates. It is also found that the deformation of tunnel periphery is almost finished within two days after the completion of tunnel lining.

Fig.8-2 shows the change of octahedral stress in the ground near to spring lining with elapsed time. From the figure it is found that the octahedral stress decreased with elapsed time at first two days and after then it remained almost unchanged, which shows a typical stress relaxation behavior. As the shear stress in ground decreased, the interaction between ground and lining will also change. It is reasonable to expect that the load

acting upon lining will increase to compensate for the loss of shear stress in ground.

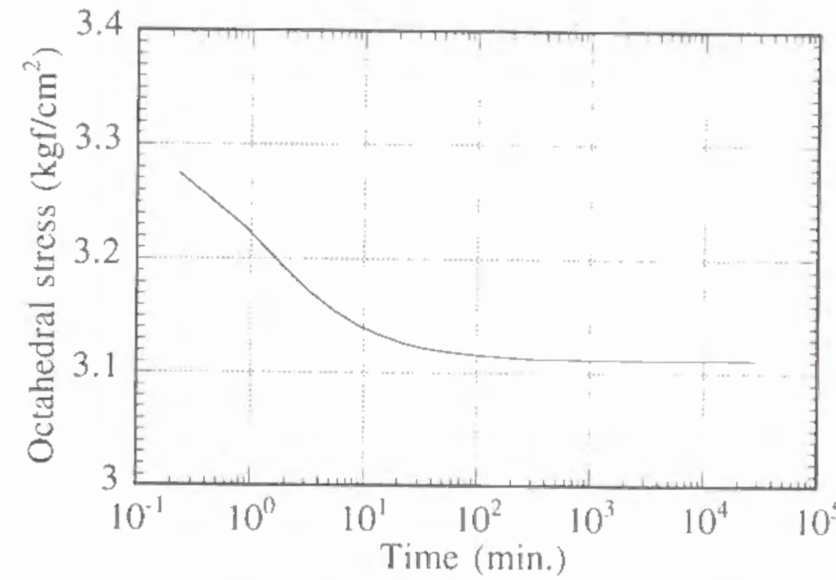

Fig.8-2 Variation of octahedral stress with time at spring line

Fig.8-3 shows the change of axial stress in lining. It is found from the figure that the axial stress in lining increased evenly around tunnel periphery. Fig.8-4 shows the variation of axial stress with elapsed time in lining at spring line. From the figure, it can also be seen that the change of the axial stress is finished almost within two days. The variation of the axial stress in lining at other position shows the similar behavior.

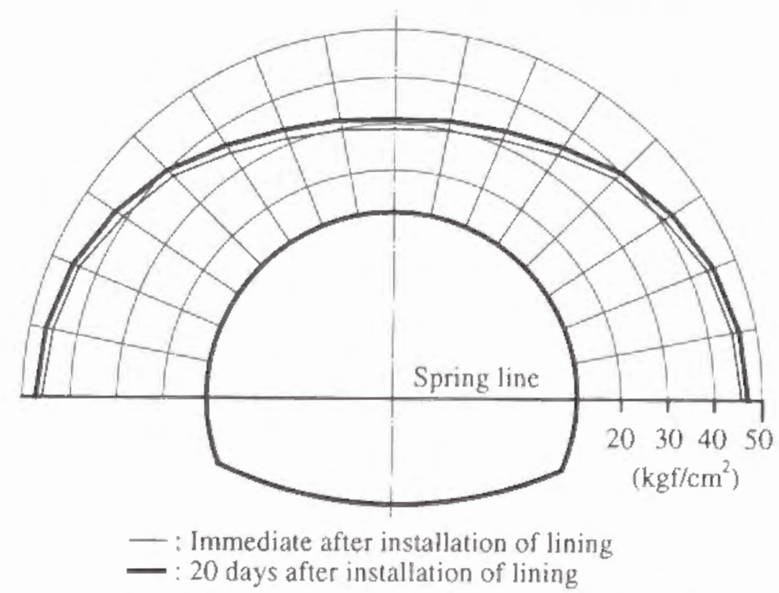

Fig.8-3 Variation of axial stress in lining with time

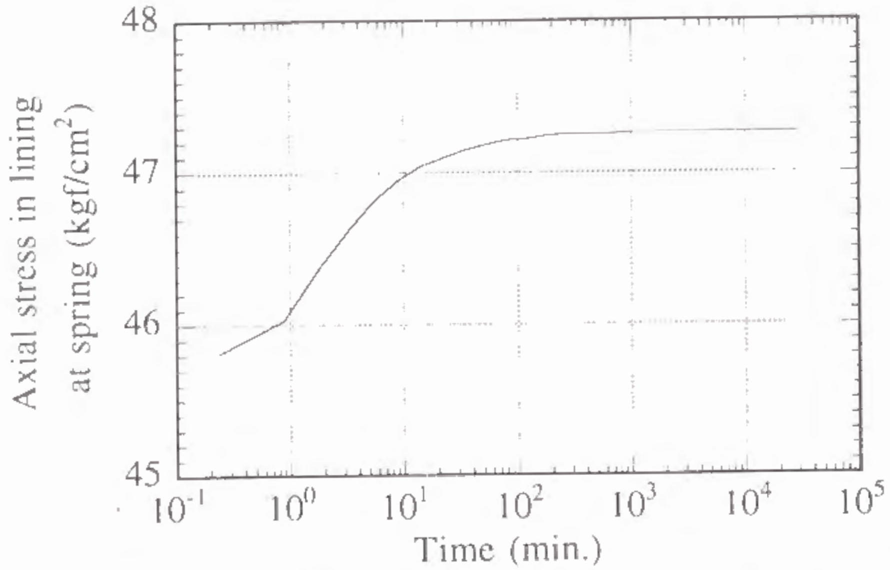

Fig.8-4 Variation of axial stress with time in lining at spring line

8-3 Conclusions

In this chapter, based on the elasto-viscoplastic model which can not only describe all the aspects of time dependency as strain rate dependency, creep and stress relaxation but also the strain softening of geologic materials, a finite element analysis is carried out to investigate the mechanical behavior of time dependency in tunnel excavation. Special attention was paid to the time dependent behavior of post tunnel excavation with lining. It is found that even if tunnel construction is completed within the stage at which no prominent plastic strain develops and the lining is installed in the linear region of characteristic curve, the time dependency of ground material cannot be neglected.

References

(1) Adachi, T. (1979) : "Research on the mechanical behavior of sedimentary rock," Doctoral Theses, Kyoto University(In Japanese).

(2) Adachi, T., Oka, F., Yashima, A., and Zhang, F. (1994) : "Analysis of earth tunnel by strain softening constitutive model," Proc. 13th ICSMFE, India, Vol.2, pp.879-882.

Chapter 9

Conclusions

The main purpose of this paper is (1) to establish fitting constitutive models which may be rather sophisticated, can describe main properties of geologic materials and (2) based on these models, to establish applicable numerical analyses by which geologic engineering problem can be solved in relation to boundary value condition.

In the beginning of the paper, a few constitutive models which are well known to us are discussed as a background of understanding later developed models. Most of the attention was paid to the constitutive models which can not only deal with strain hardening-strain softening but also time dependency. Adachi-Oka's model with strain softening was improved by adding some new ideas to the model. Especially, the evaluation of the parameters involved in the model has been generalized, which as a consequence, makes it possible for the model to be applied to numerical analyses in solving boundary value problems in geotechnical engineering.

Based on Adachi-Oka Model with strain-hardening and strain-softening, a new constitutive model with strain-softening is proposed to describe the discontinuous behavior of joint materials. Unlike most of other researchers doing, in the model, continuum theory is still used to describe the discontinuous behavior of joint materials. The dilatancy of the materials undergoing shearing is explained in elasto-plasticity theory instead of roughness of joint which is commonly used in joint analysis for geologic materials. Application of the model to the direct shear tests of geologic materials under constant normal stress and constant stiffness condition shows good agreement between the experiment results and the computed results based on the model.

In finite element and joint element analyses based on the constitutive models with strain softening, a new numerical technique is proposed and its capability to obtain a convergent solution for the boundary problem concerning strain softening is proved mathematically. Some laboratory tests such as direct shear test and conventional triaxial tests were analyzed concerning the relevant boundary value conditions. The new technique is also compared and checked with other numerical procedures in plane strain and axisymmetric conditions. It is found that the numerical procedure used in this chapter does not need any special precaution in relation to localization and the analytical results are independent of the mesh size used for spatial discretization.

The mechanical behavior of ground and lining in tunnel construction is investigated using a series of finite element and joint element analyses based on Adachi-Oka's model with strain softening. As a fundamental study, a trapdoor problem in model ground is investigated with FEM and JEM. It is found that the ground convergence curve of trapdoor can be simulated. It is also found that the load method is more suitable than the displacement method in simulating mechanical behavior of trapdoor.

It is found in the numerical analyses that the mechanical behaviors of shallow and deep tunnel are quite different and should be dealt with distinctively. Two different types of case studies were carried out. One is related to a relatively deep tunnel excavation and another is concerned with a shallow tunnel construction in which discontinuous deformation was observed in tunnel excavation. In the analyses, the parameters involved in the constitutive model are based on in-situ measurement or laboratory tests and the influence of anisotropy is taken into consideration. It is found that the discontinuous deformation observed in the shallow tunnel excavation can be well simulated by introducing joint elements into the finite element mesh along possible sliding surfaces. The deformation patterns around tunnel show much difference in different analyses when the ground around the tunnel periphery becomes softening and artificially introduced joints become yielding. It is better not to use finite element method without joint elements to simulate shallow tunnel construction. In deep tunnel, such restriction is not necessary. The analyses based on the constitutive model with strain softening can well describe the ground convergence characterized by so called Fenner-Pacher curve in tunneling with NATM.

Based on Adachi-Oka's model with strain softening, an elasto-viscoplastic model with memory is proposed for geologic materials. The comparison of analytical results based on the model with experimental results indicate that it can not only describe all the aspects of time dependency as strain rate dependency, creep and stress relaxation but also the strain softening behavior for geologic materials. Most of the parameters involved in the model can be determined in the same way used in Adachi-Oka's model with

strain softening. The new parameters introduced in this model can also be definitely determined by triaxial tests and drained creep tests.

As a major application of the elasto-viscoplastic model proposed in this paper, progressive failure of cut slope in model ground is investigated. It is found from the numerical analyses that the main factors related to instability of cut slope such as deterioration of ground and progressive failure can be simulated in relation to specified boundary value condition. The numerical result is also compared the predicted results using classical method in soil mechanics. It is found that the cut slope in model ground will not fail by the classical method, while for the finite element analysis, localized failure occurs in the cut slope of model ground.

Another application of the elasto-viscoplastic model is to investigate the mechanical behavior of time dependency in tunnel excavation. Special attention was paid to the time dependent behavior of post tunnel excavation with lining. It is found that even if tunnel construction is completed within the stage at which no prominent plastic strain develops and the lining is installed in the linear region of the characteristic curve known as Fenner-Pacher curve, the time dependency of the ground material cannot be neglected.